Membrane Processes for Water Recovery from Brown Coal Flue Gases

Hirra Azher

Submitted in total fulfilment of the requirements of the degree of Doctor of Philosophy

February, 2015

Department of Chemical and Biomolecular Engineering

The University of Melbourne

Australia

Abstract

Victorian brown coal has a significantly higher moisture content compared to black coal. Hence, it is possible that significant quantities of water can be recovered from high temperature brown coal flue gases and recycled in the process given that it is a high enough purity. The presence of CO_2 and SO_x will result in acidic water that may cause corrosion issues. The use of membranes to selectively permeate water over other flue gas components such as N_2 and CO_2 has the potential to provide a water stream of high purity. While N_2 is the major component in flue gas, in this instance the presence of CO_2 also needs to be investigated because of its high acidity. This work considered the separation performance of Nafion 115, Sulphonated Poly (Ether Ether) Ketone (SPEEK) and 6FDA – TMPD (2, 2 – bis (3, 4 – dicarboxyphenyl) hexafluoropropane dianhydride – 2, 3, 5, 6 – tetramethyl – 1, 4 – phenylenediamine) at elevated temperatures. Water, CO_2 and N_2 permeation properties of these membranes were investigated on a novel high temperature mixed gas rig that utilized mechanical agitation to eliminate concentration polarization.

The permeation of water, CO_2 and N_2 through Nafion 115 was investigated as a function of water activity at 70 – 150 °C. It was found that all permeances increased with increasing water activity but reduced with increasing temperature. This data was supplemented by sorption analysis at lower temperature which conversely showed decreasing solubility as temperature increased. The sorption results were modelled using a modified Dual Mode Sorption Model where Arrhenius expressions were used to model the effect of temperature on the water concentration absorbed into the polymer. The changes in solubility and permeance with water activity were attributed to membrane swelling as water activity increased. A comparison with a thinner perfluorosulphonic acid polymer (Fumapem F - 920) from an alternate supplier suggested that permeance did not scale linearly with membrane thickness, reflecting non – linear water activity gradients within the membrane and thus inhomogeneity in membrane swelling.

The effect of temperature on water vapour and CO_2 permeation properties of Sulphonated Poly (Ether Ether) Ketone (SPEEK) with two different ion exchange

capacities (IEC) were investigated. These were Fumapem E - 630 and Fumapem E - 540 - GF with IEC 1.6 meq/g and IEC 1.9 meq/g, respectively. It was found that both permeabilities increased with increasing water activity due to increased water solubility as water concentration increased. This was supported by FTIR spectra that measured peaks for water sorbed into the SPEEK polymer and confirmed the presence of the water as clusters. Both water vapour and CO_2 permeabilities increased as temperature increased up to 50 °C. This was due to the increase in diffusion of the penetrating molecules. However as temperature increased further, increased water uptake appeared to result in significant formation of water clusters that hindered the diffusion of isolated molecules. This decrease in diffusion coupled with a reduction in solubility with increasing temperature resulted in a significant drop in water permeability above 50 – 70 °C. Similar results have been obtained by other researchers and were attributed to the reduction in solubility overcoming the increase in diffusivity with increasing temperature. The permeabilities at 70 – 150 °C were modelled using Arrhenius expressions. Activation energies of permeation of ~ -46 kJ/mol for IEC 1.6 meq/g and ~ -43 kJ/mol for IEC 1.9 meq/g were obtained for this temperature range. SPEEK with IEC 1.9 meq/g exhibited higher permeation and selectivity than IEC 1.6 meq/g. This is due to the increased presence of the sulphonic acid groups that are known to improve the performance of any membrane.

Water vapour and gas permeation properties of 6FDA – TMPD from 25 – 150 °C were investigated. The water sorption properties from 25 – 35 °C were also investigated and resulting sorption parameters used to model water permeability at the same temperature range. It was found that the infinitely dilute Fickian diffusion constant is temperature – dependant probably due to water sorbed in the polymer plasticizing the membrane and forming clusters at higher water activities and temperatures. A similar permeability trend to SPEEK was obtained where water vapour, CO_2 and N_2 permeability increased with temperature up to 50 °C but decreased above this. This was likely due to a significant reduction in solubility as temperature increases. It might also be influenced by the formation of clusters that hinder diffusion. Similar results for this polymer were reported by others with “anti – plasticization” or clustering behaviour observed in other polymers. It is also

well known that the presence of water reduces the glass transition temperature. It appears that 6FDA – TMPD transitions from a glassy to a rubber state at a T_g of ~ 55 °C. Furthermore, CO_2 and N_2 permeabilities decrease with increasing feed water activity which suggests the competitive sorption of water. These competitive sorption and plasticization effects were investigated further at high temperatures by comparing water permeability data from a H_2O/CO_2 feed mixture to that from a H_2O/N_2 feed mixture. It was found that at low temperatures, the competitive sorption of water reduces sorption of both CO_2 and N_2. This results in similar water permeabilities through the membrane for both gas mixtures. However as temperature increases the sorption of water is reduced, resulting in increased water permeability for H_2O/CO_2 feed mixture. This is due to the increased sorption of CO_2 and consequently increased CO_2 plasticization effects.

The permeance data for water and CO_2 at 150 °C were compared for all five polymers. The highest H_2O/CO_2 selectivity was for Nafion 115 followed by Fumapem F - 920, Fumapem E - 540 - GF and Fumapem E - 630 with 6FDA – TMPD having the lowest selectivity. The permeance data was modelled within Aspen HYSYS and it was found that a permeate stream with pH 5.67 is achievable with Nafion 115 at 150 °C. However, the membrane areas required for this are very large indicating that there exists a trade – off between permeate purity and membrane area. A high purity product is required for reuse in the process therefore pH adjustment of the recovered stream would be needed regardless of the membrane material used.

Declaration

This is to certify that:

- The thesis comprises only my original work towards the PhD except where indicated in the Acknowledgements,
- Due acknowledgement has been made in the text to all other material used,
- The thesis is fewer than 100 000 words in length, exclusive of tables, maps, bibliographies and appendices.

Hirra Azher

February, 2015

Preface

Journal Publication

The 4th Chapter of this thesis has been published:

H. Azher, C.A. Scholes, G. Stevens, S.E. Kentish, *Water permeation and sorption properties of Nafion 115 at elevated temperatures,* JOURNAL OF MEMBRANE SCIENCE, 459 (2014), 104 – 113.

The papers on Chapter 5 and 6 are in progress:

H. Azher, C.A. Scholes, G. Stevens, S.E. Kentish, *The effect of Sulphonation degree and temperature on permeation properties of Sulphonated Poly (Ether Ether) Ketone,* IN PROGRESS.

H. Azher, C.A. Scholes, G. Stevens, S.E. Kentish, The effect of temperature on w*ater permeation properties of polyimide membrane,* IN PROGRESS.

Acknowledgments

This research work would not have been possible without significant support and contributions from a number of people. I would like to begin by acknowledging the immense support of my three supervisors; Prof. Sandra Kentish, Dr. Colin Scholes and Prof. Geoff Stevens.

To my primary supervisor, Prof. Sandra Kentish, firstly thank you for encouraging me to apply for this project when the opportunity arose in 2010. Your encouragement and constant support has allowed me to remain focused and finish this project. Thank you for taking such a keen interest in my work and providing valuable feedback on the papers and thesis. Your accessible nature has always made it easy for me to approach you whenever I needed guidance or support. Your special attentions to ensuring my dietary requirements have been met at conferences and symposiums have been especially heartwarming.

To Dr. Colin Scholes, thank you for all your input into my papers and thesis. Thank you for trying your best to fix the sorption analyzer for my project. I greatly appreciate all your efforts in trying to get me to finish this project in a timely manner.

To Prof. Geoff Stevens, thank you for your valuable input in this project. Your helpful feedback on my papers and thesis are greatly appreciated.

I would like to sincerely thank Dr. George Chen and Dr. Shinji Kanehashi for their continuous support in my work. Thanks George for all your help with modeling and always replying to my emails even when you were no longer at the University of Melbourne. To Shinji, you have always expressed a great interest in my work and have helped me immensely with making sense of my results. Thank you for being so invested in my project and for synthesizing the polyimide polymer used in this work.

This project would not have been possible without the financial support from Brown Coal Innovations Australia (BCIA). Thank you to BCIA for providing the funding for this project as well as giving me the opportunity to be part of the brown coal research community. Thanks to the Cooperative Research Centre for

Greenhouse Gas Technologies (CO2CRC) for providing me the use of their advanced research laboratories and the opportunity to attend various CO2CRC symposiums.

I would like to acknowledge the University of Melbourne, the Department of Chemical and Biomolecular Engineering, the Engineering Workshop and the Polymer Science Group. A very special thank you to Mr. Kevin Smeaton and Mr. Justin Fox for all their help and guidance in building the high temperature mixed gas permeation rig. Thank you to members of the Polymer Science Group; especially Dr. Paul Gurr, Dr. Andri Halim and Mr. Joel Scofield for helping me understand polymer synthesis.

To the great friends I have made in CO2CRC solvents and membranes groups and the Department over the course of my PhD. Your friendship and lively conversations have made my research years very entertaining. I am very grateful for having had the opportunity to work with such great people.

To my parents; Dr. Muhammad Saleemi and Dr. Fauzia Saleemi, thank you for always encouraging me to be the best I can. You both have been a great motivation for me and I would not have achieved what I have without your faith and love. Thank you for giving me the opportunity to study in Australia and for your unconditional support throughout my life. To my sisters; Hinna, Simra and Nimra, coming home to your jovial natures always put a smile on my face. Thanks for all your support, love and encouragement over the course of my PhD. To my friends; Ms. Lara Joachim-Rovira, Ms. Anita Bonnici and Mr. Mohamed Jamal Ed-dine, thanks for always listening to my endless stories about my research and giving me great advice at times.

Last but definitely not least, a very heartfelt thanks to my husband, Saadat. This project will absolutely not have been possible without your continuous support, encouragement and unconditional love. Thank you for believing in me and never losing faith that I will finish it. I feel truly blessed to have had you by my side through this trying experience.

Table of Contents

List of Figures

List of Tables

Nomenclature

A: Effective membrane area (cm^2)

A': Interaction of the vapour molecule and the microvoid

a: Water vapor activity (-)

b: Langmuir affinity constant

C: Sorbed Penetrant concentration (cm^3 (STP)/cm^3 Polymer)

C': Maximum sorption capacity

C_m: Mobile concentration

$\overline{C_p}$: weighted mean value of the sorption capacity of a polymer

D: Fickian Diffusivity (cm^2/s)

D_0: Infinitely dilute Fickian diffusion coefficient (cm^2/s)

E: Activation energy (kJ/mol)

EW: Equivalent Weight (g/mol SO_3H)

f: Fugacity (atm)

f_0: Saturated fugacity of vapour

F: Immobilization Factor

FFV: Fractional Free Volume

FGD: Flue Gas Desulphurisation unit

F_R: Thermodynamic Resistance

G: Cluster Integral

IEC: Ion Exchange Capacity (meq/g)

J: Flux (cm^3 (STP)/cm^2.s)

k_{abs}: rate coefficient of absorption in Equation 2.17

k_{des}: rate coefficient of desorption in Equation 2.17

k_D: Henry's law constant

k': Interaction between vapour molecules and the polymer

l: Active layer thickness (cm)

m: sample weight (g)

MW: Molecular weight (g/mol)

p: Partial pressure (atm)

p_{sat}: Saturated vapour pressure (atm)

P: Permeability (Barrer)

$\bar{P}$: Permeance (GPU)

Q_{per}: Permeate flow rate (cm^3 (STP)/s)

R: Universal gas constant (J/mol.K)

RH: Relative Humidity (%)

S: Solubility (cm3 [STP]/cm3 polymer. atm)

SD: Sulphonation degree (%)

T_g: Glass Transition Temperature (K)

T_{exp}: Experimental Temperature (K)

u: Penetrant velocity (cm/s)

V: Polymer specific volume (cm^3/g)

V_o: Volume occupied by polymeric chains (cm^3/g)

V_w: van der Waals Volume (cm^3/g)

W_i: weight fraction of component i

Wt%: mass uptake (%)

x: Mole fractions in the feed stream

y: Mole fractions in the permeate stream

Greek Letters

α: Selectivity

β: Concentration dependant diffusion parameter [cm^3.polymer/cm^3 [STP])

λ: Water uptake (mol/mol SO_3H)

λ_m: Monolayer sorption capacity

μ: Chemical potential

ρ: bulk density of polymer (g/cm^3)

φ: penetrant volume fraction

Subscripts

1: Downstream/permeate conditions

2: Upstream/feed conditions

A: H_2O

B: CO_2

C: N_2

D: Henry's Law component

H: Langmuir component

i: component *i*

j: component *j*

p: Permeation

P: Polymer

V: Microvoid region

X: Polymer matrix region

Chapter 1 Introduction

The growing world population has resulted in global energy consumption being at an all time high. In response, fuel consumption has also increased with a projected increase of 30% in coal consumption alone over the next 20 years [1]. In 2012, Australia was reported as the 3rd major coal producer with a global coal production of 6.3% after China (47.5%) and United States (13.9%) [2]. Large quantities of high-quality black coal are situated all over Australia, with New South Wales and Queensland containing 42% and 53% of the Australian black coal resources. Similarly, brown coal reserves are located in all states however 96% of this is found in Victoria [3].

Water security is a major issue in many parts of the world and industrial processes use large amounts, including the coal industry with ~2.4 t/MWh of cooling water usage alone [4]. Importantly, coal – fired power plants produce large amounts of wet flue gases containing CO_2, N_2, O_2, nitrogen oxides (NO_x), sulphur dioxides (SO_2) and fly ash. The composition and water content of the flue gas depends on a number of factors, including the coal grade. For example, black coal has a low moisture content compared to brown coal, which contains anywhere up to 48 – 70% moisture [5]. Hence, there is potential to recover water from brown coal flue gases and recycle this back into the process as boiler feed water or cooling water, as long as it is the necessary purity.

Water vapour has been recovered from flue gases using various technologies, including desiccant drying systems and condensers [6]. However, desiccant systems are expensive and condensers generate low quality water with impurities that is not suitable for reuse. The desiccant drying systems have an additional disadvantage of being energy – intensive as they require energy to regenerate the desiccant. Membrane technology is a superior alternative to these conventional technologies due to its smaller footprint, easy operation and low energy requirements [7]. Until recently, research into membranes for flue gas separation applications has mostly focused on the removal of CO_2 for carbon capture and storage purposes [7-13]. However, recent aims to improve energy efficiency and

preserve fresh water resources have led to an additional focus into the recovery of water vapour from flue gases [6, 14].

A schematic of a conventional coal – fired power plant is shown in Figure 1.1. Coal is burned in a furnace – boiler, the energy from which heats the incoming water to steam. This steam operates the turbine which in turn generates electricity via the generator (G). The steam is then cooled and recycled back to the boiler. The flue gases from the furnace – boiler are conventionally sent to a flue gas desulphurisation (FGD) unit which removes SO_x (SO_2, SO_3 and SO_4) after removal of fly ash in electrostatic precipitators. This unit considerably lowers the temperature of the flue gases from 200 – 250 °C to approximately 50 °C. Due to the presence of CO_2 and water, sending the cool flue gases to the exhaust stack would lead to water vapour condensation and thus corrosion. To prevent this, flue gas is reheated to increase the temperature to approximately 60 – 80 °C which adds to the energy costs [6, 15]. This conventional process is most commonly used by countries that have strict restrictions on the amount of SO_x that can be released into the environment.

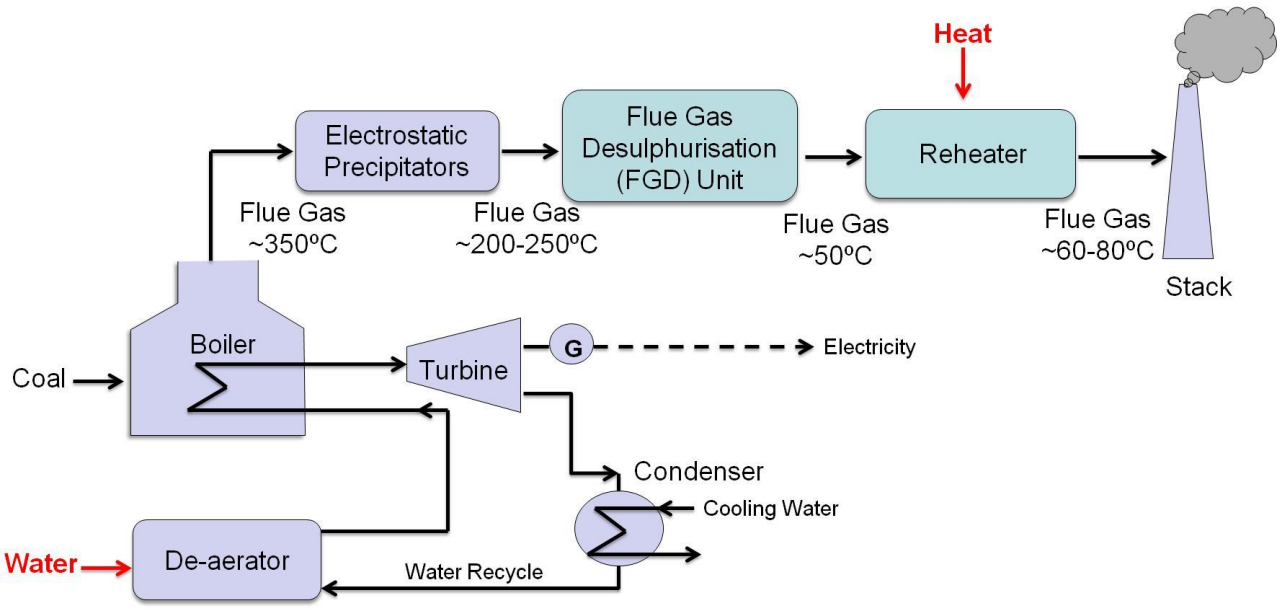

Figure 1.1: Schematic diagram of a coal-fired power plant with a reheater unit to prevent condensation of flue gas water vapour (Reproduced from [6]).

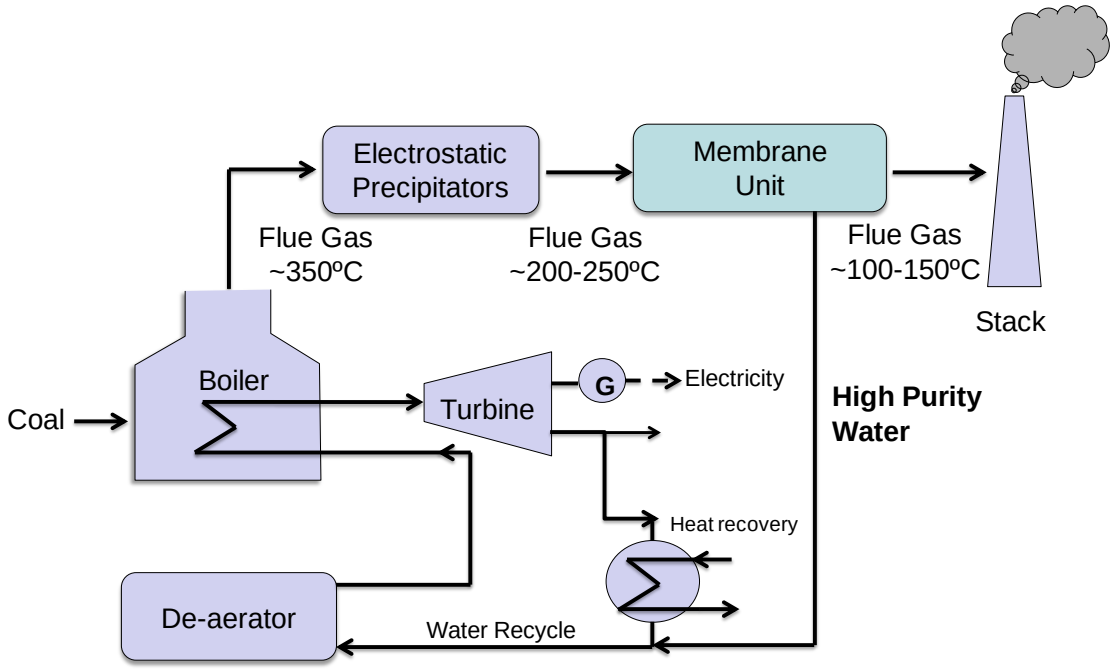

Figure 1.2: Schematic diagram of a coal-fired power plant with a membrane unit to recover and recycle water vapour (Adapted from [6]).

In many cases, particularly in Australia and in other countries, such as China, there is no FGD unit and the SO_2 emissions are dispersed via the stack. In those cases, the flue gases are emitted at a high temperature [16] as shown in Figure 1.2. The higher water vapour pressures at these temperatures means that these flue gases will have a high volume of water vapour.

Water recovered from these flue gas streams may be recycled and reused in the process as boiler feed or cooling tower make up water, preserving fresh water resources. However, for this purpose, the water recovered needs to be of a high purity. In particular, the presence of significant levels of CO_2, SO_x and NO_x in the recovered water will make it acidic and could cause corrosion issues.

Research into flue gas dehydration via membranes is quite recent and very few studies have been conducted so far that have explicitly considered water – selective membranes for this particular application [6, 14]. Most work looks at water permeable membranes in the context of fuel cells [17-26]. While the results obtained from these studies give an insight into the types of membranes that are water – selective, work specific to flue gases needs to be undertaken to gain a

comprehensive understanding of how the membranes behave under these conditions.

Gas separation membranes are essentially thin barriers that selectively permeate one or more gaseous components. This differential transport is driven by the concentration difference within and across the membrane [27]. This is individually attributed to the sorption and diffusion properties of the membrane. In comparison with conventional separation methods such as cryogenic distillation, solvent absorption and adsorption; membrane separation is a simple process with no moving parts. As long as a driving force exists across the membrane, separation of gases will occur continuously. Other advantages include low maintenance and labor costs, low space requirements, easy scale up and operation flexibility due to the modular design of the unit and low environmental impact [27]. However, regardless of these advantages membrane separation does experience issues similar to more conventional methods. One example is that membranes are fouled easily due to the presence of a wide range of minor compounds and fly ash in flue gases, especially at high temperatures [15].

Membranes are characterized by two properties; the permeability (P) (or pressure independent flux) of gases through the material and the selectivity (α), which is the ratio of one gas permeability relative to another. Conventionally, there exists a trade – off between selectivity and permeability were efforts to improve one usually results in a decrease of the other [15, 27, 28]. Despite these shortcomings, gas separation membranes have replaced conventional separation methods for a variety of applications shown in Table 1.1.

Table 1.1: Gas Separation Membrane Application [27, 29, 30].

Common Gas Separation	Application	Suppliers
O_2/N_2	Oxygen enrichment, inert gas separation	Permea (Air products), Cynara, Separex
$H_2/Hydrocarbons$	Refinery hydrogen recovery	Prism by Permea
H_2/N_2	Ammonia purge gas	Permea
H_2/CO	Syngas ratio adjustment	Separex, Permea
$CO_2/Hydrocarbons$	Acid gas treatment, landfill gas upgrading	Cynara, Separex, Permea
$H_2O/Hydrocarbons$	Natural gas dehydration	Cynara, Separex, Permea
$H_2S/Hydrocarbons$	Sour gas treating	Cynara, Separex, Permea
$He/Hydrocarbons$	Helium separation	Cynara, Separex, Permea
He/N_2	Helium Recovery	Cynara, Separex, Permea
$Hydrocarbons/Air$	Hydrocarbons recovery, pollution control	Membrane Technology and Research, Aluminium Rheinfelden/GKSS, NKK
H_2O/Air	Air dehumidification	Permea, Ube Industries, Perma Pure

The inherent ability of membranes to separate mixtures was known as early as the 19th century. In 1866, Graham used natural rubber membranes to produce oxygen – enriched air. Weller and Steiner did research on separation of oxygen from air and helium from natural gas in 1950 [13]. This work highlighted the industrial relevance of membranes; however the limited selectivity and membrane production as well as the large surface areas required deemed this process unfeasible at the time [13, 27, 28]. Research on membranes continued during the following years with major developments including Monsanto Prism membranes for hydrogen separation and Cynara and Separex systems for CO_2 separation from natural gas. Significant improvements in the design of kidney dialysis occurred during the 1940s and 50s [13]. In 1980s, it was a German company, GFT that

introduced pervaporation systems for alcohol dehydration [7]. Later work, most of which still continues to this day, includes research into novel membrane materials, improvement of existing membrane development processes, membrane configurations and its various applications [8, 27].

The most common type of membranes used for gas separation are polymeric in nature. These polymeric membranes can be divided into two classes; glassy or rubbery, depending upon the temperature at which they are used. Glassy polymers are tough, rigid polymers that operate below the glass transition temperature (T_g). Due to the rigid state of these polymers, they generally possess excellent selectivity [13, 31]. Hence, glassy membranes will be the main focus of this research as the proposed application requires membranes that specifically have high water selectivity.

This thesis aims to investigate permeation properties of candidate polymeric membranes for the recovery of high purity water from high temperature brown coal flue gases for reuse as boiler or cooling tower makeup feed. A novel steam permeation apparatus is developed for investigating the permeabilities of water and gases through polymeric membranes at high temperatures (70 – 150 °C) and pressures (1 – 5 bar). The effect of temperature on water, CO_2 and N_2 permeation and sorption properties of polymeric membranes is investigated. The change in H_2O/CO_2 and H_2O/N_2 selectivity at 150 °C for these membranes is then used to model membrane areas and the purity of the recovered stream to determine their suitability for the proposed application.

Chapter 2 Literature Review

2.1 Introduction

This chapter provides a critical literature review of research done in areas of vapour/gas separation and particularly any work done for flue gas dehydration applications. It reviews a list of potential candidate membranes and based on literature offers three membranes which will be investigated for high temperature flue gas dehydration. The basic chemistry of these dense membranes is introduced and common sorption and transport phenomena detailed.

To understand the effect of water vapour on other gases, water vapour sorption, transport and permeation characteristics are discussed. Plasticization, competitive sorption and the clustering behaviour of water vapour are reviewed. Moreover, the mathematical models developed to date in literature to characterise the sorption, transport and permeation behaviour of water in multi – component systems are summarised.

2.2 Polymeric Membranes

Membranes are essentially thin barriers that allow certain components to permeate through at a higher flux than other components (Figure 2.1). This selective behaviour results in the formation of two streams; a preferred component – rich stream (permeate) and a rejected component – rich stream (retentate).

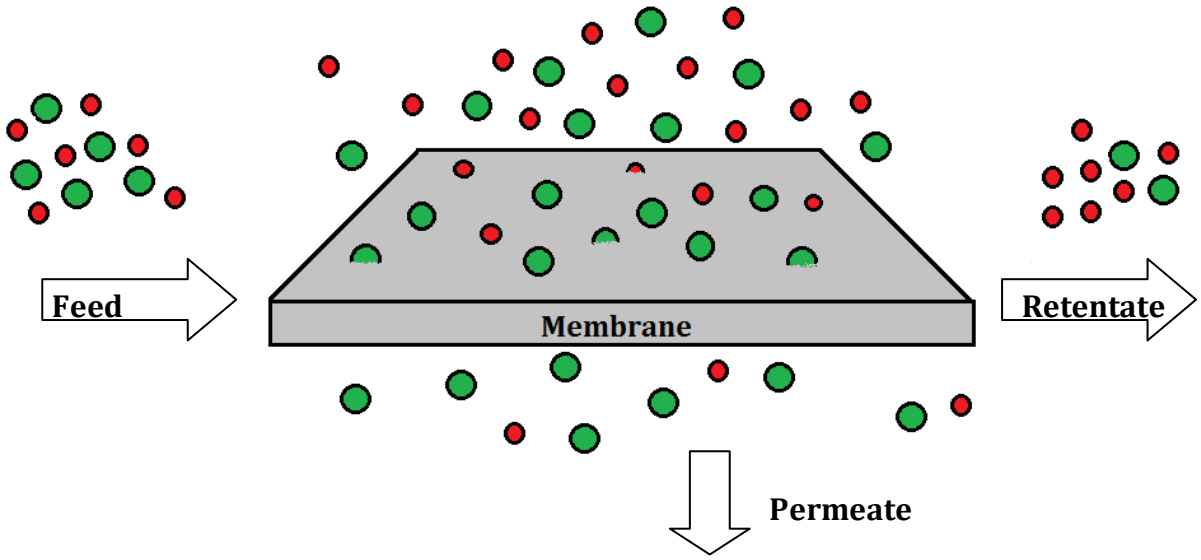

Figure 2.1: Schematic diagram for membrane based separation process

Separation membranes can be fabricated from either inorganic or organic materials. This thesis will focus on the more common organic polymeric membranes. Polymeric membranes can be further divided into two groups; porous and non – porous [7, 32]. Porous membranes consist of large interconnected voids or pores. They are well established for filtration processes like ultra, micro and nanofiltration where separation occurs based on molecule sizes of 1 nm to 10 μm. Conversely, non – porous membranes are commonly used for separation applications where the molecules size is < 1 nm. This is most commonly the case for gas/vapour separation applications. As the name suggests, these types of membranes lack any pores. Rather, the imperfect packing of the polymeric chains and their restricted movement results in free volume in the membrane. Separation in these membranes is based on the molecular interaction between the polymeric membrane and the diffusing gas species.

Polymeric membranes are often divided into glassy and rubbery polymers. A glassy polymer operates at temperatures below the glass transition temperature (T_g) [33]. Polymer dynamic motion is slow; therefore the microscopic polymer morphology never obtains an equilibrium state. This results in the formation of microvoids in the glassy polymeric matrix (Figure 2.2). As the temperature of the glassy polymer is increased to a point above T_g, the dynamic motion of the polymer chains are more fluid – like and the polymer morphology achieves an equilibrium state. Hence, as a result polymer segment rotation can occur and an elastic rubbery polymer is formed. The mobility of the polymeric chains allows components to permeate easily resulting in a high diffusion coefficient due to increased fractional free volume [7, 34].

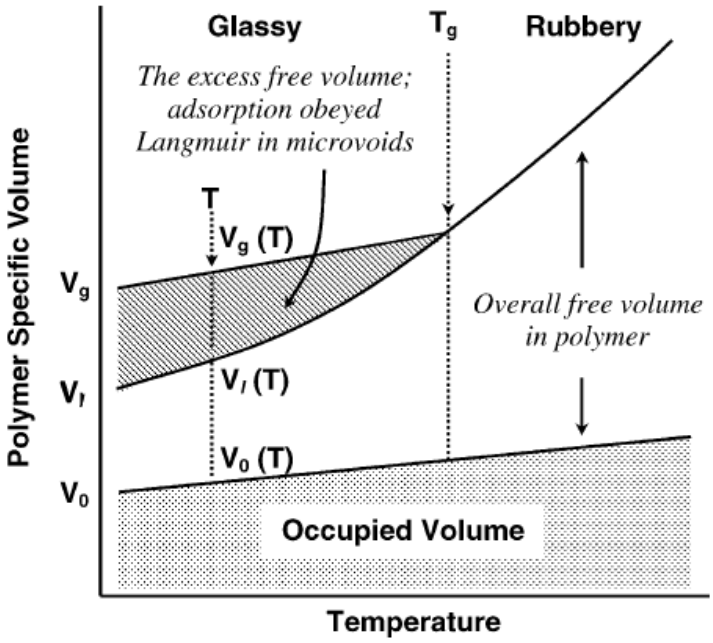

Figure 2.2: The effect of temperature on polymer specific volume for glassy and rubbery polymers. (Reproduced from [35]).

In glassy polymers, the total polymer specific volume (V) is the sum of the volume occupied by the polymeric chains in the polymeric matrix and the free volume in the microvoids. It is the reciprocal of the bulk density (ρ) and is given by:

$$V = \frac{1}{\rho} \qquad 2.1$$

From Figure 2.2, fractional free volume (FFV) is the space unoccupied by the polymer chains due to conformational constraints (bond angles, steric bulk etc) that can be occupied by gas molecules [36]. It is a fraction of the free volume in the polymer defined by subtracting the occupied volume (V_0) from the polymer specific volume (V):

$$\boldsymbol{FFV = \frac{V - V_o}{V}} \qquad \textbf{2.2}$$

The volume occupied by the polymeric chains can be predicted by using the van der Waals volume (V_w) estimate of the repeating polymer unit through a group contribution method, commonly known as Bondi's Method [37]. The van der Waals volume (V_w) is estimated based on the average atomic volume and therefore is a function of variables such as intermolecular forces, types of bonding and even quantum mechanical factors [38]. Bondi's Method also proposes that the occupied volume (V_0) is related to the van der Waals volume (V_w) by:

$$\boldsymbol{V_o = 1.3 V_w} \qquad \textbf{2.3}$$

Bondi [37] derived the factor 1.3 based on the packing densities of the molecular crystals at absolute zero. This assumption is applied to all structures and types of functional groups.

A rubbery polymer has a higher FFV and consequently a high permeability but low selectivity. Glassy polymers on the other hand have a more defined structure that hinders molecule movement by increasing tortuosity and reduces diffusion of larger species. They are inherently more shape and size selective, hence they have significantly lower permeability but higher selectivity compared to rubbery polymers [39, 40]. A possible approach to achieving reasonable permeability and selectivity is through formation of copolymers. These are designed to contain two different segments; a hard rigid segment that improves polymer selectivity and a soft flexible amorphous segment that ensures good permeability [41, 42]. PEBAX is a good example of a copolymer combining rubbery Polyethylene Oxide (PEO) with a glassy polyamide [14]. The current research requires membranes that specifically have high water selectivity; therefore glassy membranes will be the main focus of this research.

It should be noted that penetrant sorption is known to reduce the glass transition temperature of a polymer by plasticizing the membrane [43-45]. This change in glass transition temperature can be estimated using the Fox Equation, which is valid for homogeneous blend systems [46]:

$$\frac{1}{T_g} = \frac{W_p}{T_{g,p}} + \frac{W_a}{T_{g,a}} \qquad 2.4$$

Where T_g is the theoretical glass transition temperature of the polymer – penetrant mixture in K. $T_{g,p}$ [K] and $T_{g,a}$ [K] are the glass transition temperatures of pure polymer and penetrant a, respectively and W_p [-] and W_a [-] are the weight fractions of the polymer and the penetrant a, respectively.

2.3 Gas Transport Mechanism

Knudsen diffusion, molecular-sieve effect, capillary condensation, surface diffusion and solution-diffusion mechanism are the main processes by which gas transport occurs through membranes [7, 27, 36, 47]. The first four transport mechanisms are specific to porous membranes whereas solution – diffusion is most common in dense non – porous membranes. These processes are shown in Figure 2.3. Membranes considered in this research are dense non – porous membranes hence solution – diffusion is the main transport mechanism.

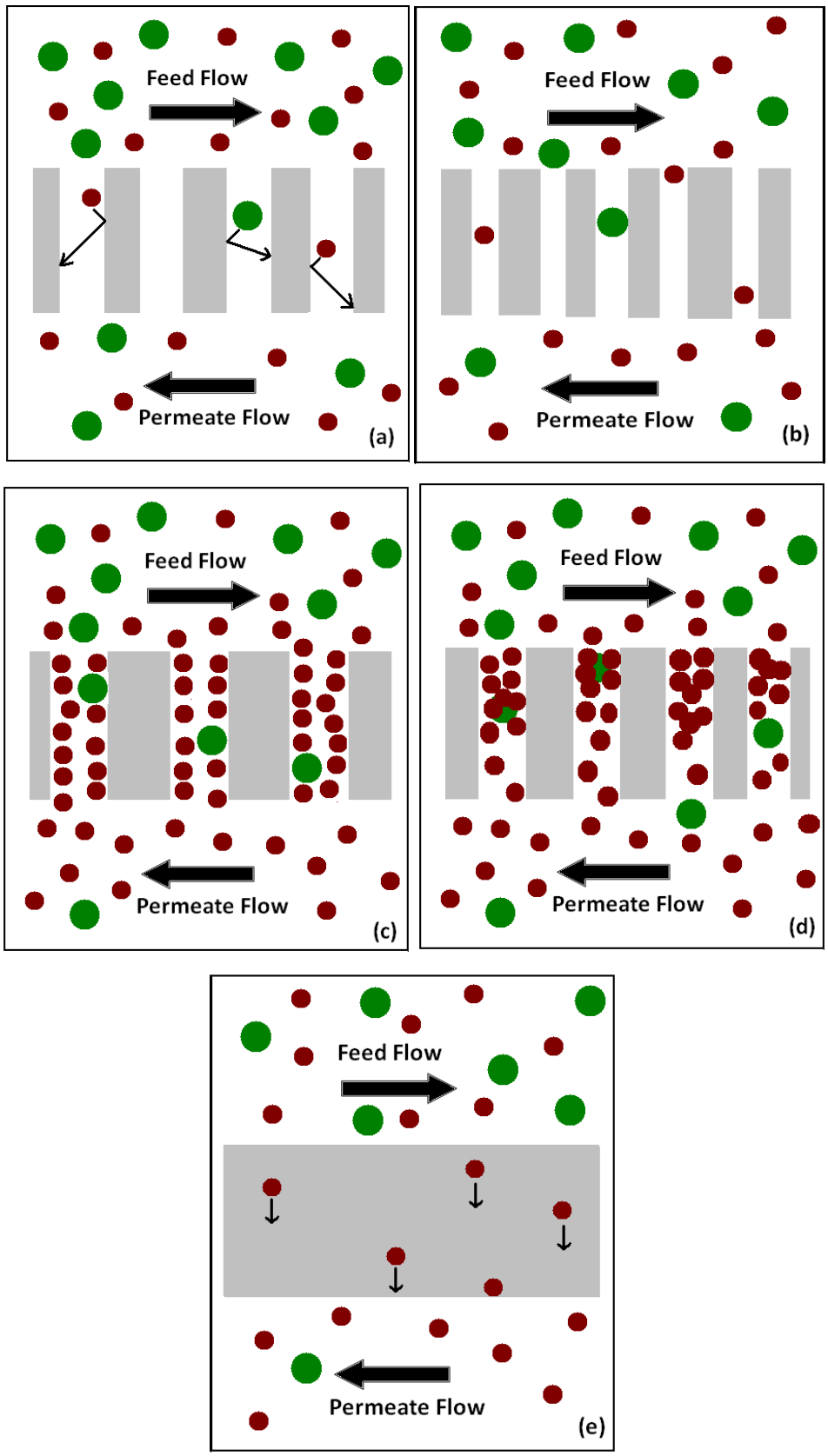

Figure 2.3: (a) Knudsen Diffusion (b) Molecular – Sieving (c) Surface Diffusion (d) Capillary Condensation (e) Solution – Diffusion Mechanism (Reproduced from [48]).

2.3.1 *Porous Membranes Transport Mechanisms*

2.3.1.1 Knudsen Diffusion

Kinetic diameter is a reflection of the smallest effective dimension of a given molecule while mean free path is the average distance between collisions of a gas molecule with other molecules. Knudsen diffusion occurs for membranes that have pore diameters slightly larger than the penetrant's kinetic diameter but smaller than its mean free path (Figure 2.3a). Hence, the diffusing molecules have more collisions with the walls of the pores compared to other molecules and move independently of each other. The permeability of a gas through the membrane is proportional to the inverse square root of its molecular weight. Hence, the selectivity of the membrane is based on the square root of the ratio of the molecular weights where subscripts denote the different permeate species.

$$\alpha_{i/j} = \sqrt{\frac{MW_i}{MW_j}} \qquad 2.5$$

This mechanism is used to describe the transport behaviour for porous inorganic and carbon membranes. It is also often observed if a non – porous membrane is defective with larger pores or holes present.

2.3.1.2 Molecular-Sieving

In this instance, membranes have pores with diameters that are in between the gas diameters to be separated. Hence, gas molecules are separated based on their size with smaller molecules diffusing through the membranes via pores while the larger molecules are blocked (Figure 2.3b).

2.3.1.3 Surface Diffusion

With this mechanism the gas molecules selectively absorb to pore walls, especially if they are condensable, and migrate along the surface (Figure 2.3c). An increase in the condensability of a gas increases the amount of surface adsorption and enhances the contribution of surface diffusion to gas permeation [7]. Furthermore, the permeability of the non – condensable gas is reduced due to the decrease in the effective pore diameter caused by adsorbed component [29].

2.3.1.4 Capillary Condensation

This is similar to surface diffusion where gas molecules adsorb to the pore walls. Interactions between these molecules result in the formation of multilayers where if the pressure conditions are close to the partial pressure of the gas in small pores, condensation will occur [49]. Hence, pores are completely filled by the condensable component and the permeability of the non – condensable component is low (Figure 2.3d) [29].

2.3.2 *Solution – Diffusion Mechanism*

This is a three stage gas transport mechanism proposed by Thomas Graham more than a century ago [36]. As mentioned previously, it is most commonly applied in dense, non – porous membranes. In this case, the gas molecules dissolve into the membrane material and diffuse across it. They are then released on the permeate side (Figure 2.3e). The diffusion across the membrane is based on a concentration difference across the two faces of the membrane. The separation of gases is achieved because of the different solubilities and diffusivities of the molecules [7, 27, 36]. This dependence on both the solubility and diffusivity allows more flexibility for refining membrane permeation properties. This solubility selective mechanism cannot be achieved in a Knudsen diffusion or molecular sieving process. This solubility based separation is the key for rubbery membranes that achieve separation of higher hydrocarbons from small penetrant molecules such as nitrogen or hydrogen. For rubbery polymers, the permeability (P) of a gaseous component is a product of the solubility (S) and the diffusivity (D) of that component. The selectivity is therefore given by:

$$\alpha_{i/j} = \frac{S_i.D_i}{S_j.D_j} \qquad 2.6$$

Conversely, glassy polymeric membranes often achieve separation of penetrating components though differences in the penetrant's kinetic diameter [50]. The presence of free volume or gaps within glassy polymers allows for penetrating species to diffuse through the polymer by "jumping" from one gap to another. Hence, the selectivity of a glassy polymer can be controlled by controlling the size as well as size distribution of the free volume [51]. This diffusion based selectivity

is often used to separate light vapour/gases from larger molecules (e.g. CO_2 from N_2 and CH_4, and H_2 purification) [52].

Table 2.1: Kinetic Diameter and Molecular Weight of gas molecules commonly encountered in gas separation applications [48]

Gas Molecule	Kinetic Diameter, [Å]	Molecular Weight, (MW) [g/mol]
H_2O	2.65	18
H_2	2.89	2
CO_2	3.30	44
O_2	3.46	32
N_2	3.64	28
CH_4	3.80	16

2.4 Penetrant Sorption and Transport

The performance of a membrane is judged by the diffusivity and selectivity of the penetrating species. Both of these characteristics are ultimately dependent on the membrane's intrinsic properties.

Permeability (P) is dependent on the flux of the penetrating species through the membrane. It is related to the steady state flux, the chemical potential/pressure driving force, and the active layer thickness (l). If the active layer thickness cannot be easily defined, as is the case for inorganic and composite/asymmetric membranes or for membranes that swell, permeance may be used. Consequently, permeance ($\bar{P}$) is independent of the active layer thickness and can be related to P by:

$$\bar{P} = \frac{P}{l} \qquad 2.7$$

Where, P is permeability in Barrer (10^{-10} cm^3 (STP)cm/cm^2.s.cmHg), l is the active layer thickness (cm) and $\bar{P}$ is the permeance in GPU (10^{-6} cm^3 (STP)/cm^2.s.cmHg).

The flux (J) of the penetrant through the membrane is defined as the product of the concentration of the sorbed species in the polymer (C), and the penetrant velocity through the membrane (u). Thermodynamically, the transport of a penetrant is driven by the chemical potential gradient across the membrane ($\partial\mu/\partial z$) against the thermodynamic resistance exhibited by the membrane (F_R) [13].

$$\boldsymbol{J = C.u = -\frac{C}{F_R}.\frac{\partial \mu}{\partial z}} \qquad \textbf{2.8}$$

Chemical potential can be defined in terms of fugacity, f:

$$\boldsymbol{\mu = \mu^o + R.T.\ln(f)} \qquad \textbf{2.9}$$

Substituting this into Equation 2.8, gives flux in terms of fugacity [13]:

$$\boldsymbol{J = C.u = -\frac{C}{f}.\frac{RT}{F_R}\frac{\partial f}{\partial z}} \qquad \textbf{2.10}$$

Solubility (S) is defined as the concentration of penetrant sorbed in polymer divided by the fugacity in gaseous phase ($S = C/f$). The thermodynamic diffusion coefficient (D) of a penetrant is defined as ($D = RT/F_R$). Substituting these definitions of solubility and diffusivity into equation 2.10 gives an expression of flux:

$$\boldsymbol{J = -D.S.\frac{\partial f}{\partial z}} \qquad \textbf{2.11}$$

Since permeability is a measure of flux, it is often defined as the product of thermodynamic diffusivity and penetrant solubility (Equation 2.12) which will be discussed further in the following sections.

$$\boldsymbol{P = D.S} \qquad \textbf{2.12}$$

Ideal selectivity (α) of a membrane material for components i and j is defined as the ratio of the permeability of the two components (Equation 2.13) whereas the real selectivity (α^*) is the ratio of the mole fractions of the gases i and j in feed (x) and permeate (y) streams (Equation 2.14).

$$\boldsymbol{\alpha_{i/j} = \frac{P_i}{P_j}} \qquad \textbf{2.13}$$

$$\boldsymbol{\alpha_{i/j}{}^* = \frac{y_i/x_i}{y_j/x_j}} \qquad \textbf{2.14}$$

For real gas mixtures, the fugacity of individual gases on the feed and permeate side must be taken into account but it is more common to quote the ideal selectivity.

2.5 Solubility

2.5.1 *Gas Sorption*

A Dual Mode Sorption Model (DMS) is often used to describe gas sorption in glassy polymer. Glassy polymeric membranes consist of two specific regions: a polymeric matrix known as the Henry's Law Region and the microscopic voids created when the polymeric chains pack imperfectly known as the Langmuir Adsorption Region (as described previously in Figure 2.2). Gas molecules are assumed to directly dissolve into the polymeric matrix and adsorb on the walls of microscopic voids. A Dual Mode Sorption Model takes into account concentration of the sorbed species in both these regions [53-55].

Sorption in the Henry's Region follows Henry's law and is linearly proportional to the solubility of a gas and the applied pressure. This relationship has been found to adequately describe the concentration of gases in rubbery polymers at low concentrations [56]. Hence, the sorption of gases in Henry's Law Region is given by:

$$C_D = k_D f \qquad 2.15$$

Where C_D is the concentration in the Henry's law region, k_D is the Henry's constant and f is the fugacity. This linear relationship is shown clearly in Figure 2.4 by the Henry's Law Sorption curve.

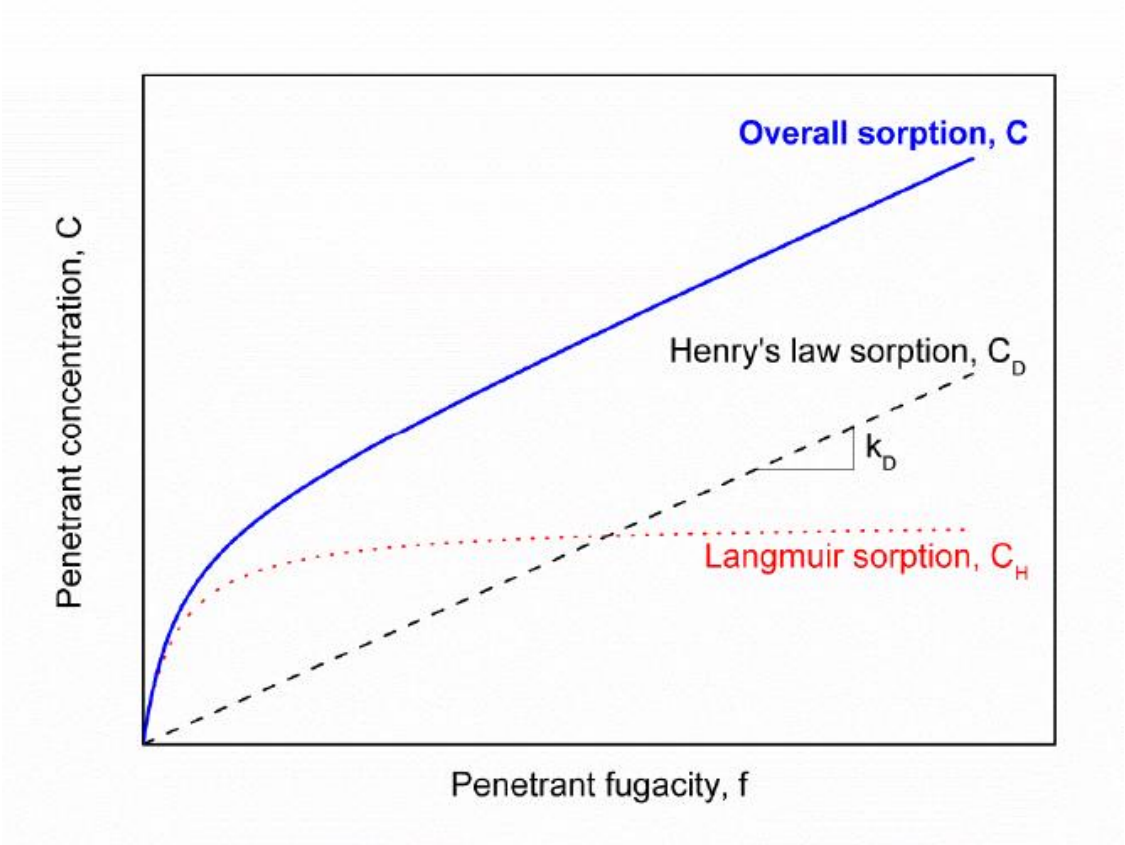

Figure 2.4: A sorption isotherm for penetrant gas sorption in glassy polymers [35].

The sorption of penetrant in the microvoids of the polymer is described by the standard Langmuir adsorption relationship:

$$C_H = \frac{C'_H.b.f}{1+bf} \qquad 2.16$$

Where C_H is the concentration of penetrant gas in the microvoids, C'_H is the maximum adsorption capacity and b is the Langmuir affinity constant which is dependent on the rate coefficients of adsorption and desorption by:

$$b = \frac{k_{abs}}{k_{des}} \qquad 2.17$$

Langmuir sorption shows a rapid increase at low fugacities as the penetrant molecules fill the free volume within the polymer but reaches a plateau soon after (Figure 2.4).

Hence, the overall penetrant sorption described by the DMS model is the addition of the sorption in Henry's Region and the Langmuir Region.

$$C = C_D + C_H = k_D.f + \frac{C'_H.b.f}{1+bf} \qquad 2.18$$

It is strongly influenced by Langmuir sorption at low fugacities where it is concave to the axis and follows Henry's sorption and increases linearly as fugacity increases (Figure 2.4).

2.5.2 *Clustering*

In hydrophobic or weakly hydrophilic polymers, polar species such as water may interact preferentially with each other resulting in the formation of clusters [57, 58]. Nguyen *et al.* [59] and Favre *et al.* [60, 61] observed similar clustering behaviour of alcohol in hydrophobic Poly (dimethylsiloxane) (PDMS) membranes. The isotherms of these types cannot be modelled by simple Flory – Huggins model or Dual Mode Sorption Models. An Engaged Species Induced Clustering (ENSIC) model has been developed to take into account the affinity of the solvent to either a polymer segment or a solvent molecule already sorbed into the polymer matrix [62-65]. These sorbed solvent molecules undergo self hydrogen bonding and diffuse through the polymeric matrix as a cluster unit rather than a single molecule. Hence, these clusters are larger in size compared to a single molecule but are not large enough to possess the properties of bulk liquid water or alcohols [65]. For water, these clusters can obstruct the pathways in the polymeric matrix and hinder the diffusion of other gaseous species. Furthermore, these clusters diffuse slower than individual water molecules and result in a reduction of water diffusivity [42, 58, 65].

Zimm and Lundberg [66] proposed a relation to quantify the clustering tendency of molecules in a two component system. At low activities, the interactions between individual molecules are smaller than those between these molecules and the polymer. However, as the penetrant concentration increases, the increased interactions between molecules cause them to aggregate together and form clusters [54, 65-67].

The Zimm and Lundberg clustering function may be used to study the extent to which the diffusion of a species through the membrane is influenced by clustering [14, 45, 68].

$$\frac{G}{V_i} = (1 - \varphi)\left[\frac{\partial(a/\varphi)}{\partial a}\right] - 1 \qquad 2.19$$

Where a is the penetrant vapour activity, φ is the penetrant volume fraction in the polymer as determined from the equilibrium sorption isotherms, V_i is the molar volume of the penetrant (cm^3/mol) and G is the cluster integral [14].

- If $G/V_w < -1$: the molecules in the solution are isolated from each other in solution, i.e. penetrant molecules are distributed in the matrix and excess coordination of these molecules by surrounding molecules does not occur.
- If $G/V_w > -1$: the forces between the penetrant molecules are significant enough for them to accumulate and form clusters.

2.5.3 *Vapour Sorption*

The DMS model described previously (Section 2.5.1) sufficiently describes the sorption of most gases in glassy polymers. However, for species such as water with high condensability and hydrogen bonding affinity, sorption isotherms of varying shapes are observed as shown in Figure 2.5 in both glassy and rubbery polymers, where C is the concentration and a is the penetrant vapour activity in the polymer [69-74].

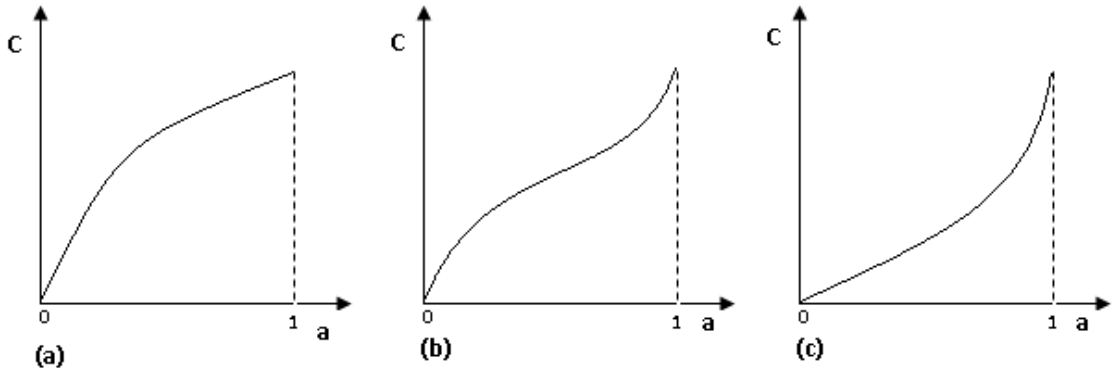

Figure 2.5: Vapour sorption isotherms in glassy polymers.

The conventional DMS model can only adequately describe the sorption isotherm depicted in Figure 2.5a. The sorption isotherm in Figure 2.5b is sigmoidal in shape with an inflection point. These are modelled by a multilayer adsorption model such as the Brunauer – Emmett – Teller (BET) equation which is applicable for penetrant activities up to 0.35 – 0.4, or its modified form, the Guggenheim – Anderson – de Boer (GAB) equation which is valid for experimental data at

activities up to 0.8 – 0.9 [72, 75]. The sorption isotherms of type (c) in Figure 2.5 are convex to the activity axis and often exhibited by highly condensable species like hydrocarbon or water. These species undergo clustering as mentioned in Section 2.5.2 and are well characterized by the Engaged species induced clustering (ENSIC) model [62, 76].

While the models mentioned above are effective, it is difficult to compare intrinsic sorption properties in different glassy polymers. Recently, a new modified Dual Mode Sorption model has been proposed which can effectively describe vapour sorption for all three vapour sorption types [72, 75]. It is based on the GAB Model described above but with the following four assumptions:

- Vapour sorption in glassy polymers occurs in two regions; the Henry's Law region/polymeric matrix and the Langmuir Region/ microvoids.
- All the molecules in the polymer matrix region undergo the same sorption mechanism.
- First layer sorption of vapour molecules in the Langmuir region occurs through GAB sorption.
- Vapour sorption in the subsequent layers of the Langmuir region undergoes the same sorption mechanism as that in the Henry's Law region.

This modified Dual Mode Sorption model is given by the equation 2.21:

$$\boldsymbol{C_A = C_{XA} + C_{VA}} \qquad \textbf{2.20}$$

$$\boldsymbol{C_A = \frac{\overline{C_p} k' \frac{f_A}{f_o}}{1 - k' \frac{f_A}{f_o}} + \frac{\overline{C_p}(A' - 1) k' \frac{f_A}{f_o}}{1 + (A' - 1) k' \frac{f_A}{f_o}}} \qquad \textbf{2.21}$$

Where, C_{XA} and C_{VA} are concentrations of penetrant A in the Henry's Law region and the Langmuir region, respectively, $\overline{C_p}$ is the weighted mean value of the sorption capacity of a polymer to a vapour, k' indicates the interaction between the vapour molecule and the polymer molecule segment, and A' is a measure of the interaction of the vapour molecule and the microvoid. $A' = 1$ for a rubbery polymer. Comparing this model (Equation 2.20 and 2.21) to the traditional DMS model (Equation 2.18), the vapour concentration in the microvoids can be re-arranged to:

$$C_{VA} = \frac{C'_H.b.f}{1+bf} = \frac{\overline{C_p}(A'-1)k'\frac{f_A}{f_o}}{1+(A'-1)k'\frac{f_A}{f_o}} \quad 2.22$$

Where the microvoid affinity constant (equivalent to the Langmuir affinity constant) for the vapour is:

$$b_A = \frac{(A'-1)k'}{f_o} \quad 2.23$$

A significant advantage of this approach is that it can successfully characterise vapour sorption of all three types with just three adjustable parameters ($\overline{C_p}$, k' and A').

Because of the separation of the penetrant sorption into the polymeric matrix and the microvoids region, competitive sorption effects in a multi – component system can be readily incorporated into this model [50].

2.5.4 *Competitive sorption in a multi-component system*

The Langmuir affinity constant of a gaseous component is a function of the critical temperature of the gas as shown in Figure 2.6. Critical temperatures of some components commonly encountered in gas separation applications are presented in Table 2.2. As shown, water has a high critical temperature compared to other gases. This means that water will adsorb more readily in the polymer free volume and consequently a higher Langmuir affinity constant is observed in Figure 2.6. Due to this high critical temperature and affinity constant, even small amounts of water compete very strongly with other penetrants for adsorption sites in the Langmuir voids of the polymer, reducing the solubility of these other species [77, 78] and consequently retarding the permeabilities of other components [77, 79, 80]. Pye *et al.* [79] found that the permeabilities of H_2 and CH_4 were severely depressed by the presence of water vapour. Chern *et al.* [77] studied the decrease in CO_2 permeability for Kapton film in the presence of water. They summarised that this decrease was due to two reasons; one being the competitive sorption of water in Langmuir sites resulting in reduced penetrant solubility and secondly, the diffusion of the gas molecules being hindered by water molecules. Sorption and transport of water vapour in various polyimides (e.g. BPDA-ODA/DABA, BPDA - DDBT, 6FDA-MPD and 6FDA-TMPD) were studied by Okamoto *et al.* [81], Lokhandwala *et al.*[82] and Sato *et al.* [83] and similar results were obtained

where water diffusivities increased with increasing vapour activities while gas diffusivities decreased.

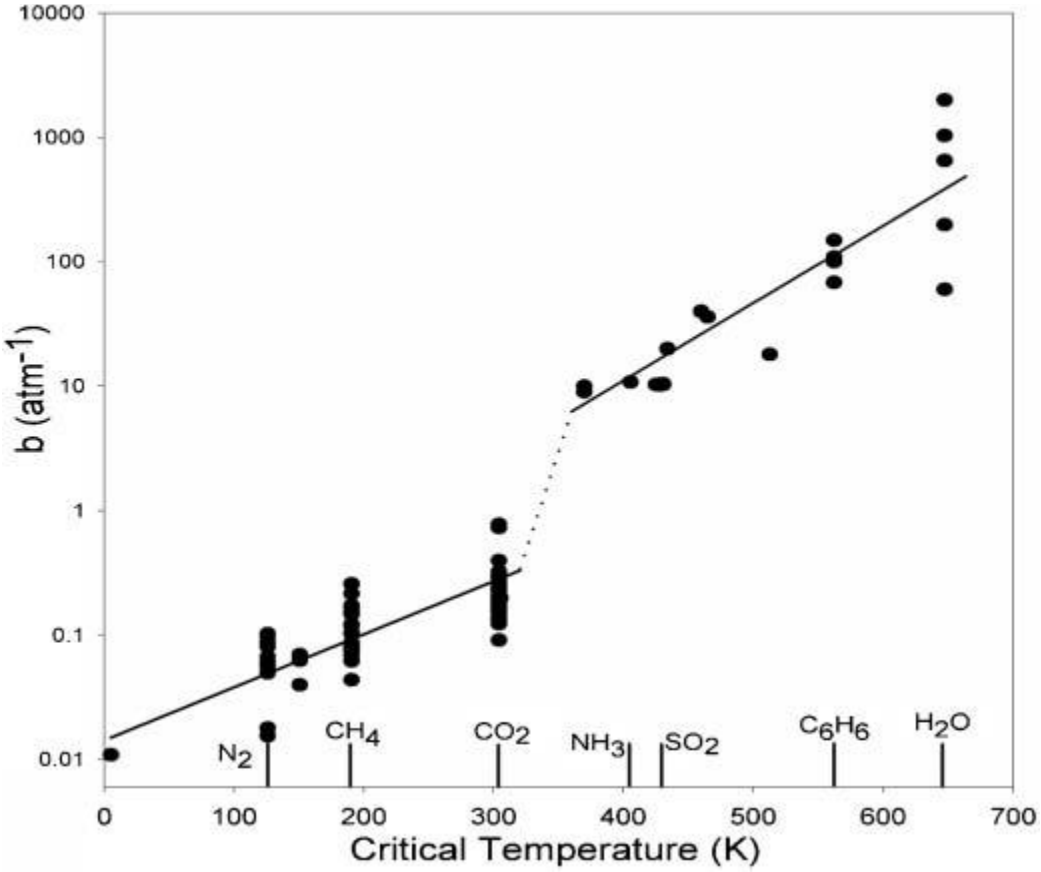

Figure 2.6: Langmuir affinity constant for a range of gases as a function of gas critical temperature in various polymers [48].

Table 2.2: Critical Temperature of various molecules encountered commonly in gas separation applications (Reproduced from [48]).

Gas Molecule	Critical Temperature [K]
H_2O	647.3
CO_2	304.2
CH_4	190.6
O_2	154.6
N_2	126.2
H_2	33.2

Koros *et al.* [84, 85] accounted for the competitive sorption effects by extending the dual mode sorption model. This model is based on the assumption that the competitive sorption between penetrants only occurs for the Langmuir/microvoid regions and the Henry's law component of the model behaves ideally. Hence, the concentration of gas B in the presence of other gases is given by:

$$C_B = C_{DB} + C_{HB} = k_{DB} f_B + \frac{C'_{HB} b_B f_B}{1 + b_A f_A + b_B f_B + b_C f_C \ldots} \qquad 2.24$$

As expected, the concentration absorbed of each individual gas would be reduced compared to the single gas case due to competitive sorption effects. The sorption also depends heavily on the relationship between the Langmuir affinity constant (b_i) and fugacity of all gases.

2.5.5 *Diffusivity*

Diffusion through a membrane occurs when penetrating species travel through the membrane due to random molecular motion that is primarily driven by concentration, chemical potential, fugacity or partial pressure differences across the two surfaces of the membrane. The diffusion coefficient is a constant that characterizes the relationship between the flux of the penetrating species and the concentration difference across the membrane. It is dependent on the size of the gaseous species and the size and distribution of microvoids through the polymer. This size and distribution of microvoids is indicated by the FFV of the polymer as discussed in section 2.4. Therefore according to Fujita's free volume theory, FFV can be related to the penetrant diffusivity by constants A_D and B_D [86, 87].

$$D = A_D e^{\left(\frac{-B_D}{FFV}\right)} \qquad 2.25$$

2.5.5.1 *Immobilization Theory*

The diffusion of penetrating species through the Langmuir void region may be hindered due to the presence of "dead ends" relative to the diffusion in the Henry's Law region [88, 89]. This essentially means there is no pathway for the molecule to continue diffusing forward through the polymeric matrix. An immobilization factor (F) can be used to characterize this restricted mobility of the penetrating species [89]. It is described as the ratio of the diffusion coefficient in Langmuir region to that in the Henry's law region:

$$F = \frac{D_H}{D_D} \quad 2.26$$

Paul and Koros [88] developed a partial immobilization model in which they assumed that the total gas concentration in the polymer can be divided into two parts; a mobile concentration (C_m) and an immobilized concentration ($C - C_m$). This means that all of the penetrant dissolved in the polymeric matrix (C_D) is mobile along with a fraction F of penetrant in the Langmuir region (C_H). The remaining (1-F) of C_H has no mobility and diffusion of these penetrating species in completely arrested by the "dead ends". Since concentration in a polymer is given by the sorption in both Henry and Langmuir regions:

$$C = C_D + C_H \quad 2.27$$

Therefore, the mobile concentration can be expressed by incorporating the immobilization factor into equation 2.27 to give:

$$C_m = C_D + FC_H = k_D.f + \frac{F.C'_H.b.f}{1+bf} \quad 2.28$$

2.5.6 *Plasticization*

Plasticization refers to a swelling or slight solvation of polymers by a penetrant. It occurs due to the strong interactions of the penetrant with the glassy polymer chains which affords them greater mobility. The swelling of the polymer results in increased fractional free volume (decreased T_g) which in turn results in increased gaseous diffusivity (and hence permeability) and reduced selectivity [90-93]. While plasticization can be caused by interactions of various gaseous species such as CO_2, SO_2, H_2S and water with the polymeric membrane [48], plasticization by CO_2 has been studied extensively [53, 86, 94, 95]. The extent of the swelling depends on a range of factors such as time, temperature and membrane thickness. It is strongly dependant on pressure as a high partial pressure leads to a high penetrant concentration within the membrane. Plasticisation can be reduced through thermal treatment, cross – linking and use of hybrid materials that make polymers less prone to swelling [96, 97].

Water or water clusters can also plasticize a polymer, resulting in increased polymer free volume. This consequently increases the diffusivity as a function of increasing water activity [81, 98, 99].

Conversely, water clusters can also exhibit "anti – plasticization" behaviour by filling the free volume within the polymer. This decrease in free volume reduces the diffusivity and consequently the permeability of penetrant molecules [83, 100]. The performance of the membrane depends upon whether the plasticization/swelling effects or pore filling/anti –plasticization effects are prevailing.

2.5.7 *Permeability Models*

At steady state, permeability of a penetrant through a membrane is given by:

$$\boldsymbol{P} = \frac{\boldsymbol{J.l}}{\boldsymbol{f_2 - f_1}} \qquad \textbf{2.29}$$

As detailed by Paul and Koros [88], the penetrant concentration can usually be assumed to change linearly across the membrane, if the diffusion coefficient is independent of the penetrant concentration. Then based on the immobilization theory described in section 2.5.5.1, Equation 2.29 can be rewritten to express permeability in terms of mobile penetrant concentration:

$$\boldsymbol{J} = -\frac{\boldsymbol{1}}{\boldsymbol{l}} \int_{\boldsymbol{C_{m2}}}^{\boldsymbol{C_{m1}}} \boldsymbol{D}\, \boldsymbol{dC_m} = -\frac{\boldsymbol{1}}{\boldsymbol{l}}\, \boldsymbol{D}(\boldsymbol{C_{m1}} - \boldsymbol{C_{m2}}) \qquad \textbf{2.30}$$

$$\boldsymbol{P} = \frac{\boldsymbol{D}(\boldsymbol{C_{m2}} - \boldsymbol{C_{m1}})}{\boldsymbol{f_2 - f_1}} \qquad \textbf{2.31}$$

$$\boldsymbol{P} = \frac{\boldsymbol{D}}{\boldsymbol{f_2 - f_1}} \left[\left(\boldsymbol{k_D} + \frac{\boldsymbol{FC'_H b}}{\boldsymbol{1 + b f_2}} \right) \boldsymbol{f_2} - \left(\boldsymbol{k_D} + \frac{\boldsymbol{FC'_H b}}{\boldsymbol{1 + b f_1}} \right) \boldsymbol{f_1} \right] \qquad \textbf{2.32}$$

Based on the competitive sorption principles discussed in section 2.5.4, the permeability equation 2.32 can be modified to include the effects of competitive sorption of other gases. Hence, the steady state permeability of penetrant *B* under a dry binary feed stream containing gas *B* and *C* becomes [101]:

$$\boldsymbol{P_B} = \frac{\boldsymbol{D_B}}{\boldsymbol{f_{B2} - f_{B1}}} \left[\left(\boldsymbol{k_{DB}} + \frac{\boldsymbol{F_B C'_{HB} b_B}}{\boldsymbol{1 + b_B f_{B2} + b_C f_{C2}}} \right) \boldsymbol{f_{B2}} - \left(\boldsymbol{k_{DB}} + \frac{\boldsymbol{F_B C'_{HB} b_B}}{\boldsymbol{1 + b_B f_{B1} + b_C f_{C1}}} \right) \boldsymbol{f_{C1}} \right] \qquad \textbf{2.33}$$

The presence of water vapour in multi – component system yields an even more complex model as it is necessary to include both a concentration dependent diffusion coefficient, a more complex Dual Mode Sorption Model to account for water solubility and the competitive sorption effects. Using equations 2.21 and 2.24, the complex DMS model gives the mobile concentration of water [101] by:

$$C_{mA} = \frac{\overline{C_p} k' \left(f_A / f_o\right)}{1 - k' \left(f_A / f_o\right)} + \frac{F_A \overline{C_p} b_A f_A}{1 + b_A f_A + b_B f_B + b_C f_C} \quad \textbf{2.34}$$

As discussed in previous section 2.5.6, the diffusion coefficient of gases may increase due to the plasticization or swelling effect of water. Conversely, the diffusion coefficient may also fall due to the formation of water clusters that hinder gas diffusion. Hence, diffusion coefficient depends strongly on the penetrant concentration and is often expressed as an exponential function [101]:

$$D(C_A) = D_{A0} e^{\beta_A C_A} \quad \textbf{2.35}$$

Where D_{A0} is the Fickian diffusion coefficient (cm^2/s) at infinite dilution ($C_A \rightarrow 0$), and β_A is a parameter for concentration dependant diffusion (cm^3.polymer/cm^3 [STP]) that depends on the nature of the penetrant – polymer system and the temperature. A positive value of β_A is referred to as the penetrant plasticizing ability [101] reflecting a swelling of the polymer structure as concentration increases. A negative β_A reflects a fall in the diffusion coefficient as the penetrant concentration increases and is usually attributed to water cluster formation [101]. Similar plasticization or anti – plasticization behaviour for a positive or negative β_A respectively is presented by Sato *et al.* [83]; however they have defined β_A in terms of the penetrant activity:

$$D_A(\alpha) = D_{A0} e^{\beta_A \alpha} \quad \textbf{2.36}$$

Where:

$$\alpha = \frac{p}{p_{sat}}$$

Assuming that the diffusion coefficient of water vapour is a function of only the mobile water vapour concentration in the polymer, Equation 2.35 can be written as:

$$D_A = D_{A0} e^{\beta_A C_{mA}} \quad \textbf{2.37}$$

Substituting this into equation 2.30, gives:

$$J = -\frac{1}{l} \int_{C_{mA2}}^{C_{mA1}} D_{A0} e^{\beta_A C_{mA}} \, dC_{mA} \quad \textbf{2.38}$$

$$J = -\frac{1}{l} \frac{D_{A0}}{\beta_A} \left(e^{\beta_A C_{mA2}} - e^{\beta_A C_{mA1}}\right) \quad \textbf{2.39}$$

Substituting equation 2.34 and 2.39 into equation 2.29 gives:

$$P_A = \frac{D_{A0}}{\beta_A(f_{A2} - f_{A1})}\left(e^{\beta_A C_{mA2}} - e^{\beta_A C_{mA1}}\right)$$

$$P_A = \frac{D_{A0}}{\beta_A(f_{A2} - f_{A1})}\left(e^{\left(\beta_A\left(\frac{C_p k'\left(\frac{f_{A2}}{f_0}\right)}{1-k'\left(\frac{f_{A2}}{f_0}\right)} + \frac{F_A C_p b_A f_{A2}}{1 + b_A f_{A2} + b_B f_{B2} + b_C f_{C2}}\right)\right)} - e^{\left(\beta_A\left(\frac{C_p k'\left(\frac{f_{A1}}{f_0}\right)}{1-k'\left(\frac{f_{A1}}{f_0}\right)} + \frac{F_A C_p b_A f_{A1}}{1 + b_A f_{A1} + b_B f_{B1} + b_C f_{C1}}\right)\right)}\right) \quad 2.40$$

2.5.7.1 Temperature Effects

Permeability is often modelled as a function of temperature using an Arrhenius expression [53, 102, 103] (Equation 2.41) where P_o is the pre – exponential factor (independent of temperature), R is the universal gas constant and E_p is the apparent activation energy of permeability:

$$P_A = P_o e^{\frac{-E_p}{RT}} \quad 2.41$$

Since, permeability is a product of diffusivity and solubility (Equation 2.12), both diffusivity and solubility of a component can also be expressed using Arrhenius equation and a Van't Hoff Relationship [104]:

$$D_A = D_o e^{\frac{-E_D}{RT}} \quad 2.42$$

$$S_A = S_o e^{\frac{-\Delta H_s}{RT}} \quad 2.43$$

Therefore:

$$P_o e^{\left(\frac{-E_p}{RT}\right)} = D_o e^{\left(\frac{-E_D}{RT}\right)} . S_o e^{\left(\frac{-\Delta H_s}{RT}\right)} \quad 2.44$$

$$E_p = E_D + \Delta H_s \quad 2.45$$

Where, E_D is the apparent activation energy for water diffusion and ΔH_s is the heat of water sorption. In general, ΔH_s is negative, while E_D is positive, so both are usually larger in magnitude than E_p.

2.6 Concentration Polarization

Concentration polarization is a phenomenon more commonly observed in liquid filtration processes [105]. Due to mass transfer resistance in the boundary layer, the concentration of the rejected species builds up at the membrane surface which reduces the concentration of the permeating species (Figure 2.7). This reduction in concentration limits permeation and reduces membrane performance.

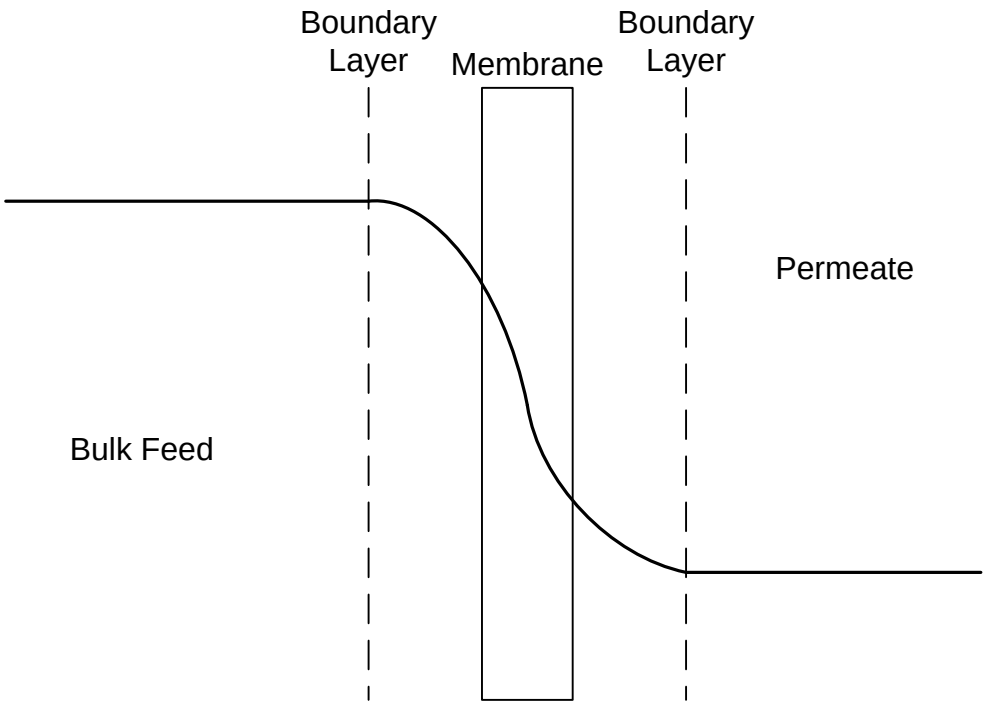

Figure 2.7: Schematic representation of changing concentration profile across the membrane surface.

Generally, in gas separation, concentration polarization effects are less significant due to the much greater resistance of the membrane itself. As a result, there is less penetrant depletion or accumulation on the surfaces of the membrane. However with rapidly permeating species like water, concentration polarization effects become significant. Therefore, in water vapour separation processes if the effects of concentration polarization are not taken into account, the estimation of the permeability and selectivity values may be inappropriately low. This can be avoided by calculating the boundary layer resistances associated with concentration polarisation and subtracting them from the total resistance [6, 106]. However this is often an inaccurate approach. Hence, it is easier to eliminate

concentration polarization by ensuring the gas – vapour mixture is well mixed and the boundary layer resistance is low. This may be achieved by increasing the cross flow stream flow rate to increase turbulence or employing a stirring device. As the chaotic flow in a system increases, the mass transfer rate also increases until it stabilises. This constant level is indicative of the true permeability where effects of concentration polarization are minimised. Hence, investigation into cross flow rates and stirrer speeds are often needed to ensure a well mixed system is achieved.

2.7 Overview of Water Permeable Polymers

Water vapour permeabilities and selectivity of various membranes at 30 °C have been researched extensively and are summarised in Figure 2.8.

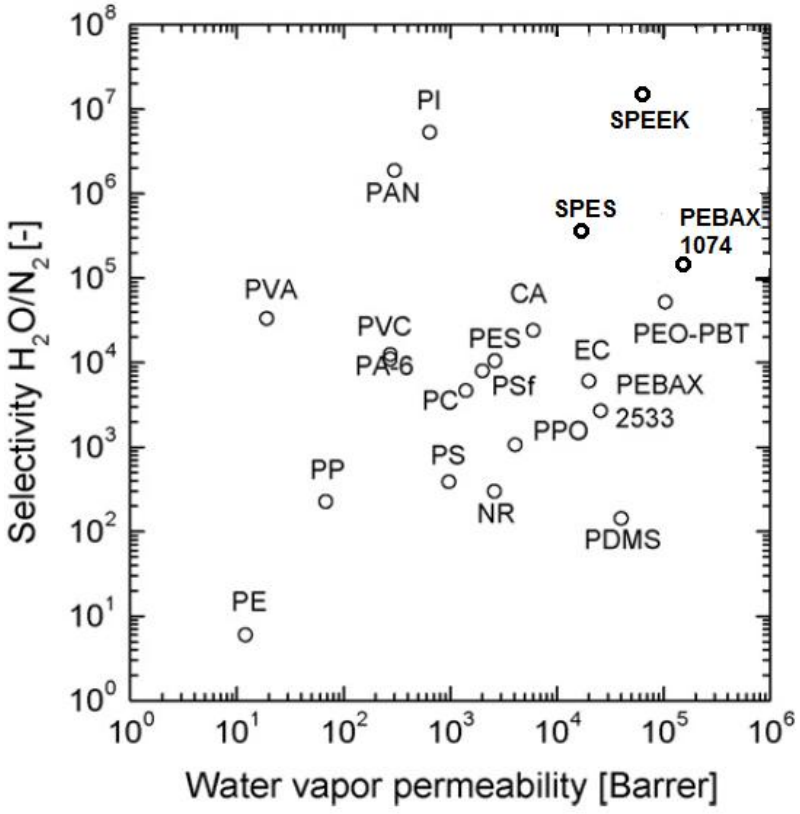

Figure 2.8: Water Vapour permeability vs. Water vapour/N_2 selectivity of polymeric membranes at 30°C [6].

Membranes with good water selectivity are paramount to ensure a high purity water stream is recovered. As a result, membranes in the top right hand corner of Figure 2.8 are ideal candidates for this application. These include Sulphonated Poly (Ether Ether) Ketone (SPEEK), Polyimide (PI), Sulphonated Poly Ether Sulphone

(SPES) and PEBAX 1074. So far, these membranes have mostly been researched for Proton Exchange Membrane Fuel Cell (PEMFC) application [17, 20, 23-25, 107-110], with only recent work undertaken into flue gas separations [6, 14, 102, 111-113].

2.7.1 *PFSA Polymers*

A Polymer Electrolyte Membrane Fuel Cell (PEMFC) directly transforms chemical energy into electrical energy by conducting protons through a membrane from the anode to the cathode. They are an energy efficient and environmentally friendly option for transportation, remote locations and portable power applications that use either hydrogen or methanol as fuel [23]. Currently, the most common electrolyte membrane used is the perfluorosulphonic acid (PFSA) membrane, Nafion. It has two domains; a hydrophobic polytetrafluoroethylene (PTFE) backbone with side chains of perfluorinated vinyl ethers ending with hydrophilic sulphonic acid groups (Figure 2.9). These hydrophilic groups aid in water sorption; which consequently swells the membrane and provides improved means for water diffusion through the membrane. Water uptake and transport in the PEM is essential to successful operation of the cell which also makes it useful for dehydration purposes. It is used commercially for this purpose at ambient temperatures.

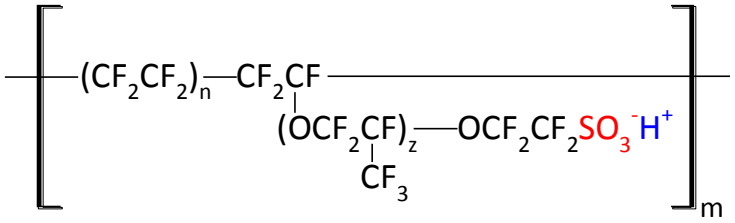

Figure 2.9: Structure of Nafion, a perfluorosulphonated polymer

A range of different models have been proposed to suggest the changes in domain structure of the polymer, particularly in the presence of water [114-119]. Many of the models in use today are based on the cluster – network model initially suggested by Hsu and Gierke [120]. This proposed an inverted – micelle structure where the hydrophilic sulphonic acid group and the polar water molecules separate from the hydrophobic fluorocarbon matrix into a spherical domain as

shown in Figure 2.10. The spherical clusters are connected by narrow channels and their size is dependent on the amount of water sorbed.

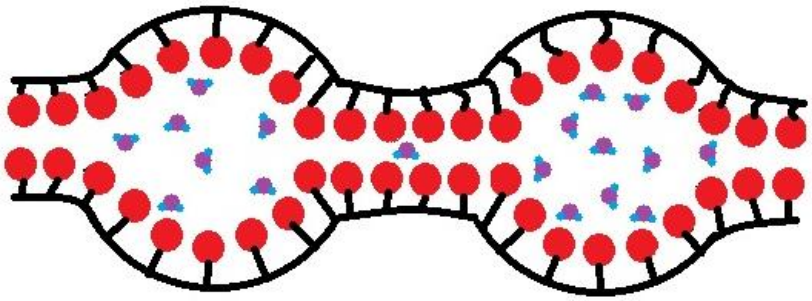

Figure 2.10: Inverted micelle clusters in Nafion membranes where the red indicates the SO_3H groups extending from the hydrophobic backbone and lining the water channels (Reproduced from [120]).

Nafion has good chemical and physical stability and high proton conductivities. This high proton conductivity is essential to successful operation of the fuel cell and is indeed dependant on the amount of water present in the membrane. Various studies have reported threshold water humidity for PFSA polymers below which there is no ion conductivity. However, as water concentration or volume fraction increases above this threshold, the conductivity increases which indicates percolation through the ionic clusters [121]. The amount of water uptake by PFSA polymers depends upon a number of things including membrane pre – treatment. Studies have shown that the pre – treatment method is crucial to ensuring reproducible results [122, 123]. They have also found that untreated Nafion membranes have a water uptake of 27 wt% in liquid water whereas those pre – treated have a water uptake of 34 wt% [124].

Some studies also show the measured water uptake for Nafion under saturated water vapour conditions (100% RH) is often less than that from immersion in liquid water at the same temperature [124, 125]. This phenomenon is referred to as Schroeder's paradox and is the focus of much debate [126-130]. Zawodzinski *et al.* believe the condensation of water vapour into the pores of the polymeric matrix constitutes an additional resistance which is not present in liquid equilibrated samples. Hence, the water content in vapour is lower than that for liquid

equilibrated samples [124]. Similarly, Hinatsu *et al.* argue that the presence of water as vapour poses an extra resistance where the water has to condense onto the pores first before it can diffuse across the membrane. This is made difficult by the hydrophobic nature of the fluorinated Nafion matrix [126]. Choi and Datta reported more water molecules sorbing onto the sulphonic acid site in the liquid phase as compared to vapour and attributed this to the differences in the surface energy of the sorption sites in the two phases [127]. However, Onishi *et al.* found no distinction in water uptake from saturated vapour and liquid immersion and believe that the differences observed in studies up to date are due to the differences in the thermal history of the membrane. They believe that pre – treatment of Nafion membrane, especially drying at high temperatures, severely affects the polymer morphology. According to them, given enough time water uptake in vapour equilibrated samples will equal that in liquid immersion [128].

The extensive application of Nafion is limited by high cost, the inability to withstand high temperatures and high methanol permeability which leads to catalyst poisoning and reduced fuel cell efficiency [17, 92]. At high temperatures (> 100 °C), the ion conductivity of Nafion decreases significantly, reportedly due to water loss from the membrane [92, 131-135]. At low pressures, the water partial pressure is limited to this total pressure and thus cannot reach its saturation partial pressure. This effectively limits the water activity in the membrane [121]. This can be overcome by operating at higher total pressures to allow for a greater partial pressure of water. Furthermore, this loss of conductivity is often related to the anisotropic deformation that occurs when the membrane is constrained between two electrodes. It is claimed that the loss does not occur when the membrane is free to swell isotropically [92, 136], as would be the case for a permeation application.

New materials with better conductivity and thermal stability are also claimed to provide a solution. Many recent studies have focused on investigating the performance of shorter – side – chain perfluorosulphonic acid (SSC – PFSA) polymers such as Hyflon ion and Aquivion [137-141]. Due to the shorter side chains, these PFSA polymers possess a higher crystallinity and increased glass transition temperatures than longer side chain polymers like Nafion [140]. This

means that even at high water concentrations, operation can be maintained above the glass transition temperature (see Equation 2.4). However, Vrentas *et al.* [142] have shown that there can be a step change in diffusion coefficient at the glass transition temperature, and this is believed to be the cause of the loss of proton conductivity above this temperature. Furthermore, SSC – PFSA polymers are known to have comparable water sorption to Nafion for the same equivalent weight (EW) at lower temperatures [143, 144]. Hence, it is claimed that these SSC – PFSA polymers are able to operate at high temperatures with no loss of conductivity [139, 141].

To date, research into Nafion for such dehydration applications includes extensive studies on water sorption from 30 – 140 ^{o}C [114, 124-126, 128, 145-149] and diffusion at 30 – 80 °C [114, 122, 150] as well as some studies on water flux below 100 °C [22, 150, 151]. The permeation of CO_2 through dried and hydrated Nafion has also been the focus of a few studies [146, 152, 153]. However, there is no information available on mixed gas water or CO_2 permeation above 100 ^{o}C. This is due at least partly to the observed decrease in fuel cell performance above 80 ^{o}C and at lower relative humidities [152, 154, 155].

Various researchers have reported that the water uptake in Nafion increases as a function of both temperature and water activity [130, 146, 156]. According to Majsztrik *et al.* increased water concentration at higher water activity increases the size of 'hydrophilic' channels through which water diffusion occurs. This is shown in Figure 2.11 where at low water concentrations, the water fills the free volume in the polymer. As water concentration increases, the water sorbs into the channels lined with hydrophilic sulphonic acid groups and away from the hydrophobic matrix which 'shrinks', resulting in increasing pore size ($p_{d,o} < p_{f,o}$) for water transport [156, 157].

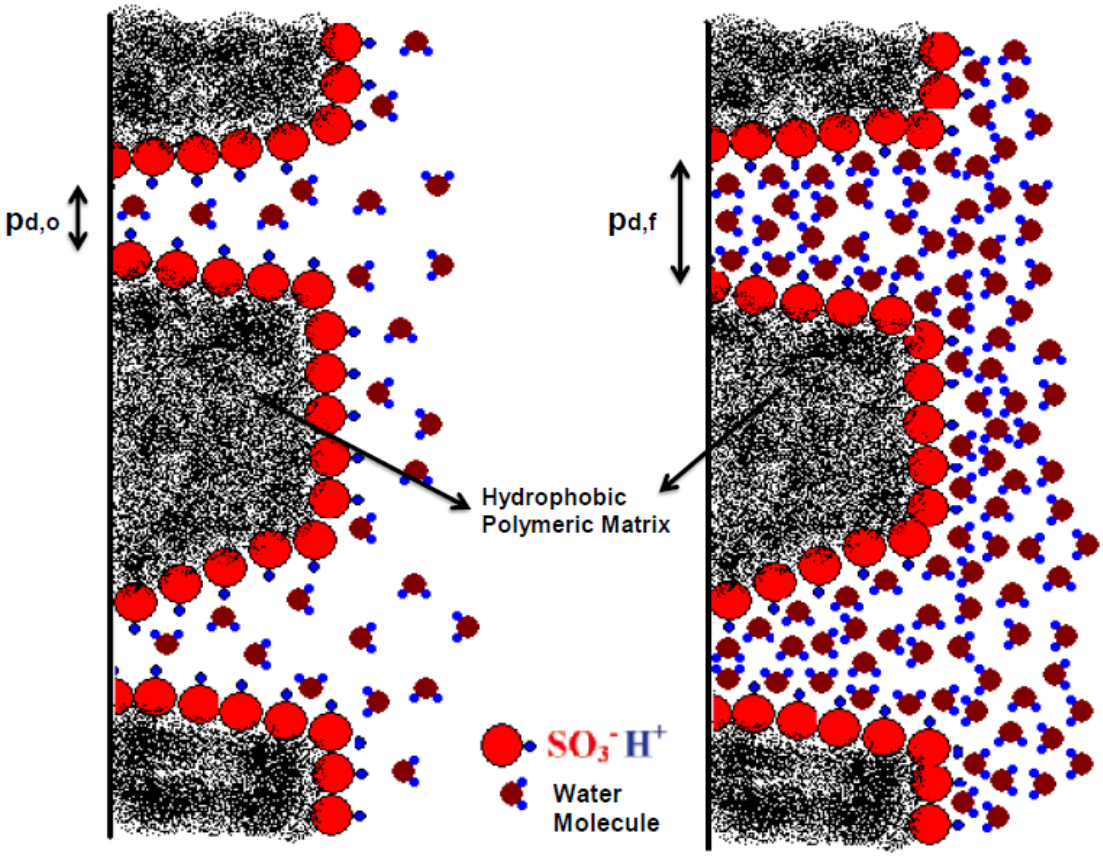

Figure 2.11: Change in structure of Nafion polymer with increasing water concentration (Reproduced from [157]).

The measured density of Nafion is known to decrease with increasing water activity. This is attributed to the increase in free volume caused by the formation and expansion of water clusters at higher water activities [130]. The increase in water uptake with increasing temperature is due to the relaxation of the polymeric matrix. This softening of the polymer allows for greater hydrophobic matrix shrinkage and therefore water to be absorbed by the polymer [156].

Other researchers have shown that the permeability of CO_2 through Nafion also increases with water activity [138, 139, 146]. At high water concentrations, the hydrophilic channels swell which increases diffusion of CO_2 through them. Conversely, it is claimed that CO_2 permeability only increases up to a temperature of 50 °C but then decreases. Ma and Skou attributed this interesting change in mechanism to three processes occurring simultaneously [158]. At low temperatures, the increase in thermal energy increases diffusion which accounts for the initial increase. However, as temperature continues to increase, the water

solubility of the membrane decreases. This reduces the size of the hydrophilic channels through which CO_2 diffusion occurs [146]. Similarly, as temperature increases, the CO_2 solubility also decreases which impacts the overall permeation rate [153, 158].

2.7.2 *Other Sulphonated Polymers*

Many alternative electrolyte membranes such as Sulphonated Poly (Ether Ether) Ketone (SPEEK), Sulphonated Poly (Ether) Sulphone (SPES) and Sulphonated Polyimide (SPI) have been investigated for fuel cell applications. Since water acts as a carrier for protons, proton conductivity is a good indication of the water permeability i.e. high proton conductivity indicates high water permeability [159]. Studies done on these polymers suggested improvements in polymer performance can be achieved through increase in sulphonation degree.

Sulphonated Poly (Ether Ether) Ketone (SPEEK) is a non – perfluorinated sulphonated polymer that possesses excellent proton conductivities [6, 102, 103, 160-168] (Figure 2.12). The presence of hydrophilic $-SO_3H$ end group increases water uptake in a polymer by increasing interactions between the water molecules and the end groups [161, 166, 169-171].

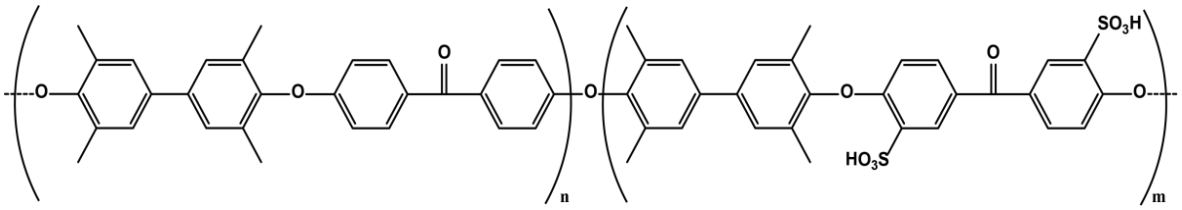

Figure 2.12: Structure of Sulphonated Poly (Ether Ether) Ketone.

It can be synthesized via direct polymerization of sulphonated monomers or post – sulphonation of Poly (Ether Ether) Ketone (PEEK) [12, 172]. PEEK is a crystalline thermoplastic that has a high chemical resistance and is only soluble in very concentrated nitric and sulphuric acids. It is this hydrophobic backbone that provides the mechanical and thermal stability of the SPEEK polymer. The addition of hydrophilic sulphonic acid end groups ($-SO_3H$) makes SPEEK an amorphous polymer that has both hydrophilic and hydrophobic regions [12]. The degree of hydrophilicity of SPEEK is determined by the degree of sulphonation (SD) of the polymer.

It is well known that sulphonation of a polymer improves the water permeation properties [12, 102, 103, 161, 172-174]. Addition of sulphonate group increases the hydrophilicity of the polymer which increases both water vapour permeability and selectivity over other gases through increased interactions between polymer and water [161, 166, 169-171]. Jiang *et al.* [161] observed two distinct types of behaviour where at low vapour activity (< 0.75), there was only a small increase in water uptake but as vapour activity increased above 0.75, there was a sharp increase in water content in the membrane. This latter increase was more pronounced in higher sulphonated degree membranes and was attributed to the increased presence of the $-SO_3H$ groups [161]. Jia *et al.* studied the effect of the sulphonation degree on nitrogen and water vapor permeation properties of PEEK [102]. The permeability of water increased with increasing sulphonation degree while the nitrogen permeability decreased. The decrease in nitrogen permeability was attributed to the increased presence of the $-SO_3H$ groups that reduced the free volume within the polymer. Consequently, the selectivity of H_2O/N_2 increased, making sulphonation an effective method for improving membrane separation performance. Similar results have been obtained by Liu *et al.* [160] and Sijbesma *et al.* [6] where water selectivity increased with increasing sulphonation degree. These authors have attributed this behavior to the amorphous nature of the SPEEK structure. The sulphonated end groups that represent the hydrophilic region in the polymer, aggregate with water molecules to form transport channels through which water diffusion readily occurs [6, 12, 160, 166, 171].

There have been a number of studies that have looked at the effect of temperature on SPEEK permeation properties. Most recently, Wessling *et al.* considered the permeation of pure water, CO_2 and N_2 and mixed gases through SPEEK at 30 °C, 50 °C and 70 °C [6]. They found the pure gas permeabilities to be very low due to the rigid structure of SPEEK which allows no chain mobility. The presence of water in the mixed gas experiments (water and N_2) showed considerably higher gas permeabilities for wet SPEEK compared to dry state. This was due to high membrane swelling degree which resulted in increased free volume. The effect of temperature on water permeability was complex where permeability increased with temperature initially but decreased above 70 °C. This was believed to be due

to the two contrasting effects; increased diffusivity of water at high temperature due to increased swelling but reduced solubility of water in the polymer matrix [6]. In contrast, Jia *et al.* [102] found that water permeability increased as temperature increased from 25 – 50 °C and attributed this to the increase in diffusivity. Similar results were obtained by Wang *et al.* [112] who found that both water and N_2 permeabilities increased with increasing temperature from 30 – 50 °C.

Potreck *et* al analyzed the kinetic sorption behavior of water vapour in SPEEK [45]. They studied the effect of water sorption on the glass transition temperature (T_g) of SPEEK using the Fox equation (Equation 2.4) and showed that it continuously decreased as water concentration in the polymer increased (Figure 2.13). It is well known that plasticization by penetrant depresses T_g of a polymer [43, 44, 175]. They found that both SPEEK polymers transitioned from a glassy to a rubbery state when the T_g decreased to the experimental temperature of 20 °C at a water concentration of ~ 600 cm^3 [STP]/cm^3.polymer.

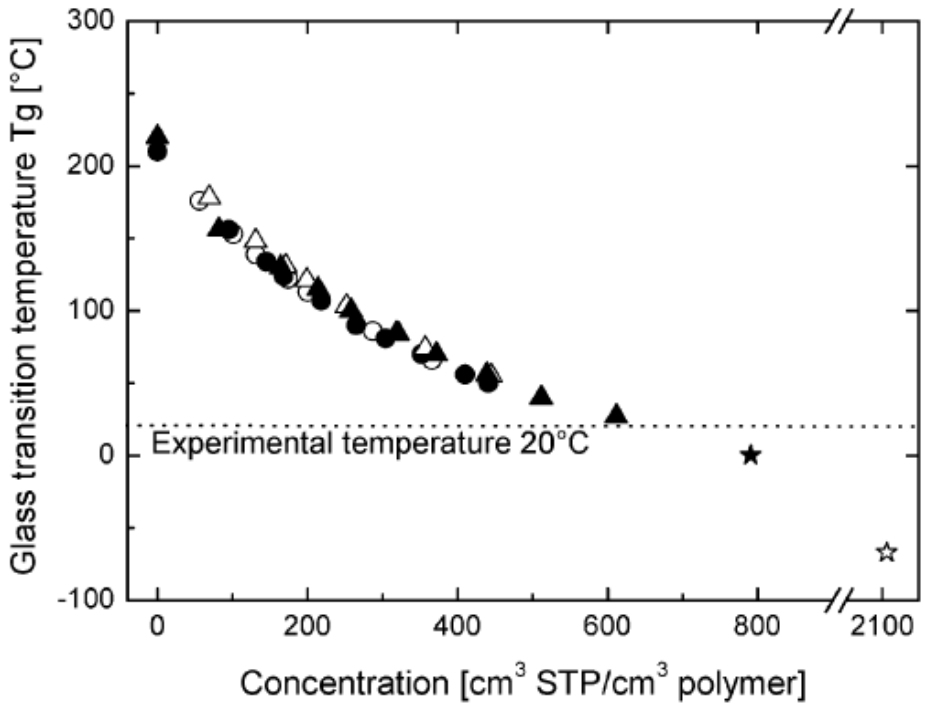

Figure 2.13: Theoretical glass transition temperature (T_g) as a function of water concentration in SPEEK with Sulphonation Degree (SD) of 59% (circles) and 79% (triangles) for sorption (open data points) and desorption (closed data points) runs [45].

Potreck *et al.* also calculated the Fickian diffusion coefficient of water vapour in SPEEK during sorption and desorption (Figure 2.14). In both runs, they observed an initial increase in Fickian diffusion as a function of water concentration in the membrane. The Fickian diffusion coefficient of the polymer with SD of 75 % was lower than that for 59 % in sorption runs. A similar trend with SD was obtained by Piroux *et al.* for sulphonated copolyimides who attributed this decrease in diffusion to the decrease in FFV caused by the increased presence of the bulky SO_3H groups [113].

However, the Fickian diffusion coefficient in both SPEEK sorption and desorption runs reached a plateau at a water concentration of ~ 300 cm^3 [STP]/cm^3.polymer and then began to decrease. Potreck *et al.* attributed this drop in diffusion to the polymer transitioning from a glassy to a rubbery state. They argue that while in a glassy state, both Fickian diffusion and relaxational changes occur. However, as the polymer transitions to a rubbery state, it becomes fully relaxed and only Fickian sorption kinetics play a role. They also suggest that at these high water concentrations, the buildup of the diffusion profile is too fast in thin membranes and that this may lead to inaccuracies in the measurement of the Fickian diffusion coefficient.

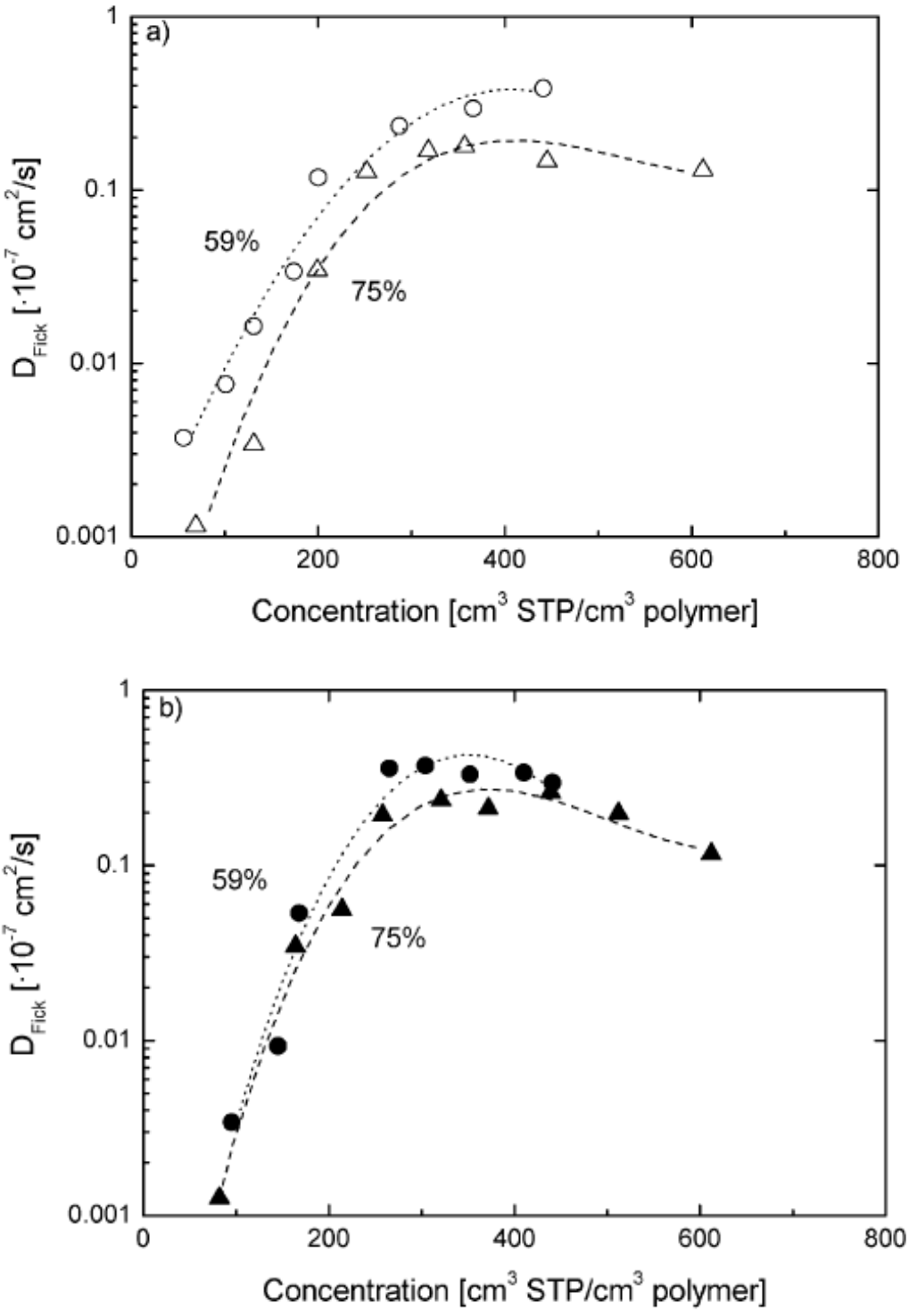

Figure 2.14: Fickian diffusion of water vapour in SPEEK for sorption (open data points) and desorption (closed data points) [45].

Furthermore, while they performed a Zimm – Lundberg clustering analysis shown in Figure 2.15, they interestingly proposed that the formation of clusters only occurs when the cluster integral is above zero. This is in contradiction to the popular definition of clusters forming when the cluster integral is above -1 [65,

101, 176-178]. According to their definition, they observed a positive cluster integral at very high water concentrations and attributed this to inaccuracies in the measurements. Hence, they reported no water cluster formation in their membranes. However, if the commonly held definition of cluster formation occurring when $G/V > -1$ is employed, it becomes apparent that cluster formation does indeed occur for the two SPEEK polymers when the water concentration reaches ~ 270 – 350 cm^3 STP/cm^3 polymer. This is consistent with the point at which the diffusion coefficient is observed to plateau.

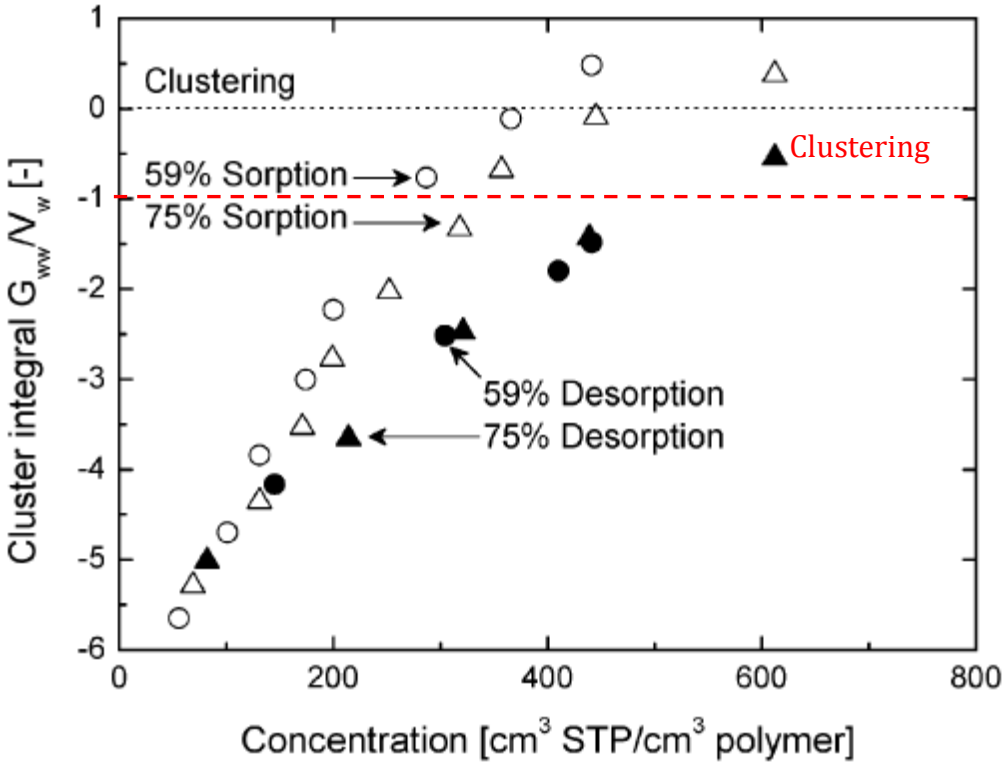

Figure 2.15: Cluster integral as a function of water concentration in SPEEK polymer for sorption (open points) and desorption (closed points).

A study conducted by Khan *et al.* [179] focused on CO_2 and N_2 permeabilities. They found that CO_2/N_2 selectivity increased with increasing sulphonation degree (SD) of SPEEK. As discussed, increased sulphonation degree causes a reduction in polymer free volume resulting in reduced diffusion coefficients. However, solubility coefficients of CO_2 in particular increased with an increasing degree of sulphonation due to the interactions of the CO_2 quadrupole with the polar SO_3^- groups in the polymer. Hence, the increase in CO_2 solubility compensated the

decrease in diffusion resulting in greater permeability at higher sulphonation degrees.

As well as SPEEK, Jia *et al.* [103] also studied the mixed gas behaviour of water vapour and N_2 through Sulphonated Poly (Ether) Sulphone (SPES) and found that the permeability of water increased with increasing sulphonation degree whereas the permeability of N_2 decreased. They believe this is because the introduction of sulphonic acid groups causes chain stiffness which explains the decrease in N_2 permeability [103]. Later work by Wang *et al.* [180] included investigating permeabilities of water vapour, H_2, CO_2, O_2, N_2, and CH_4 gases through non – sulphonated and modified Poly (Aryl Ether Sulphone) membranes at 30 – 100 °C. They found that polymers with bulky side groups had high gas permeabilities due to increase fractional free volume whereas those with strongly hydrophilic carboxylate groups had increased interactions with water and hence had high water permeabilities [180]. Work done by Chen *et al.* [181] confirmed this, where the gas permeabilities increased for polymers with bulky side groups.

A Sulphonated Polyimide (SPI) was considered by Piroux *et al.* who conducted a series of studies investigating water vapour and gas permeation [113, 182, 183]. Investigation into pure water vapour permeation found that it took place in both sulphonated and non – sulphonated phases of the copolymer. The polarity and the free volume associated with non – sulphonated monomers influences the water uptake, i.e. synthesizing a copolymer with a bulky non – sulphonated CARDO monomer increases fractional free volume in the polymer and leads to increased water permeability. Despite this, the sulphonated phase was primarily responsible for water absorption where water uptake increased due to sulphonated phase hydration [113]. Another study investigated the permeabilities of H_2, O_2, CO_2 and N_2 at 20 °C. The CO_2 permeability decreased with increasing sulphonated block content, hence they established that CO_2 permeability primarily occurs through the free volume associated with the non – sulphonated phase. This supports the results obtained by Chen and Wang [180] for SPES where gas permeability increases with increased free volume. Similar trends are observed for other gases where the gas diffusivities (and hence permeabilities) decrease as the sulphonated phase content increases. Hence, it was established that gas diffusivity was the most

important parameter in the transport phenomenon [182]. Tanaka *et al.* [184] did similar work and explained that the decrease in permeability is due to the increased intermolecular forces caused by the sulphonic groups. This restricts chain mobility, hence decreases gas permeability with increasing sulphonated content. A third study by Piroux investigating the permeability of CO_2 in hydrated conditions showed that it decreased for relative humidity of up to 50 % and increased again thereafter. This was because at high humidity, the gas transport through the sulphonated phase is high due to the increased interactions between the polar gas and the water contained in the polymer as well as the increased hydrophilic channel size due to water uptake [183].

The effect of water activity on the water diffusion coefficient of a SPI has been studied by Detallante *et al.* [178] and is presented in Figure 2.16. As shown, the diffusion increases initially as the water activity increases, passes through a maximum and then begins to decrease. They attributed this initial increase to the dual-mode sorption of water into the sorption sites and then the free volume. As water activity increases above 0.3, the diffusion begins to decrease due to the formation of water clusters.

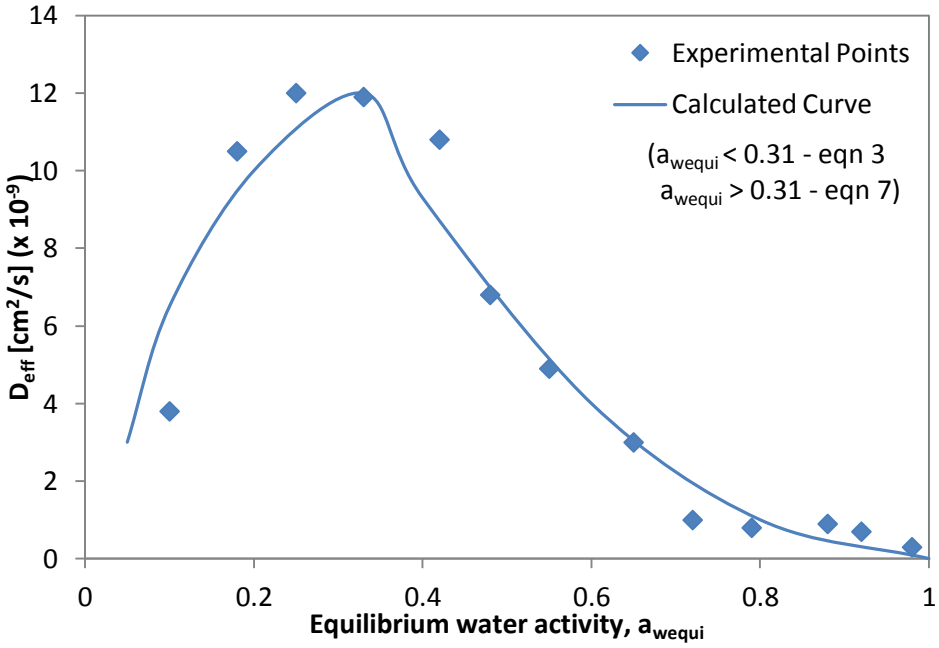

Figure 2.16: Effective diffusion coefficient as a function of water activity for Napthalenic Sulphonated Polyimide (Reproduced from [178]).

2.7.3 *PEBAX*

A study performed by Potreck *et al.* [14] looked at the Fickian Diffusion coefficient and clustering phenomenon (presented in Figure 2.17) of water vapour in PEBAX at 20 – 70 °C. They reported a decrease in the Fickian diffusion coefficient of water at 70 °C, particularly at high water activities. They attributed this to the lower degree of plasticization caused by water at high temperatures that results in low free volume for water molecules to diffuse through.

They reported a very strong tendency for water molecules to form clusters in rubbery PEBAX. Furthermore, they attributed the diminished increase in Fickian diffusion at water activities of ~ 0.5 – 0.7 to the slower diffusion rates of large water clusters. However, as water activity continues to increase, the newly sorbed water molecules enter an environment with similar properties to that of bulk liquid water that reduces their tendency to form clusters.

Interestingly, Potreck *et al.* found that water permeability in PEBAX increased with increasing temperature initially but decreased at 70 °C. They attributed this solely to the relatively large decrease in water solubility at high temperatures. The N_2 permeability increased consistently with increasing temperature because the increase in gas diffusion dominated the decrease in gas solubility [14]. Sijbesma *et al.* [6] also studied the permeabilities of pure water, CO_2 and N_2 and mixed gases through PEBAX at 30 °C, 50 °C and 70 °C. They reported high pure gas permeabilities due to the presence of free volume in the rubbery segments. PEBAX showed higher N_2 and pure CO_2 permeability, the latter of which was due to the ether linkages present in the PEO building block [6].

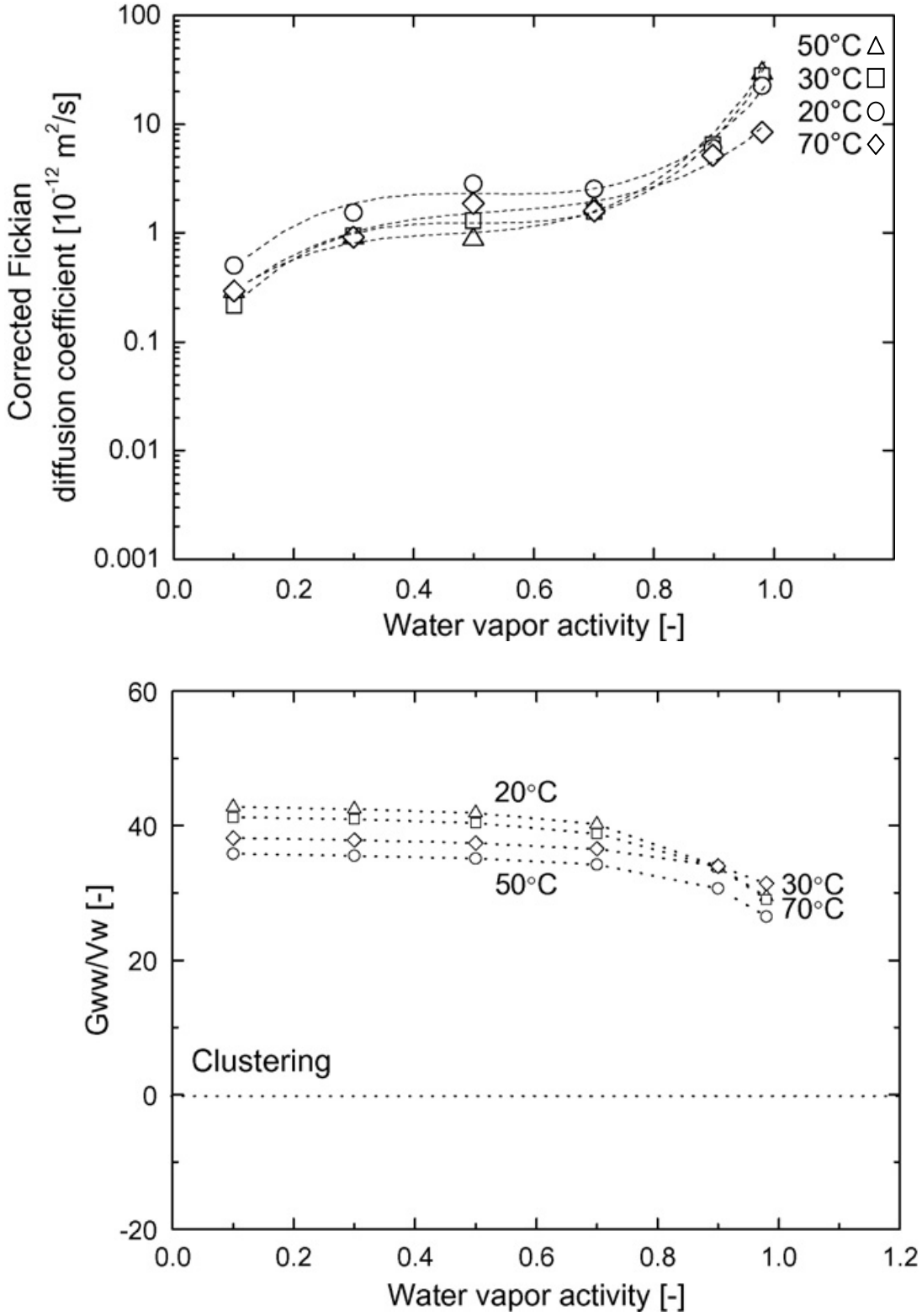

Figure 2.17: Fickian Diffusion coefficient (Top) and Clustering analysis (Bottom)of water vapour in PEBAX 1074 [14].

2.7.4 *Polyimides*

Polyimide membranes such as Kapton, Matrimid, 6FDA and BPDA containing polyimides have been extensively researched for membrane gas separation applications, such as carbon capture [53, 54, 86] and natural gas dehydration [82] and purification [77, 185]. To date, many researchers have studied the effect of CO_2 – induced plasticization [86, 95, 185-188], thermal and mechanical properties [189, 190], operating temperature and pressure [53, 191] and water transport and sorption properties [54, 81, 83, 101, 192, 193] of these polyimide membranes but none have focused on high temperature dehydration applications of these polymers.

6FDA – TMPD (2,2 – bis (3,4 – dicarboxyphenyl) hexafluoropropane dianhydride – 2, 3, 5, 6 – tetramethyl – 1,4 – phenylenediamine) is a rigid glassy polyimide that when fabricated as a non – porous membrane shows high CO_2 permeabilities while retaining reasonable selectivities against N_2 and CH_4. The chemical structure is shown in Figure 2.18. There has been some work done to investigate water permeation properties of 6FDA – TMPD but there is a considerable gap in knowledge in the mixed vapor/gas permeation behavior of this polymer, especially as a function of temperature. There is real potential to investigate this polymer for high temperature flue gas dehydration application. It should be noted that this polymer is also commonly referred to as 6FDA - durene, 6FDA - TMPDA, 6FDA - TeMPD and 6FDA - TeMPDA.

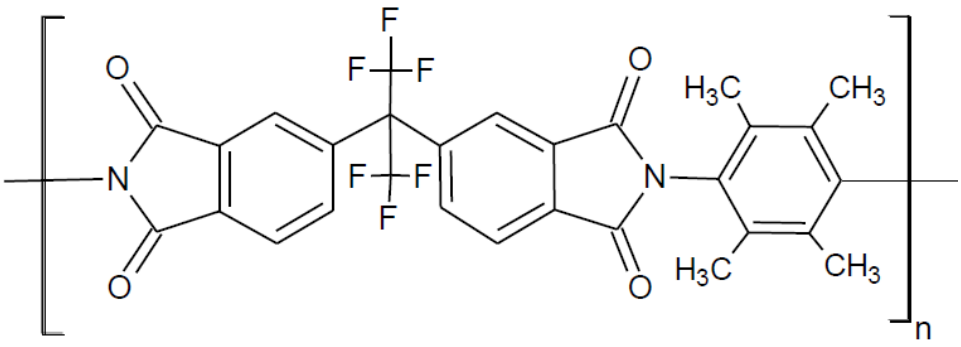

Figure 2.18: Structure of 6FDA – TMPD (2,2 – bis (3,4 – dicarboxyphenyl) hexafluoropropane dianhydrid - 2, 3, 5, 6 – tetramethyl - 1,4 - phenylenediamine)

Chen *et al.* [54, 101] studied the water permeation properties of 6FDA – durene at 35 °C and developed a mathematical model that models water permeability in a multi – component system by taking into account the competitive sorption effects of gases present (see section 2.5.7). They found that water concentration and permeability increased with increasing water activity due to water – induced plasticization as well as increased water solubility. However, this increase was somewhat restricted by the presence of water clusters expected to form at high water activity. These water clusters resulted in reduced diffusivity of water but also other gases. Similar results have been obtained by Stern *et al.* [82], Okamoto *et al.* [81] and Ansaloni *et al.* [194] for similar polyimides. Furthermore, Chen *et al.* [54] observed a decrease in CO_2 and CH_4 permeability with increasing water activity and attributed this to successful competitive sorption of water as well as the presence of water clusters that hinders diffusion. Similar competitive sorption behavior was observed by Chern *et al.* [77] for CO_2 permeability in the presence of water vapour for a Kapton polyimide membrane. Chen *et al.* [101] successfully modeled the water and gas permeability using a mathematical model that takes competitive sorption of other gases into account. They reported the infinitely dilute Fickian diffusion coefficient (D_0), plasticization factor (β) and immobilization factor (F) for water vapour, CO_2 and CH_4 and found them to be in good agreement with that reported by Duthie *et al.* [53] and Sato *et al.* [83].

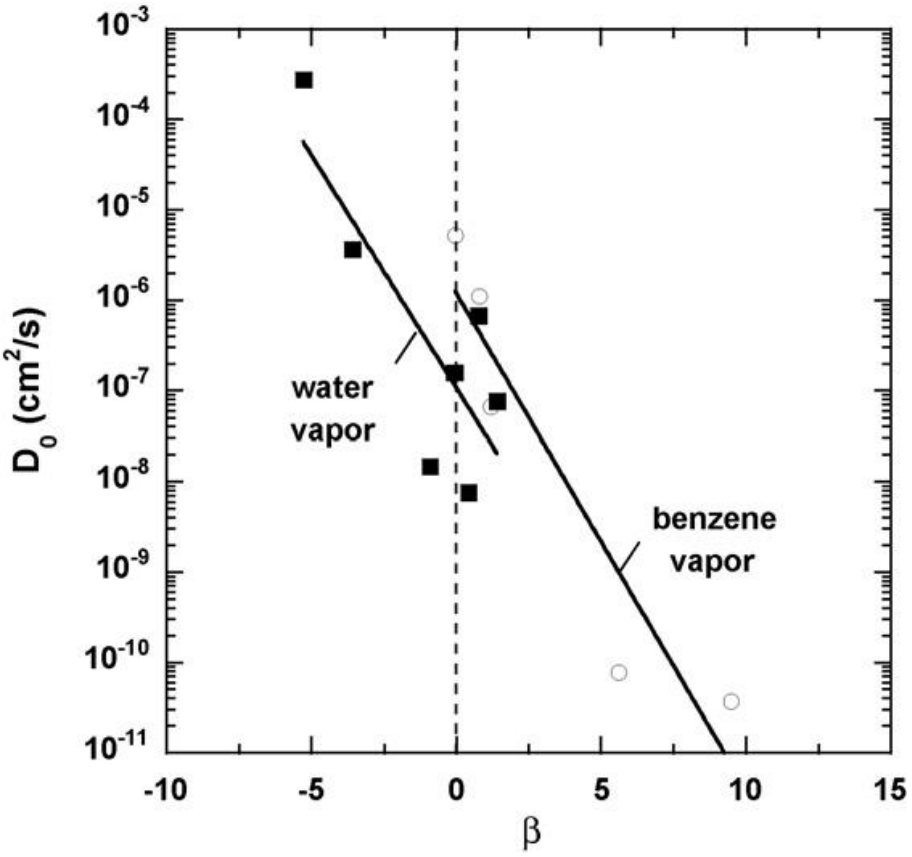

Figure 2.19: Infinite – dilution diffusion coefficient (D_0) as a function of pressure dependant plasticization parameter (β) for water and benzene vapour for a range of polymers (PDMS, PTMS – based and 6FDA – based polyimides) [83].

Sato *et al.* [83] studied the effect of water vapour presence on plasticization ability of a range of rubbery and glassy polymers including 6FDA – TeMPD. They reported infinite – dilution diffusion coefficient (D_0) for water and benzene vapour as a function of plasticization parameter (β) for a range of polymers (Figure 2.19). It should be noted that they defined β in terms of the vapour activity of penetrant (Equation 2.36). A positive β is indicative of plasticization while a negative β is indicative of 'anti – plasticization'. This "anti – plasticization" behavior was exhibited where formation of water clusters in the membrane was likely to occur. A β value of -0.081 for 6FDA – TeMPD for water vapour confirmed that water vapour has the tendency to cause either plasticization or 'anti – plasticization' in this particular polymer as the value lies very close to $\beta = 0$.

This is more clearly shown in Figure 2.20, where the presence of water vapour in rubbery and glassy polymers with low T_g induces 'anti – plasticization' effects with

negative β values obtained. As T_g increases, β also increases and the presence of water vapour induces plasticization effects in these glassy polymers. It is interesting to note that while β value does becomes positive, the plasticization effects of water vapour are still not as severe benzene vapour and indeed lie very close to $\beta = 0$, even for glassy 6FDA based membranes with $T_g \sim 300 - 400$ °C.

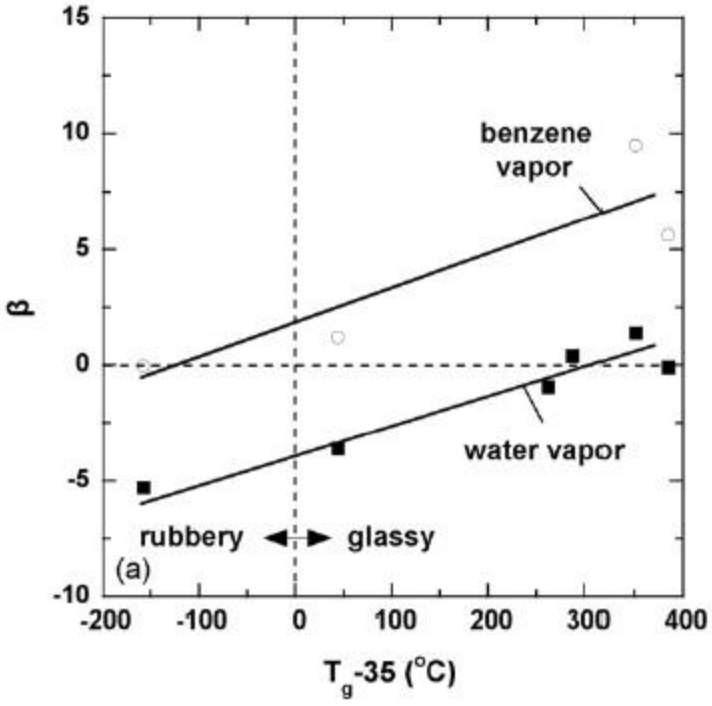

Figure 2.20: β effects of water vapour and benzene vapour as a function of T_g for a range of glassy and rubbery polymers [83].

Duthie *et al.* [53] studied the effect of operating temperature on CO_2 induced plasticization of 6FDA polyimide. They found that the solubility of CO_2 decreased with increasing temperature from 21 – 77 °C and modeled these curves successfully using the Dual Model Sorption Model (Equation 2.18). Permeability of CO_2, N_2 and O_2 were also measured, with N_2 and O_2 permeability increasing with temperature while CO_2 permeability decreased. These changes were attributed to a combination of increased diffusivity with temperature but a significant reduction in CO_2 solubility. This meant that the onset of plasticization was delayed at higher temperatures. Chung *et al.* [191] observed similar trends where N_2 permeability increased with temperature while CO_2 permeability and solubility decreased. Duthie *et al.* [53] also modeled the CO_2 permeability and diffusivity data to obtain

the infinitely dilute Fickian diffusion coefficient (D_0), CO_2 plasticization ability (β) and the immobilization factor (F) and found these to be a function of temperature. As expected, D_0 increased as temperature increased but both β and F were found to decrease. They attributed the decrease in the CO_2 plasticization ability (β) to the higher fugacities needed to induce plasticization at higher temperatures. The immobilization factor (F) is ratio of diffusion coefficients in Langmuir region to that in the Henry's Law region. As temperature increased, the diffusion in the Henry's region dominates over the diffusion in the Langmuir region and hence F decreases. Okamoto *et al.* [195] obtained similar values of D_0 to Duthie *et al.* [53] over a temperature range of 35 - 80 °C for a similar polyimide.

2.8 Scope of the Thesis

The permeabilities of pure water, CO_2 and N_2 for membranes discussed at length in the previous sections have only been investigated at temperatures below 100 °C. Water/CO_2 selectivities at 30 °C for a few of these membranes are presented in Figure 2.21. Most studies have also only considered the mixed gas behaviour of water vapour and N_2 as indicated by the H_2O/N_2 selectivity presented in Figure 2.8 [14, 102, 112]. High purity recovered water is compromised by the downstream permeation of CO_2 which causes acidification and corrosion. Therefore, while N_2 is the major component in flue gases and has been studied exclusively so far, CO_2 permeability needs to be studied in conjunction with water vapour and N_2 and at high temperature to accurately determine the effectiveness of membranes for flue gas dehydration applications, specifically in Australian Brown coal – fired power plants.

We have chosen to investigate mixed gas water, CO_2 and N_2 permeation properties of Nafion, SPEEK and 6FDA – TMPD at elevated temperatures. There has been limited work on investigating the separation performance of these membranes especially at elevated temperatures and their potential appears high for the proposed application. A comparison of the properties of these membranes as investigated in the literature is presented in Table 2.3.

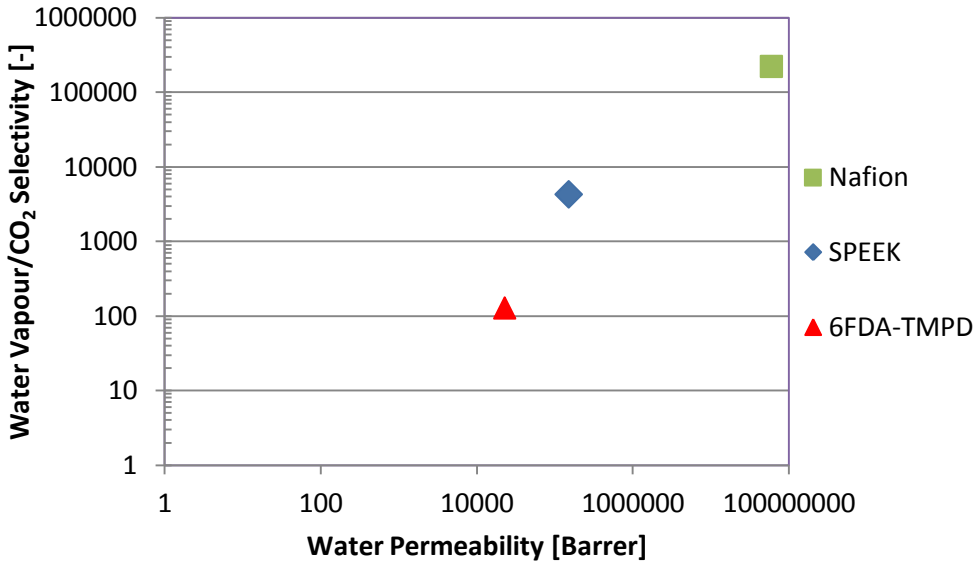

Figure 2.21: Water vapour permeability vs. Water vapour/CO_2 selectivity for Nafion, SPEEK, PEBAX, SPES and 6FDA durene at 30 °C (Note: These values have been derived from taking pure water and CO_2 permeabilities due to the lack of studies conducted on mixtures of water/CO_2).

Table 2.3: A comparison of the properties of the selected polymeric membranes.

Name	Density [g/cm³]	Fractional Free Volume (FFV)	Ion Exchange Capacity [meq/g]	Glass Transition Temperature [°C]
Nafion	1.65 – 2.19 [196, 197]	0.041 – 0.044 [198]	0.6 – 1.25 [156]	100 – 150 [199-202]
SPEEK	1.07 – 1.2 [203, 204]	0.11 – 0.16 [100, 204]	1.48 – 2.74 [164, 203]	220 – 250 [102, 103, 205-207]
6FDA – TMPD	1.3 – 1.33 [86, 191]	0.180 – 0.182 [86, 191]	NA	370 – 430 [53, 86, 186, 208]

Chapter 3 focuses on explaining the experimental methods and techniques used to investigate membrane performance, especially the one developed to measure steam permeation at high temperature. The physical and chemical properties of chosen membranes such as membrane density and thermogravimetric analysis are discussed. Single and multi – component gas permeation rigs used to measure

water and gas permeabilities at a range of temperatures as well as the gravimetric sorption analyser used to determine solubility are described.

Chapter 4 focuses on the first candidate membrane; Perfluorosulphonic acid (PFSA) based Nafion 115. The water permeation properties at elevated temperatures from 70 – 150 °C are investigated and reported. Furthermore, the water sorption isotherms at 20 – 40 °C are modelled using the Zimm – Lundberg clustering analysis and a modified Dual Mode Sorption Model. The temperature – dependence of water sorption parameters at these temperatures are reported using an Arrhenius relationship. Water, CO_2 and N_2 permeance at 70 – 150 °C as a function of water activity and pure gas permeabilities at 35 – 150 °C are investigated.

Chapter 5 focuses on the second candidate membrane; Sulphonated Poly (Ether Ether) Ketone or SPEEK. The effect of sulphonation degree and temperature on permeation properties of SPEEK membranes is investigated. FTIR is employed to study the state of water in membranes with varying Ion Exchange Capacities (IEC)/sulphonation degrees; IEC 1.6 meq/g and IEC 1.9 meq/g. Water, CO_2 and N_2 permeabilities at 30 – 150 °C as a function of water activity for the two membranes are investigated.

Chapter 6 focuses on the third candidate membrane; 6FDA – Durene polyimide. The effects of temperature and water activity on permeation properties of this membrane are investigated. Water, CO_2 and N_2 permeabilities at 25 – 150 °C as a function of water activity are measured. Water sorption isotherms at 25 – 35 °C are modelled and sorption parameters used to model the water permeabilities at corresponding temperatures. This provides an insight into the solubility and diffusivity behaviour through a glassy polyimide membrane.

Chapter 7 is a comparison chapter in which properties of Nafion, SPEEK and 6FDA investigated are compared against one another to determine suitability of these membranes to the proposed application. This is done using a membrane module designed on ASPEN HYSYS to investigate membrane areas and pH of the recovered stream based on the H_2O/CO_2 selectivity of these individual membranes at 150 °C.

Chapter 3 Experimental Methods

This chapter details the materials and polymer synthesis as well as experimental techniques utilized to acquire results in this research.

3.1 Materials and Membrane Treatment

3.1.1 *Polymers and Polymers Synthesis*

The membrane materials under investigation in this research are summarised in Table 3.1.

Table 3.1: Characteristics of the membrane materials used in this work

Name	Equivalent Weight (EW) [g/mol SO_3H]	Ion Exchange Capacity (IEC) [meq/g]	Supplier
Nafion 115	1100	0.9	DuPont
Fumapem F - 920	900	1.1	FuMA-Tech GmbH
Fumapem E - 630	630	1.6	FuMA-Tech GmbH
Fumapem E - 540 - GF	530	1.9	FuMA-Tech GmbH
6FDA – TMPD	NA	NA	6FDA – Aldrich TMPD - Fluka

Nafion 115 was purchased from DuPont as flat sheets. It was the thinnest Nafion membrane available from Dupont in a small order size. The membranes were pre – treated according to a standard procedure [125, 126, 209]. They were boiled in 3% H_2O_2 for an hour, rinsed several times and then boiled in purified H_2O for half an hour, boiled in 1M sulphuric acid for an hour followed by rinsing and boiling in purified H_2O for another half an hour. Studies have shown that this pre – treatment method is crucial to ensuring reproducible results (see section 2.7.1) [122, 123]. The membranes for permeation experiments were then stored in purified water at room temperature whereas those for sorption experiments were dried under vacuum at 35 °C.

A perfluorosulphonic acid (PFSA) based membrane similar to Nafion (Fumapem F - 920) was kindly provided by FuMA – Tech GmbH, Germany. This membrane had a thickness of 20 μm. It was removed from a PET support layer and tested as supplied as it was too delicate to undergo the pre – treatment method described above.

Sulphonated Poly (Ether Ether) Ketone (SPEEK) membranes with two different ion exchange capacities (IEC); Fumapem E630 (IEC 1.6 meq/g) and glass fibre reinforced Fumapem E540-GF (IEC 1.9 meq/g) were kindly supplied by FuMA – Tech GmbH, Germany. The membranes were received as A4 sized flat sheets on PET foils. The membranes were peeled away from the PET support and were used as supplied.

6FDA – TMPD was synthesised in house by Dr Shinji Kanehashi using the monomers 4,4 – (hexafluoroisopropylidene) diphthalic anhydride (6FDA) and 2, 3, 5, 6 – tetramethyl – 1,4 – phenylene – diamine (TMPDA) as supplied without any purification [186]. The chemical imidization reaction involved the formation of a polyamic acid through the addition of TMPD diamine to an N, N – dimethylacetamide (DMAc) solution in a purged round bottom flask. The solution was stirred for 30 minutes before 6FDA was slowly added to the solution with constant stirring over an ice bath to remove reaction heat. After 30 minutes, the ice bath was removed and the reaction left to proceed for 12 hours under nitrogen atmosphere at room temperature. The imidization process for ring closure was performed at room temperature using pyridine and acetic anhydride. The reaction was allowed to occur for 5 hours with constant stirring before precipitation of the polymer solution was carried out in excess methanol. The purification step was carried out numerous times to ensure the removal of unreacted monomers, oligomers, pyridine and acetic anhydride and DMAc.

A 3.5 wt% casting solution was prepared by dissolving the 6FDA – TMPD polymer in dichloromethane at room temperature overnight. The solution was filtered and ultrasonicated to remove any bubbles. The homogenous solution was cast into casting rings on a glass plate, covered and dried at room temperature overnight for at least 12 hours. The membranes were removed from the glass plate and further

dried under vacuum at 80 °C for 24 hours and annealed at 150 °C for 48 hours. They were gradually cooled down in the vacuum oven to room temperature and stored in a dessicator for a week before direct use.

3.1.2 *Gas Supply and Analysis*

Gases were purchased from BOC Gases Australia Limited and used without further purification.

Table 3.2: Gas Purities and Compositions

Name	Grade	Purity
Nitrogen, N_2	High Purity	99.99%
Carbon Dioxide, CO_2	Industrial	99.9%
Helium, He	Ultra High Purity	99.999%
Argon, Ar	High Purity	99.99%
Compressed Air	Zero Grade	21% O_2 in N_2
10%CO_2/90%N_2	NATA Certified	± 0.2%

3.2 Measurement of Physical & Chemical Properties

3.2.1 *Membrane Thickness*

The membrane thicknesses were measured using a micrometer (Mitutoyo, Japan) with an accuracy of approximately ± 1 μm. The commercial membranes were supplied as A4 sheets and were found to be uniform in thickness. However, the dense cast 6FDA – TMPD membranes formed a meniscus on the glass plate with a thick membrane edge close to the casting ring and a thinner central area. The effective membrane area that was tested was cut from the centre of this central area. In order to be consistent, the membrane thicknesses for all membranes; commercial and those prepared in – house, were measured at approximately 15 locations around the cut effective membrane area and averaged. These are presented in Table 3.3.

Table 3.3: Average measured thickness of membranes being investigated.

Polymer	Thickness [µm]
Nafion 115	122 ± 5
Fumapem F - 920	22 ± 2
Fumapem E - 630	32 ± 3
Fumapem E - 540 - GF	40 ± 3
6FDA - TMPD	52 ± 10

3.2.2 *Membrane Density*

A standard technique used for measuring bulk membrane densities is the Buoyancy Technique [210-212]. The weight of the membranes was measured using a Mettler Toledo AB204-5 top loading balance. A pre-dried membrane sample was weighed in air (m_{air}) and then in ethanol (Undenatured AR 100%, Chem-Supply, Australia) ($m_{ethanol}$) in mg. The densities of the polymers were calculated according to the equation 3.1 and are presented in Table 3.4 :

$$\rho_{polymer} = \left(\frac{m_{air}}{m_{air} - m_{ethanol}}\right)\rho_{ethanol} \qquad 3.1$$

Table 3.4: Polymer densities of Membranes at 25°C

Polymer	Density [g/cm^3]
Nafion 115	1.82 ± 0.05
Fumapem F - 920	1.96 ± 0.14
Fumapem E - 630	1.24 ± 0.03
Fumapem E - 540 - GF	1.65 ± 0.03
6FDA - TMPD	1.32 ± 0.04

The higher density of Fumapem E - 540 - GF relative to other SPEEK membrane (E - 630) reflects the glass fibre reinforcement.

3.2.3 *Thermogravimetric Analysis*

Thermogravimetric analysis (TGA) measures mass loss of a sample at a defined increase in temperature. It is commonly used to gain information about the rate of solvent loss and polymer degradation as a function of temperature [162, 172, 213].

A Perkin Elmer Diamond Thermogravimetric Analyser (USA) was used. Samples of approximately 1 mg were sandwiched between two aluminium pans with the top pan perforated. TGA measurements were performed over the temperature range of 50 – 900 °C at a heating rate of 10 °C/min.

3.2.4 *Fourier Transform Infrared Spectroscopy (FTIR)*

The infra – red spectrum of sorbed water was determined on a Perkin Elmer Frontier FT – IR Spectrometer with a Universal ATR Sampling Accessory. The absorbance of samples was measured for the full wavenumber range of 550 – 4000 cm^{-1}. The membranes were first dried in a vacuum over overnight at 30 °C and an FTIR spectrum was measured. The membranes were then suspended in containers with saturated salt solutions of LiCl, K_2CO_3, $NaNO_3$ and KCl that had relative humidities of 15 %, 45 %, 65 % and 85 % respectively in the space above the solutions at 20 °C. These samples were left to equilibrate for one week. The FTIR spectrum of these humidified samples was then measured and the subtraction method was used to obtain the spectra of the sorbed water [214].

3.3 Measurement of Penetrant Transport Properties

3.3.1 *Pure Gas Permeation Set-up*

Pure gas permeability was measured on a constant volume - variable pressure (CVVP) experimental rig described in detail by Duthie *et al.* [215] (Figure 3.1). The membrane cell and a heating loop were housed in a fan forced oven (Scientific Equipment Manufactures). The oven was modified to incorporate ¼'' Swagelok fittings and stainless steel tubing through the sides of the oven. The permeate/downstream side was sent to a temperature controlled water bath and is of a known constant calibrated volume. A membrane sample with a surface area of 11.95 cm^2 was placed in the membrane cell and both downstream and upstream were evacuated to < 10^{-4} mbar using a vacuum pump. Before introducing feed gas,

the downstream side was isolated from vacuum to determine the leak rate of air into the constant volume from fittings and tubing. This was done by measuring the increase in the rate of pressure of the evacuated constant volume. The feed gas was supplied to the upstream side at a set temperature and pressure. The increase in pressure on the downstream side due to gas permeation through the membrane was monitored. The feed and permeate pressures were determined by a MKS Baraton 0 - 6895 kPa transducer and a MKS Baraton 0 - 1.33 kPa transducer, respectively. The permeate side transducer was protected by a pressure relief valve.

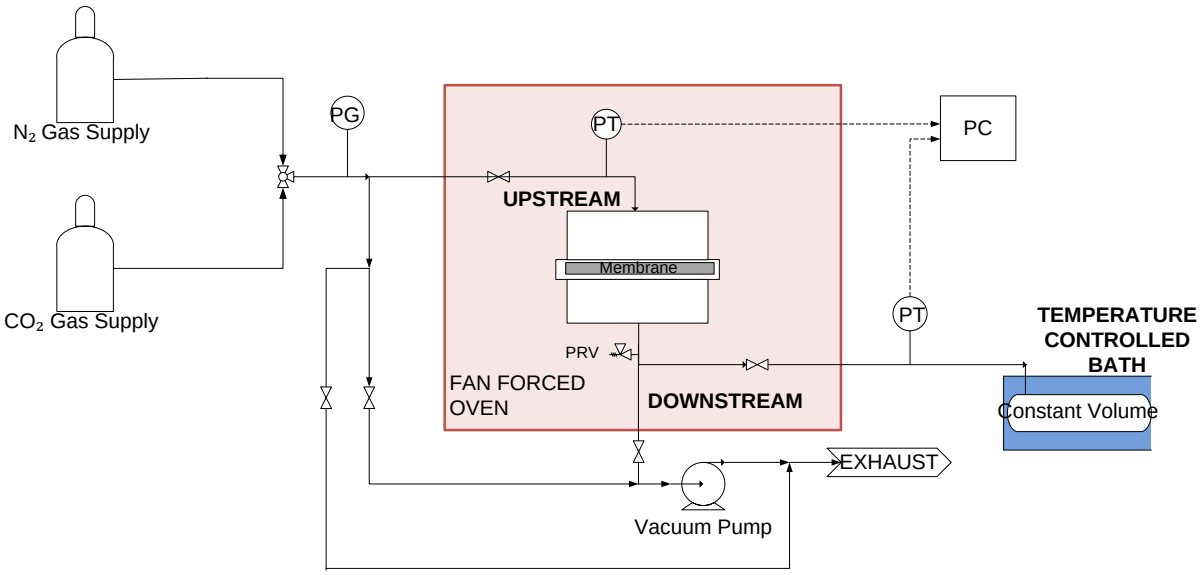

Figure 3.1: Constant Volume - Variable Pressure (CVVP) set – up used to measure pure gas permeabilities and selectivity

The signal outputs from the pressure transducers and thermo couples were relayed via a National Instruments data logging card and then logged electronically using NI Labview X, at 1 sec intervals. The volume in the CVVP permeation apparatus, V_c, was calibrated with a standard Styrex polystyrene film (Mitsubishi Plastics, Japan). The Styrex polystyrene film had a thickness of 40 μm and an oxygen permeability of 2.27 x 10^{10} $cm^3.cm/cm^2.s.cmHg$ at 30 °C under a feed pressure of 1 atm.

The permeability of the gas is then determined using steady state pressure gradient using the following equation:

$$P = \frac{273.2 \times 10^{10}}{760} \cdot \frac{lV_c}{AT\frac{(p_f \times 76)}{14.7}} \cdot \left[\frac{dp}{dt} - \left(\frac{dp}{dt}\right)_{leak}\right] \quad 3.2$$

Where, P is the steady state permeability in Barrer (1 Barrer= 10^{-10} $cm^3.cm/cm^2.s.cmHg$), l is the membrane thickness in cm, V_c the volume of calibrated downstream chamber in cm^3, A is the effective area of the film in cm^2, T is the operating bath temperature in K, p_f is the absolute feed pressure in psia, dp/dt is the slope of pressure increase in the permeate side known volume versus time in $mmHgs^{-1}$, and $(dp/dt)_{leak}$ is the rate of ambient air leaking into the system determined before each gas permeation testing in $mmHgs^{-1}$.

3.3.2 *Low Temperature Mixed Gas Permeation Set-up*

A variable volume – constant pressure experimental rig was designed and constructed by Chen *et al.* [54] to measure simultaneous water vapour and gas permeability for a wide range of temperature (20 – 60 °C) and pressure (1 – 10 bar) [50] (Figure 3.2). A feed gas supply (either pure or gas mixture) was fed into a saturator filled with water followed by a demister to remove any water droplets. Both the saturator and demister were housed in a temperature controlled bath which allowed fine control of the water vapour activity of the humidified feed stream. Stainless steel tubing from the outlet of the demister to the inlet of the fan forced oven was constantly heated by a flexible heating tape (Cole - Parmer) to ensure no water condensation occurred [54].

The humidified gas stream was then passed through a humidity and temperature transmitter (HMT, Probe type 334, Vaisala Oyj, Finland, measurement range: 0 - 100% RH, operating ranges: 70 - 180 °C, 0 - 100 bar) which was fitted into the fan forced oven. The oven also contained a membrane permeation cell with another HMT housed on the permeate side. The membranes with a surface area of 10.75 cm^2 were supported by a porous stainless steel plate and had stainless steel wool placed on both feed and permeate side to promote mixing. The temperature of the gas stream entering the oven was always set to be slightly higher than the operating temperature of the oven. The total pressure and flowrate (mass flow indicator MFI 1, Aalborg) of the feed and retentate streams were controlled by the back pressure controller (BPC, Cole - Parmer) in the retentate stream. The

permeate side of the membrane used argon (UHP Ar, BOC Australia) as the sweep gas to remove any components permeated through the membrane. The water vapour permeability was calculated using HMT2 and gas analysis was performed by a gas chromatography (450-GC, Varian, Inc.). The temperature and RH % of HMT 1 and 2, as well as the gas composition of the permeate stream were recorded in 10 minutes interval until the system equilibrium was reached (typical 1 - 2 hours for each water activity) [54].

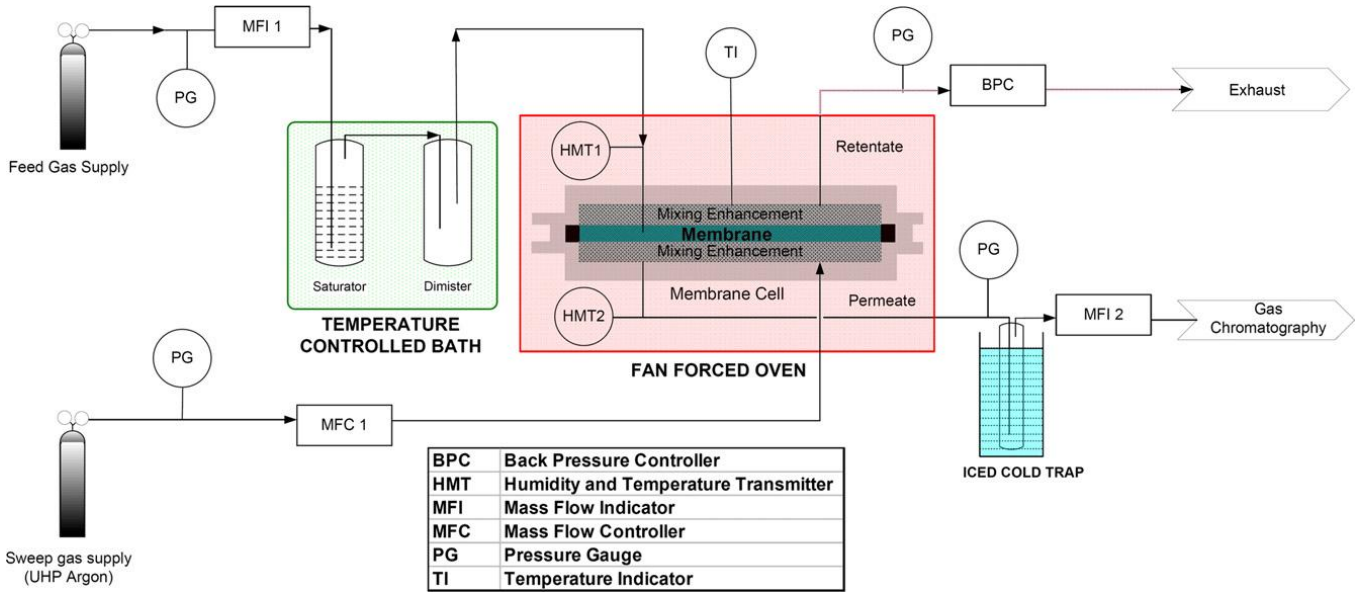

Figure 3.2: Water Vapour Permeation Apparatus [54].

3.3.3 *High Temperature Mixed Gas Permeation Set-up*

A novel mixed gas permeation set-up (Figure 3.3) was developed in this work for measuring the permeability of steam and mixed gases for a range of pressures and temperatures (0.5 – 5 bar and 70 – 150 °C).

Pure CO_2 (0.5 - 4 Bar) or N_2 (0.5 - 4 Bar) was fed to a temperature controlled oven. It was preheated by passing it through a heating coil before being mixed with steam in a mixing bomb. The steam was supplied by a Simon Boiler (SB2S Series) at a maximum pressure of 6.5 bars and 168 ^{0}C. The pressure of the steam was controlled using a steam pressure regulator to 1 – 4 Bar, which subsequently controlled the temperature of the steam supplied to the rig. A Tec fluid M21/G steam flow meter (MFI1, 0 – 6 kg/hr, Process Control Services) with a needle valve placed upstream was used to control the flow rate of the steam supplied. The flow

meter was calibrated for 6 bar steam. Hence, deviations from this operating pressure required a "Pressure Correction Factor" (k_p) to get an accurate estimate of the flow rate supplied.

$$\boldsymbol{k_p = \sqrt{\frac{P_1}{P_{cal}}}}$$

$$\boldsymbol{F_1 = k_p . F_{cal}}$$

Where, P_{cal} and F_{cal} are the calibrated pressure and flow rate reading from the flow meter, respectively and P_1 and F_1 are the working pressure and flow rate, respectively. The total pressure of the combined feed stream changed from approximately 0.5 to 4 bars based on its temperature.

The humidity of the water/gas mixture was controlled by the flow rates of the gases being mixed. Pure CO_2 and N_2 flow rates were controlled using Aalborg Mass Flow Controllers (MFC2 and MFC3, 0 – 5 L/min). The wet steam feed mixture was passed through a humidity and temperature transmitter (HMT1, Probe type 334 Vaisala Oyj, Finland, measurement range: 0 - 100% RH, operating ranges: -70 to 180 °C, 0 - 100 bar) custom fitted into the oven and into an inverted membrane cell. While gases are pre – heated prior to mixing with steam to ensure no water condensation occurs, the membrane cell was inverted to ensure any condensed water did not accumulate on the surface of the membrane. Furthermore, this cell was specially designed to contain a magnetically driven stirring mechanism on both feed and permeate side in order to eliminate concentration polarisation (Figure 3.4). The circular membrane had an effective surface area of 15.90 cm^2 and was supported by a porous stainless steel circular disk to withstand high feed pressures.

Argon (HP Ar, BOC Australia) and helium (HP He, BOC Australia) were used as a sweep gases on the permeate side to continuously remove permeated components from the membrane cell. Sweep gas pressure was set at 60 kPa while the flow rate was controlled using an Aalborg Mass Flow Controller (MFC1, 0 – 250 mL/min). A second humidity transmitter (HMT2), similar to the feed side HMT, was used to determine the permeate water content. The permeate stream was then chilled in

an iced cold trap before being passed through a rotameter (MFI2, Cole – Parmer). The dehydrated permeate stream was finally sent to a gas chromatography unit (GC 7820A, Agilent Technologies) to analyse the CO_2 and N_2 composition. Argon was used for CO_2 permeation experiments while helium was used for N_2 permeation experiments as both argon and N_2 had the same retention times.

A membrane was placed in the membrane cell and the system sealed and heated to the desired temperature. During this time, dry gases were fed through both feed and permeate side to calibrate the humidity probes by reducing the humidity to below 1% which generally took 2 – 3 hours. Once this was achieved, steam was introduced in the rig. The system was allowed to reach steady state which generally took 1 – 2 hours for each water activity. The temperature and humidity from HMT 1 and 2 as well as the gas composition from the GC was then recorded. The humidity and temperature transmitters measure the vapour content of the streams and were calibrated monthly using a HMK 15 salt bath calibrator (Vaisala Oyj, Finland) to ensure their accuracy.

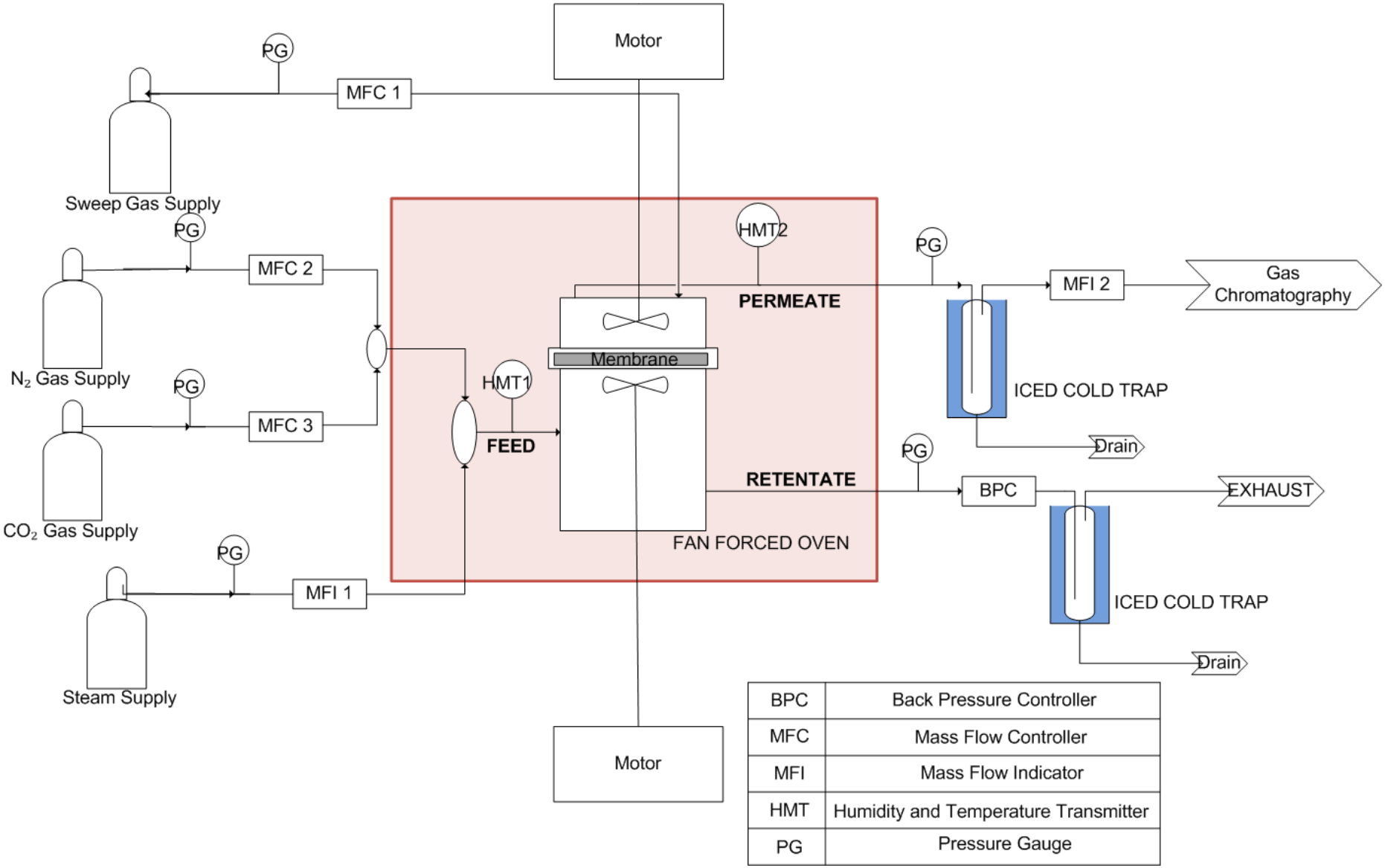

Figure 3.3: Schematic of High Temperature Steam and Mixed Gas Permeation Experimental Rig.

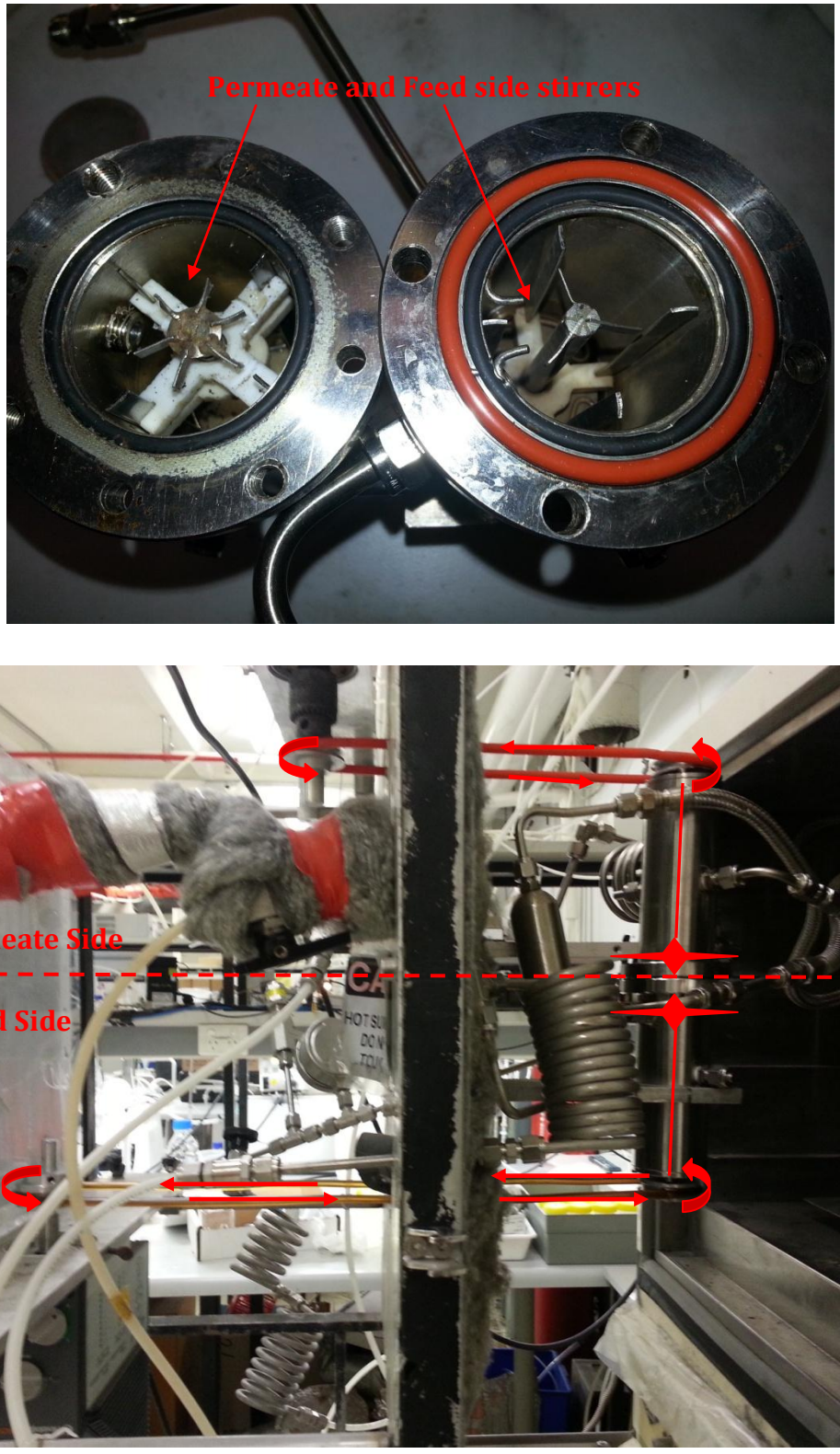

Figure 3.4: Photographs of the mechanical stirrers on feed and permeate side.

3.4 Concentration Polarisation Elimination

Concentration polarisation occurs when water permeation through a membrane is fast compared to other permeating components as discussed in section 2.6. Hence, before taking permeability measurements, it is essential to ensure that concentration polarisation does not affect the results. Figure 3.5 shows the effects of stirrer speed on permeance measurements at low water activities at 70 °C and 150 °C for Nafion 115. As shown, the water permeance for 70 °C increases with increasing stirrer speed up to 630 rpm above which no significant increase in visible. This is the minimum stirrer speed for these conditions above which concentration polarisation effects are insignificant. The permeance is lower for 150 °C due to reduced water solubility at higher temperatures; therefore the effect of concentration polarisation is lower compared to that at 70 °C. Based on this preliminary work, all subsequent experiments for Nafion 115 were conducted at a stirrer speed of 700 rpm to ensure the effect of concentration polarization was truly eliminated.

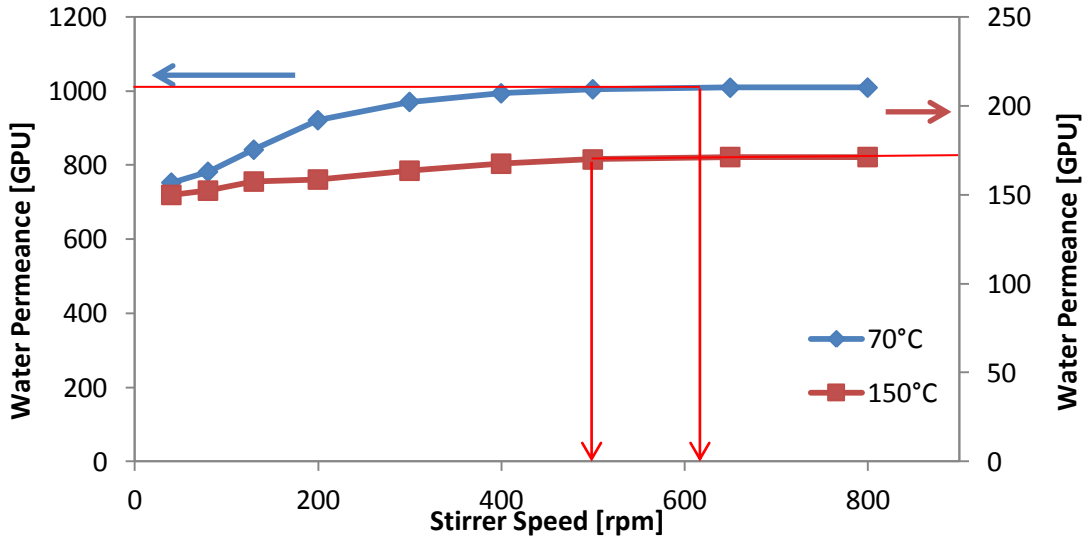

Figure 3.5: Water permeance as a function of feed side stirrer speed for 70 °C and 150 °C at low feed water activity of 0.18 for Nafion 115.

Concentration polarization might also occur on the permeate side if the permeated water is not removed continuously. Hence, investigation of the sweep gas flow rate needed to eliminate concentration polarization is also required. As shown above, the effect of concentration polarization for a given water activity is less severe at a

higher temperature. Therefore, only the sweep gas flow rate at 70 °C was investigated. It was found that the water permeance at 70 °C and low water activity increases with increasing sweep gas flow rate up to 48 mL/min above which no significant increase was observed (Figure 3.6). Based on this, all subsequent experiments were conducted with a sweep gas flow rate of 60 mL/min to ensure the effect of concentration polarization was truly eliminated on the permeate side.

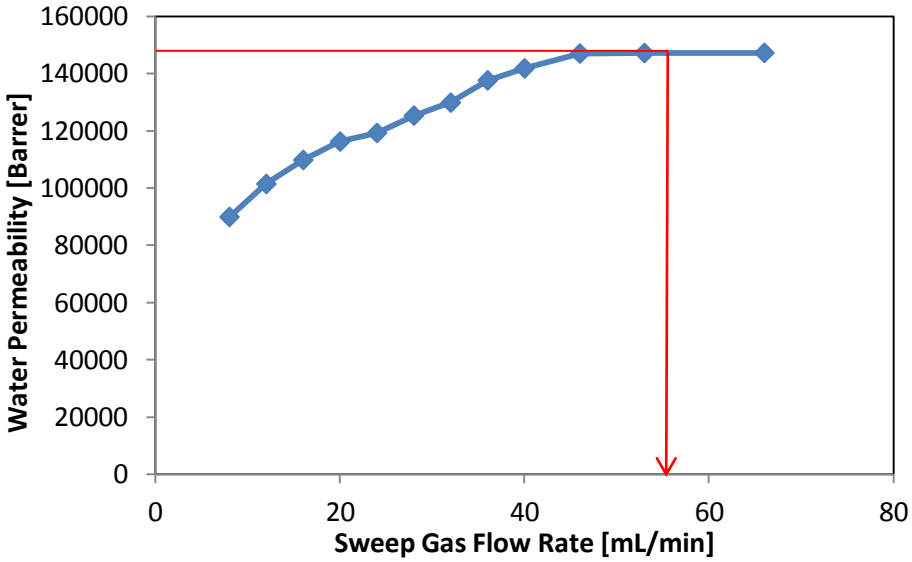

Figure 3.6: Water permeability through Nafion 115 as a function of sweep gas flow rate at 70 °C and low feed water activity of 0.18.

For investigation of SPEEK permeation properties, concentration polarisation was removed using mechanical stirrers on both feed and permeate sides. Figure 3.7 shows the feed stirrer speed needed to eliminate it for the two SPEEK membranes. SPEEK IEC 1.9 meq/g has a higher sulphonation degree and as a result a greater water permeance compared to IEC 1.6 meq/g. For this reason, the minimum stirrer speed required to eliminate concentration polarization for IEC 1.9 meq/g is 500 rpm compared to 300 rpm for IEC 1.6 meq/g. These are the speeds above which no change in water permeance is observed. All subsequent experiments were conducted with a feed side stirrer of 600 rpm to ensure concentration polarisation is eliminated on the feed side.

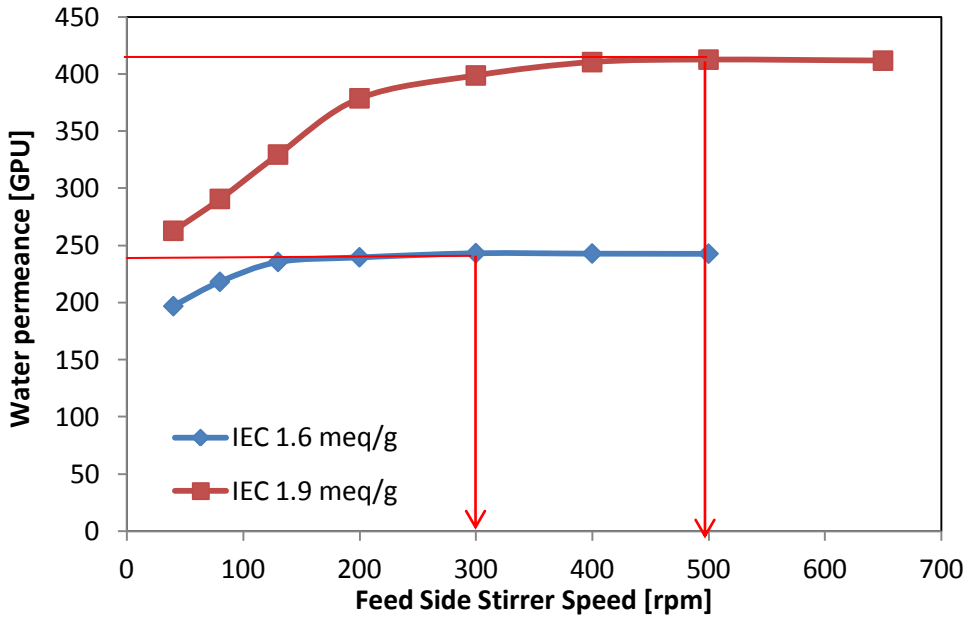

Figure 3.7: Water permeance as a function of feed side stirrer speed for SPEEK IEC 1.6 meq/g and IEC 1.9 meq/g at 70 °C and a feed water activity of 0.20.

As with the feed side, it is essential to eliminate concentration polarization on the permeate side. Figure 3.8 shows the permeate side stirrer speed needed to achieve this for the two SPEEK membranes. Again, IEC 1.9 meq/g has a higher water permeance and thereby requires a greater stirrer speed of 170 rpm compared to 150 rpm needed for IEC 1.6 meq/g. All subsequent experiments were conducted with a permeate side stirrer speed of 200 rpm to ensure concentration polarisation was truly eliminated on permeate side.

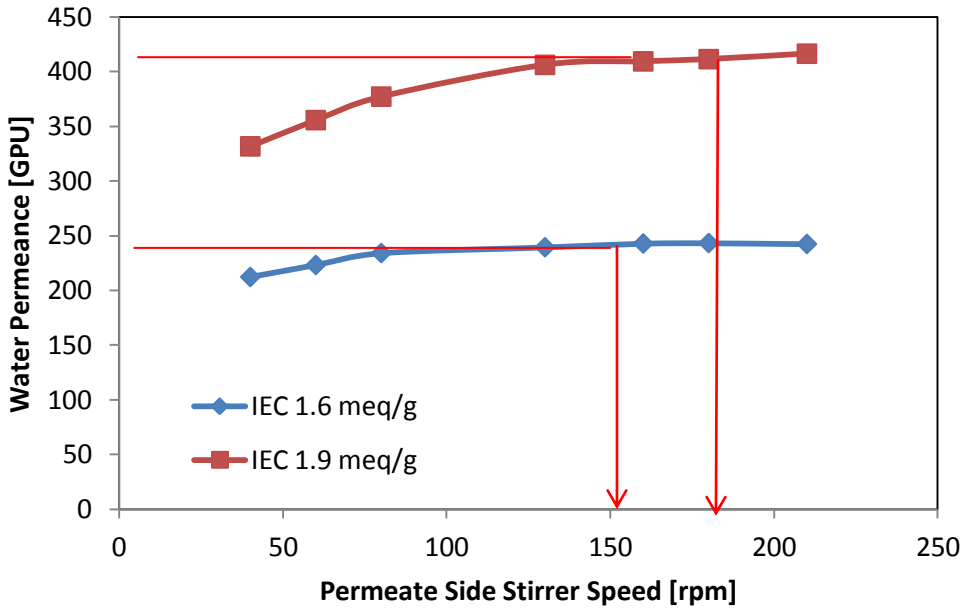

Figure 3.8: Water permeance as a function of permeate side stirrer speed for SPEEK IEC 1.6 meq/g and IEC 1.9 meq/g at 70 °C and a feed water activity of 0.20.

Similarly, the minimum stirrer speeds required to eliminate concentration polarization on feed and permeate sides for 6FDA – TMPD were 350 rpm and 150 rpm, respectively (Figure 3.9). These are the speeds above which no change in water permeability was observed hence all measurements were taken with a feed side and permeate side stirrer speed of 400 rpm and 200 rpm, respectively.

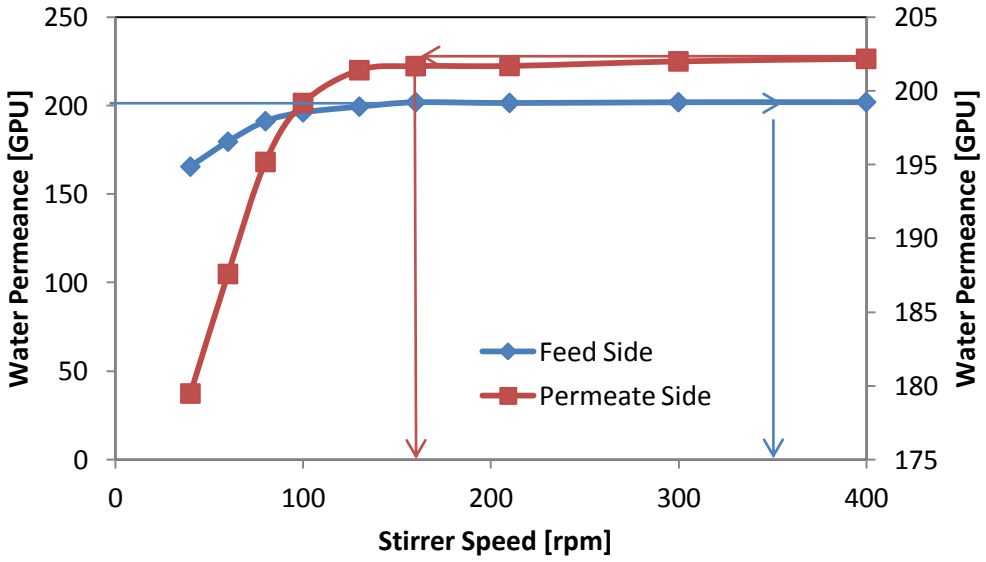

Figure 3.9: Water permeance as a function of feed and permeate side stirrer speed for 6FDA -durene at 70 °C and a feed water activity of 0.20.

3.5 Permeability Evaluation

The water activity is related to the relative humidity (RH) by the following equation where p_{H2O} is the partial pressure of water vapour and p_{sat} is the saturated vapour pressure at the stream temperature:

$$a_w = \frac{RH}{100} = \frac{p_{H_2O}}{p_{sat}} \quad \textbf{3.3}$$

The flux through the membrane is given by Equation 3.4 where Q_{per} is the dehydrated permeate flow rate (cm^3 (STP)/s), A_{eff} is the effective membrane area (cm^2), y_i is the mol fraction of the gas component i in permeate stream. For water vapour and CO_2, this is calculated from the HMT partial pressures and from gas composition from GC, respectively. The dry permeate stream is considered to be an ideal gas ($\gamma_i = 1$) as it contains mostly argon at atmospheric pressure with trace amounts of CO_2.

$$J_i = \frac{Q_{per} y_i \gamma_i}{A_{eff}} \quad \textbf{3.4}$$

3.6 Water Vapour Sorption Measurement

3.6.1 *Gravimetric Sorption Analyser*

A Gravimetric Sorption Analyser (GHP-FS, with a Cahn D-200 balance, VTI Scientific Instruments, Florida) was used to conduct sorption measurements, as shown in Figure 3.10.

The sorption analyser was operated in flow mode for water vapour sorption experiments. This is due to the condensable nature of water vapour and is the most accurate approach to measuring water sorption [216]. A membrane sample (> 10 mg) was placed in the temperature controlled sample holder. The system was evacuated and heated to 50 °C to remove any air and existing water vapour from the samples. The sample chamber and vapour saturator are set to the desired temperature. This consequently determines the maximum water partial pressure that can be achieved. Dry helium gas was bubbled through water in vapour saturator to produce a fully water-saturated stream. Humidified gas of varying humidities was then obtained by mixing varying amounts of dry helium with this

water-saturated stream. Humidified stream of a certain RH % was continuously passed over the sample at slightly higher than atmospheric pressures. The weight gain associated with water sorption was recorded until it varied by <0.01%. The RH % of the humidified stream was then increased step by step to achieve a sorption isotherm. Desorption runs were carried out in the opposite manner where water activity was reversed step by step.

The calculations for the sorption isotherms were based on the dry volume of membrane as shown in Equation 3.5. This volume will change as the membrane swells but the data was not corrected to account for this. Furthermore, the Gravimetric sorption analyser failed towards the end of the project limiting the measurements that could be undertaken.

$$\boldsymbol{C = \frac{(m_f - m_{i,dry}).V_{H2O}}{V_{p,dry}.MW_{H2O}}} \qquad \textbf{3.5}$$

Where, C [cm^3[STP]/cm^3.polymer] is the water concentration in the polymer, m_f [g] is the final equilibrium mass of the polymer and the water absorbed and $m_{i,dry}$ [g] is the initial dry weight of the polymer. V_{H2O} is the volume of 1 mol of water at standard temperature and pressure [22,414 cm^3 .STP/mol], $V_{p,dry}$ is the volume of dry polymer and MW_{H2O} is the molecular weight of water [18 g/mol].

3.6.1.1 Liquid Water Uptake

Membranes were dried in vacuum oven overnight before being weighed and placed in liquid water at 25 – 70 °C for a week. The samples were removed, blotted dry with kim wipes to remove excess water and weighed. The water uptake (wt %) was measured by the following equation, where m_f and m_i are the final and initial mass of the sample, respectively :

$$\boldsymbol{Water\ Uptake\ (wt\%) = \frac{m_f - m_i}{m_i} \times 100} \qquad \textbf{3.6}$$

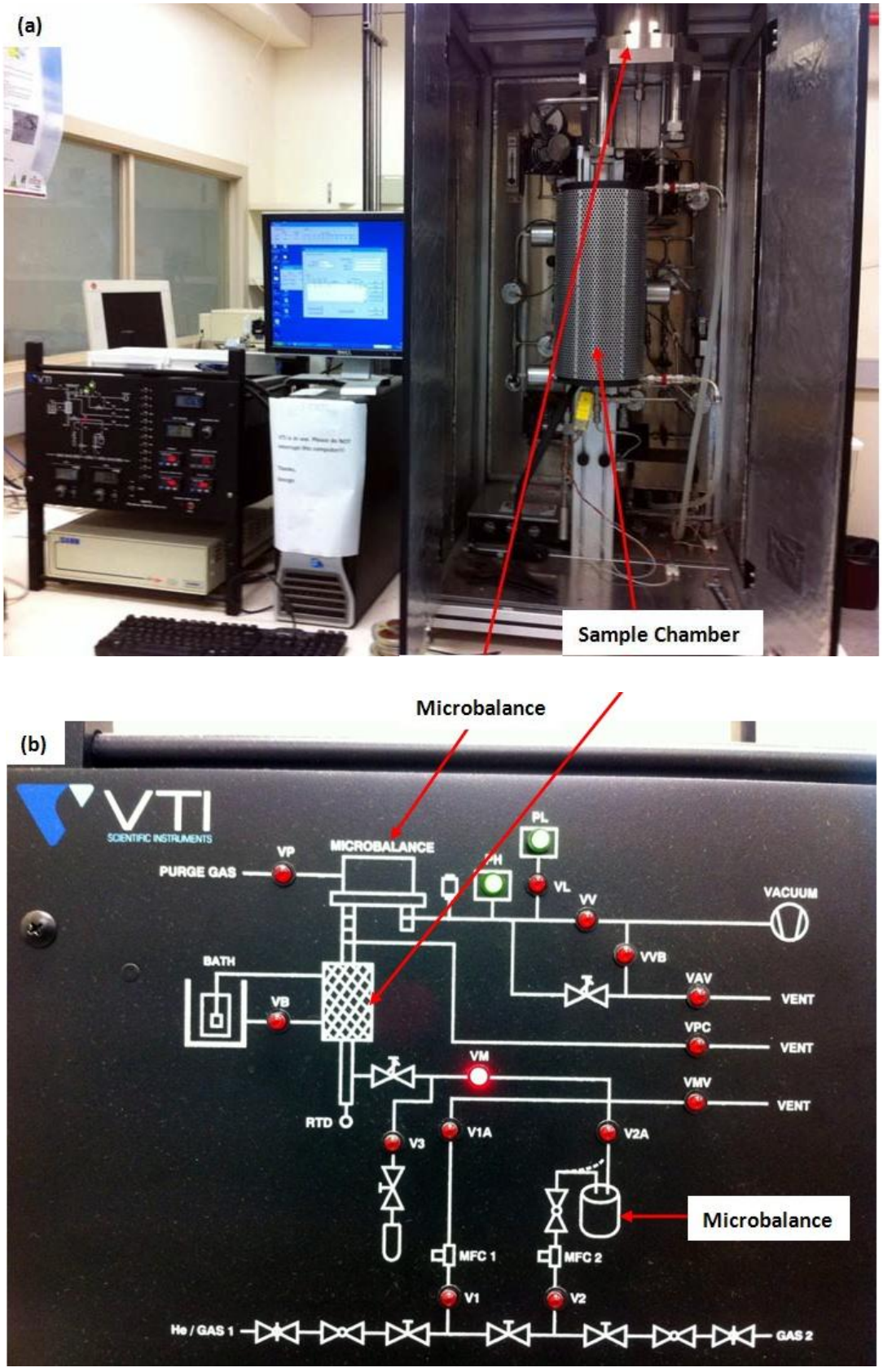

Figure 3.10: Photograph (a) and Schematic diagram (b) of the Gravimetric Sorption Analyser.

Chapter 4 Water Permeation & Sorption Properties of Nafion 115 at Elevated Temperatures

4.1 Introduction

Perfluorosulphonic acid (PFSA) based membranes such as Nafion 115 have been extensively researched for fuel cell applications as presented in section 2.7.1. These studies have focused on water flux through Nafion at temperatures below 100 °C. To consider its application for flue gas dehydration purposes, Nafion behaviour at elevated temperatures needs to be understood. Therefore, the aim of this work is to investigate the water, CO_2 and N_2 permeation properties of Nafion 115 as a function of water activity at 70 – 150 °C. Furthermore, water sorption properties of Nafion at 20 – 40 °C will also be investigated and modelled using the modified Dual Mode Sorption Model discussed in section 2.5.3.

4.2 Water Sorption and Modelling

The concentration of water in the DuPont Nafion 115 membrane as a function of temperature is presented in Figure 4.1. The isotherm curve is concave to the pressure axis at low activities but convex at high activities. Water sorption isotherms of this form have been observed for Nafion by Choi and Datta [127], Morris and Sun [130], Jalani and Datta [156], Devanathan *et al.* [217-219], De Anglis *et al.* [140] and Hinatsu *et al.* [126]. At low activities, water molecules solvate the hydrophilic sulphonate groups and fill the free volume within the polymer. This water filling behaviour is more obvious when the solubility is plotted (Figure 4.2). As the activity increases, this solubility falls rapidly as the free volume is filled. At higher water activities swelling of the membrane causes the uptake to rise resulting in a convex curve shape [126, 130, 156]. This increase is obvious in the concentration data (Figure 4.1) but only has a significant impact upon solubility at water activities greater than 0.9 (Figure 4.2).

An increase in temperature also results in an increase in water concentration at any given water activity. This reflects an increasing equilibrium water partial pressure (p_{sat}), which in turn results in an increased water partial pressure at a given activity. Once the concentration is divided by this water partial pressure to

give the solubility parameter (Figure 4.2) the temperature trend inverts, with the greatest solubility at the lowest temperature. Higher temperatures increase the mean kinetic energy of the water molecule which weakens forces between water and polymer thereby resulting in reduced solubility at high temperatures; a phenomenon consistent with most polymeric materials [54, 156, 220]. Concentration data from Morris and Sun [130], Rivin *et al.* [221], Zawodzinski *et al.* [124] and Jalani and Datta [156] were converted to solubility by dividing with partial pressures and these were found to be in good agreement with the solubility data obtained in this study. The heat of sorption calculated using equation 2.43, gives ΔH_s = -40.8 ± 2.4 kJ/mol for a water activity of 1. This is comparable to heat of sorption value of -44 kJ/mol obtained for Nafion 117 by Watari *et al.* [193].

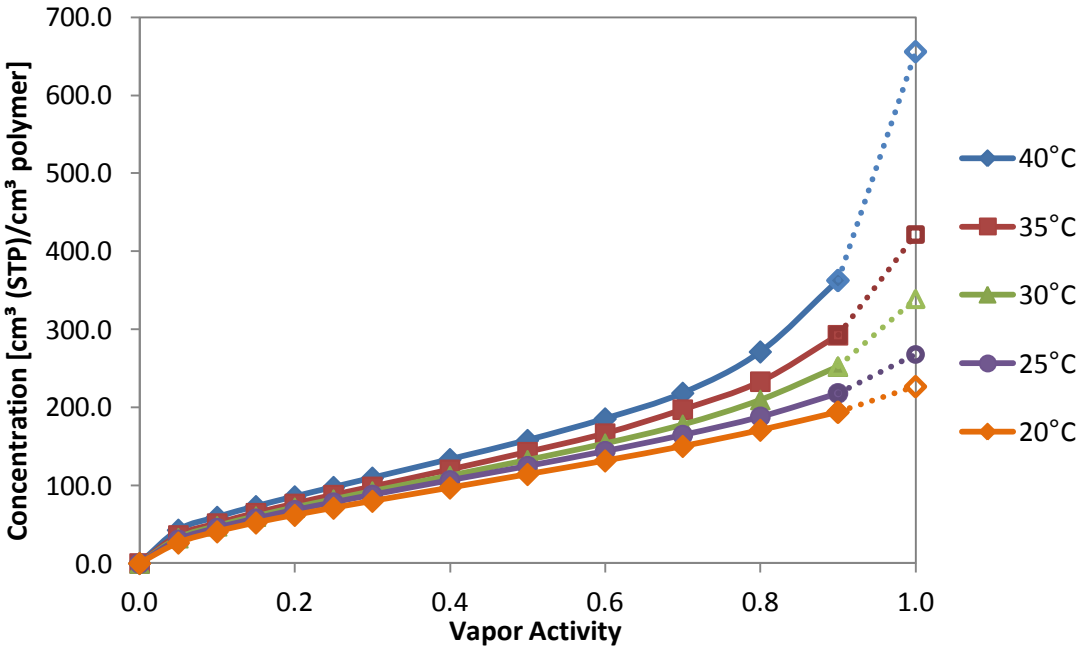

Figure 4.1: Water sorption isotherms for Nafion 115 at a range of temperatures (open data points measured in liquid water).

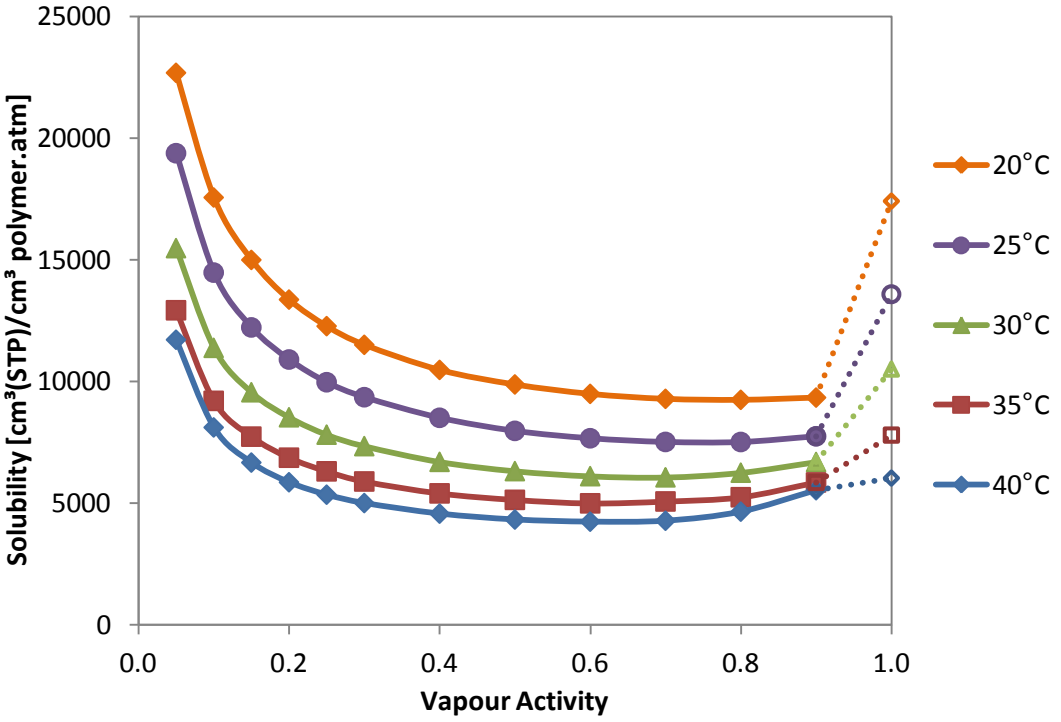

Figure 4.2: Water solubility in Nafion as a function of temperature (open data points measured in liquid water).

The Zimm and Lundberg clustering analysis (Equation 2.19) was performed on the sorption isotherms in Figure 4.1. If G/V_w > -1, the forces between the water molecules are significant enough for them to accumulate and form clusters. The cluster function (G/V_W) for Nafion 115 as a function of temperature is shown in Figure 4.3. Clusters form at higher water activities and higher temperatures due to the increased water concentration and the resultant increase in water-water interactions. It is noteworthy that while Figure 4.2 may suggest that liquid water solubility is different to that which might be recorded for vapour solubility at 100% humidity, such differences are much less apparent in Figure 4.1 and Figure 4.3, indicating that Schroeder's Paradox may not be a real phenomenon but an artefact only of the very steep increase in solubility as the water activity moves from 0.9 to 1.

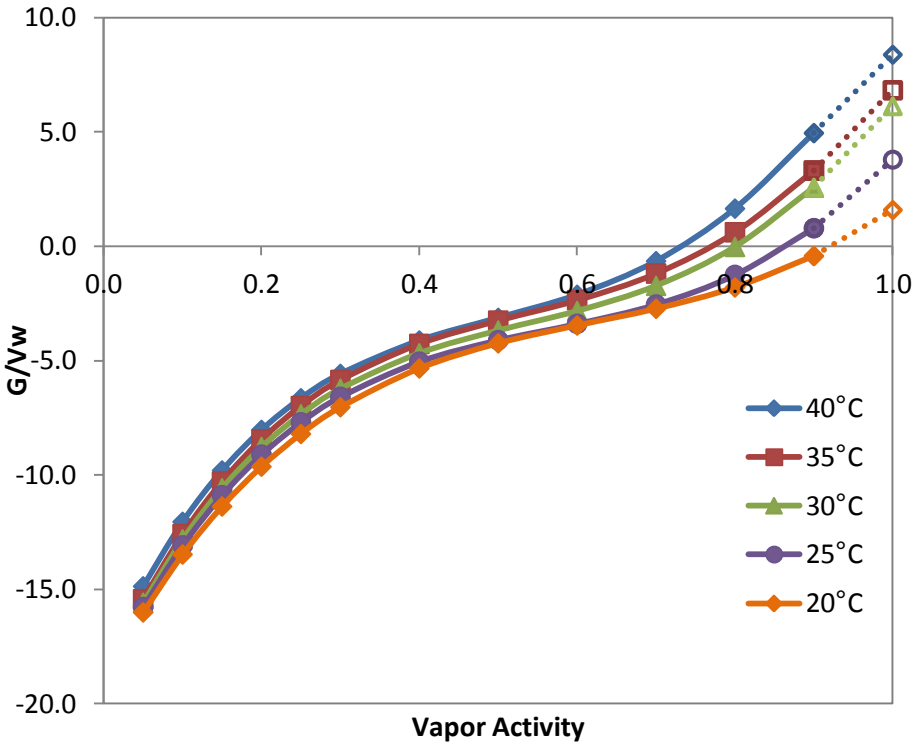

Figure 4.3: Water cluster analysis of Nafion 115 as a function of temperature (open data points measured in liquid water).

Water uptake (λ) isotherms of the type presented in Figure 4.4 can be fitted to a model based on the new modified Dual Mode sorption model discussed in section 2.5.3 [72, 75]. This is presented in Equation 4.1, in terms of the water uptake (λ) defined as the moles of water per mole of SO_3H sites in a sulphonated polymer.

$$\boldsymbol{\lambda(a_w) = \frac{\lambda_m.k'.a_w}{1-k'.a_w} + \frac{\lambda_m.(A'-1).k'.a_w}{1+(A'-1).k'.a_w}} \qquad \textbf{4.1}$$

Where, $\lambda\ (a_w)$ is the moles of water per mole of sulphonic acid site (SO_3H) at a given water activity. λ_m is the monolayer sorption capacity or the moisture content of the whole free monomolecular surface of the polymer. k' and A' have the same definitions as described in section 2.5.3. The parameters λ_m, k' and A' can be temperature dependent and represented by Arrhenius-type equations shown below:

$$\boldsymbol{\lambda_m = \lambda_o e^{\left(\frac{-E_\lambda}{RT}\right)}} \qquad \textbf{4.2}$$

$$\boldsymbol{k' = k_o e^{\left(\frac{-E_k}{RT}\right)}} \qquad \textbf{4.3}$$

$$A' = A_o e^{\left(\frac{-E_A}{RT}\right)} \quad 4.4$$

Water uptake isotherms shown in Figure 4.4 were fitted to these four equations using non-linear regression techniques and the resulting parameters are presented in Table 4.1. It was found that parameters *A'* and *k'* are temperature dependant, while within the experimental uncertainties parameter λ_m is not.

Table 4.1: Estimated fitting parameters for a range of temperatures for Nafion 115.

Parameter	Nafion 115
λ_m [mol.H_2O/mol.SO_3H]	2.77 ± 0.04
k_o [-]	100 ± 26
E_k [kJ/mo]	12.6 ± 0.7
A_o [-]	3570 ± 60
$E_{A'}$ [kJ/mol]	14.6 ± 0.4

The parameters fitted to the water uptake experimental data at 25 °C are comparable with that obtained by Li *et al.* at 25 °C as shown in Table 4.2 [75]. Furthermore, this model (dotted line) fits well to the experimental data points as shown in Figure 4.4.

Table 4.2: Comparison of fitting parameters at 25°C compared with literature.

	This Work	Y.Li *et al.*, 2013 [75]
Material	Nafion 115	Nafion 117
T [°C]	25	25
λ_m [mol H_2O / mol SO_3H]	2.83 ± 0.08	3.1
k'	0.62 ± 0.01	0.8
A'	9.90 ± 0.55	11.4

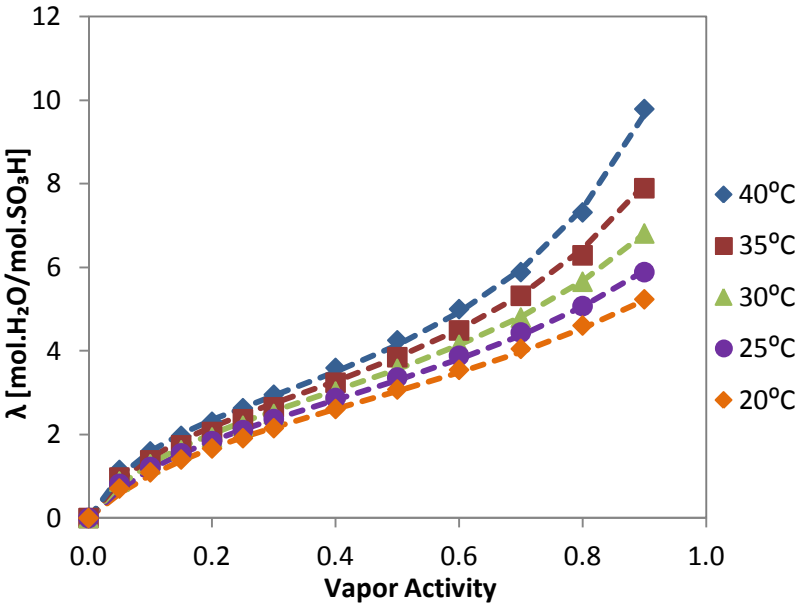

Figure 4.4: Water uptake (λ) in Nafion 115 as a function of vapour activity and temperature. The experimental data points are fitted with the fitting parameters obtained in Table 4.1 (dotted line).

4.3 Theoretical Glass Transition Temperature

The liquid water concentrations at 20 – 40 °C and the Fox equation (Equation 2.4) were used to estimate the theoretical glass transition temperature, T_g. This theoretical T_g is a function of the water sorption at a given experimental temperature and is presented in Figure 4.5. As shown, the estimated theoretical T_g for the experimental temperatures of 20 – 40 °C for Nafion 115 lies firmly in the rubbery region below the red dotted transition line. This confirms the state of Nafion 115 as a rubbery polymer in the temperature region being investigated here.

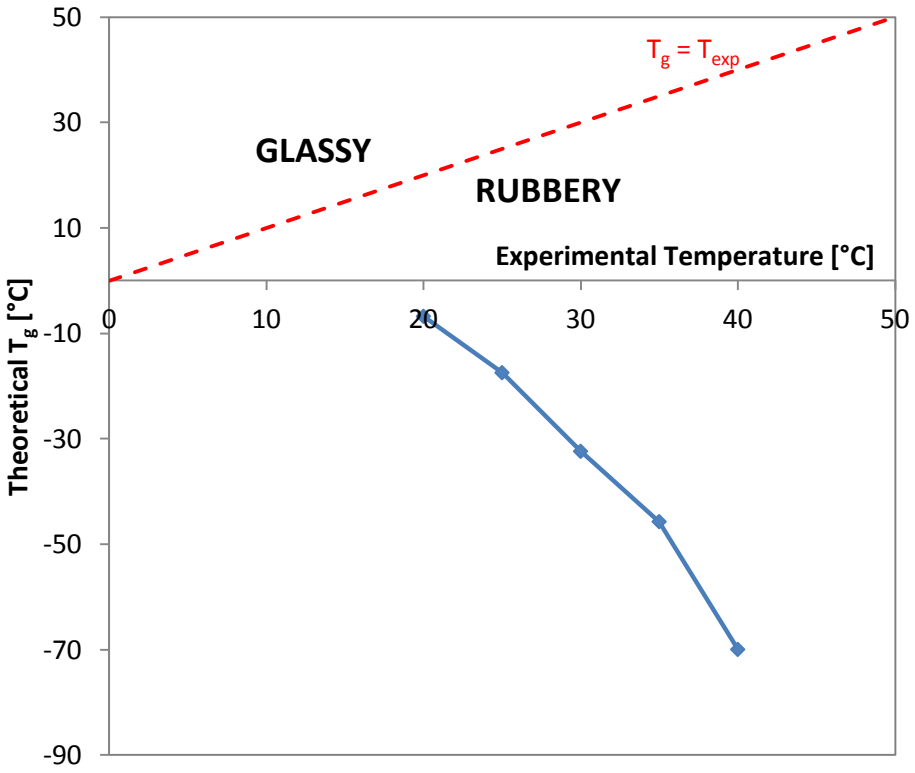

Figure 4.5: Theoretical T_g as a function of experimental temperature calculated from liquid water sorption data points. The dotted red line is the transition line between glassy and rubbery states.

4.4 Validation of Experimental Rig

The high temperature water permeation experimental set-up shown in Figure 3.3 required validation to ensure accurate permeance readings was obtained. Hence, the water permeance values obtained in this study are first compared with available literature values in Figure 4.6. Most studies report water flux through Nafion but for purposes of comparison these have been converted to water permeance using the membrane area reported in these studies. Furthermore, for simplicity Figure 4.6 only compares data obtained at an upstream feed water activity of $a \sim 0.9$. The permeance difference observed at 80 °C for Motupally and Becker [150] where the measurement is at $a = 1$ is most likely due to this difference in feed water activity. Majsztrik *et al.* [22] reported water flux through Nafion 115 at 30 – 80 °C and a range of water activities. These results compare well with the present work. Steam availability at temperatures lower than 70 °C was a limitation of the current experimental set – up. To study water permeance at

30 °C, the water permeation experimental rig constructed by Chen [54] was used. As shown, a water permeance of ~15,200 GPU was obtained using this rig and this value also compares well with the Majsztrik results.

Romero and Merida [151] have also studied the water flux through Nafion as a function of temperature. However, their values are significantly different from those obtained in this study. This is possibly because these authors did not consider the effect of concentration polarization. Romero and Merida had a set-up with stagnant saturated nitrogen on the feed side and a continuous helium flow on the permeate side. The decreased availability of water at the membrane surface acts as a barrier to water diffusivity which consequently gives reduced flux [151]. Conversely, Majsztrik *et al.* reduced concentration polarisation by ensuring a large excess flow on the feed side [22]. This figure highlights the important need to take the effect of concentration polarization into account so as to obtain the true nature of the permeation properties of a polymer.

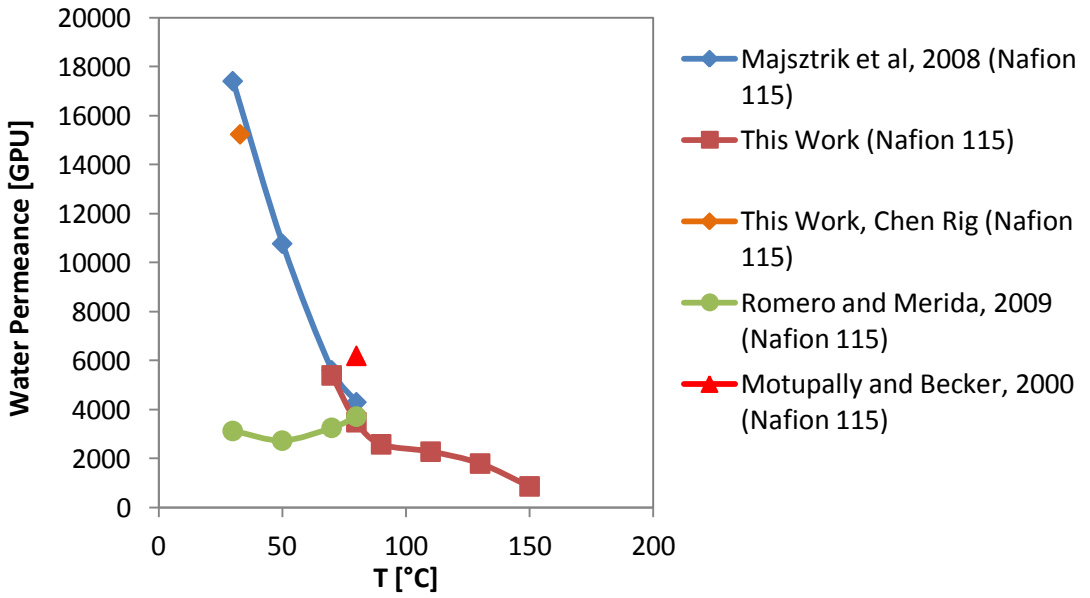

Figure 4.6: Water permeance through Nafion 115 obtained in this study compared with that from literature at upstream water activities of 0.9 to 1.0. The data for Motupally and Becker is at an activity of 1.

A detailed comparison of data for the water permeance at 70 °C and 80 °C as a function of water activity is shown in Figure 4.7. The dotted lines are the permeances obtained in this study and the solid lines are those obtained by

Majsztrik *et al.* [22]. As presented, the water permeance values compare well up to feed water activity of ~ 0.9. However, there are significant differences at a feed water activity of 1 at both temperatures i.e. ~ 17,000 GPU at 80 °C for Majsztrik compared to ~7000 GPU at the same temperature found in this study. This could be a result of the different pre-treatment methods utilised. The membranes in the current study were pre – dried whereas permeance experiments in Majsztrik study were done with fully hydrated membranes. As discussed above, the very rapid change in water solubility that occurs as the humidity reaches 100%, means that there is significant experimental uncertainty in any gas phase measurements within this humidity range [128]. It is possible that the pre-dried membranes used in our work had not indeed reached steady state at this humidity and a more extended experiment would allow the permeance to increase further.

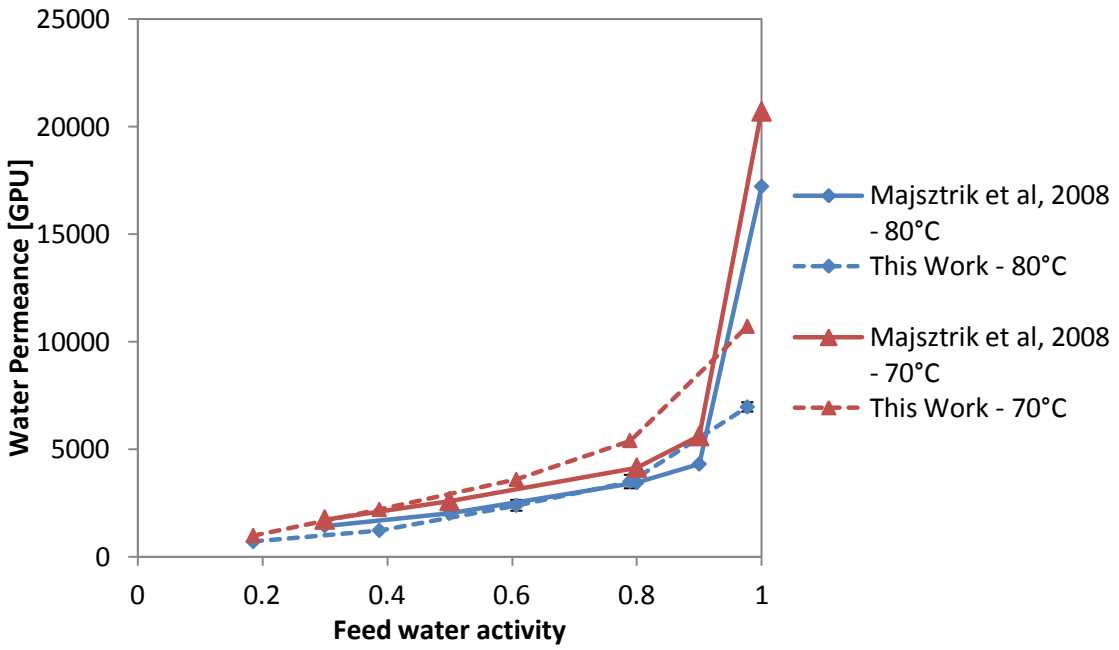

Figure 4.7: Comparison of water permeance through Nafion 115 at 70°C and 80°C with those obtained by Majsztrik *et al*, 2008 [22].

4.5 Water vapour permeance

Water vapour permeance through Nafion 115 as a function of feed water activity and partial pressure is presented in Figure 4.8. As shown, water permeance increases in a non – linear manner as a function of feed water activity, as is generally the case with most polymeric materials [22, 54]. This reflects swelling in the membrane side exposed to concentrated steam. At 70 °C, the water permeance

increased from ~980 GPU for a feed water activity of 0.18 to ~10,000 GPU for fully saturated steam. Also, for any given temperature the water permeance increases as feed water partial pressure increases as shown in the inset of Figure 4.8.

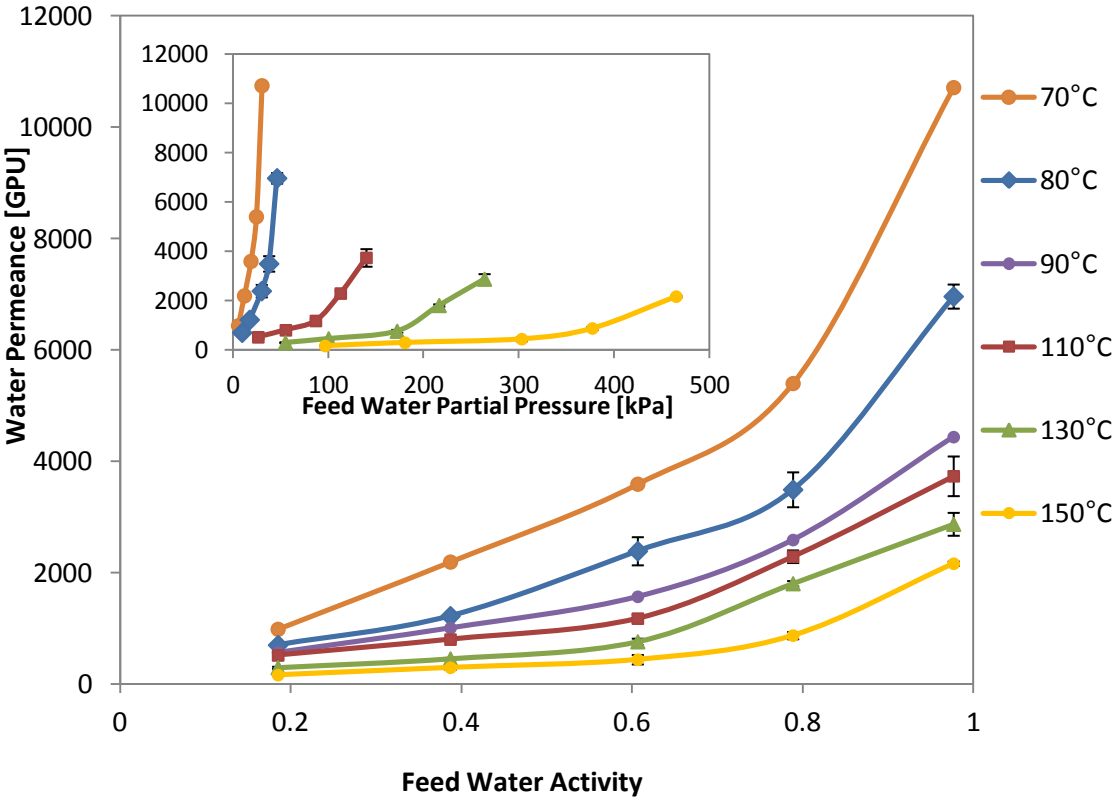

Figure 4.8: Water permeance through Nafion 115 as a function of feed water activity and feed water partial pressure. (Total feed pressure: 0.5 – 4 Barg)

An increase in temperature results in a significant decrease in water permeance as shown by the drop from ~10,700 GPU at 70 °C to ~2,100 GPU at 150 °C for fully saturated steam in Figure 4.9. This corresponds with the decrease in water solubility with increasing temperature (Figure 4.2) and implies that water permeance is dominated by this solubility and is less affected by the increase in water diffusivity that occurs with temperature. As shown in the previous section, water permeance at 70 °C and 80 °C compares well with that obtained by Majsztrik [22] but no comparison is available for water permeance higher than 80 °C.

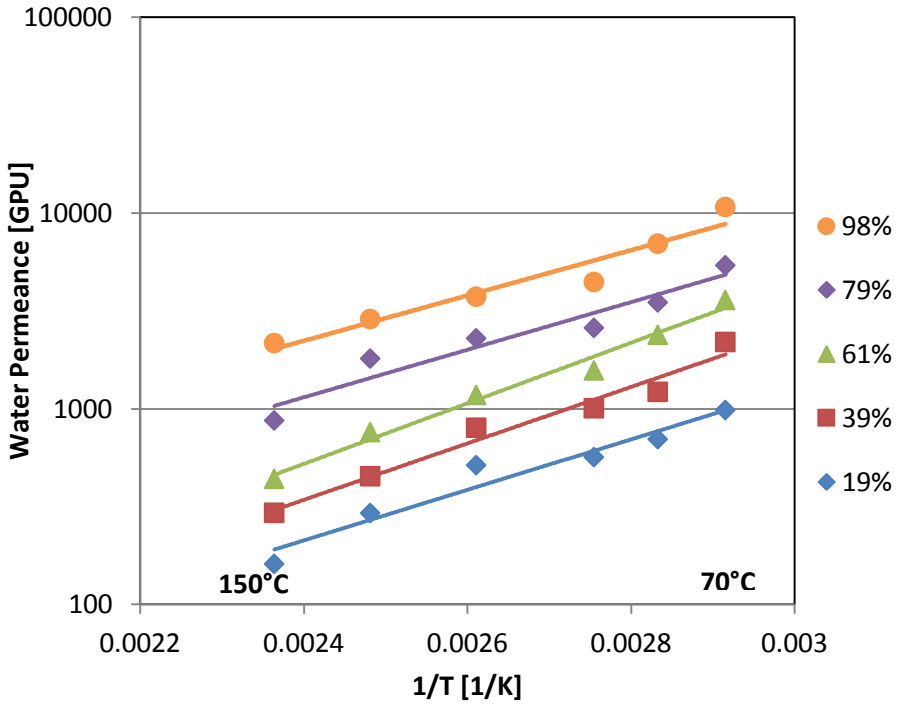

Figure 4.9: Water permeance through Nafion 115 as a function of temperature and feed RH %.

The activation energy of water permeability for Nafion determined using equation 2.41 is presented in Table 4.3. Activation energy for 70 – 150 °C obtained in this work compares well with that obtained by Majsztrik *et al.* due to similar permeance values observed in Figure 4.7. However, the E_p value obtained by Romero and Merida for the same temperature range of 70 – 80 °C is significantly different due to the increasing permeance with temperature trend observed in their work (Figure 4.6). Gorri *et al.* studied water permeance at 35 – 65 °C through a short-chain PFSA polymer with an EW of 860 g/mol SO_3H and obtained an $E_p \sim$ -29.7 kJ/mol which compares well within experimental error to the results obtained in this study.

Table 4.3: Activation energy of water permeability for Nafion 115 compared to literature.

	Temperature Range [°C]	E_p [kJ/mol]
This Work	70 - 150	-25.5 ± 3.1
Majsztrik et al. [22]	70 - 80	-21.7 ± 4.1
Romero and Merida [151]	70 - 80	13.2 ± 4.9
**Gorri et al. [137]*	35 - 65	-29.7

*Studied a short-chain PFSA polymer with an EW of 860 g/mol SO_3H.

The water permeance results were identical, within experimental error, whether N_2 or CO_2 was used as the second gas in the binary mixture. Indeed, the data in Figure 4.8 and Figure 4.9 represents the average from both experiments. This suggests that neither competitive sorption nor plasticisation by carbon dioxide influences the water permeance significantly.

4.6 CO_2 and N_2 Permeance

The CO_2 permeance through Nafion 115 as a function of feed water activity and temperature is presented in Figure 4.10. CO_2 permeance increases as water activity increases as shown by the increase from ~1.0 GPU at a water activity of 0.2 to ~2.9 GPU at a feed water of 0.8 at 70 °C. This reflects the membrane swelling at increasing water activity opening pathways for CO_2 diffusion, where uptake reduces crystallinity and the polymer transitions from a glassy to a rubbery state as discussed in section 2.7.1 [43, 200, 222]. This is reflected in the reduced glass transition temperature observed in the presence of water vapour in Figure 4.5. Similar increasing permeance trends have been observed by various researchers [138, 139, 223].

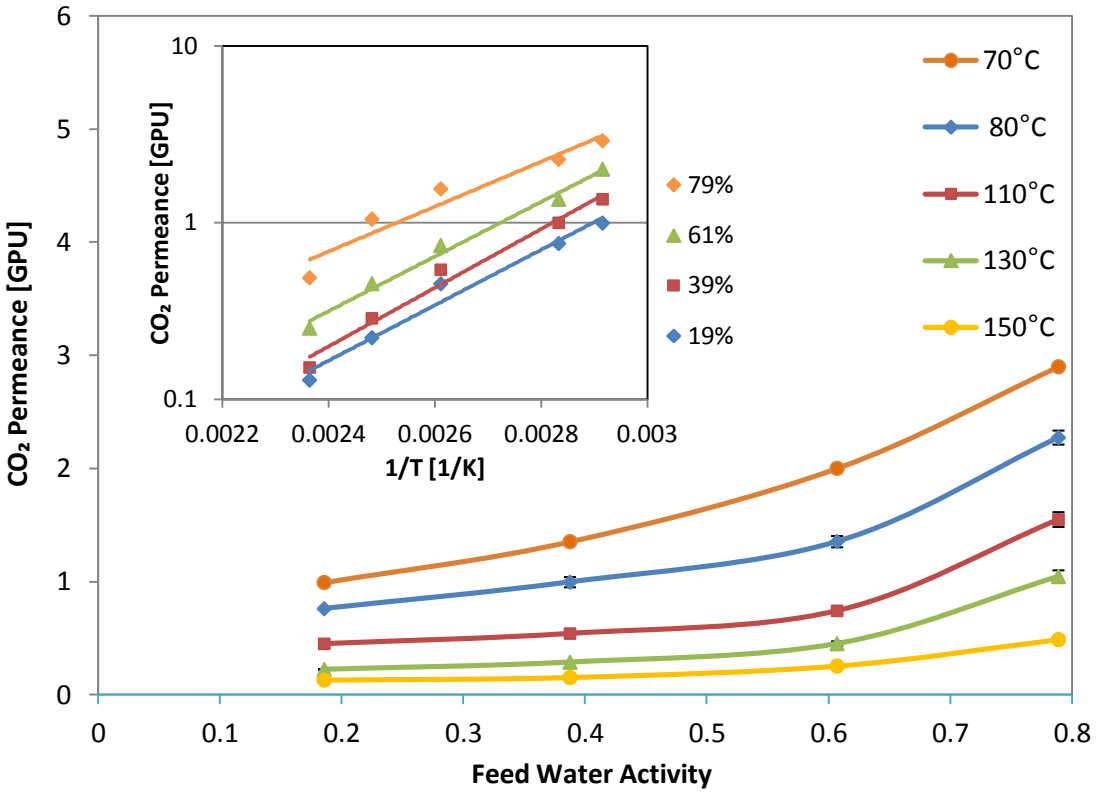

Figure 4.10: CO_2 Permeance through Nafion 115 as a function of feed water activity and temperature (inset).

CO_2 permeance decreases with increasing temperature from 70 – 150 °C as presented in the inset of Figure 4.10. This could be due to the increased formation of water clusters at high temperature, which may hinder diffusion [146]. Furthermore, the decrease in CO_2 solubility with increasing temperature will also cause a decrease in CO_2 permeance. Ma and Skou observed an initial increase in CO_2 permeance with temperature up to 40 – 50 °C. Above this range, they observed the same trend of decreasing CO_2 permeance with increasing temperature. They attributed this behaviour to the trade off between diffusivity and solubility [158]. The activation energy of CO_2 permeance in humidified conditions using equation 2.41 is presented in Table 4.4. As shown, the E_p value is in good agreement with the value obtained by Ma and Skou above 50 °C. At temperatures below 50 °C, the permeability trend inverts resulting in positive E_p value due to greater CO_2 solubility at lower temperatures. Baschetti *et al.* also observe a positive activation energy at low temperature. These trends are discussed further in Chapters 5 and 6.

Table 4.4: Activation energies of CO_2 permeance in a humid system for Nafion compared to literature.

	Temperature Range [°C]	E_p [kJ/mol]
This Work	70 - 150	-28.9 ± 3.2
Ma and Skou [158]	50 - 80	-32.4 ± 4.0
Ma and Skou [153, 158]	30 - 50	2.8 ± 1.9
Baschetti et al. [139]	25 - 50	16.1 ± 5.4

The N_2 permeance through Nafion 115 as a function of feed water activity and temperature is presented in Figure 4.11. Similar to CO_2 permeance, N_2 permeance increases with increasing water activity but decreases with an increase in temperature. Increased membrane swelling at higher water activities increases free volume for N_2 diffusion which consequently increases permeance. However, N_2 solubility decreases with increasing temperature resulting in a decreasing permeance trend. The activation energy of N_2 permeance in humidified conditions using equation 2.41 is presented in Table 4.5. Baschetti *et al.* have investigated N_2 permeance through Nafion 117 as a function of %RH but only for temperature range 25 – 50 °C [139]. They observed increasing N_2 permeance for this temperature range and consequently obtained a positive E_p value. To the best of our knowledge, no work has been done to study the effect of humidity on N_2 permeance at temperatures above 50 °C.

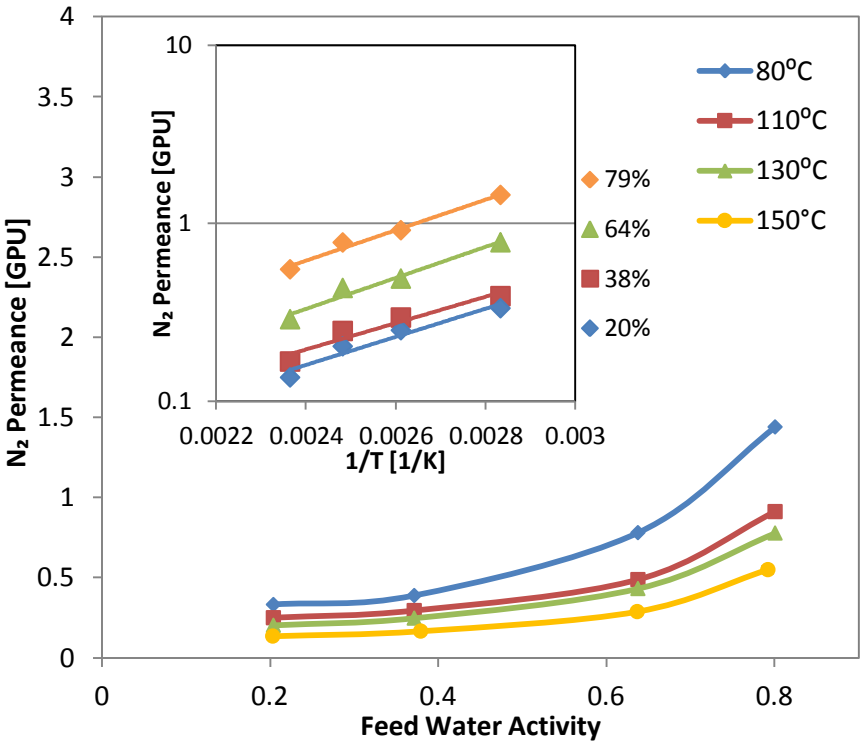

Figure 4.11: N_2 Permeance through Nafion 115 as a function of feed water activity and temperature.

Table 4.5: Activation energies of N_2 permeance in a humid system for Nafion compared to literature.

	Temperature Range [°C]	E_p [kJ/mol]
This Work	70 - 150	-15.6 ± 1.2
Baschetti et al. [139]	25 - 50	45.6 ± 3.1

N_2 and CO_2 permeance through dry Nafion 115 at a range of temperatures is presented in Figure 4.12. Both permeances increase as temperature increases due to the increase in diffusivity; as observed by various researchers [138, 139]. The permeance values compare well at 35 °C with that obtained by Chiou and Paul [152] and Catalano *et* al [138] for Nafion 117, giving a CO_2/N_2 selectivity of 12. However, the selectivity of CO_2 over N_2 decreases as temperature increases, with a value of ~2.6 at 150 °C. Furthermore, dry CO_2 and N_2 permeances are considerably lower compared to the wet permeances in Figure 4.10 and Figure 4.11,

respectively. This is due to the presence of water that results in increased volume fraction of the hydrophilic phase through which CO_2 and N_2 diffusion occurs [138, 139, 153, 158, 224]. The activation energy of dry permeability for CO_2 and N_2 are shown in Table 4.6 and are in good agreement with that obtained by various researchers. However, it is noteworthy that the dry activation energies are positive, whereas those in the presence of water are negative (Table 4.4 and Table 4.5)

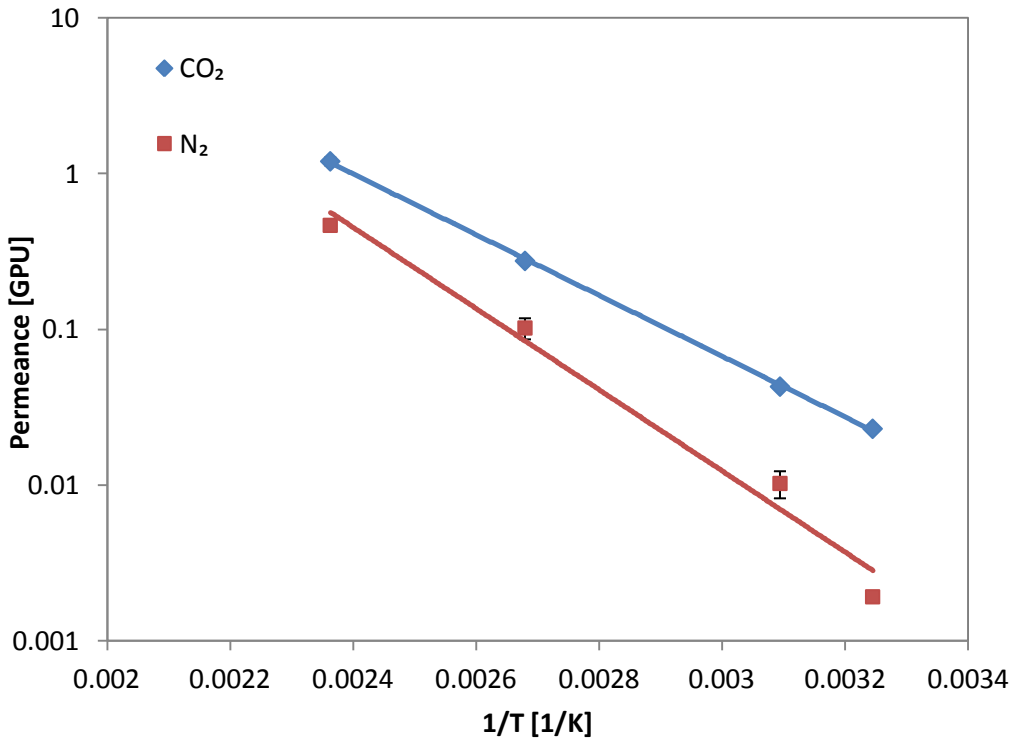

Figure 4.12: N_2 and CO_2 Permeance through dry Nafion 115 as a function of temperature.

Table 4.6: Activation energies of CO_2 and N_2 permeability for Nafion compared to literature.

	Temperature Range [°C]	$E_{p,CO2}$ [kJ/mol]	$E_{p,N2}$ [kJ/mol]
This Work	25 - 150	37.3 ± 2.1	49.9 ± 2.9
Catalano et al. [138]	35 - 65	-	49.6
Baschetti et al. [139]	25 - 65	36.7	49.7
**Catalano et al. [224]*	35 - 65	-	41.7

*Studied a short-chain PFSA polymer with an EW of 860 g/mol SO_3H.

The selectivity of H_2O over CO_2 and N_2 as a function of feed water activity and temperature is shown in Figure 4.13. As seen from the graph, there is no observable change with increasing temperature for H_2O/CO_2. However, the selectivity increases slightly at low feed water activity but remains unchanged at higher water activities. Conversely, the selectivity for H_2O/N_2 is slightly higher at low temperatures but does not appear to be a function of feed water activity.

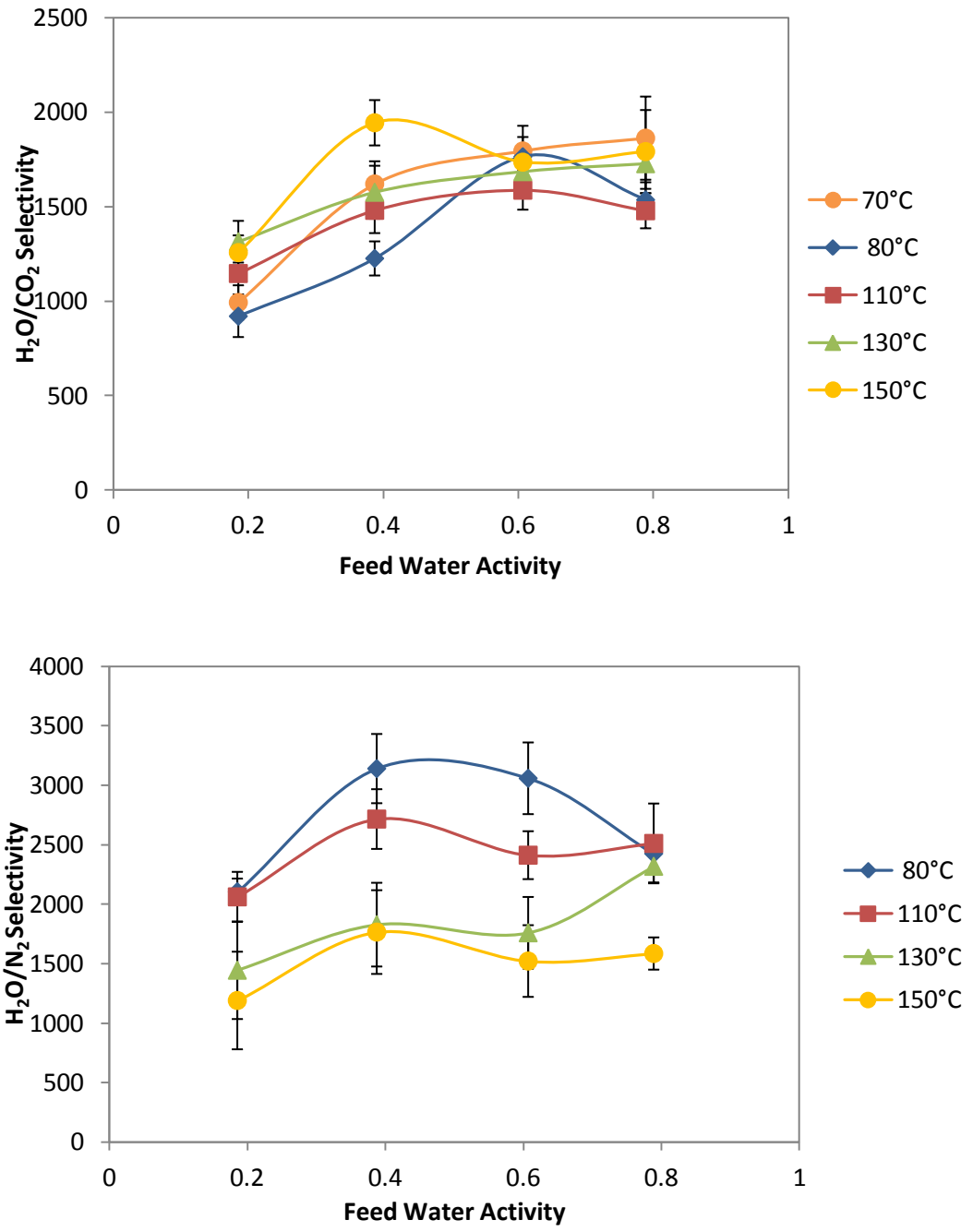

Figure 4.13: Selectivity of water over CO_2 as a function of feed water activity and temperature.

4.7 Thickness Dependence

To determine the effect of membrane thickness, a thinner Perfluorosulphonic acid based membrane similar to Nafion was examined (Section 3.1.1). The water permeance results as a function of feed water activity at 70 °C and 150 °C for the two membranes are presented in Figure 4.14. As expected, the permeance through the thinner membrane is greater. However, the permeance does not scale linearly with thickness – a six-fold reduction in thickness translates to only a three-fold increase in permeance at 70 °C and a ~1.6 fold increase at 150°C. Some of these differences may relate to differences in membrane chemistry, given they are provided by different suppliers. However, the Equivalent Weight (EW) quoted by the Suppliers would suggest that this should favour permeance through the Fumapem 20 μm membrane (Section 3.1.1, Table 3.1). Rather, it is likely that the non-linear dependence of the permeance upon thickness reflects the inhomogeneity in which the membrane swells. Water concentration and hence membrane swelling will be significantly greater in the side exposed to the concentrated steam. Conversely, the swelling on the permeate side will be negligible, leading to much lower rates of diffusion. It is likely that the transfer of water (and indeed carbon dioxide and nitrogen) will be controlled by the slower transfer on this side, meaning that the remaining membrane thickness becomes less relevant to the transfer process. Majsztrik *et al.* proposed the formation of a "hydrophobic skin" on the surface of the membrane on the permeate side. Consequently, water permeation is limited by the interfacial mass transport between this hydrophobic skin and the gas phase on permeate side [146].

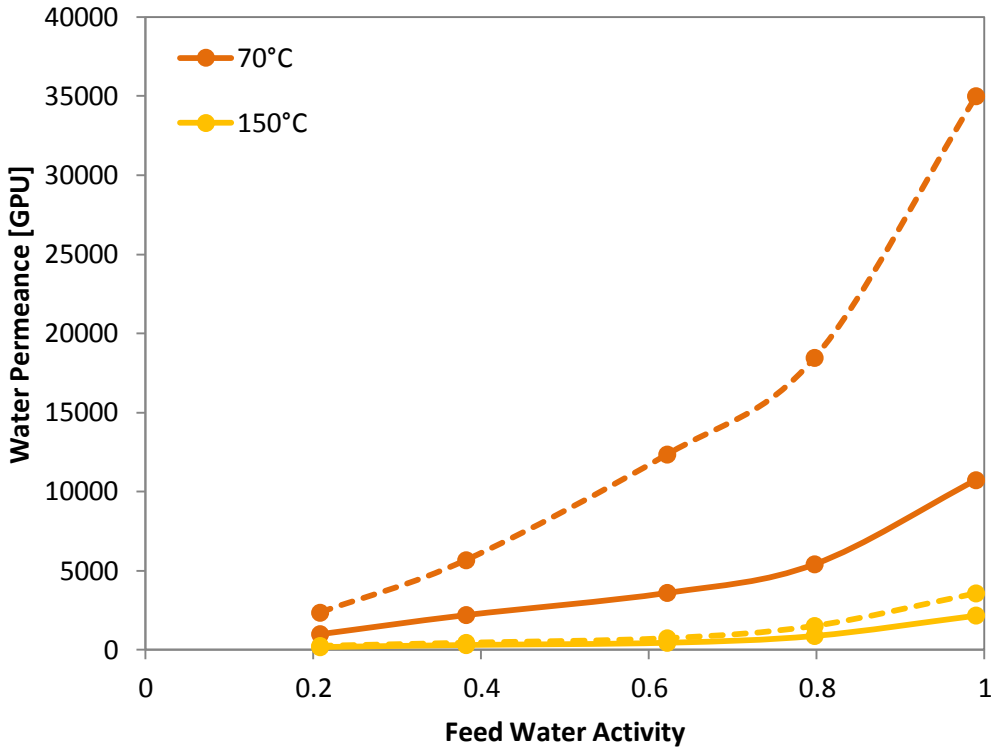

Figure 4.14: Water permeance as a function of feed water activity at 70 °C and 150 °C. The dotted and solid lines are for 20 µm and 127 µm dry thicknesses, respectively.

4.8 Conclusion

Water sorption isotherms for Nafion 115 as a function of feed water activity and temperature are presented. It was found that water uptake in the polymer increased with increasing water activity and temperature. A cluster analysis performed on these isotherms confirmed the formation of water clusters at lower water activity for high temperature. This was attributed to the increased water concentration in the membrane as temperature and the saturation water vapour pressure were increased.

Water, N_2 and CO_2 permeance through Nafion 115 as a function of feed water activity and temperature was also investigated. It was found that all permeances increased with increasing water activity. Negative activation energies were recorded for permeation of water, CO_2 and N_2 through humid systems at 70 – 150 °C. This is in contrast to the positive activation energies obtained by other workers at low temperatures. Positive activation energies for CO_2 and N_2 permeances

through a dry membrane were also observed. These trends in activation energies will be investigated further in the following chapters.

Water permeance was not found to scale linearly with membrane thickness, with the permeance at 150 ^{o}C only changing by a factor of around 1.6 between membranes of 20 and 127 μm in thickness. This reflects non-linear water activity gradients through the membrane, which means that most mass transfer resistance occurs on the low humidity, permeate side of the membrane.

Chapter 5 Effect of Sulphonation Degree and Temperature on Permeation Properties of Sulphonated Poly (Ether Ether) Ketone

5.1 Introduction

Sulphonated Poly (Ether Ether) Ketone or SPEEK has been investigated extensively for fuel cell and low temperature flue gas dehydration applications as detailed in section 2.7.2. As discussed, the few flue gas dehydration studies on SPEEK have been conducted at low temperatures (< 100 °C) and have focused solely on N_2 permeation due to the larger content of N_2 in flue gas streams. For the proposed application, it is necessary to reduce the presence of CO_2 in the recovered permeate, as high acidity would prevent re-use of the condensed water [70]. Hence, the permeation properties of CO_2 and water vapour through SPEEK need to be investigated at elevated temperatures in order to determine the suitability of SPEEK membranes for the proposed application. Furthermore, FTIR spectroscopy is also used to determine the occurrence of water clustering within the membrane.

5.2 Liquid Water Uptake

The liquid water uptake and water concentration in SPEEK samples with IEC 1.6 meq/g and IEC 1.9 meq/g is presented in Figure 5.1. It was not possible to obtain full water sorption isotherms as a function of water activity due to the failure of the gravimetric sorption analyser. Water uptake and concentration is greater for SPEEK with an IEC 1.9 meq/g compared to IEC 1.6 meq/g, reflecting the increased density of the $-SO_3H$ groups [161, 172, 213]. It should be noted that the IEC 1.9 meq/g membrane also contained glass reinforcing fibres. TGA results (Figure 5.4) suggest that these fibres represent around 25% of the total weight. Thus, the water sorption of the underlying SPEEK material is higher again, of the order of 11.4 to 20 wt% across the range of temperatures considered here. The water uptake and concentration also increases as temperature increases from 5 – 70 °C. This reflects the increasing saturation partial pressure of water as temperature increases,

which counteracts the declining solubility. The activation energy for water uptake is an average of ~8.3 ± 0.7 kJ/mol for the two sulphonation degrees. Similar trends have been observed by Hande *et al.* [225] as well as Al Lafi and Hay [226].

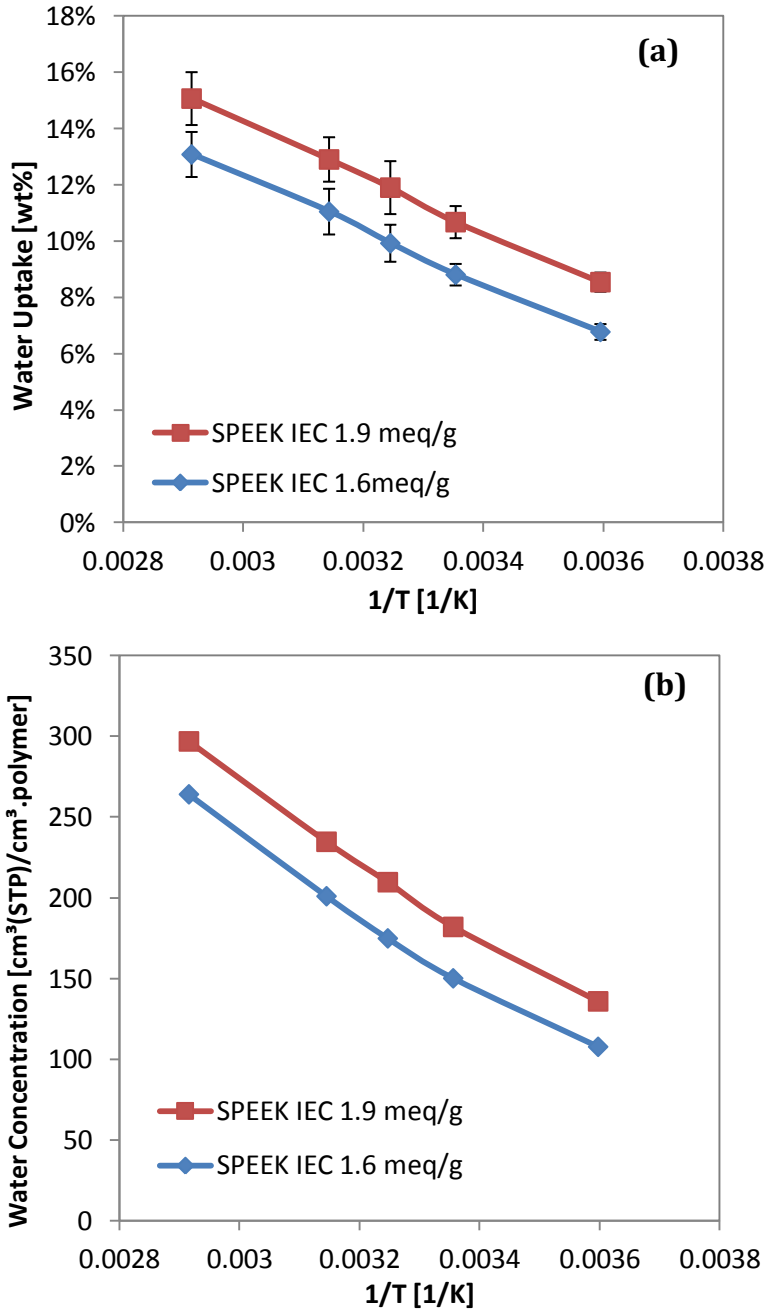

Figure 5.1: Liquid water uptake (a) and water concentration (b) in SPEEK IEC 1.6 meq/g and IEC 1.9 meq/g as a function of temperature.

Hande *et al.* obtained a water uptake of 14 wt% for SPEEK IEC 2.0 meq/g compared to 12 wt% for SPEEK IEC 1.9 meq/g obtained in this study [225].

However, these values are significantly lower than the 44 wt% obtained by Potreck *et al.* for SPEEK SD of 59 %, the reasons for which are unclear [45].

Figure 5.2 gives water solubility in SPEEK as a function of temperature. As obtained by various other researchers for a range of polymers, solubility decreases as temperature increases [54, 156, 220].

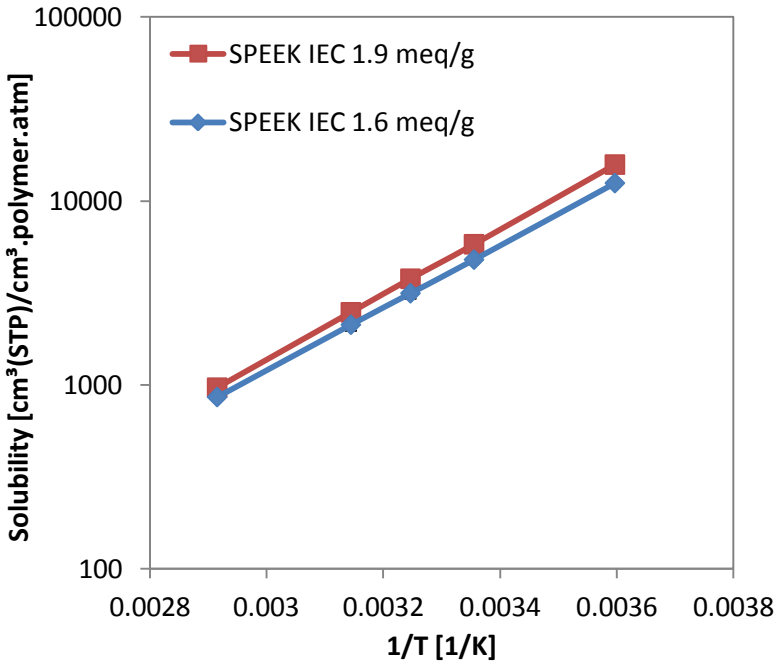

Figure 5.2: Solubility of water in SPEEK IEC 1.6 meq/g and IEC 1.9 meq/g as a function of temperature.

5.3 Theoretical Glass Transition Temperature

The liquid water uptake in Figure 5.1 and the Fox equation (equation 2.4) was used to estimate the theoretical T_g for SPEEK IEC 1.6 meq/g and SPEEK IEC 1.9 meq/g. As shown in Figure 5.3, SPEEK IEC 1.6 meq/ and IEC 1.9 meq/g are glassy below temperatures of ~58 °C and ~ 48 °C, respectively when fully loaded with water. As temperature increases above these thresholds, the SPEEK polymers transition from glassy to rubbery state. The onset of this transition is at a lower temperature (~48 °C) for the higher sulphonation degree polymer (IEC 1.9 meq/g) due to the greater water uptake of this polymer.

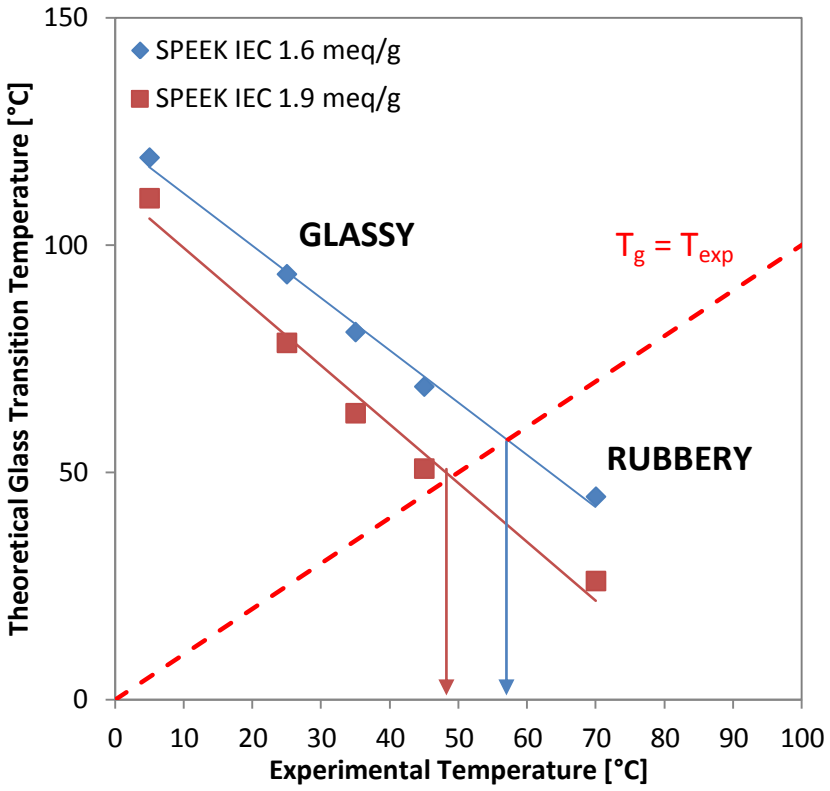

Figure 5.3: The theoretical T_g for SPEEK IEC 1.6 meq/g and SPEEK IEC 1.9 meq/g as a function of experimental temperature. The red dotted line represents the transition line between glassy and rubbery polymers.

5.4 Thermogravimetric Analysis

Thermogravimetric analysis of wet and dry SPEEK IEC 1.6 meq/g and IEC 1.9 meq/g is shown in Figure 5.4. For wet samples (dotted lines), there is an initial mass loss associated with water evaporation at ~ 100 °C irrespective of the IEC of the SPEEK polymer. This water loss is greater for IEC 1.9 meq/g at ~ 11 wt% compared to ~ 9 wt% observed for IEC 1.6 meq/g. These values match well to the liquid water uptake obtained in Figure 5.1. This water loss is clearly not observed for dry SPEEK samples. The second mass loss at ~320 – 370 °C is associated with the acid-catalytic decomposition of the $-SO_3H$ group. Commonly, this mass loss is greater for a higher sulphonated polymer due to the greater presence of $-SO_3H$ groups. In this instance, the mass loss (wt%) associated with SPEEK IEC 1.9 meq/g is less due to this membrane being reinforced with glass fibre which remains behind and adds to the residual weight after the polymer has decomposed. Similar

TGA curves for SPEEK have been observed by several researchers [103, 161, 172, 227-230].

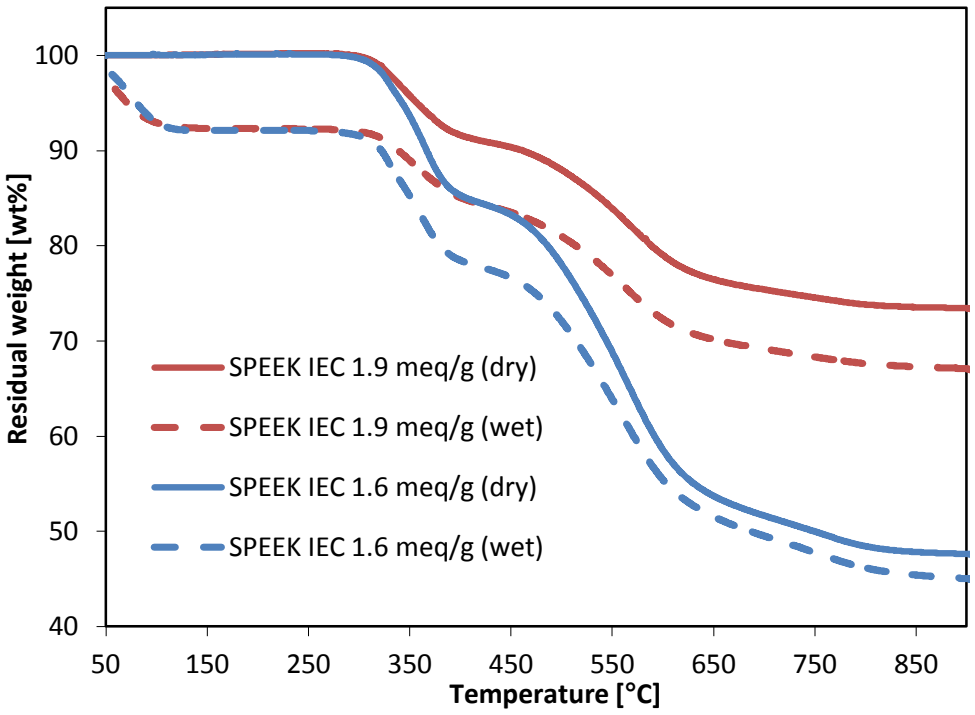

Figure 5.4: Thermogravimetric Analysis (TGA) of wet (dotted line) and dry SPEEK IEC 1.6 meq/g and IEC 1.9 meq/g.

5.5 FTIR Measurements

The FTIR spectra of the two sulphonated SPEEK membranes are shown in Figure 5.5. According to various researchers [112, 161, 163, 166, 167, 213], the presence of peaks at 1020, 1080, 1220 and 1480 cm^{-1} indicate the stretching vibrations of the sulphonic acid groups. The absorbance of these peaks is greater for a higher sulphonation degree polymer as observed in Figure 5.5.

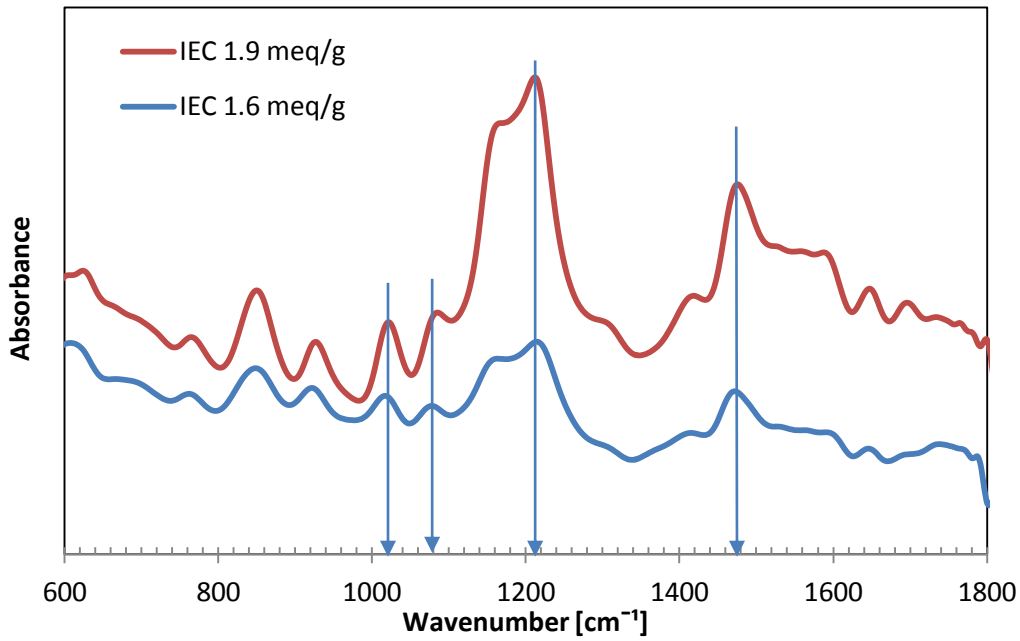

Figure 5.5: FTIR Spectra of SPEEK IEC 1.6 meq/g and IEC 1.9 meq/g.

The spectra at a range of RH after subtraction of the spectrum of a dry membrane are shown in Figure 5.6. The shape and intensity of asymmetric ν_a(OH) and symmetric ν_s(OH) stretching bands and a bending band δ(HOH) in the FTIR spectra can be used to gather information about hydrogen – bonding interactions between sorbed water and the polymer [214, 231]. Generally, hydrophobic polymers have sharp distinct bands for these three peaks that relay small or no interactions between water molecules and polymer. In these cases, the ν_a (OH) and ν_s (OH) exist at a frequency of ~ 3800 and 3700, respectively while δ (HOH) is found at ~1600. As polymers becomes more hydrophilic, the ν_a(OH) and ν_s(OH) bands shift to lower frequencies while δ(HOH) shifts to higher frequencies. Furthermore, the bands becomes broader similar to that for liquid water [214, 231]. This indicates that water molecules interact with a polar group and these interactions becomes stronger with increasing polymer hydrophilicity resulting in a greater shift. In the present case, the asymmetric ν_a (OH) peak appears at ~ 3400 cm^{-1}, while the symmetric ν_s (OH) appears at ~ 3070 cm^{-1}. It is unclear why the ν_s (OH) peak appears at a wavenumber of ~ 3070 cm^{-1} instead of the expected ~ 3200 cm^{-1}. Both peaks increase in intensity as the RH increases from 15% to 85% for both IECs. Furthermore, the increase in the ν_a(OH) band is greater for IEC 1.9 meq/g compared to IEC 1.6 meq/g due to the greater number of polar sites (-

SO_3H). However, the position of the peaks does not appear to move significantly with the IEC or the %RH.

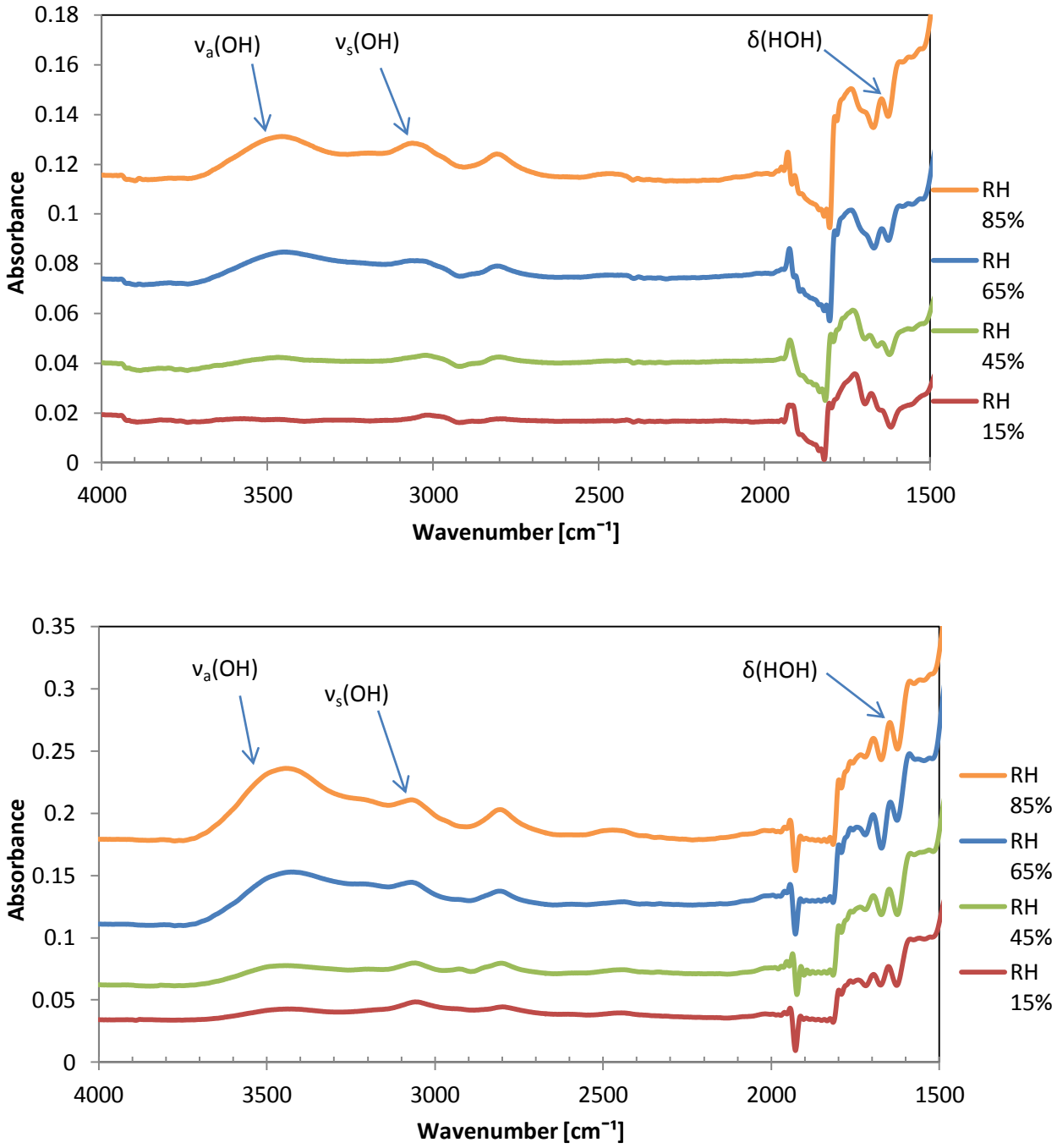

Figure 5.6: FTIR spectra of SPEEK IEC 1.6 meq/g (top) and SPEEK IEC 1.9 meq/g (bottom) containing sorbed water at a range of RH [Note: the scale of each curve has been shifted vertically to facilitate peak identification].

Kusanagi and Yukawa [214] use the relationship between the wavenumbers of the ν_a (OH) and ν_s (OH) peaks to determine the hydrophobicity/hydrophilicity of a

polymer. This figure is reconstructed in Figure 5.7. The top right hand corner consists of hydrophobic polymers which lie on a straight line (black solid line) that extends towards the gaseous phase of water and indicates the presence of isolated water molecules in the polymer. Conversely, hydrophilic polymers lie on another straight line (red) with a different slope extrapolating to the value of liquid water towards the bottom left hand corner of the graph. These low ν_a (OH) and ν_s (OH) peak frequencies indicate strong water-polar group interactions leading to the formation of liquid-like water clusters in the polymer structure. PEO is located at the crossing point of these two lines indicating its intermediate hydrophobicity [214].

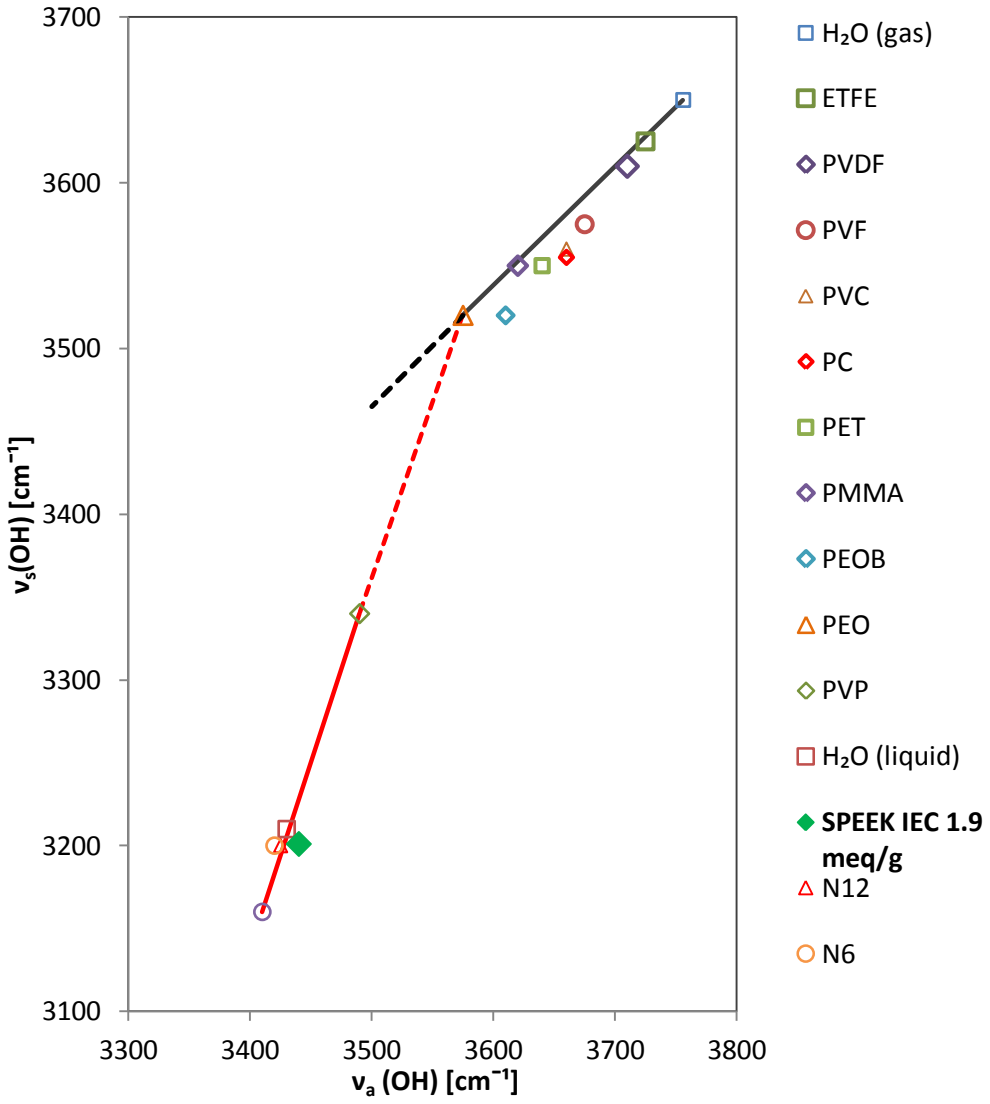

Figure 5.7: Relationship between ν_a(OH) and ν_s(OH) stretching frequencies of sorbed water molecules in different solid polymers. (Adapted from Kusanagi and Yukawa [214])

Adding the ν_a (OH) and ν_s (OH) peak values for SPEEK IEC 1.6 meq/g and IEC 1.9 meq/g places them firmly in the hydrophilic region of Figure 5.7. Hence, these membranes are indeed hydrophilic in nature and the water in these polymers is likely to be present as clusters at 20 °C.

5.6 Dry CO_2 and N_2 Permeability

The permeabilities for pure dry CO_2 and N_2 feed streams and the corresponding ideal CO_2/N_2 selectivity are presented in Figure 5.8 and Figure 5.9, respectively. These were measured on the CVVP experimental rig described in section 3.3.1. CO_2 and N_2 permeabilities are higher for the more sulphonated SPEEK membrane (IEC 1.9 meq/g). The same permeability trend was observed by Khan and Colleagues [12], however the magnitude of their permeability values are significantly greater than those observed here (Table 5.1). A possible reason for this is the presence of bulky methyl side groups in their SPEEK polymer that they argue leads to increased fractional free volume compared to other researchers. However in this work, permeability values are significantly greater than those obtained by Sijbesma and colleagues. The reason for this is unclear given that the membrane structures are the same. This may again relate to the difficulty in obtaining accurate measurements at such low permeation rates.

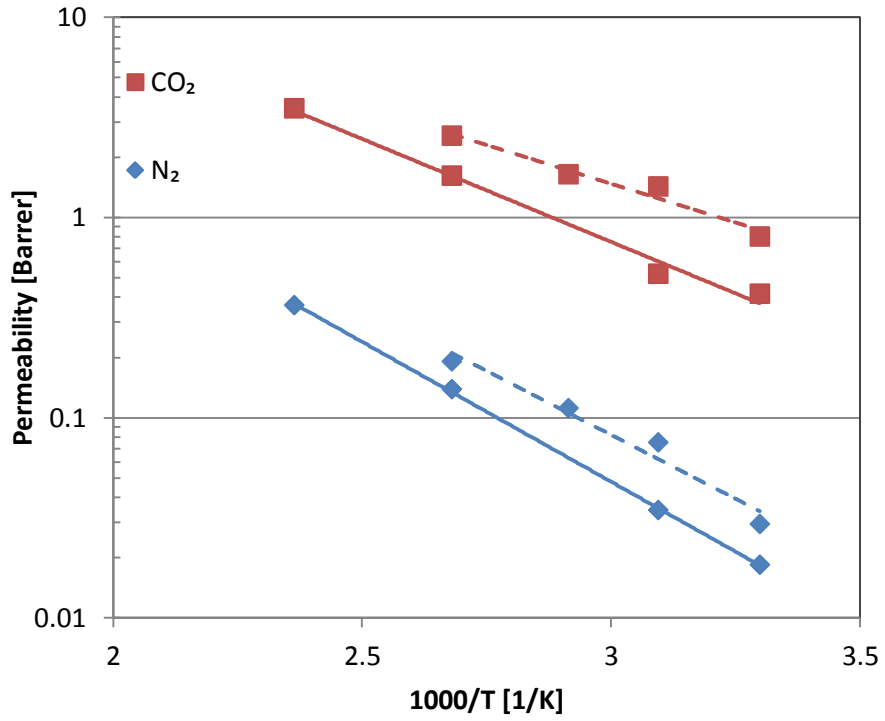

Figure 5.8: Pure CO_2 and N_2 permeability for SPEEK IEC 1.6 meq/g (Solid lines) and SPEEK IEC 1.9 (Dotted lines) meq/g as a function of temperature. The lines are exponential fits to the data.

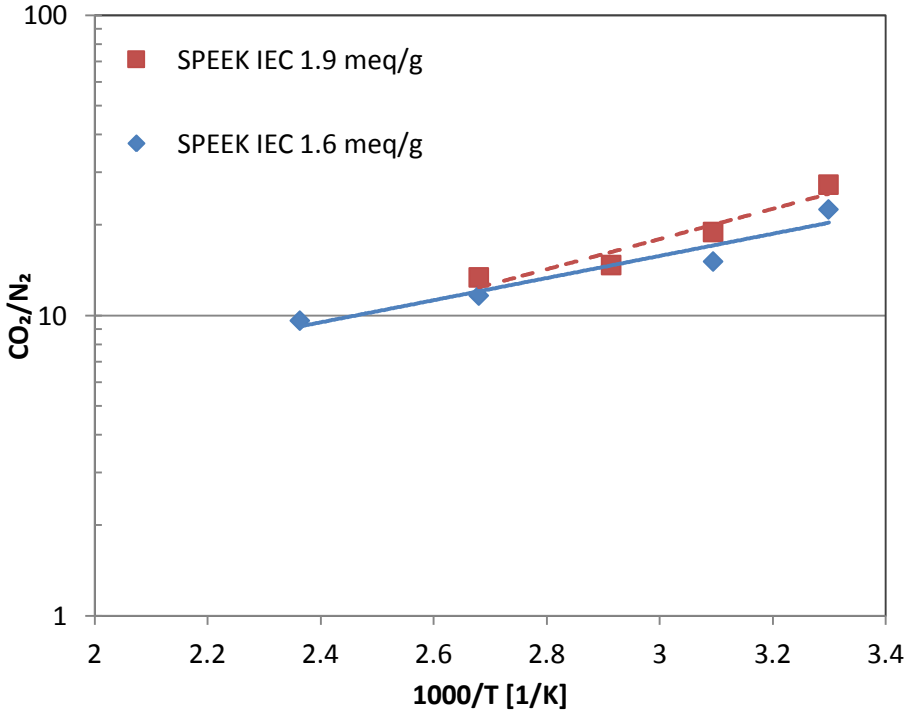

Figure 5.9: CO_2/N_2 selectivity of SPEEK IEC 1.6 meq/g and SPEEK IEC 1.9 meq/g as a function of temperature.

Table 5.1: Pure CO_2 and N_2 permeability in a dry system through SPEEK IEC 1.6 meq/g and IEC 1.9 meq/g compared to literature.

	This Work T = 30°C		Sijbesma *et al.* [6] T = 30°C	Khan *et al.* [12] T = 25°C
IEC (Meq/g)	**1.6**	**1.9**	**1.7**	**1.8**
CO_2 Permeability [Barrer]	0.42 ± 0.03	0.80 ± 0.02	0.11 ± 0.01	10.4
N_2 Permeability [Barrer]	0.018 ± 0.003	0.029 ± 0.004	0.003 ± 0.001	0.37
CO_2/N_2	22.6	27.3	36.7	28.2

From Figure 5.8, the permeability of both CO_2 and N_2 increases with increasing temperature due to an increase in diffusivity. The increase is greater for N_2 and this consequently results in a reduction in CO_2/N_2 selectivity as temperature increases observed in Figure 5.9. Similar behaviour is reported by Khan *et al.* [12]. However, the activation energies of permeation (E_p) for pure CO_2 and N_2 calculated using equation 2.41 differ significantly to that obtained by Khan and colleagues (Table 5.2). This is possibly due to the different nature of their heavily methylated SPEEK membrane as opposed to the non-methylated membrane used in this study. It is commonly known that the presence of bulky functional groups such as methyl groups hinder close packing of the polymeric matrix resulting in increased free volume and higher permeabilities [12].

Table 5.2: Comparison of Activation Energies of Permeation for CO_2 and N_2

Activation Energies, E_p	This Work		Khan *et al.* [12]	
	IEC 1.6 meq/g	IEC 1.9 meq/g	IEC 1.4 meq/g	IEC 1.8 meq/g
CO_2 [kJ/mol]	19.7 ± 0.6	14.8 ± 0.7	8.7	6.9
N_2 [kJ/mol]	26.6 ± 0.5	24.4 ± 0.6	17.0	16.1

5.7 Preliminary Permeability Results

To enable comparison with previous studies of SPEEK, the water permeability for FuMa-Tech membranes was measured at 30 °C, 50 °C and 70 °C on the low temperature mixed gas permeation apparatus described in section 3.3.2. The results are presented in Figure 5.10. As expected, the water permeability increases with increasing water activity due to the increased water sorption at higher water activities, a trend observed by several researchers [161, 167]. For any given temperature and water activity, the water permeability is also higher for the more sulphonated membrane (IEC 1.9 meq/g). The effect of temperature on water permeability gives interesting results when temperature increases from 30 °C to 50 °C. At low water activities (<0.4), the water permeability at 50 °C is lower than that at 30 °C. However as water activity increases above 0.4, the water permeability for 50 °C overtakes that for 30 °C. This change in behaviour was also observed by Sijbesma *et al.* [3] who found a crossover point at a water activity of 0.5 for similar conditions. As shown in Figure 5.10, the water permeabilities for IEC 1.6 meq/g and IEC 1.9 meq/g used in this study are in good agreement with those of Sijbesma *et al.* [6] for SPEEK of IEC 1.7 meq/litre. The results are also consistent with those of Liu *et al.* [160] who investigated water permeability through SPEEK using a cup method. They reported permeabilities at 100% RH of ~39,000 Barrer and ~110,000 Barrer at 30 °C and 50 °C, respectively, similar to the values obtained in this study.

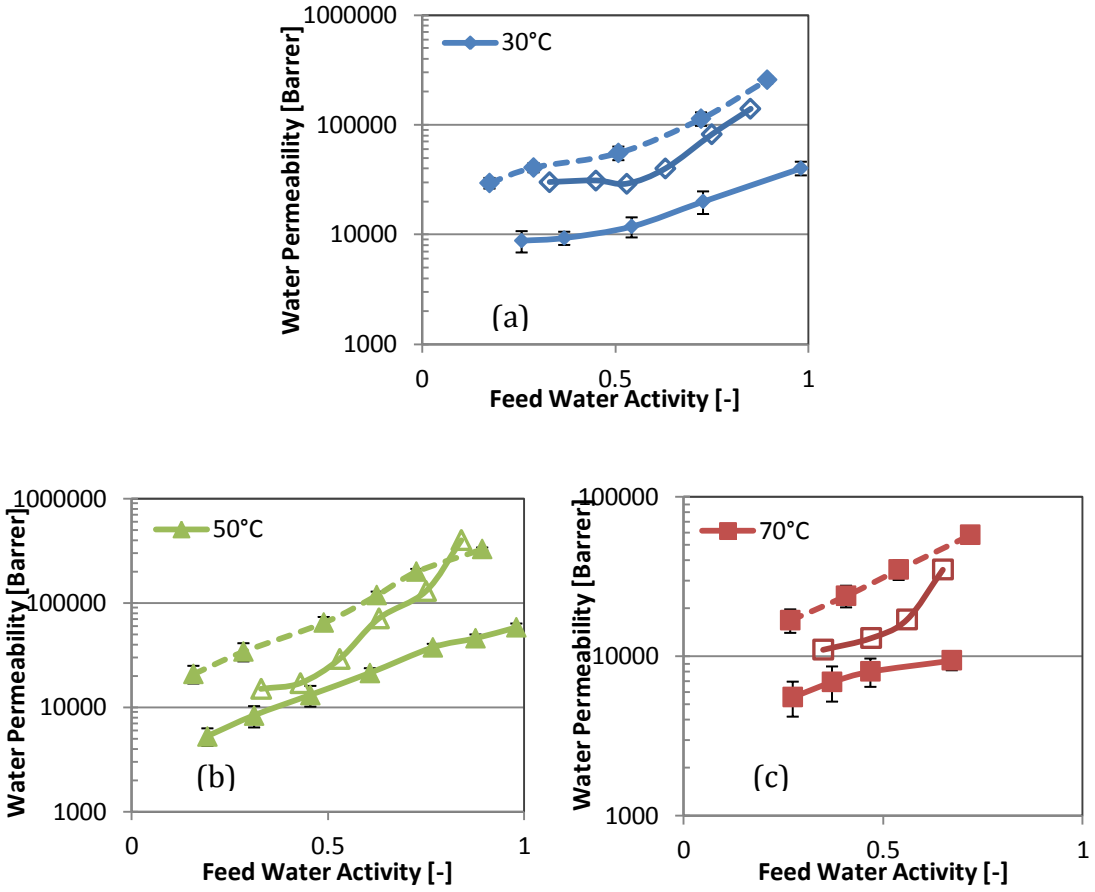

Figure 5.10: Water permeability as a function of feed water activity at 30 °C (a), 50 °C (b) and 70 °C (c) for SPEEK IEC 1.9 meq/g (Dotted Line) and IEC 1.6 meq/g (Solid Line) compared with that obtained by Sijbesma *et al,* 2008 for a membrane of 1.7 meq/g (Open Data Points) [6].

High temperature water permeabilities measurements at 70 – 150 °C were conducted on the steam permeation rig described in section 3.3.3 [70]. As a result, it is important to match the water permeabilities from the two different experimental apparatus to achieve confidence in the precision of the two rigs. This is done in Figure 5.11 which presents the water permeability obtained on the low temperature rig (dotted line) and the high temperature rig (solid line) at 70 °C. As shown, the permeability values from the two experimental rigs match well at 70 °C for the two SPEEK IECs.

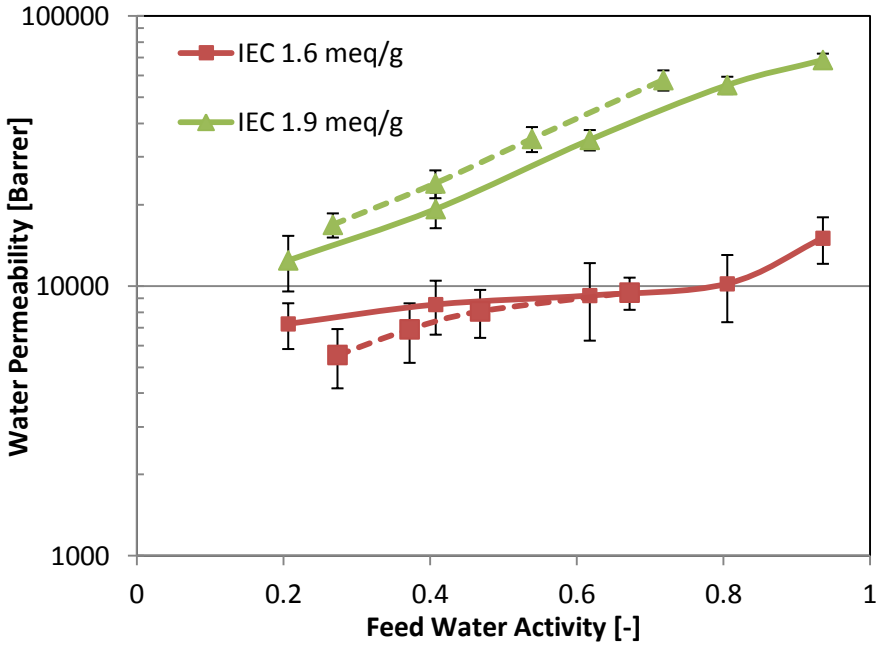

Figure 5.11: Water Permeability for SPEEK IEC 1.9 meq/g and IEC 1.6 meq/g at 70 °C obtained on the steam experimental rig (Solid Lines) and mixed gas permeation rig described by Chen *et al. [54]* (Dotted lines).

5.8 Water Vapour Permeability

Water permeability through SPEEK IEC 1.6 meq/g (solid lines) and IEC 1.9 meq/g (dotted lines) as a function of feed Relative Humidity (RH %) from 30 – 150 °C are presented in Figure 5.12.

It is apparent that water permeability increases with increasing feed RH at a given temperature. For example for SPEEK IEC 1.6 meq/g (solid line) at 150 °C, the water permeability increased from ~300 Barrer to ~1100 Barrer as feed RH increased from 21% to 94%. Furthermore, the water permeability for SPEEK 1.9 meq/g (dotted line) is greater than that for IEC 1.6 meq/g (solid line) for a given feed RH % and temperature. This is a result of the increased presence of the sulphonic acid end groups that have greater interactions with water and result in higher water solubility [6, 12, 160].

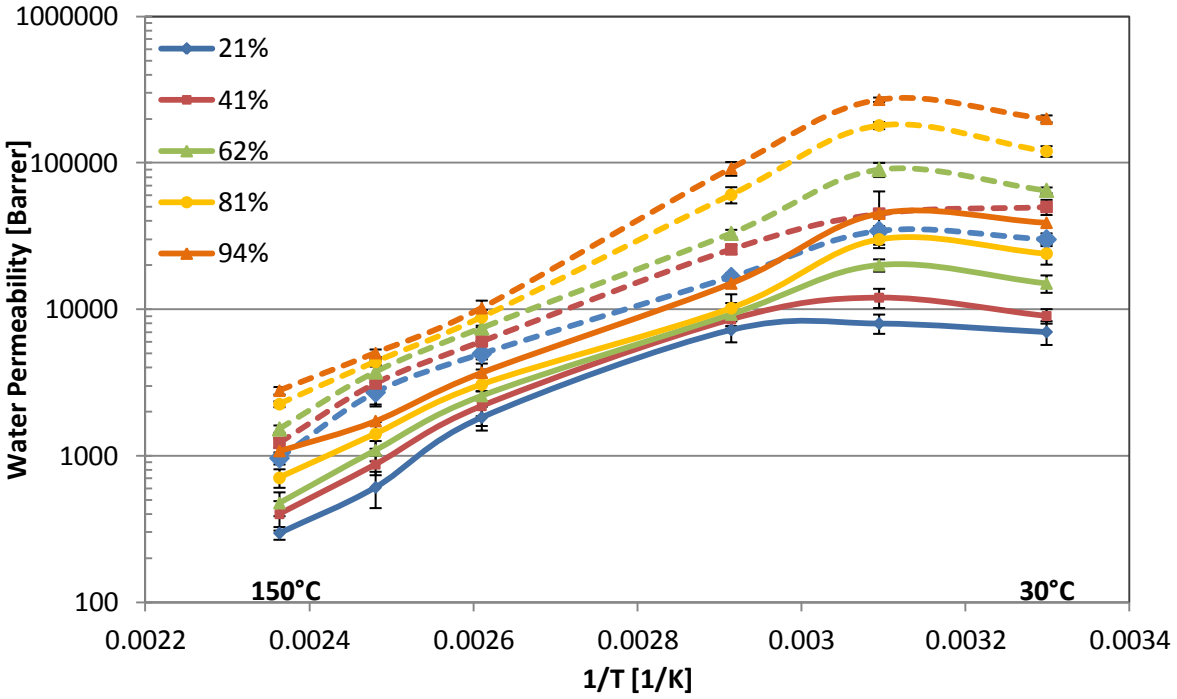

Figure 5.12: Water permeability through SPEEK IEC 1.6 meq/g (Solid lines) and IEC 1.9 meq/g (Dotted lines) as a function of temperature and feed RH (%).

The effect of temperature on water permeability described in the preliminary results is presented more clearly in Figure 5.12. There is little change in permeability as temperature increases from 30 °C to 50 °C, giving low activation energy of permeation, E_p ~ 8.8 kJ/mol and 13.9 kJ/mol for IEC 1.6 meq/g and IEC 1.9 meq/g, respectively. These are compared to activation energies of water permeability obtained by various researchers in Table 5.3. The large variation in the E_p values is due to the differences in the IEC's as well as the different functional groups of the SPEEK membranes used in these studies. These differences also likely reflect the changing shape of the permeability curve in this region.

Table 5.3: Activation energy of water permeability through SPEEK compared to literature.

	Temperature Range [°C]	E_p [kJ/mol]	
This Work	30 - 50	8.8 ± 3.1	13.9 ± 2.3
Liu et al. [160]	30 - 50	22.4	
Jia et al. [102]	25 - 50	8.2	
Wang et al. [112]	25 - 40	19.3	

As temperature increases above 50 °C, the water permeability decreases continuously reflecting an activation energy that is negative and significantly greater in magnitude. The pre-exponential values (P_o) fitted to the experimental data at 70 – 150 °C for the two membranes are presented in Figure 5.13. As expected, P_o increases with feed RH and is also larger for the higher sulphonation degree (IEC 1.9 meq/g) membrane.

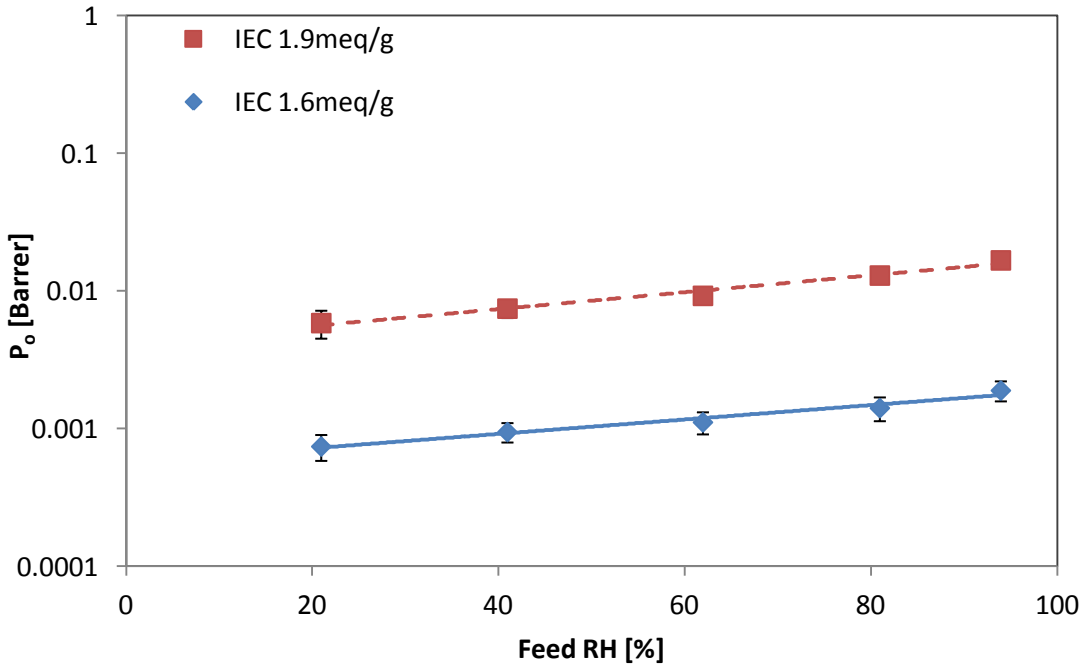

Figure 5.13: P_o values for IEC 1.9 meq/g and IEC 1.6 meq/g as a function of feed RH (%).

Table 5.4: Activation energy of water permeability for IEC 1.6 meq/g and IEC 1.9 meq/g in two temperature ranges.

	Temperature Range [°C]	E_p [kJ/mol]	
		IEC 1.6 meq/g	IEC 1.9 meq/g
This Work	30 - 50	8.8 ± 3.1	13.9 ± 2.3
	50 - 150	-46 ± 0.9	-43 ± 0.8

Table 5.4 shows the change in activation energies of water permeability for the two IEC's across the temperature range. From Figure 5.12, there appears to be a change in mechanism which occurs at ~50 – 70 °C. Indeed, closer inspection suggests that this mechanism change occurs at ~70 °C for lower humidities and

~50 °C at higher humidities. As explained in section 2.5.7 from equations 2.41 – 2.45, the changes in activation energy of permeability may reflect changes in the activation energy for diffusivity that occur as temperature increases; or changes in the heat of sorption (equation 2.45). The water solubility curve (Figure 5.2) gives no indication of such a shift in mechanism across this temperature range, indicating that solubility is probably not the cause of this behaviour. However, as discussed in section 5.2 above, the water will likely form clusters inside the membrane. These water clusters are known to hinder water diffusivity [54, 70]. It is possible that there is some change in the behaviour of these water clusters in the temperature range 50 – 70 °C that influences the rate of change in diffusivity. Assuming the heat of solution for liquid water (ΔH_s) is similar to that at other humidities (calculated from Figure 5.2 using Equation 2.43); it can be used to calculate the activation energy of diffusivity (E_D) for temperature range 30 – 50 °C using equation 2.45. The values are presented in Table 5.5.

Table 5.5: Activation Energy of water permeability and diffusivity and Heat of sorption for IEC 1.6 meq/g and IEC 1.9 meq/g.

T = 30 - 50°C	E_p [kJ/mol]	ΔH_s [kJ/mol] (from Figure 5.2)	E_D [kJ/mol]
IEC 1.6 meq/g	8.8 ± 3.1	-32.6 ± 0.5	41.4 ± 2.2
IEC 1.9 meq/g	13.9 ± 2.3	-33.9 ± 0.6	47.9 ± 1.7

Potreck *et al.* studied the sorption and Fickian diffusion of water through SPEEK membrane with two sulphonation degrees [45]. They found that the Fickian diffusion of water in both polymers increased initially as a function of water concentration in the membrane. The Fickian diffusion in the lower sulphonated polymer reached a plateau soon after while the higher sulphonated polymer diffusion went through a maximum and then began to decrease (Figure 2.14). They attributed this decrease to a transition in the polymer state from glassy to rubbery as discussed in section 2.7.2 [45]. As shown in Figure 5.3, this transition from glassy to rubbery was also observed in this work for SPEEK IEC 1.6 meq/g and IEC 1.9 meq/g at experimental temperature of ~58 °C and ~48 °C. Furthermore,

Potreck *et al.* reported no cluster formation in their study. However, a closer inspection of their work (Figure 2.15) reveals $G/V > -1$ at high water concentrations which indicates towards the formation of clusters at water concentrations ~ 270 – 350 cm^3 STP/cm^3 polymer. As discussed in section 2.5.2, clustering reduces the diffusion coefficient by hindering the diffusion of individual water molecules. Indeed, a decrease in water diffusion as a whole due to the formation of water clusters has also been reported by various researchers [14, 57, 106, 178]. Therefore, it may not only be the transition of SPEEK from a glassy to rubbery state that results in a change in mechanism but also the likely formation of large water clusters.

It is well known that the formation of clusters increases as both water vapour activity and temperature increases as detailed in the clustering analysis in section 4.2 [45, 54, 232]. This is likely one of the reasons for the change in mechanism observed for both SPEEK membranes at 50 – 70 °C. From Figure 5.1, the water uptake increases as temperature increases. Consequently, increased interactions between water molecules result in them undergoing self-hydrogen bonding and aggregating together (as obtained from Figure 5.7). It is likely that as temperature increases to 50 – 70 °C, the water concentration in these SPEEK membranes reaches a critical concentration where the size and number of water clusters begins to significantly affect the diffusion of individual water molecules. From Figure 5.1b, the water concentrations in the SPEEK polymers in the temperature range 50 – 70 °C are in the range ~250 – 310 cm^3 STP/cm^3 polymer. These are very comparable to the water concentrations of ~ 270 – 350 cm^3 STP/cm^3 polymer observed in the clustering analysis done by Potreck *et al.* in Figure 2.15, (within experimental error and varying sulphonation degrees/IECs). This coupled with the decreasing solubility observed in Figure 5.2, gives the changing water permeability behaviour observed in Figure 5.12.

This change in mechanism is similar to that observed in Chapter 4 for Nafion 115. Here again, the activation energy for permeation was observed to change sign at around 50 °C.

5.9 CO_2 Permeability in Wet Conditions

CO_2 permeability as a function of feed water activity and temperature for the two SPEEK membranes is presented in Figure 5.14. It is important to note that the permeability data at 30 °C, 50 °C and 70 °C was obtained from the mixed gas permeation rig described in section 3.3.2 while that at higher temperatures came from the steam rig described in section 3.3.3.

The dry CO_2 permeabilities are considerably lower when compared to permeabilities in the presence of water. This behaviour is reported by various researchers and is due to the plasticization of the membrane in the presence of water [6, 102, 103]. The activation energy of CO_2 permeability at low temperatures (30 – 50 °C) in humid conditions is similar to that for the same temperature range in dry conditions i.e. $E_p \sim 10.2$ kJ/mol in wet conditions compared to $E_p \sim 14.8$ kJ/mol in dry conditions (obtained from Figure 5.14). This suggests the mechanisms for permeation are comparable at low temperatures, reflecting the low concentration of water in the membrane. Furthermore, the CO_2 permeability increases as feed water activity increases due to the increased interactions between the $-SO_3H$ groups and water molecules that swell the membrane and open pathways for CO_2 diffusion. CO_2 permeability is greater for IEC 1.9 meq/g compared to IEC 1.6 meq/g, reflecting the greater swelling of the more sulphonated membrane.

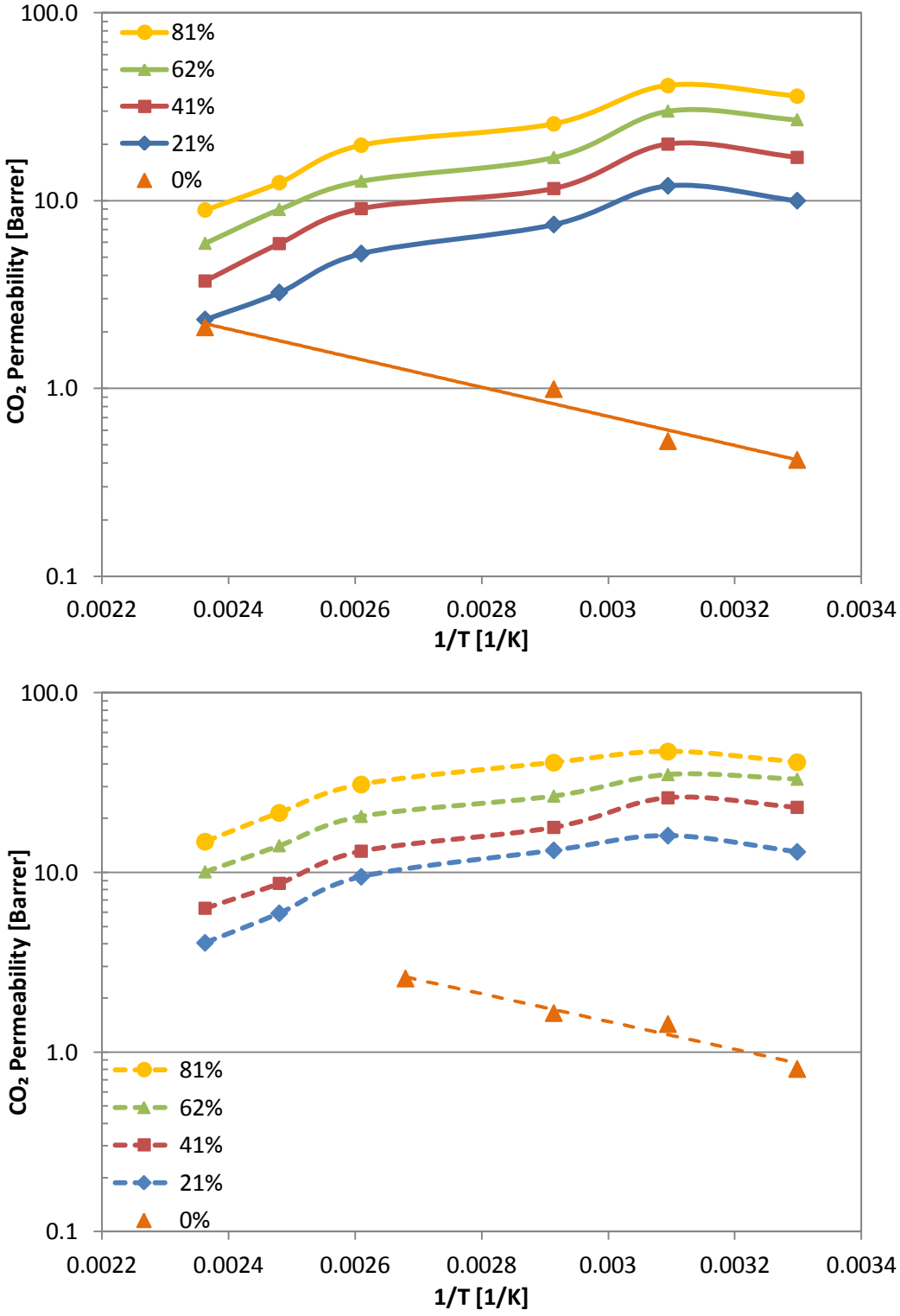

Figure 5.14: CO_2 permeability as a function of temperature for IEC 1.6 meq/g (solid line) and IEC 1.9 meq/g (dotted line) at different RH %.

Importantly, similar behaviour to the water permeability in Figure 5.12 is observed with respect to temperature. That is, the CO_2 permeability increases from

30 °C to 50 °C but decreases as temperature increases above 50 °C. Similar behaviour was observed by Ma and Skou for CO_2 permeability in hydrated Nafion membrane [158]. This again may reflect a change in the water clustering within the membrane discussed in the previous section as well as the transition from glassy to rubbery state. A decline in CO_2 diffusivity with increasing water content in the membrane has been observed by other workers [54, 86], and can again be related to increases in the number and size of water clusters, which inhibit the flow of other gases. This is often referred to as 'anti-plasticisation' (see section 2.5.6).

N_2 permeability was also measured for the two SPEEK membranes. The results obtained were similar in magnitude to those obtained by Sijbesma *et al.* [6] (< 1 Barrer); however such a low N_2 permeability is too close to the detection limit of the gas chromatography unit used in mixed gas measurements for accurate values to be reported here.

The selectivity of H_2O/CO_2 for the two IEC membranes is presented in Figure 5.15. As shown, the selectivity increases with decreasing temperature up to 50 °C below which it decreases. This is a direct result of the anomaly in the water permeability behaviour observed in Figure 5.12. Sijbesma *et al.* [6] found that the selectivity of H_2O/N_2 decreased with temperature as in this case but in fact increased with increasing feed water activity. This is because the increase in CO_2 permeation with increasing feed water activity is considerable compared to the limited changes in N_2 permeability observed in their work. As stated by many other researchers, a higher degree of sulphonation does improve the separation performance of the membranes as shown by the higher selectivity for IEC 1.9 meq/g (dotted line) compared to IEC 1.6 meq/g (solid line) at any given water activity and temperature [12, 102, 103, 172].

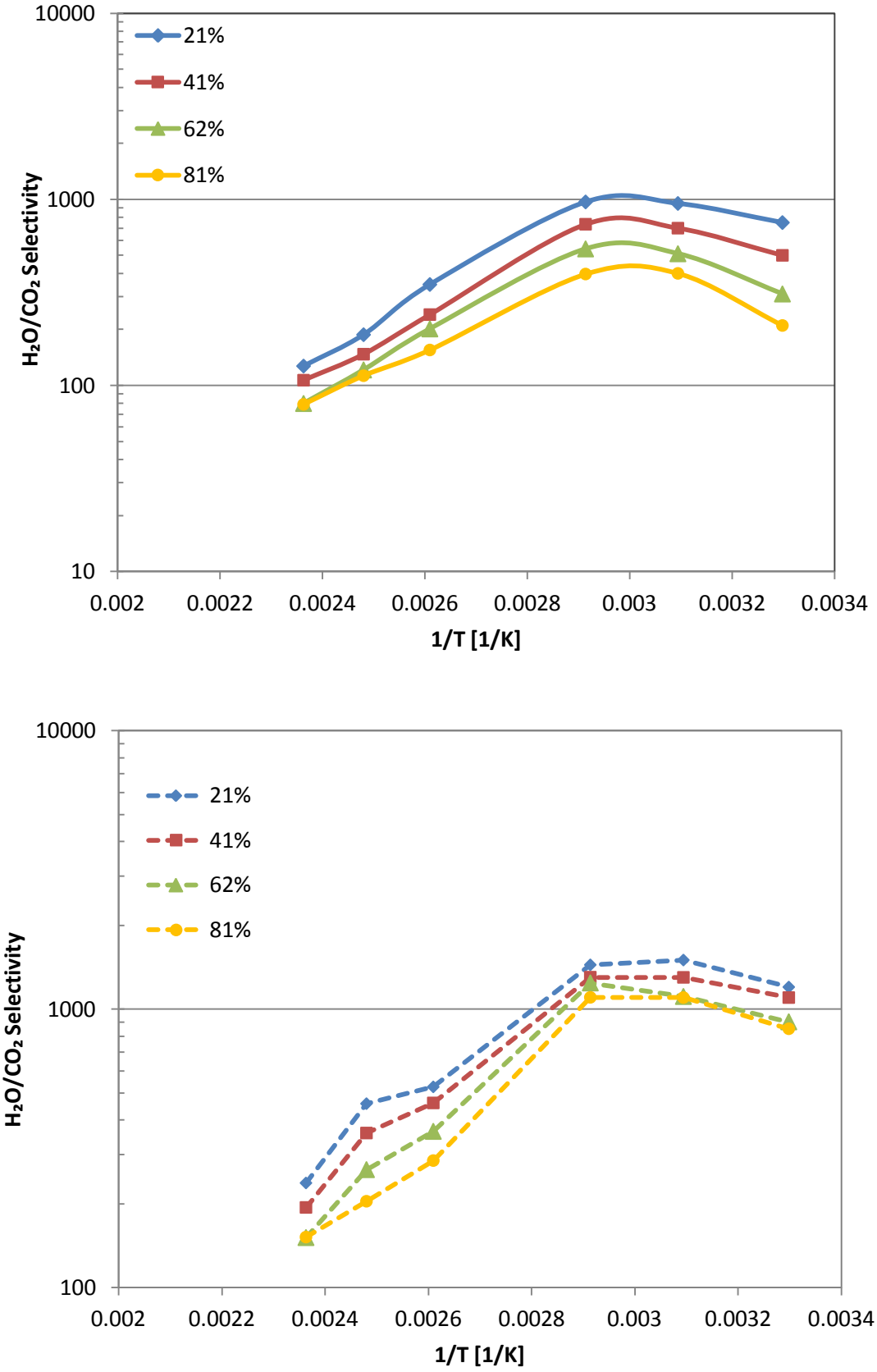

Figure 5.15: Selectivity of H_2O/CO_2 as a function of feed RH (%) and temperature for IEC 1.6 meq/g (solid line) and IEC 1.9 meq/g (dotted line).

5.10 Conclusion

The effect of sulphonation degree and temperature on permeation properties of Sulphonated Poly (Ether Ether) Ketone was studied. Water uptake and concentration increased with increasing temperature and was higher for the highly sulphonated membrane with an IEC 1.9 meq/g. FTIR spectra for the two IECs confirmed the presence of sorbed water in polymers as clusters. It was most likely the size and number of these water clusters that resulted in a change in water permeability mechanism at 50 – 70 °C for both membranes. Furthermore, an analysis of the theoretical T_g showed both polymers transitioning from a glassy to a rubbery state at experimental temperatures of ~48 – 58 °C.

Both water vapour and CO_2 permeabilities increased initially as temperature increased but decreased above 50 – 70 °C. This is possibly due to the presence of large water clusters that hinder the diffusion of both water and CO_2 or it may be a change in membrane morphology due to a transition from glassy to rubbery. The resultant decrease in both diffusivity and solubility causes the permeability to drop drastically above 50 - 70 °C. The increase in these permeabilities with increasing water activity is caused by membrane swelling in the presence of water. SPEEK membrane with IEC 1.9 meq/g had better permeation properties and separation compared to IEC 1.6 meq/g. This was due to the higher sulphonic acid content of the membrane that improved membrane performance.

Chapter 6 The Effect of Temperature on Water Permeation Properties of 6FDA - TMPD Polyimide Membrane

6.1 Introduction

6FDA – TMPD polyimide has been extensively researched for gas separation applications as discussed in section 2.7.4. This study aims to investigate water, CO_2 and N_2 permeation properties of 6FDA – durene as a function of temperature for water recovery from flue gas at elevated temperatures. To date, the majority of studies have focused on CO_2-separation performance of these membranes at temperatures below 100°C and in the absence of water. To the best of the author's knowledge, only Chen *et al.* [54] looked at water vapor permeation through 6FDA – durene and the effect of water on permeation of CO_2 and CH_4. However, they have only conducted this work at 35 °C. This work aims to investigate water, CO_2 and N_2 permeabilities at 25 – 150 °C as well as study the effect of CO_2 induced-plasticization at 70 – 150 °C. The mathematical model developed by Chen *et al.* [101] discussed in section 2.5.7 is then successfully applied to model water permeability at three different temperatures (25 – 35 °C). Water sorption isotherms and clustering analysis at these temperatures are also investigated.

6.2 Water sorption

The water sorption isotherms for 6FDA – durene at 25 – 35 °C are presented in Figure 6.1. The curves are convex to the activity axis reflecting the exponential increase predicted by multilayer sorption as vapor activity increases [45, 72]. Both Stern *et al.* [82] and Okamoto *et al.* [81] observed similar behavior with 6FDA based polyimide polymers and attributed this to the glassy polymer being strongly plasticized by water molecules at high vapor activities. Furthermore as temperature increases, the amount of water sorbed by the polymer increases, reflecting an increase in equilibrium water partial pressure. This consequently yields a slightly increased water concentration at a given water partial pressure although the differences are small, as shown in the inset of Figure 6.1. Dividing the concentration by the increased partial pressure gives an inverted trend where

solubility of liquid water decreases as temperature increases (Figure 6.2). The heat of sorption calculated using equation 2.43 gives ΔH_s = -12.1 kJ/mol. Similar behavior was observed for water sorption isotherms in Nafion 115 as a function of temperature (Section 4.2) and has been observed by various researchers for SPEEK [161, 164, 167]. However, the magnitude of ΔH_s is smaller than that of Nafion and SPEEK (Chapter 4 and 5) due to the absence of the $-SO_3H$ groups.

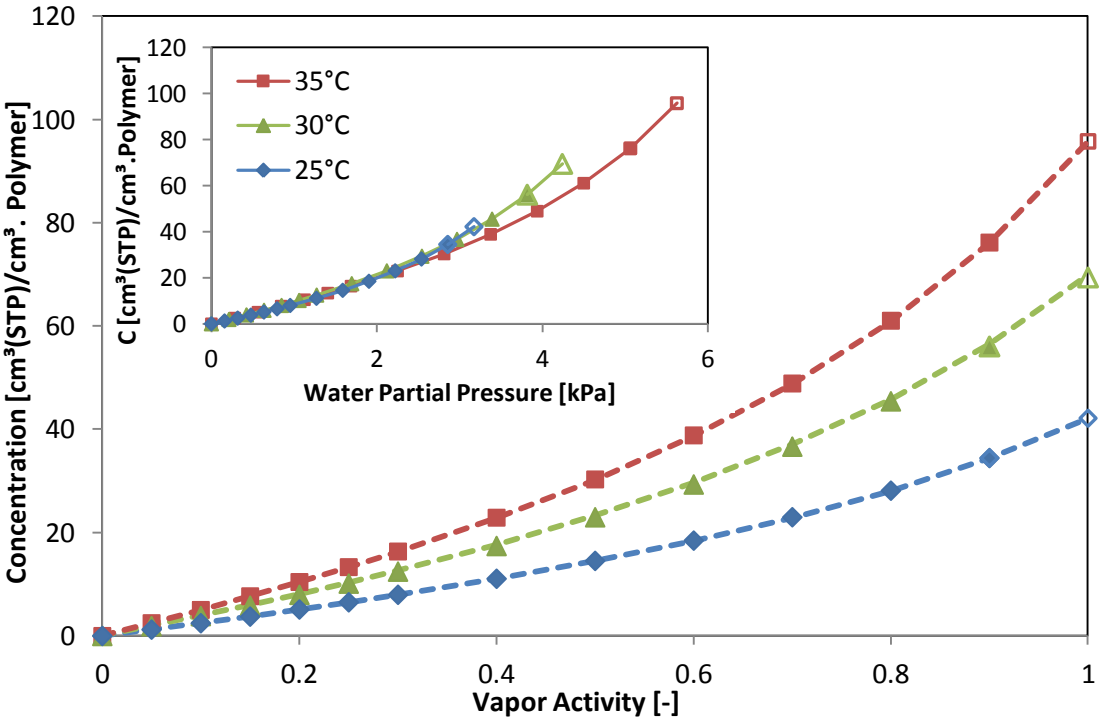

Figure 6.1: Water vapour sorption isotherms for 6FDA - durene at three temperatures (Note: Experimental data points have been fitted with the NDMS model and parameters obtained in Table 6.1 [dotted line]. Inset shows water concentration as a function of water partial pressure. Open data points are measured in liquid water)

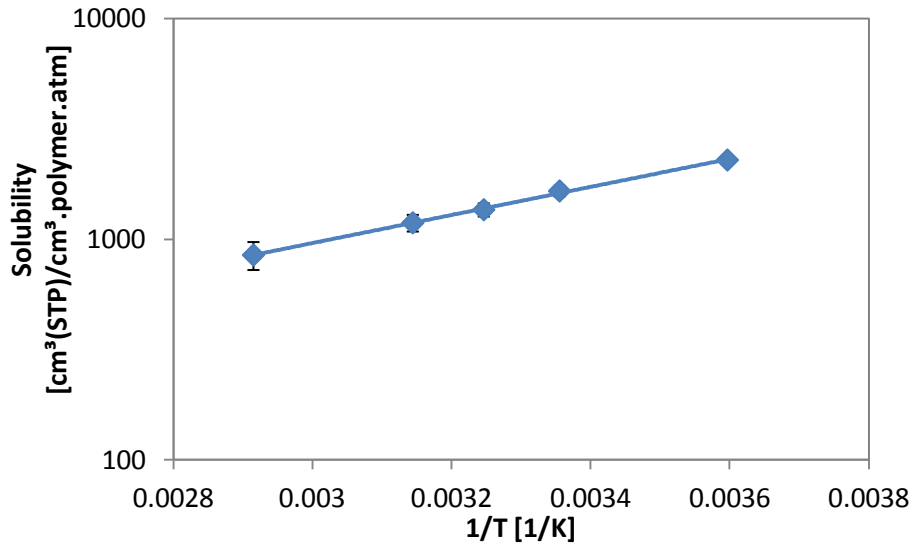

Figure 6.2: Liquid water solubility in 6FDA - TMPD as a function of temperature.

The water sorption isotherms in Figure 6.1 were modelled using the modified Dual Mode Sorption (equation 2.21) described in section 2.5.3. Furthermore, it was found that both $\overline{C_p}$ and k' are temperature-dependant and were modelled using Arrhenius Equations below:

$$\overline{C_p} = C_o e^{\left(\frac{-E_C}{RT}\right)} \qquad 6.1$$

$$k' = k_o e^{\left(\frac{-E_k}{RT}\right)} \qquad 6.2$$

The fit performed using non-linear regression techniques gives the parameters presented in Table 6.1.

Table 6.1: Estimated fitting parameters of 6FDA – TMPD.

Parameter	6FDA - TMPD
A'[-]	1.51 ± 0.02
k_o [-]	10.4 ± 1.3
E_k [kJ/mo]	7.2 ± 0.7
C_o [cm^3(STP)/cm^3.polymer]	4.82 ± 0.01 x 10^9
E_c [kJ/mol]	47 ± 5

The parameters fitted to the water sorption experimental data at 35 °C are comparable with that obtained by Chen *et al.* [101] at 35 °C as shown in Table 6.2. Furthermore, this model fits well to the experimental data points as shown by the dotted line in Figure 6.1.

Table 6.2: Comparison of fitting parameters for NDMS model for 6FDA - TMPD at 35 °C.

	This Work	Chen *et al.*, 2012 [101]
C_p $[cm^3(STP)/cm^3.polymer]$	52 ± 4	50 ± 8
k' [-]	0.62 ± 0.01	0.66 ± 0.03
A'[-]	1.51 ± 0.02	1.61 ± 0.25
$b_A=k'(A'-1)/f_0$ $[atm^{-1}]$	5.68	7.14

A Zimm – Lundberg clustering analysis (using Equation 2.19) was performed on these sorption isotherms. The clustering analysis is presented in Figure 6.3. As expected, the clustering integral (G/V_w) becomes more positive as the vapour activity increases. This is due to the increased water concentration as vapour activity increases observed in Figure 6.1 that results in increased water-water interactions and water clustering and has been reported by various researchers [45, 81, 178]. As temperature increases from 25 – 35 °C, the vapour activity above which clustering occurs decreases from ~0.8 to ~0.5, i.e. the onset of water cluster formation occurs at lower vapour activity at higher temperatures. This is due to the increase in water vapour concentration observed as temperature increases (Figure 6.1).

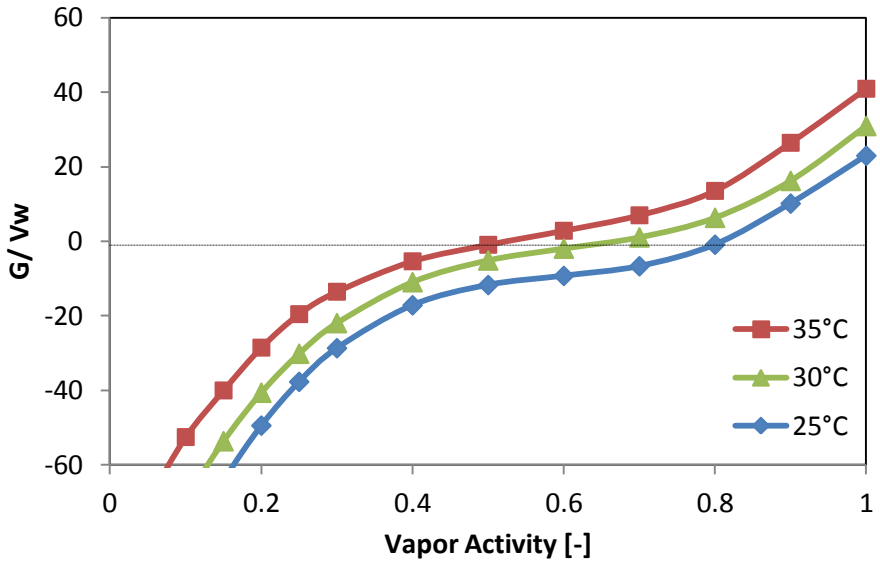

Figure 6.3: Zimm-Lundberg analysis of clustering for 6FDA – TMPD based on water vapour sorption isotherms.

6.3 Theoretical Glass Transition Temperature

The theoretical T_g for 6FDA – durene was calculated using water sorption isotherms in Figure 6.1 (a = 1) and the Fox equation 2.4 and is presented in Figure 6.4. As shown, in the presence of liquid water 6FDA – durene transitions from a glassy to a rubbery polymer at an experimental temperature of ~ 55 °C. Therefore, 6FDA – durene likely exists as a glassy polymer at 25 – 55 °C and as a rubbery polymer above 55 °C.

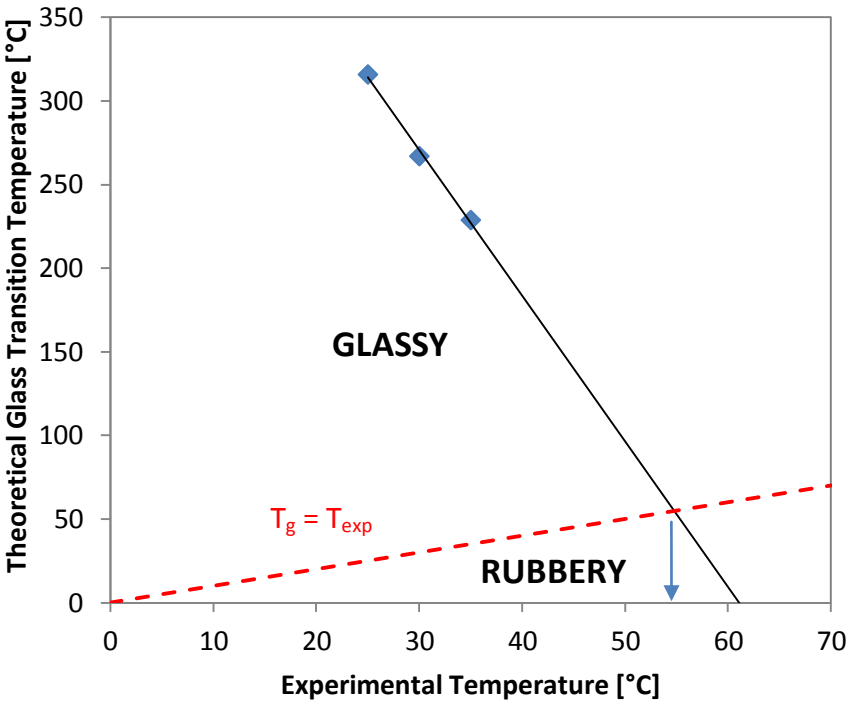

Figure 6.4: Theoretical T_g as a function of experimental temperature for 6FDA - TMPD in the presence of liquid water. The red dotted line represents the transition line between glassy and rubbery states.

6.4 Low Temperature Permeability Modeling

The model derived by Chen *et al.* [101] and discussed in section 2.5.7 was used to characterize the permeation of water vapor in a multi-component system. The water permeability data at 25 – 35 °C in Figure 6.5 was fitted to equation 2.32 using water sorption parameters presented in Table 6.1 and sorption parameters for CO_2 and N_2 obtained from literature (Table 6.3) to account for the competitive sorption effects. Fugacity based CO_2 sorption parameters have been reported by Duthie *et al.* [53] for a range of temperatures and have been interpolated for temperatures here. Similarly, N_2 sorption parameters have been investigated by Chung *et al.* [94, 95] for 6FDA - durene and have been extrapolated for temperatures here.

Table 6.3: Sorption parameters of CO_2 and N_2 in 6FDA - TMPD from literature.

	CO_2 [a]			N_2 [b]		
T [°C]	25	30	35	25	30	35
k_D $[cm^3(STP)/cm^3.atm]$	4.06	3.65	3.20	0.257	0.211	0.172
C'_H $[cm^3(STP)/cm^3]$	62.9	60.0	58.8	31.4	29.3	27.5
b $[atm^{-1}]$	0.73	0.65	0.55	0.051	0.048	0.045

[a] Data interpolated from Duthie *et al.* [53].

[b] Data extrapolated from Chung *et al.* [94, 95].

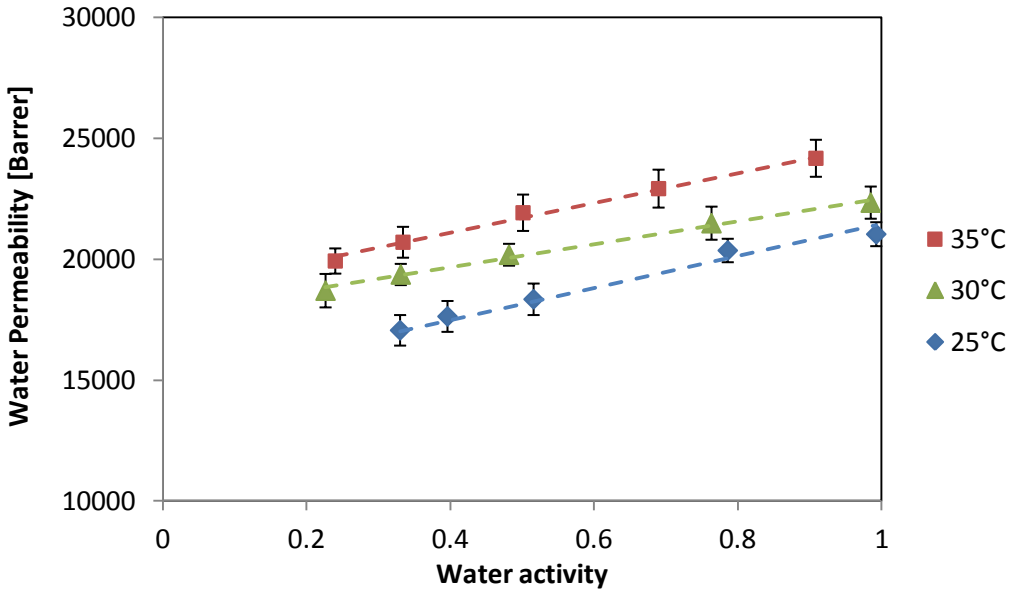

Figure 6.5: Water permeability through 6FDA - TMPD as a function of water activity and temperature (Data points: experimental data and Dotted line: fitted model).

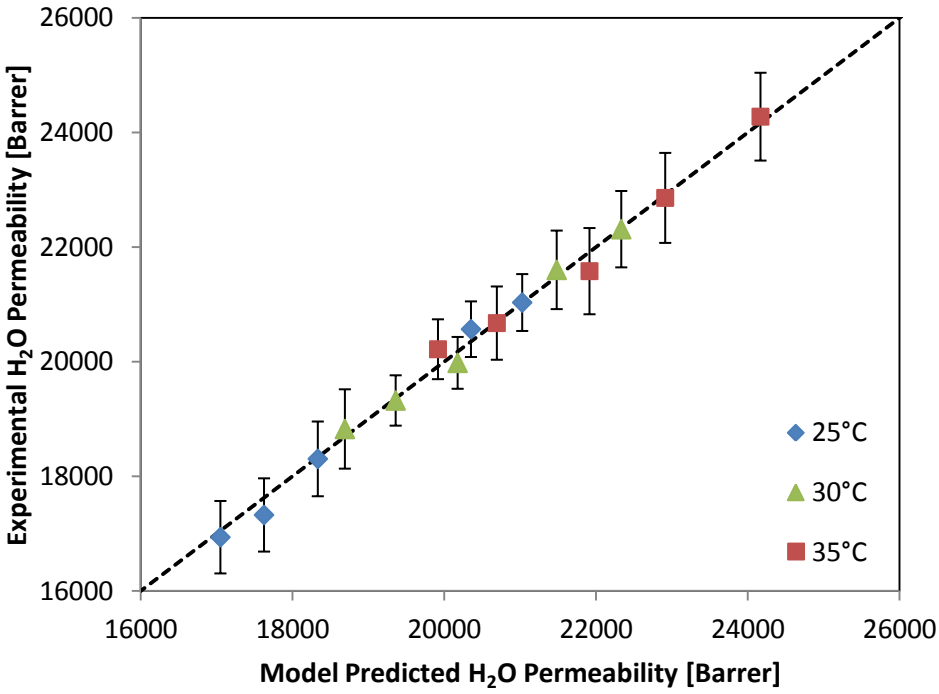

Figure 6.6: Experimental H_2O permeability plotted against the modelled H_2O permeability for 6FDA - TMPD at 25 – 35 °C.

As shown in Figure 6.5 and Figure 6.6, the experimental water permeability are fitted well by the model obtained by Chen *et al.* [101] for all three temperatures. The infinitely dilute Fickian diffusion coefficient (D_{A0}), immobilization factor (F_A) and concentration dependant diffusion constant (β_A) for the three temperatures are presented in Table 6.4. Furthermore, it was found that infinitely dilute Fickian diffusion coefficient (D_{A0}) is temperature-dependant and can be expressed as an Arrhenius expression:

$$\boldsymbol{D_{A0} = D_0 e^{\left(\frac{-E_{0,D}}{RT}\right)}} \qquad \textbf{6.3}$$

Table 6.4: Fitted parameters for modelling water vapour permeability for 6FDA - TMPD.

	This Work			Chen *et al.*, 2012 [101]
T [°C]	25	30	35	35
D_{A0} [cm^2/s]	1.94 ± 0.03 x 10^{-7}	2.02 ± 0.02 x 10^{-7}	2.11 ± 0.02 x 10^{-7}	2.17 ± 0.02 x 10^{-7}
D_0 [cm^2/s]		2.38 ± 0.09 x 10^{-8}		-
$E_{o,D}$[kJ/mol]		6.21 ± 0.07		-
F_A		0.65 ± 0.22		0.61 ± 0.04
β_A [cm^3/cm^3]	-0.029 ± 0.004	-0.022 ± 0.002	-0.017 ± 0.004	-0.017 ± 0.001

As a comparison, the fitted parameters obtained in this study at 35 °C are compared to and found to be in good agreement with that obtained by Chen *et al.* [101]. As expected, the infinitely dilute Fickian diffusion coefficient (D_{A0}) increases as temperature increases (Table 6.4) due to the increased kinetic energy of the water molecules; supporting the literature [53, 192, 193]. The empirical constant for concentration dependant diffusion (β_A) is negative for all three temperatures which is indicative of the formation of water clusters that ultimately hinder diffusion [101]. However, the β value becomes less negative as temperature increases. The immobilization factor (F_A) is the ratio of diffusion coefficients in Langmuir region to Henry's Law region. The change in diffusion coefficients in the two regions is effected by temperature to the same extent, hence the value of F_A was found to be independent of temperature.

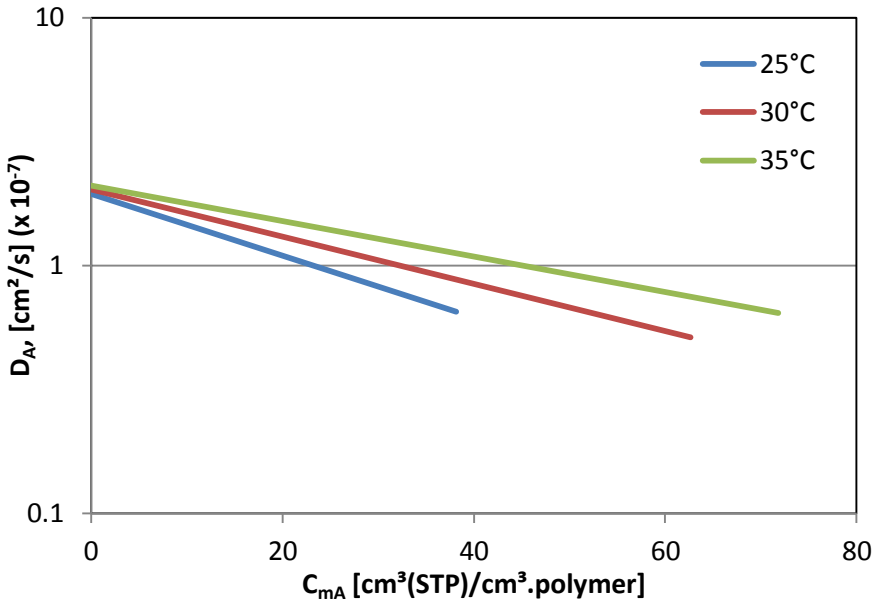

Figure 6.7: Fickian diffusion coefficient, D_a as a function of the mobile concentration of water, C_{mA} and temperature.

Figure 6.7 shows the Fickian diffusion coefficient, D_A through 6FDA - durene as a function of the mobile water concentration (C_{mA}) and temperature (calculated using equations 2.34 and 2.37, respectively). The Fickian diffusion coefficient (D_A) decreases as water concentration increases due to the increased pore-filling effects which block diffusional pathways [65, 101]. However as temperature increases, this decrease in D_A is greater due to the increased water concentration in the polymer at a higher temperature. This consequently results in significantly greater pore – filling effects as well as the increased formation of water clusters as temperature increases (as shown previously in Figure 6.3). These water clusters hinder the diffusion of individual water molecules and result in a decrease in D_A. Similar result was obtained by Stern *et al.* [82] and Detallante *et* al [178] who both attributed the decreasing D_A with increasing water activity solely to the formation of water clusters that hinder diffusion. However, it is noteworthy that the trend is opposite to that observed by Potreck *et al.* for SPEEK (Figure 2.14). As expected, the Fickian diffusion coefficient is larger at a higher temperature for any given C_{mA} value due to increased FFV at 35 °C compared to 25 °C (Figure 6.1).

6.5 Water Vapour Permeability

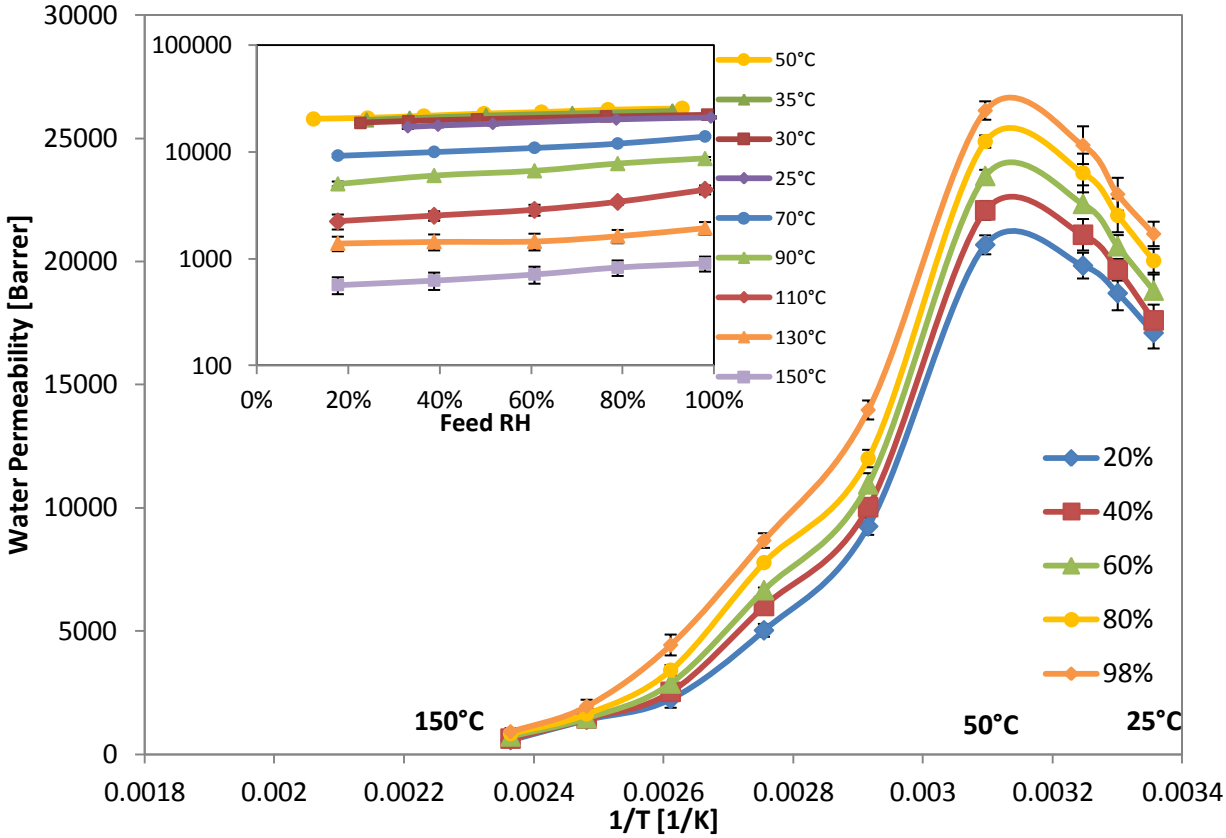

Figure 6.8: Water permeability through 6FDA - durene as a function of temperature (For clarity, water permeability as a function of feed RH is presented as an inset)

Water permeability through 6FDA - durene across a wide range of temperatures is presented in Figure 6.8. The permeability data at 25 – 70 °C was investigated using the mixed gas permeation rig described in section 3.3.2 while high temperature permeability data at 70 – 150 °C was investigated using the high temperature steam permeation set – up described in section 3.3.3. The water permeability data at 70 °C for the two experimental rigs was found to be in good agreement. As expected, water permeability increases as feed RH increases from 20% to 98% as shown from the inset of Figure 6.8. This is due to the increased sorbed water vapour concentration as well as water-induced plasticization observed at high vapour activities [54, 81].

As observed in Figure 6.8, there is a clear maximum in the permeability between 40 – 50 °C suggesting a change in mechanism. This change may correlate with the transition of 6FDA - durene from glassy to rubbery at ~55 °C (Figure 6.4). It is

possible that the nature of water clusters in a rubbery system differs to that in the glassy state and this results in a reduction in diffusion coefficient. Decreases in the diffusion coefficient have been observed By Potreck *et al.* [14] for rubbery PEBAX, Chang *et al.* [233] for Poly (acrylic acid) and Armstrong *et al.* [234] for Ethyl Cellulose as it transitions to a rubbery state at high water concentrations. Furthermore, Dettalante *et al.* [178] and Okamoto *et al.* [81] report the presence of water vapour as clusters particularly in a hydrophobic polymeric matrix such as non-sulphonated 6FDA based polyimides as is the case here. Additionally, solubility decreases as temperature increases (Figure 6.2) and this may dominate changes in diffusivity resulting in the net decrease in water permeability above 50 °C observed in Figure 6.8. This behavior is consistent for rubbery polymers that are solubility selective. Overall, the change in mechanism observed above 50 °C is a result of various effects including changes in diffusivity as a result of changing glassy/rubbery states and clustering as well as the decrease in solubility; a phenomenon observed for SPEEK in Chapter 5 and by many researchers [6, 53, 82, 83, 153, 158]. Sato *et al.* studied the change in the infinitely dilute Fickian diffusion coefficient (D_{A0}) and concentration dependant diffusion (β_A) as a function of the glass transition temperature of a range of 6FDA based polyimides. They found that the β_A becomes more negative for rubbery polymers as shown in Figure 2.20. They also reported the ability of water to cause both plasticization and clustering in 6FDA-TeMPD [83].

As observed in previous chapters, there is also a change in the activation energy of water permeation from a positive to a negative value at ~50 °C for 6FDA - durene as shown in Table 6.5.

Table 6.5: Activation energy of water permeability for 6FDA - TMPD in two temperature ranges.

	Temperature Range [°C]	E_p [kJ/mol]
This Work	25 - 50	6.6 ± 0.1
	50 - 150	-38 ± 1

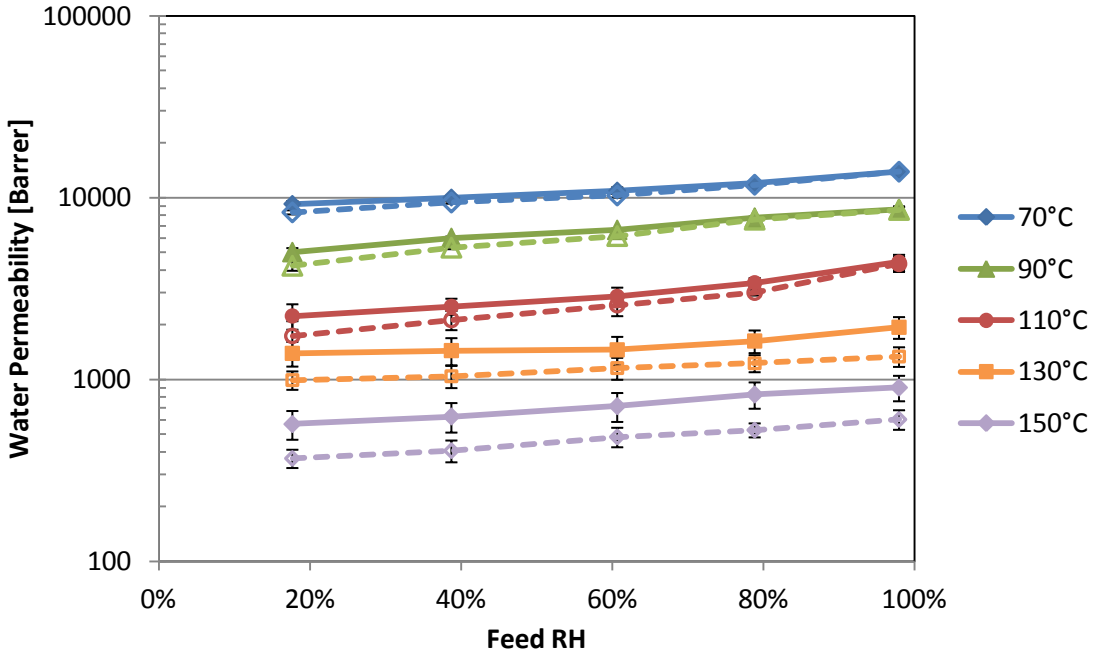

Figure 6.9: Water permeability through 6FDA - TMPD at 70 – 150 °C with steam/CO_2 (Solid lines) and steam/N_2 (dotted line) feed mixtures.

The plasticization effects of CO_2 at high temperature (70 – 150 °C) were studied using steam/CO_2 (solid lines) and steam/N_2 (dotted lines) feed streams with the results presented in Figure 6.9. The plasticization effects of CO_2 are more pronounced at low feed water activity where the water permeability with pure CO_2 stream is higher than that obtained with N_2 for any given temperature. This is because the plasticization ability of water is limited at these low water activities allowing the CO_2 induced plasticization effects to be visible. Furthermore, competitive sorption by CO_2 may also limit the increase in water solubility. It is well known that plasticization by CO_2 can occur at partial pressures well below the critical plasticization fugacities [53, 81, 195]. However as water activity increases, water-induced plasticization becomes significant enough to mask any plasticization caused by CO_2 resulting in no significant difference observed between the CO_2 and N_2 water permeabilities. Similar results at low water activity were observed by Chen *et al.* [54] at 35 °C.

As temperature increases, the difference in water permeabilities observed between the two feed streams becomes significant. This is mainly the result of high CO_2 pressures needed to make steam/CO_2 mixtures at 150 °C. This consequently

results in increased CO_2 partial pressures at high temperatures that give increased water permeability in the presence of CO_2.

6.6 CO_2 & N_2 Permeability

Figure 6.10 presents dry CO_2 and N_2 permeabilities (RH 0%) through 6FDA - durene as a function of temperature at 35 – 150 °C. N_2 permeability increases with increasing temperature due to increasing diffusivity while CO_2 permeability decreases as solubility effects dominate. Similar trends for these two gases were observed by Duthie *et al.* [53] with increasing temperature. Both Duthie *et al.* [53] and Chung *et al.* [208] obtained pure CO_2 and N_2 gas permeabilities of ~ 440 – 570 Barrer and ~ 35 - 47 Barrer at 35 °C and 10 bar, respectively that match well against the ~470 Barrer and ~36 Barrer measured in this study. Similar results have been observed by various other researchers [184, 187, 191, 208].

CO_2 and N_2 permeability as a function of temperature (25 – 150 °C) and feed RH (20 – 80 %) is also presented in Figure 6.10. As feed RH increases from 20% to 80%, both CO_2 and N_2 permeabilities decrease. This is due to competitive sorption with water molecules in the Langmuir region where increased feed RH leads to increased water sorption and reduced gas sorption. Similar result was reported by Chen *et al.* [54] for CO_2 and CH_4 mixtures with increasing water activity and by various researchers [77, 235].

Both figures show similar behavior to water permeability in Figure 6.8 with respect to temperature. Both CO_2 and N_2 permeability increase initially as temperature increases from 25 °C to 50 °C. However, as temperature increases above 50 °C, both permeabilities drop due to the prominent decrease in penetrant solubility. It is interesting to note that the decrease in water permeability as temperatures increases from 50 °C to 70 °C in Figure 6.8 is significantly greater (~ 50%) compared to the 30% and 32% permeability drop observed for CO_2 and N_2 respectively for the same temperature range. A possible reason for this is the reduced water solubility in the polymer as temperature increases (Figure 6.2) that consequently results in reduced competitive sorption of CO_2 and N_2 with water molecules.

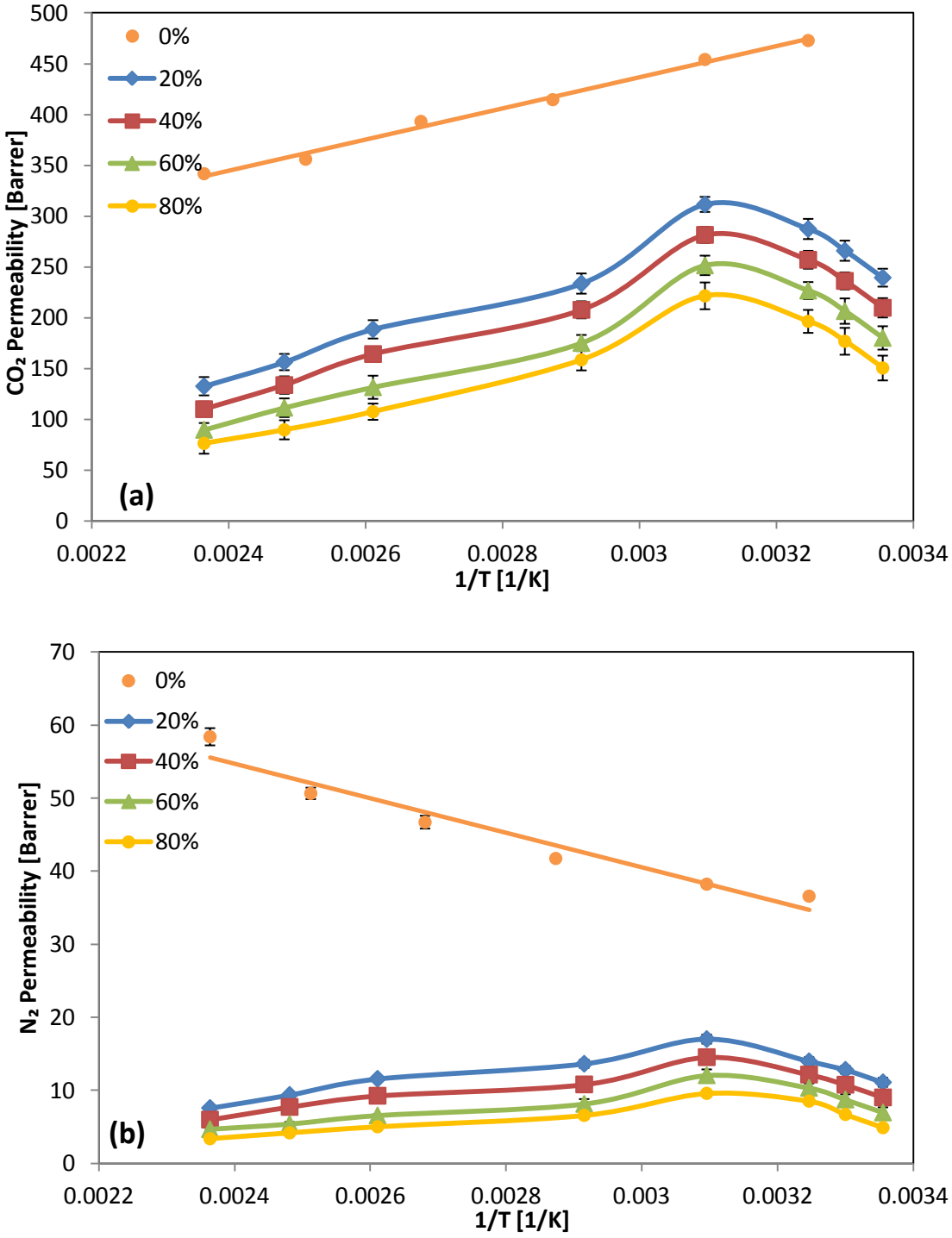

Figure 6.10: CO_2 permeability (a) and N_2 permeability (b) through 6FDA - TMPD as a function of temperature and feed RH (%).

The dry CO_2 and N_2 permeabilities at RH 0% are significantly higher when compared against the wet permeabilities shown in Figure 6.10. This further supports the occurrence of competitive sorption with water molecules that results in reduced gas sorption. It may also be a result of the presence of water clusters

that hinder diffusion of these gas molecules. Hence, these lower diffusivity and solubility effects combine to produce lower CO_2 and N_2 permeabilities in the presence of water.

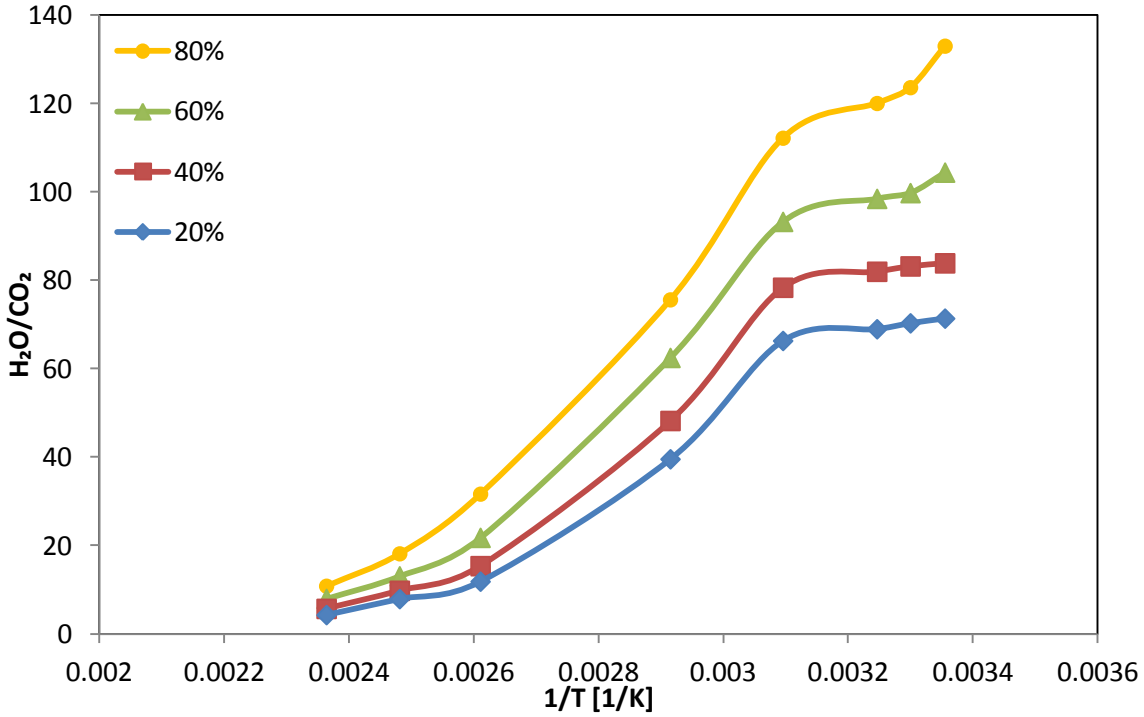

Figure 6.11: H_2O/CO_2 selectivity through 6FDA - TMPD as a function of temperature and feed RH (%).

Figure 6.11 shows H_2O/CO_2 selectivity of 6FDA - durene as a function of feed RH and temperature. As feed RH increases from 20% to 80%, the selectivity of H_2O/CO_2 also increases. This is a direct reflection of the increase and decrease in water and CO_2 permeabilities observed in Figure 6.8 and Figure 6.10a, respectively. However as temperatures increases, H_2O/CO_2 selectivity decreases. The drop in selectivity is small at low temperatures of 25 – 50 °C due to the similar increases in water and CO_2 permeability observed. However as discussed previously, the decrease in water permeability (Figure 6.8) at temperatures above 50°C is significantly greater than that observed for CO_2 permeability in Figure 6.10a. Consequently at temperatures above 50°C, the H_2O/CO_2 selectivity reflects this significant drop in water permeability.

6.7 Conclusion

The Zimm – Lundberg clustering analysis performed on 6FDA – TMPD water sorption isotherms found that water clusters increased as temperature and water vapor activity increased. Water, CO_2 and N_2 permeability data at 25 – 35 °C was modeled and it was found that the infinitely dilute Fickian Diffusion Coefficient (D_0) increased and the water plasticization parameter (β) became less negative as temperature increased. This reflected increased concentrations of water in the polymer. Water, CO_2 and N_2 permeability was investigated at 25 – 150 °C and as a function of water activity. It was found that all permeabilities increased as temperature increased from 25 °C to 50 °C due to an increase in diffusion. However as temperature increased above 50 °C, the reduction in solubility resulted in a significant decrease in permeability of all three components. A similar change in the sign of the activation energy of water permeation to previous chapters was observed. Water permeability increased with increasing water activity due to increased solubility at higher activities while CO_2 and N_2 permeability decreased due to increased competitive sorption of water as well as the presence of water clusters at higher activities.

Chapter 7 Comparison of the Selected Investigated Membranes

7.1 Membrane Performance

The water permeances as a function of feed water activity for the investigated membranes at 150 °C are presented in Figure 7.1. As shown, the two PFSA based membranes have the highest water permeance while 6FDA - durene has the lowest. This is due to the presence of the $-SO_3H$ groups in PFSA membranes that aids in water sorption and consequently water permeability. This is further indicated by the rate of increase of water permeance as a function of feed water activity especially at high water activities. This rate is greatest for sulphonated membranes that swell in the presence of water such as Fumatech F - 920, Nafion 115, SPEEK IEC 1.6 meq/g and IEC 1.9 meq/g. 6FDA - durene has no sulphonic acid groups and consequently does not swell at high water activities. A further contributing factor is the differences in membrane thickness, with the thinner Fumatech F - 920 outperforming the thicker Nafion membrane.

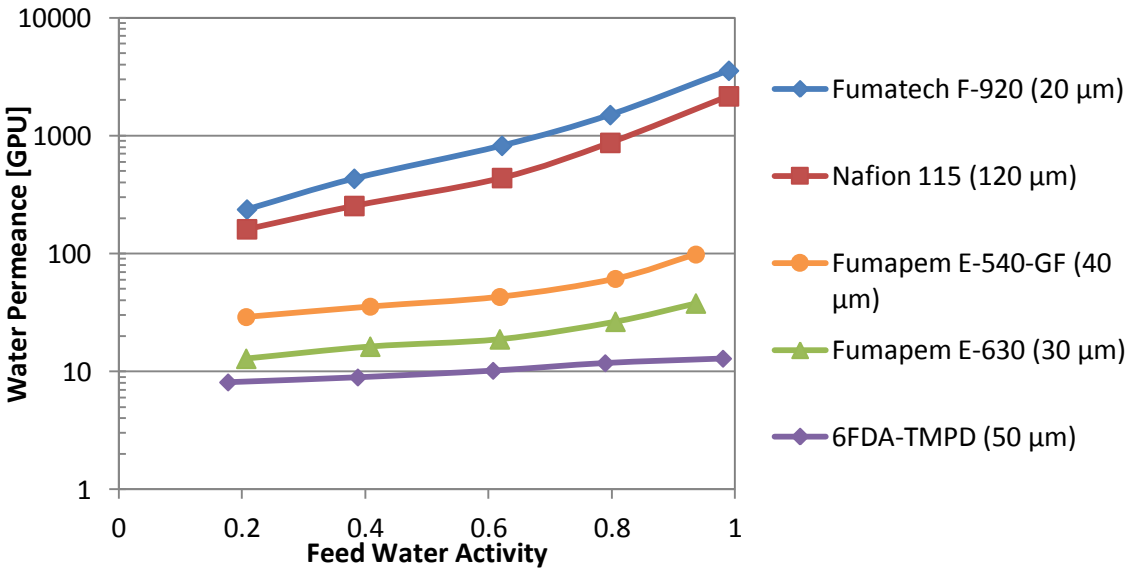

Figure 7.1: Water permeance (GPU) for tested membranes as a function of feed water activity at 150 °C

CO_2 permeances as a function of feed water activity for the investigated membranes at 150 °C are shown in Figure 7.2. For sulphonated membranes that

swell in the presence of water, the CO_2 permeances increase as feed water activity increases. This is due to the opening of pathways through which CO_2 diffusion occurs. However for 6FDA - durene, the CO_2 permeance decreases as feed water activity increases. This is due to the competitive sorption effects of water that reduces CO_2 solubility as well as a decrease in diffusion caused by water clustering that consequently results in reduced permeability through the membrane.

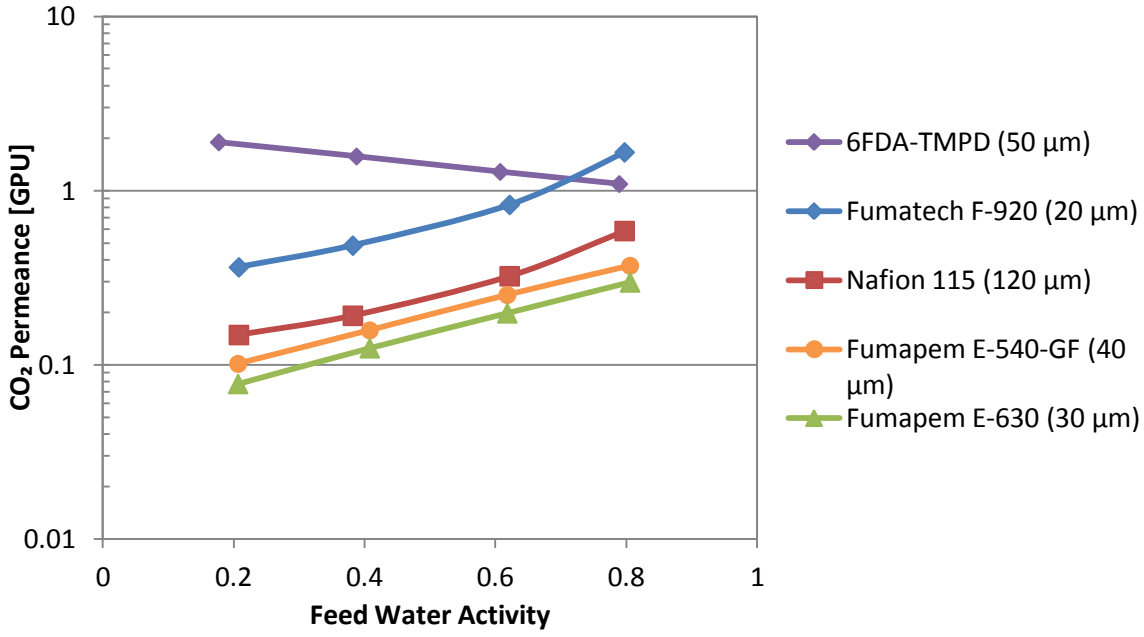

Figure 7.2: CO_2 permeance (GPU) for tested membranes as a function of feed water activity at 150 °C

Figure 7.3 shows H_2O/CO_2 selectivity for the investigated membranes based on Figure 7.1 and Figure 7.2. As expected, the H_2O/CO_2 selectivity of Fumatech F - 920 is the highest while 6FDA - durene is the lowest. There is a very small increase in H_2O/CO_2 selectivity of these membranes with increasing water activity due to the greater increase in water permeance observed in Figure 7.1. In contrast, the H_2O/CO_2 selectivity of SPEEK membranes decreases with increasing water activity due to the greater increase in CO_2 permeance relative to water permeance for these membranes. 6FDA - durene shows increasing H_2O/CO_2 selectivity with increasing water activity due to the increased competitive sorption of water that reduces CO_2 solubility.

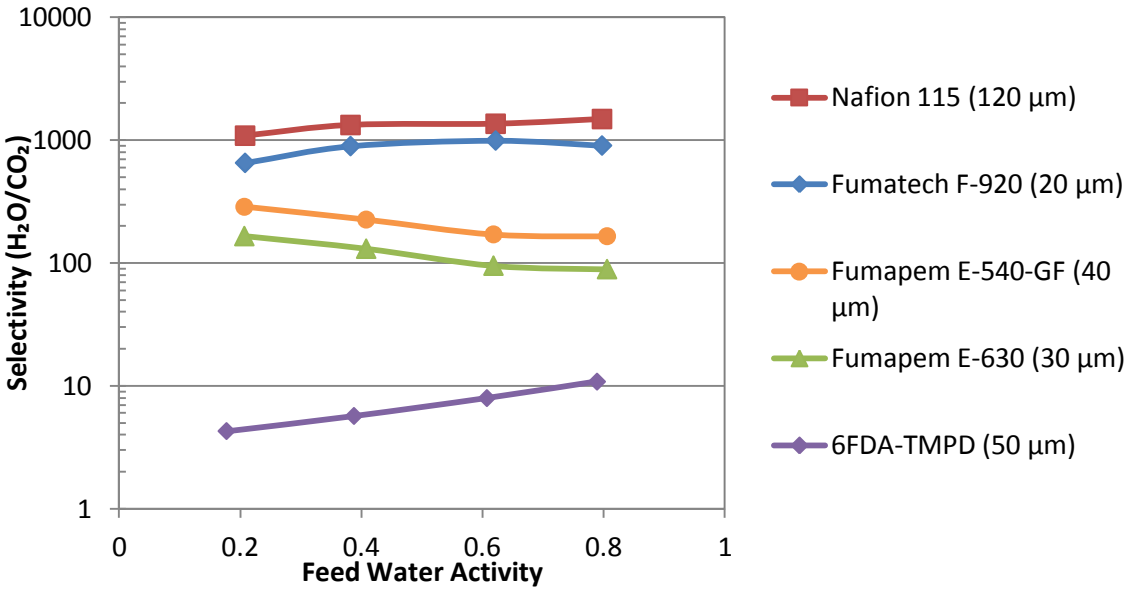

Figure 7.3: H_2O/CO_2 selectivity of investigated membranes at 150°C.

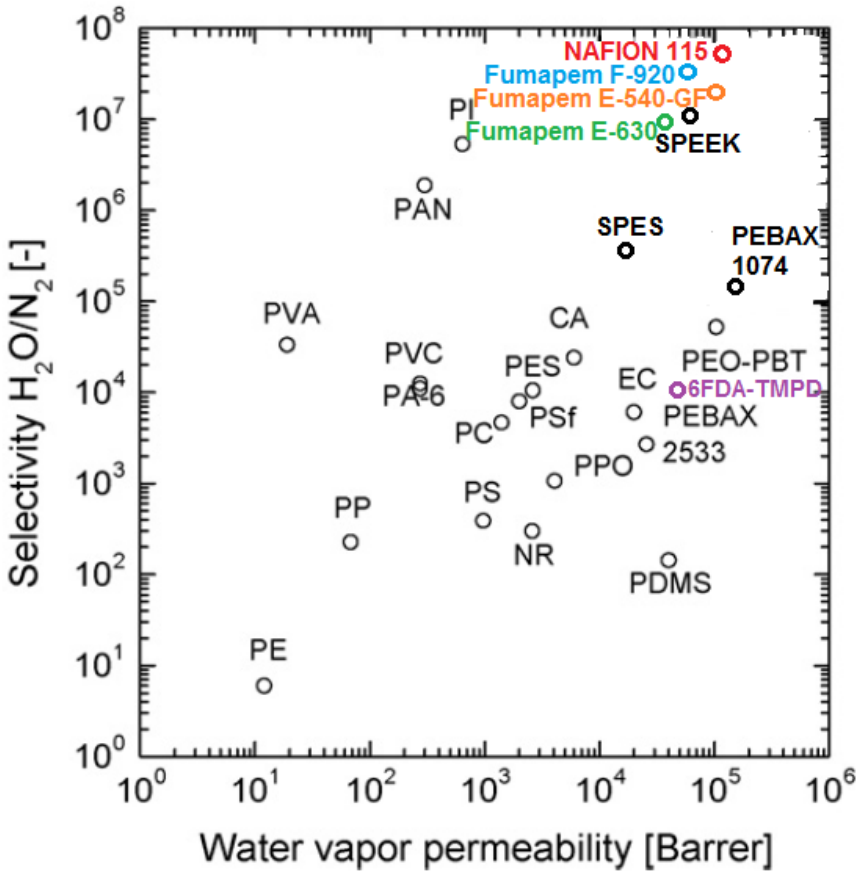

Figure 7.4: H_2O/N_2 selectivity vs water permeability plot updated with membranes from this work at 30°C [6].

Figure 7.4 shows the H_2O/N_2 Robeson's plot reported by Wessling *et al.* [6] at 30°C. This plot has been updated to show the results from this thesis where all membranes except 6FDA – TMPD lie within the targeted area of high selectivity and high permeability. Since this figure is based on permeability which accounts for membrane thickness, the effects of thicknesses are not considered. It should be noted that in this work much care was taken to eliminate concentration polarization. Similar efforts may not have been used in other work which would lead to lower permeabilities and selectivities than in the data presented here.

Figure 7.5 presents H_2O/CO_2 and H_2O/N_2 selectivity as a function of water permeance at 150 °C. The H_2O/N_2 selectivity at 150°C for SPEEK is slightly higher than PFSA polymers. This is due to the significant drop in N_2 permeability for PFSA membranes as compared to SPEEK. However, the selectivities are considerably lower than H_2O/N_2 at 30 °C (Figure 7.4) due to the lower permeabilities at the higher temperature. The H_2O/CO_2 selectivity follows the same trend as Figure 7.4 where Nafion 115 has the highest selectivity while 6FDA – TMPD has the lowest.

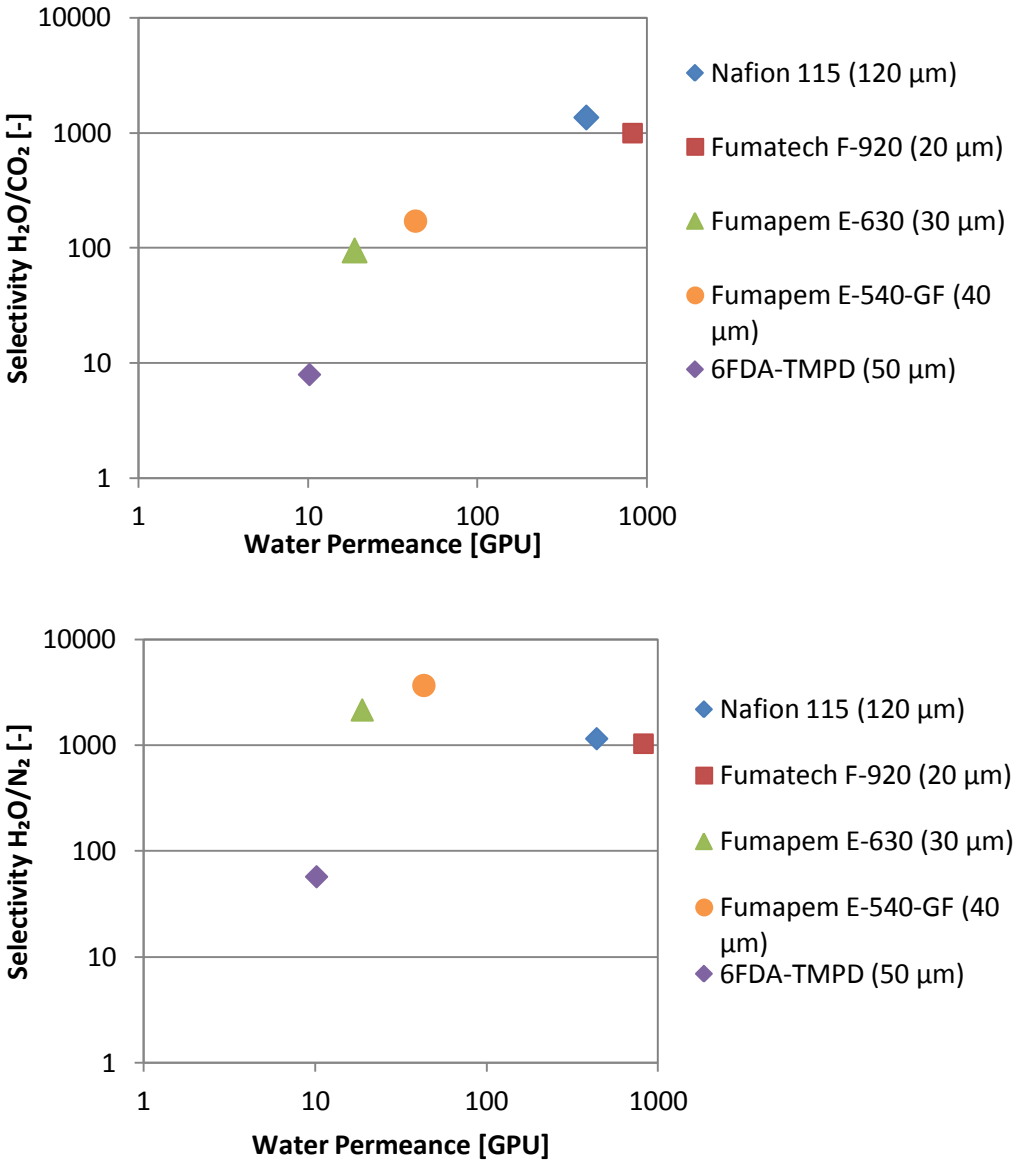

Figure 7.5: H_2O/CO_2 selectivity vs. water permeance (top) and H_2O/N_2 selectivity vs. water permeability (bottom) for the selected membranes at 150 °C.

A comparison of the heat of sorption and activation energy of water permeation for the selected membranes is presented in Table 7.1. All heat of sorption and activation energy values are negative indicating towards decreasing solubility and permeability trends as temperature increases for these selected membranes.

Table 7.1: Comparison of heat of sorption and activation energy of water permeation for the selected membranes.

	ΔH_s [kJ/mol]	E_a, [kJ/mol]
Nafion	-40.8 ± 2.4	-25.5 ± 3.1
SPEEK IEC 1.9 meq/g	-33.9 ± 0.6	-43.0 ± 0.8
SPEEK IEC 1.6 meq/g	-32.6 ± 0.5	-46.0 ± 0.9
6FDA - TMPD	-12.1 ± 0.3	-38.0 ± 0.9

7.2 HYSYS Modeling Results

A simulation was performed to determine the possible permeate composition if these membranes were exposed to a brown coal flue gas at 150 °C and 1 Bar. The experimental permeance values along with feed composition, temperature and pressure were entered into a membrane extension within ASPEN HYSYS® Version 7.3 and using the Peng Robinson Fluid Package. The schematic with the input variables are shown in Figure 7.6. This extension is an in – house programmed module that is based on mass transfer equations for counter – current flow configurations [236]. For a feed stream at 150 ^{0}C and 1 Bar containing 25 mol% water, there is no potential for heat recovery as the maximum available partial pressure of water is ~25 kPa on the feed side. Hence, all simulations were performed for a downstream permeate pressure of 10 kPa to determine the purity of the liquid water stream at 40 ^{o}C.

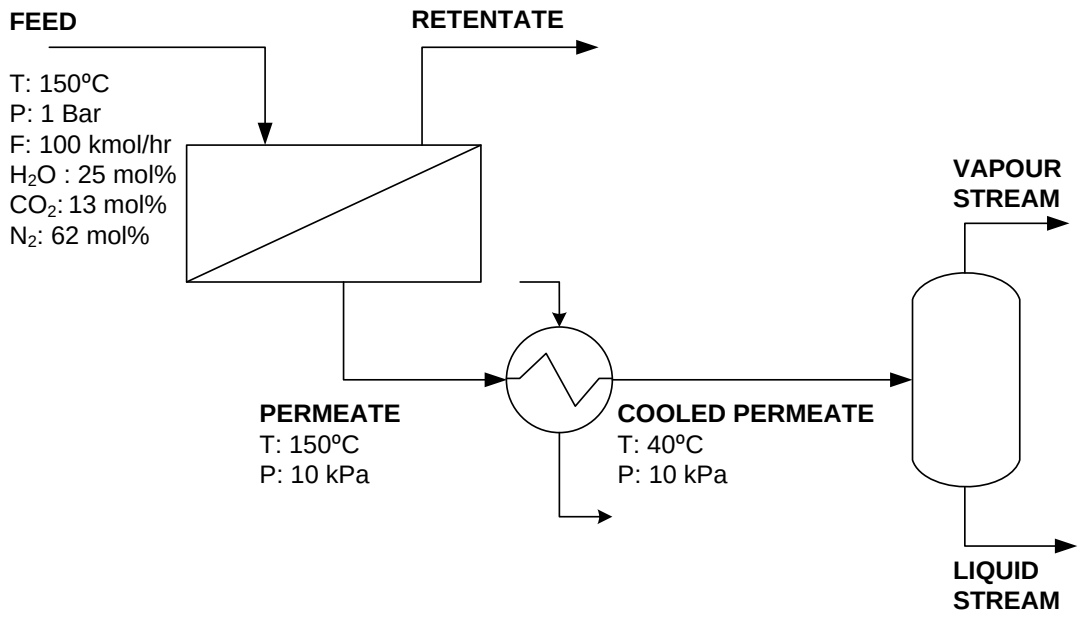

Figure 7.6: Schematic of the membrane module with input variables.

Water, CO_2 and N_2 permeabilities used in the simulations for the investigated membranes are presented in Table 7.2. It should be noted that while the simulation module takes into account the changes in composition of both feed and permeate streams along the length of the module, it does not account for the impacts of concentration polarisation within the membrane unit. Such concentration polarisation would tend to reduce the water permeabilities and increase the permeability of other gases, so that the results here probably reflect the worst case.

Table 7.2: Input permeabilities and dry membrane thickness for simulations (Calculated from experimental data based on feed composition provided in [237])

	Nafion 115	Fumapem F – 920 – RF	SPEEK IEC 1.6 meq/g	SPEEK IEC 1.9 meq/g	6FDA - TMPD
CO_2 [Barrer]	12.2	2.5	2.82	5.15	149
N_2 [Barrer]	12.3	2.8	0.10	0.15	9.1
H_2O [Barrer]	14150	2889	215	550	519
Dry Thickness [µm]	127	20	30	40	50

The permeate pH was calculated using the mole fraction of CO_2 and H_2O in the permeate stream from the HYSYS simulation. The change in permeate pH as a function of water recovery was insignificant for all membranes. The average pH values are presented in Table 7.3. Nafion 115 gave the highest pH of 5.67 compared to pH of 4.27 for 6FDA - TMPD. This better separation is due to the higher selectivity of Nafion 115 compared to 6FDA - TMPD [238].

Table 7.3: pH of the recovered liquid stream for the investigated membranes.

Material	Liquid Stream pH
Nafion 115	5.67 ± 0.06
Fumapem F - 920	5.35 ± 0.05
Fumapem E - 540 - GF (IEC 1.9 meq/g)	5.07 ± 0.07
Fumapem E - 630 (IEC 1.6 meq/g)	4.96 ± 0.06
6FDA - TMPD	4.27 ± 0.08

The membranes area (for 100 kmol/hr of feed flow rate) required for these membranes as a function of water recovery are presented in Figure 7.7. For one stage process, the membrane areas required are very large due to the low feed water content and partial pressure. Membranes with high selectivities like Nafion 115 and Fumapem F - 920 require the largest membrane areas compared to 6FDA - TMPD with a low selectivity. Furthermore as water recovery increases, the

membrane areas required to achieve this also increase. Similar results have been obtained by Merkel *et al.* [238] who modelled the membrane areas required for post-combustion CO_2 capture. They reported a trade off between purity of the permeate stream and membrane areas where areas required to recover pure streams for highly selective membranes are very large compared to those required to recover less pure streams by membranes with lower selectivity. This is indeed the case here where largest membrane areas are obtained for Nafion 115 and Fumapem F - 920 that gave highest selectivities and liquid stream pH.

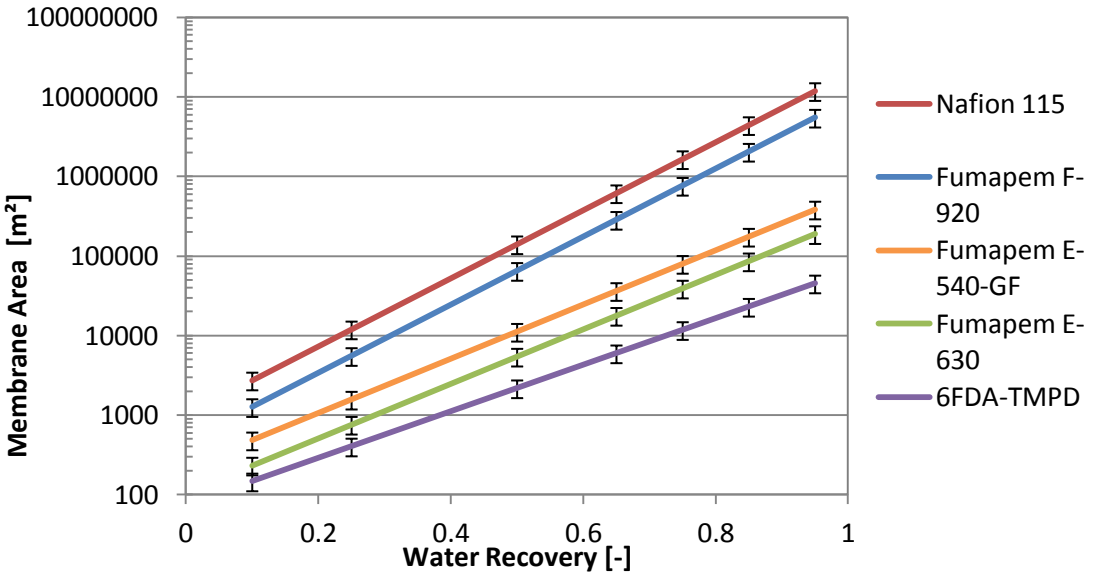

Figure 7.7: Membrane areas required for investigated membranes as a function of water recovery (for feed flow rate of 100kmol/hr).

Based on permeate pH alone, the best possible option for the proposed application is Nafion 115 with a permeate pH of 5.67. However, the membrane areas required for separation are very large and this needs to be taken into account. Regardless a higher purity product is required; hence any water recovered through these membranes would have to undergo pH adjustment to ensure it is suitable for recycle into the process.

Chapter 8 Conclusions & Future Perspectives

8.1 Conclusions

Water vapour from high temperature brown coal flue gases can be recovered using water-selective polymeric membranes. Several researchers have looked at using polymeric membranes for this application. However, the performance of these membranes has only been investigated at low temperature for mixed gas behaviour of water vapour and N_2. While N_2 is the major component in flue gas, in this instance the presence of CO_2 also needs to be investigated to determine its effect on the performance of membrane and consequently the recovered stream. This work considered the separation performance of Nafion 115, Sulphonated Poly (Ether Ether) Ketone and 6FDA – TMPD at elevated temperatures. Water, CO_2 and N_2 permeation properties of these membranes were investigated on a novel high temperature mixed gas rig.

For all three membrane types, the water uptake and concentration in the polymer increased as temperature increased. This is due to increasing saturation vapour pressure and consequently partial pressure at a given water activity. However, solubility decreased as temperature increased which is consistent with most polymeric materials. The formation of clusters at high water concentrations was confirmed using Zimm-Lundberg clustering analysis and FTIR spectra. This was attributed to increased water-water interactions at higher water concentrations.

These membranes showed a peak in permeability at ~ 50 – 70 °C. The initial increase with temperature was related to the increase in diffusivity. As temperature continued to increase, there was likely a decrease in diffusion due to the formation of large water clusters as well as a transition from glassy to rubbery state. This coupled with the decreasing solubility resulted in a change in mechanism of permeation observed at ~ 50 – 70 °C. This caused a change in the signs of the activation energy of permeation at around 50 °C. Furthermore, the CO_2 and N_2 permeabilities were also influenced by this change in mechanism where a peak in permeability at ~50 – 70 °C was also observed for these gases.

In particular, the permeation of water, CO_2 and N_2 through Nafion 115 was investigated at 70 – 150 °C. All three permeances and water solubility increased with increasing water activity. These changes in solubility and permeance were attributed to membrane swelling as water concentration in the polymer increased at higher water activities. A calculation of theoretical T_g suggested the rubbery state of Nafion for the entire experimental temperature range considered in this chapter. A comparison with a thinner PFSA polymer showed inhomogeneity in membrane swelling where water, CO_2 and N_2 permeances did not scale linearly with membrane thickness, reflecting non-linear water activity gradients within the membrane.

The effect of temperature on water vapour and CO_2 permeation properties of SPEEK at two different IEC was investigated. Water concentration and solubility increased with increasing water activity due to membrane plasticization. This resulted in an increase in the permeability as a function of water activity. SPEEK with IEC 1.9 meq/g exhibited higher permeation and selectivity than IEC 1.6 meq/g. This is due to the increased presence of the sulphonic acid groups that interact more strongly with water molecules resulting in greater water uptake.

Water vapour and gas permeation properties of 6FDA - TMPD from 25 – 150 °C were investigated. Modelling of the water sorption at 25 – 35 °C showed that the water sorbed in the polymer exists as clusters causing a decline in diffusivity with increasing concentration. While water permeability increased with increasing water activity, CO_2 and N_2 permeabilities decreased due to competitive sorption of water. These competitive sorption and plasticization effects were investigated at high temperatures by comparing water permeability data from a H_2O/CO_2 feed mixture to that from a H_2O/N_2 feed mixture. It was found that at low temperatures, the competitive sorption of water reduces sorption of both CO_2 and N_2 resulting in similar water permeabilities through the membrane for both gases. However as temperature increases, the sorption of water is decreases resulting in increased water permeability for H_2O/CO_2 feed mixture. This is due to the increased sorption of CO_2 and consequently increased CO_2 plasticization effects.

The permeance data for water and CO_2 at 150 °C were compared for all five polymers. The highest H_2O/CO_2 selectivity was for Nafion 115 followed by Fumapem F - 920, Fumapem E - 540 - GF and Fumapem E - 630 with 6FDA - TMPD having the lowest selectivity. The permeance data was modelled within Aspen HYSYS and it was found that a permeate stream with pH 5.67 is achievable with Nafion 115 at 150 °C. However, the membrane areas required for this are very large indicating that there exists a trade-off between permeate purity and membrane areas. For reuse in the process, a high purity/pH product is required therefore pH adjustment of the recovered stream would be needed regardless of whichever membrane material is chosen and used.

8.2 Future Perspectives

There are various suggestions for future researchers considering the investigation of polymeric membranes for high temperature flue gas dehydration:

- The sorption properties of Nafion, SPEEK and 6FDA - durene membranes at high temperatures as a function of water activity need to be investigated to accurately determine the water sorption and clustering effects. For this, a gravimetric sorption analyser needs to be specially designed and constructed for high temperature water sorption analysis. These sorption parameters will consequently enable permeability modelling at high temperatures.
- Positron Annihilation Lifetime Spectroscopy (PALS) characterisation can be carried out to study the effect of water presence on free volume within these polymers. This will further explain the presence of clusters.
- The effect of fly ash, SOx and NOx on the performance of these membranes needed to be investigated, especially at high temperatures.
- The effect of high temperatures on mechanical properties of these membranes needs to be investigated to determine their suitability for this application.
- Other candidate materials including Polyvinyl Alcohol (PVA), sulphonated polyimides (SPI) and sulphonated Poly Ether Sulphones (SPES) should also be investigated for the proposed application.

Chapter 9 References

1. International Energy Agency, *World Energy Outlook*, 2013.
2. BP, *Statistical Review of World Energy*. June 2013. Last accessed on 27/10/14, <http://www.bp.com/content/dam/bp/pdf/statistical_review/statistical_review_of_world_energy_2013.pdf>
3. Australian Government, *Energy in Australia 2011*. Department of Resources, Energy and Tourism, 2011. Last accessed on 27/10/14, < http://data.daff.gov.au/data/warehouse/pe_abares99001789/Energy_in_Aust_2011_13f.pdf>
4. Stevens, G., Mumford, K, Quyn, D, Kentish, S, Scholes, C, Webley, P, Lee, S, Ho, M, Wiley, D, Qader, A, Hooper, B, Hoadley, A and Harkin, T *Post-combustion Carbon Dioxide Capture Technologies for Brown Coal Power Generation - Final report for Brown Coal Innovation Australia (Full Version)*. 2011, Cooperative Research Centre for Greenhouse Gas Technologies, Canberra, Australia, .
5. State Government Victoria, *Lignite/Brown Coal*, by: Department of Primary Industries, State Government Victoria, Melbourne, Last accessed on 27/10/14, <http://www.energyandresources.vic.gov.au/earth-resources/victorias-earth-resources/coal >
6. Sijbesma, H., et al., *Flue gas dehydration using polymer membranes.* Journal of Membrane Science, 2008. **313**(1-2): p. 263-276.
7. Baker, R.W., *Membrane technology and applications*. 2004: J. Wiley.
8. Baker, R.W., *Future Directions of Membrane Gas Separation Technology.* Industrial & Engineering Chemistry Research, 2002. **41**(6): p. 1393-1411.
9. Meisen, A. and X. Shuai, *Research and development issues in CO2 capture.* Energy Conversion and Management, 1997. **38**(Supplement 1): p. S37-S42.
10. Granite, E.J. and T. O'Brien, *Review of novel methods for carbon dioxide separation from flue and fuel gases.* Fuel Processing Technology, 2005. **86**(14-15): p. 1423-1434.
11. Scholes, C.A., S.E. Kentish, and G.W. Stevens, *Carbon Dioxide Separation through Polymeric Membrane Systems for Flue gas applications.* Recent Patents on Chemical Engineering, 2008. **1**(1): p. 52-66.

12. Khan, A.L., X. Li, and I.F.J. Vankelecom, *Mixed-gas CO_2/CH_4 and CO_2/N_2 separation with sulfonated PEEK membranes.* Journal of Membrane Science, 2011. **372**(1-2): p. 87-96.
13. Baker R.W., W.J.K., E.L. Cussler, R.L. Riley, W. Eykamp, H. Strathmann, *Membrane separation systems: recent developments and future directions*, ed. R.W. Baker. 1991: Noyes Data Corp.
14. Potreck, J., et al., *Mixed water vapor/gas transport through the rubbery polymer PEBAX® 1074.* Journal of Membrane Science, 2009. **338**(1-2): p. 11-16.
15. Aaron, D. and C. Tsouris, *Separation of CO_2 from Flue Gas: A Review.* Separation Science & Technology, 2005. **40**(1-3): p. 321-348.
16. Cooperative Research Centre for Coal in Sustainable Development, *Power Station Emissions Handbook*, Cooperative Research Centre for Coal in Sustainable Development, Australia, 2009.
17. Zhong, S., et al., *Crosslinked sulfonated poly(ether ether ketone) proton exchange membranes for direct methanol fuel cell applications.* Journal of Power Sources, 2007. **164**(1): p. 65-72.
18. Gil, M., et al., *Direct synthesis of sulfonated aromatic poly(ether ether ketone) proton exchange membranes for fuel cell applications.* Journal of Membrane Science, 2004. **234**(1-2): p. 75-81.
19. Kaliaguine, S., et al., *Properties of SPEEK based PEMs for fuel cell application.* Catalysis Today, 2003. **82**(1-4): p. 213-222.
20. Shuhua, Z., C. Nguyenthi Que, and K. Dukjoon. *Cross-linked poly (ether ether ketone) as a proton exchange membrane for fuel cell applications*. in *Nanotechnology (IEEE-NANO), 2010 10th IEEE Conference on*. 2010.
21. Smitha, B., S. Sridhar, and A.A. Khan, *Solid polymer electrolyte membranes for fuel cell applications--a review.* Journal of Membrane Science, 2005. **259**(1-2): p. 10-26.
22. Majsztrik, P., A. Bocarsly, and J. Benziger, *Water Permeation through Nafion Membranes: The Role of Water Activity.* The Journal of Physical Chemistry B, 2008. **112**(51): p. 16280-16289.
23. Jiang, R., H.R. Kunz, and J.M. Fenton, *Composite silica/Nafion® membranes prepared by tetraethylorthosilicate sol-gel reaction and solution casting for direct methanol fuel cells.* Journal of Membrane Science, 2006. **272**(1-2): p. 116-124.
24. Sundar, S., et al., *Crosslinked sulfonated polyimide networks as polymer electrolyte membranes in fuel cells.* Journal of Polymer Science Part B: Polymer Physics, 2005. **43**(17): p. 2370-2379.

25. Su, Y.-H., et al., *Increases in the proton conductivity and selectivity of proton exchange membranes for direct methanol fuel cells by formation of nanocomposites having proton conducting channels.* Journal of Power Sources, 2009. **194**(1): p. 206-213.
26. Nikolić, V.M., et al., *Performance comparison of modified poly(vinyl alcohol) based membranes in alkaline fuel cells*. International Journal of Hydrogen Energy, 2011. **36**(17): p. 11004-11010.
27. Abedini, R., *Application of Membrane in Gas Separation Processes: Its Suitability and Mechanisms.* Ropa a uhlie, 2010. **52**(2): p. 69.
28. Kohl, A.L. and R.B. Nielsen, *Gas purification*. 5th ed. 1997: Gulf Pub.
29. Noble, R.D. and S.A. Stern, *Membrane separations technology: principles and applications*. 1995: Elsevier.
30. Freeman, B. and Y. Yampolskii, *Membrane Gas Separation*. 2010: John Wiley & Sons.
31. Townsend, R.P., *Handbook of separation process technology Edited by R. W. Rousseau, Wiley-Interscience, New York, 1987. pp. xiv + 1010, price £64.15. ISBN 0-471-89558-X.* Journal of Chemical Technology & Biotechnology, 1989. **44**(4): p. 330-331.
32. Schmeling, N., et al., *Functionalized copolyimide membranes for the separation of gaseous and liquid mixtures.* Beilstein Journal of Organic Chemistry, 2010. **6**: p. 789-800.
33. Hill Anita, J. and R. Tant Martin, *The Structure and Properties of Glassy Polymers*, in *Structure and Properties of Glassy Polymers*. 1999, American Chemical Society. p. 1-20.
34. Sperling, L.H., *Introduction to physical polymer science*. 4th ed. 2006: Wiley-Interscience.
35. Kanehashi, S. and K. Nagai, *Analysis of dual-mode model parameters for gas sorption in glassy polymers.* Journal of Membrane Science, 2005. **253**(1–2): p. 117-138.
36. Maier, G., *Gas Separation with Polymer Membranes.* Angewandte Chemie International Edition, 1998. **37**(21): p. 2960-2974.
37. Bondi, A., *Physical properties of molecular crystals, liquids and glasses.* Vol. 7. 1968, New York: Wiley. 502.
38. Park, J.Y. and D.R. Paul, *Correlation and prediction of gas permeability in glassy polymer membrane materials via a modified free volume based group contribution method.* Journal of Membrane Science, 1997. **125**(1): p. 23-39.
39. Rousseau, R.W., *Handbook of Separation Process Technology*. 1987, John Wiley & Sons. p. 897-907.

40. Brandrup, J., et al., *Polymer Handbook* 2005, John Wiley & Sons. p. 77-85.
41. Metz, S.J., M.H.V. Mulder, and M. Wessling, *Gas-Permeation Properties of Poly(ethylene oxide) Poly(butylene terephthalate) Block Copolymers.* Macromolecules, 2004. **37**(12): p. 4590-4597.
42. Metz, S.J., et al., *Mixed gas water vapor/N2 transport in poly(ethylene oxide) poly(butylene terephthalate) block copolymers.* Journal of Membrane Science, 2005. **266**(1-2): p. 51-61.
43. Corti, H.R., F. Nores-Pondal, and M. Pilar Buera, *Low temperature thermal properties of Nafion 117 membranes in water and methanol-water mixtures.* Journal of Power Sources, 2006. **161**(2): p. 799-805.
44. Chow, T.S., *Molecular Interpretation of the Glass Transition Temperature of Polymer-Diluent Systems.* Macromolecules, 1980. **13**(2): p. 362-364.
45. Potreck, J., et al., *Sorption induced relaxations during water diffusion in S-PEEK.* Physical Chemistry Chemical Physics, 2009. **11**(2): p. 298-308.
46. Fox, T.G., *Influence of diluent and of copolymer composition on the glass temperature of a polymer system.* Bull Am Phys Soc, 1956. **1**(2): p. 123.
47. Koros, W.J. and G.K. Fleming, *Membrane-based gas separation.* Journal of Membrane Science, 1993. **83**(1): p. 1-80.
48. Scholes, C.A., S.E. Kentish, and G.W. Stevens, *Effects of Minor Components in Carbon Dioxide Capture Using Polymeric Gas Separation Membranes.* Separation & Purification Reviews, 2009. **38**(1): p. 1-44.
49. Uchytil, P., et al., *Influence of capillary condensation effects on mass transport through porous membranes.* Separation and Purification Technology, 2003. **33**(3): p. 273-281.
50. Chen, G.Q., *Water Vapor Permeation through Glassy Polyimide Membranes and Its Impact upon Carbon Dioxide Capture Operations*, in *Department of Chemical and Biomolecular Engineering*. 2012, The University of Melbourne: Melbourne.
51. Takeuchi, H., *A jump motion of small molecules in glassy polymers: A molecular dynamics simulation.* The Journal of Chemical Physics, 1990. **93**(3): p. 2062-2067.
52. Shantarovich, V.P., et al., *Positron Annihilation Lifetime Study of High and Low Free Volume Glassy Polymers: Effects of Free Volume Sizes on the Permeability and Permselectivity.* Macromolecules, 2000. **33**(20): p. 7453-7466.
53. Duthie, X., et al., *Operating temperature effects on the plasticization of polyimide gas separation membranes.* Journal of Membrane Science, 2007. **294**(1–2): p. 40-49.
54. Chen, G.Q., et al., *Water vapor permeation in polyimide membranes.* Journal of Membrane Science, 2011. **379**(1–2): p. 479-487.

55. Merkel, T.C., et al., *Gas sorption, diffusion, and permeation in poly(dimethylsiloxane).* Journal of Polymer Science Part B: Polymer Physics, 2000. **38**(3): p. 415-434.
56. Paul, D.R.Y.s., Yuri.P. , *Polymeric gas separation membranes*. 1994: CRC Press.
57. Barrie, J.A. and B. Platt, *The diffusion and clustering of water vapour in polymers.* Polymer, 1963. **4**(0): p. 303-313.
58. Hsu, W.P., et al., *Sorption and diffusion of water vapour in hydrogen-bonded polymer blends.* Polymer, 1993. **34**(3): p. 597-603.
59. Nguyen, Q.T., et al., *Clustering of solvents in membranes and its influence on membrane transport properties.* Journal of Membrane Science, 1996. **113**(1): p. 137-150.
60. Favre, E., et al., *Sorption, diffusion and vapor permeation of various penetrants through dense poly(dimethylsiloxane) membranes: a transport analysis.* Journal of Membrane Science, 1994. **92**(2): p. 169-184.
61. Favre, E., et al., *Sorption of organic solvents into dense silicone membranes. Part 1.-Validity and limitations of Flory-Huggins and related theories.* Journal of the Chemical Society, Faraday Transactions, 1993. **89**(24): p. 4339-4346.
62. Favre, E., et al., *The engaged species induced clustering (ENSIC) model: a unified mechanistic approach of sorption phenomena in polymers.* Journal of Membrane Science, 1996. **117**(1–2): p. 227-236.
63. Favre, E., et al., *Mechanistic modelling of sorption phenomena in polymers: the Engaged Species Induced Clustering (ENSIC) model.* J. Membr. Sci, 1996. **117**: p. 227-236.
64. Jonquières, A., et al., *Modelling of vapour sorption in polar materials: Comparison of Flory–Huggins and related models with the ENSIC mechanistic approach.* Journal of Membrane Science, 1998. **147**(1): p. 59-71.
65. Modesti, M., et al., *Mathematical model and experimental validation of water cluster influence upon vapour permeation through hydrophilic dense membrane.* Journal of Membrane Science, 2004. **229**(1–2): p. 211-223.
66. Zimm, B.H. and J.L. Lundberg, *Sorption of Vapors by High Polymers.* The Journal of Physical Chemistry, 1956. **60**(4): p. 425-428.
67. Zimm, B.H., *Simplified Relation Between Thermodynamics and Molecular Distribution Functions for a Mixture.* The Journal of Chemical Physics, 1953. **21**(5): p. 934-935.
68. Zhao, Q., P. Majsztrik, and J. Benziger, *Diffusion and Interfacial Transport of Water in Nafion.* The Journal of Physical Chemistry B, 2011: p. null-null.

69. Lim, L.-T., I.J. Britt, and M.A. Tung, *Sorption and transport of water vapor in nylon 6,6 film.* Journal of Applied Polymer Science, 1999. **71**(2): p. 197-206.
70. Azher, H., et al., *Water permeation and sorption properties of Nafion 115 at elevated temperatures.* Journal of Membrane Science, 2014. **459**(0): p. 104-113.
71. Jonquières, A., et al., *Comparison of UNIQUAC with related models for modelling vapour sorption in polar materials.* Journal of Membrane Science, 1998. **150**(1): p. 125-141.
72. Feng, H., *Modeling of vapor sorption in glassy polymers using a new dual mode sorption model based on multilayer sorption theory.* Polymer, 2007. **48**(10): p. 2988-3002.
73. Huang, J., et al., *Sorption and transport behavior of water vapor in dense and asymmetric polyimide membranes.* Journal of Membrane Science, 2004. **241**(2): p. 187-196.
74. Okuno, H., K. Renzo, and T. Uragami, *Sorption and permeation of water and ethanol vapors in poly(vinylchloride) membrane.* Journal of Membrane Science, 1995. **103**(1–2): p. 31-38.
75. Li, Y., et al., *Water sorption in Nafion® membranes analyzed with an improved dual-mode sorption model—Structure/property relationships.* Journal of Membrane Science, 2013. **439**(0): p. 1-11.
76. Favre, E., et al., *Sorption of organic solvents into dense silicone membranes. Part 2.-Development of a new approach based on a clustering hypothesis for associated solvents.* Journal of the Chemical Society, Faraday Transactions, 1993. **89**(24): p. 4347-4353.
77. Chern, R.T., et al., *"Second component" effects in sorption and permeation of gases in glassy polymers.* Journal of Membrane Science, 1983. **15**(2): p. 157-169.
78. De Bo, I., H. Van Langenhove, and J. De Keijser, *Application of vapour phase calibration method for determination of sorption of gases and VOC in polydimethylsiloxane membranes.* Journal of Membrane Science, 2002. **209**(1): p. 39-52.
79. Pye, D.G., H.H. Hoehn, and M. Panar, *Measurement of gas permeability of polymers. II. Apparatus for determination of permeabilities of mixed gases and vapors.* Journal of Applied Polymer Science, 1976. **20**(2): p. 287-301.
80. Kruczek, B. and T. Matsuura, *Limitations of a constant pressure-type testing system in determination of gas transport properties of hydrophilic films.* Journal of Membrane Science, 2000. **177**(1–2): p. 129-142.

81. Okamoto, K.-I., et al., *Sorption and diffusion of water vapor in polyimide films.* Journal of Polymer Science Part B: Polymer Physics, 1992. **30**(11): p. 1223-1231.
82. Lokhandwala, K.A., S.M. Nadakatti, and S.A. Stern, *Solubility and transport of water vapor in some 6FDA-based polyimides.* Journal of Polymer Science Part B: Polymer Physics, 1995. **33**(6): p. 965-975.
83. Sato, S., et al., *Permeability, diffusivity, and solubility of benzene vapor and water vapor in high free volume silicon- or fluorine-containing polymer membranes.* Journal of Membrane Science, 2010. **360**(1–2): p. 352-362.
84. Koros, W.J., et al., *A model for permeation of mixed gases and vapors in glassy polymers.* Journal of Polymer Science: Polymer Physics Edition, 1981. **19**(10): p. 1513-1530.
85. Koros, W.J., *Model for sorption of mixed gases in glassy polymers.* Journal of Polymer Science: Polymer Physics Edition, 1980. **18**(5): p. 981-992.
86. Kanehashi, S., et al., *Effects of carbon dioxide-induced plasticization on the gas transport properties of glassy polyimide membranes.* Journal of Membrane Science, 2007. **298**(1–2): p. 147-155.
87. Fujita, H., *Diffusion in polymer-diluent systems*, in *Fortschritte Der Hochpolymeren-Forschung*. 1961, Springer Berlin Heidelberg. p. 1-47.
88. Paul, D.R. and W.J. Koros, *Effect of partially immobilizing sorption on permeability and the diffusion time lag.* Journal of Polymer Science: Polymer Physics Edition, 1976. **14**(4): p. 675-685.
89. Petropoulos, J.H., *Quantitative analysis of gaseous diffusion in glassy polymers.* Journal of Polymer Science Part A-2: Polymer Physics, 1970. **8**(10): p. 1797-1801.
90. Duthie, X., et al., *Operating temperature effects on the plasticization of polyimide gas separation membranes.* Journal of Membrane Science, 2007. **294**(1-2): p. 40-49.
91. Wessling, M., et al., *Plasticization of gas separation membranes.* Gas Separation & Purification, 1991. **5**(4): p. 222-228.
92. Casciola, M., et al., *On the decay of Nafion proton conductivity at high temperature and relative humidity.* Journal of Power Sources, 2006. **162**(1): p. 141-145.
93. de Almeida, S. and Y. Kawano, *Thermal Behavior of Nafion Membranes.* Journal of Thermal Analysis and Calorimetry, 1999. **58**(3): p. 569-577.
94. Cheng, S.-X., et al., *Gas-sorption properties of 6FDA–durene/1,4-phenylenediamine (pPDA) and 6FDA–durene/1,3-phenylenediamine (mPDA) copolyimides.* Journal of Applied Polymer Science, 2003. **90**(8): p. 2187-2193.

95. Shao, L., et al., *The effects of 1,3-cyclohexanebis(methylamine) modification on gas transport and plasticization resistance of polyimide membranes.* Journal of Membrane Science, 2005. **267**(1–2): p. 78-89.

96. Kanehashi, S., et al., *Effects of carbon dioxide-induced plasticization on the gas transport properties of glassy polyimide membranes.* Journal of Membrane Science, 2007. **298**(1-2): p. 147-155.

97. Reijerkerk, S.R., et al., *On the effects of plasticization in CO2/light gas separation using polymeric solubility selective membranes.* Journal of Membrane Science, 2011. **367**(1-2): p. 33-44.

98. Potreck, J., et al., *Mixed water vapor/gas transport through the rubbery polymer PEBAX® 1074.* Journal of Membrane Science, 2009. **338**(1–2): p. 11-16.

99. Despond, S., E. Espuche, and A. Domard, *Water sorption and permeation in chitosan films: Relation between gas permeability and relative humidity.* Journal of Polymer Science Part B: Polymer Physics, 2001. **39**(24): p. 3114-3127.

100. Xie, W., et al., *Effect of Free Volume on Water and Salt Transport Properties in Directly Copolymerized Disulfonated Poly(arylene ether sulfone) Random Copolymers.* Macromolecules, 2011. **44**(11): p. 4428-4438.

101. Chen, G.Q., et al., *Modeling of the sorption and transport properties of water vapor in polyimide membranes.* Journal of Membrane Science, 2012. **409–410**(0): p. 96-104.

102. Jia, L., et al., *Sulfonation of polyetheretherketone and its effects on permeation behavior to nitrogen and water vapor.* Journal of Applied Polymer Science, 1996. **60**(8): p. 1231-1237.

103. Jia, L., et al., *Permeation of nitrogen and water vapor through sulfonated polyetherethersulfone membrane.* Journal of Polymer Science Part B: Polymer Physics, 1997. **35**(13): p. 2133-2140.

104. Costello, L.M. and W.J. Koros, *Thermally stable polyimide isomers for membrane-based gas separations at elevated temperatures.* Journal of Polymer Science Part B: Polymer Physics, 1995. **33**(1): p. 135-146.

105. Strathmann, H., *Membrane Separation Processes, 4. Concentration Polarization and Membrane Fouling*, in *Ullmann's Encyclopedia of Industrial Chemistry*. 2000, Wiley-VCH Verlag GmbH & Co. KGaA.

106. Metz, S.J., et al., *Transport of water vapor and inert gas mixtures through highly selective and highly permeable polymer membranes.* Journal of Membrane Science, 2005. **251**(1-2): p. 29-41.

107. Carbone, A., et al., *Influence of post-casting treatments on sulphonated polyetheretherketone composite membranes.* Journal of Power Sources, 2010. **195**(18): p. 6037-6042.
108. Ohkubo, T., et al., *Molecular dynamics simulations of Nafion and sulfonated polyether sulfone membranes. I. Effect of hydration on aqueous phase structure.* Journal of Molecular Modeling, 2011. **17**(4): p. 739-755.
109. Shahi, V.K., *Highly charged proton-exchange membrane: Sulfonated poly(ether sulfone)-silica polyelectrolyte composite membranes for fuel cells.* Solid State Ionics, 2007. **177**(39-40): p. 3395-3404.
110. Li, L. and Y. Wang, *Sulfonated polyethersulfone Cardo membranes for direct methanol fuel cell.* Journal of Membrane Science, 2005. **246**(2): p. 167-172.
111. Bondar, V.I., B.D. Freeman, and I. Pinnau, *Gas transport properties of poly(ether-b-amide) segmented block copolymers.* Journal of Polymer Science Part B: Polymer Physics, 2000. **38**(15): p. 2051-2062.
112. Wang, F., T. Chen, and J. Xu, *Synthesis of poly(ether ether ketone) containing sodium sulfonate groups as gas dehumidification membrane material.* Macromolecular Rapid Communications, 1998. **19**(2): p. 135-137.
113. Piroux, F., et al., *Water vapour transport mechanism in naphthalenic sulfonated polyimides.* Journal of Membrane Science, 2003. **223**(1-2): p. 127-139.
114. Zhao, Q., P. Majsztrik, and J. Benziger, *Diffusion and Interfacial Transport of Water in Nafion.* The Journal of Physical Chemistry B, 2011. **115**(12): p. 2717-2727.
115. Duan, Q., H. Wang, and J. Benziger, *Transport of liquid water through Nafion membranes.* Journal of Membrane Science, 2012. **392–393**(0): p. 88-94.
116. Weber, A.Z. and J. Newman, *Modeling Transport in Polymer-Electrolyte Fuel Cells.* Chemical Reviews, 2004. **104**(10): p. 4679-4726.
117. Roche, E.J., et al., *Small-angle scattering studies of nafion membranes.* Journal of Polymer Science: Polymer Physics Edition, 1981. **19**(1): p. 1-11.
118. Schmidt-Rohr, K. and C. Qiang, *Parallel cylindrical water nanochannels in Nafion fuel-cell membranes.* Nature Materials, 2008. **7**(1): p. 75-83.
119. Mauritz, K.A., *Review and Critical Analyses of Theories of Aggregation in Ionomers.* Journal of Macromolecular Science, Part C, 1988. **28**(1): p. 65-98.
120. Hsu, W.Y. and T.D. Gierke, *Ion transport and clustering in nafion perfluorinated membranes.* Journal of Membrane Science, 1983. **13**(3): p. 307-326.
121. Laporta, M., M. Pegoraro, and L. Zanderighi, *Perfluorosulfonated membrane (Nafion): FT-IR study of the state of water with increasing humidity.* Physical Chemistry Chemical Physics, 1999. **1**(19): p. 4619-4628.

122. Hallinan, D.T. and Y.A. Elabd, *Diffusion of Water in Nafion Using Time-Resolved Fourier Transform Infrared–Attenuated Total Reflectance Spectroscopy.* The Journal of Physical Chemistry B, 2009. **113**(13): p. 4257-4266.
123. Berezina, N.P., S.V. Timofeev, and N.A. Kononenko, *Effect of conditioning techniques of perfluorinated sulphocationic membranes on their hydrophylic and electrotransport properties.* Journal of Membrane Science, 2002. **209**(2): p. 509-518.
124. Zawodzinski, T.A., et al., *A Comparative Study of Water Uptake By and Transport Through Ionomeric Fuel Cell Membranes.* Journal of The Electrochemical Society, 1993. **140**(7): p. 1981-1985.
125. Zawodzinski, T.A., et al., *Determination of water diffusion coefficients in perfluorosulfonate ionomeric membranes.* The Journal of Physical Chemistry, 1991. **95**(15): p. 6040-6044.
126. Hinatsu, J.T., M. Mizuhata, and H. Takenaka, *Water uptake of perfluorosulfonic acid membranes from liquid water and water vapor.* Journal of The Electrochemical Society, 1994. **141**(6): p. 1493-1498.
127. Choi, P. and R. Datta, *Sorption in Proton-Exchange Membranes.* Journal of The Electrochemical Society, 2003. **150**(12): p. E601-E607.
128. Onishi, L.M., J.M. Prausnitz, and J. Newman, *Water–Nafion Equilibria. Absence of Schroeder's Paradox.* The Journal of Physical Chemistry B, 2007. **111**(34): p. 10166-10173.
129. Takamatsu, T., M. Hashiyama, and A. Eisenberg, *Sorption phenomena in nafion membranes.* Journal of Applied Polymer Science, 1979. **24**(11): p. 2199-2220.
130. Morris, D.R. and X. Sun, *Water-sorption and transport properties of Nafion 117 H.* Journal of Applied Polymer Science, 1993. **50**(8): p. 1445-1452.
131. Alberti, G., et al., *Polymeric proton conducting membranes for medium temperature fuel cells (110–160°C).* Journal of Membrane Science, 2001. **185**(1): p. 73-81.
132. Yang, C., et al., *Approaches and technical challenges to high temperature operation of proton exchange membrane fuel cells.* Journal of Power Sources, 2001. **103**(1): p. 1-9.
133. Tsonos, C., L. Apekis, and P. Pissis, *Water sorption and dielectric relaxation spectroscopy studies in hydrated Nafion® (-SO3K) membranes.* Journal of Materials Science, 2000. **35**(23): p. 5957-5965.
134. Shao, Z.-G., P. Joghee, and I.M. Hsing, *Preparation and characterization of hybrid Nafion–silica membrane doped with phosphotungstic acid for high temperature*

operation of proton exchange membrane fuel cells. Journal of Membrane Science, 2004. **229**(1–2): p. 43-51.

135. Savinell, R., et al., *A Polymer Electrolyte for Operation at Temperatures up to 200°C.* Journal of The Electrochemical Society, 1994. **141**(4): p. L46-L48.
136. Alberti, G., et al., *More on Nafion conductivity decay at temperatures higher than 80 °c: Preparation and first characterization of in-plane oriented layered morphologies.* Industrial and Engineering Chemistry Research, 2013. **52**(31): p. 10418-10424.
137. Gorri, D., et al., *Water and methanol permeation through short-side-chain perfluorosulphonic acid ionomeric membranes.* Journal of Membrane Science, 2008. **322**(2): p. 383-391.
138. Catalano, J., et al., *The effect of relative humidity on the gas permeability and swelling in PFSI membranes.* International Journal of Hydrogen Energy, 2012. **37**(7): p. 6308-6316.
139. Giacinti Baschetti, M., et al., *Gas permeation in perflurosulfonated membranes: Influence of temperature and relative humidity.* International Journal of Hydrogen Energy, 2013. **38**(27): p. 11973-11982.
140. De Angelis, M.G., et al., *Water sorption and diffusion in a short-side-chain perfluorosulfonic acid ionomer membrane for PEMFCS: effect of temperature and pre-treatment.* Desalination, 2006. **193**(1–3): p. 398-404.
141. Li, J., M. Pan, and H. Tang, *Understanding short-side-chain perfluorinated sulfonic acid and its application for high temperature polymer electrolyte membrane fuel cells.* RSC Advances, 2014. **4**(8): p. 3944-3965.
142. Vrentas, J.S. and C.M. Vrentas, *Solvent Self-Diffusion in Glassy Polymer-Solvent Systems.* Macromolecules, 1994. **27**(20): p. 5570-5576.
143. Arcella, V., C. Troglia, and A. Ghielmi, *Hyflon Ion Membranes for Fuel Cells.* Industrial & Engineering Chemistry Research, 2005. **44**(20): p. 7646-7651.
144. Merlo, L., et al., *Membrane Electrode Assemblies Based on HYFLON® Ion for an Evolving Fuel Cell Technology.* Separation Science and Technology, 2007. **42**(13): p. 2891-2908.
145. Zawodzinski, T.A., et al., *The water content dependence of electro-osmotic drag in proton-conducting polymer electrolytes.* Electrochimica Acta, 1995. **40**(3): p. 297-302.
146. Majsztrik, P.W., et al., *Water sorption, desorption and transport in Nafion membranes.* Journal of Membrane Science, 2007. **301**(1-2): p. 93-106.
147. Hallinan, D.T. and Y.A. Elabd, *Diffusion and Sorption of Methanol and Water in Nafion Using Time-Resolved Fourier Transform Infrared–Attenuated Total*

Reflectance Spectroscopy. The Journal of Physical Chemistry B, 2007. **111**(46): p. 13221-13230.

148. Alberti, G. and R. Narducci, *Evolution of permanent deformations (ormemory) in nafion 117membranes with changes in temperature, relative humidity and time, and its importancein the development of medium temperature PEMFCs.* Fuel Cells, 2009. **9**(4): p. 410-420.
149. Alberti, G., R. Narducci, and M. Sganappa, *Effects of hydrothermal/thermal treatments on the water-uptake of Nafion membranes and relations with changes of conformation, counter-elastic force and tensile modulus of the matrix.* Journal of Power Sources, 2008. **178**(2): p. 575-583.
150. Motupally, S., A.J. Becker, and J.W. Weidner, *Diffusion of Water in Nafion 115 Membranes.* Journal of The Electrochemical Society, 2000. **147**(9): p. 3171-3177.
151. Romero, T. and W. Mérida, *Water transport in liquid and vapour equilibrated Nafion™ membranes.* Journal of Membrane Science, 2009. **338**(1–2): p. 135-144.
152. Chiou, J.S. and D.R. Paul, *Gas permeation in a dry Nafion membrane.* Industrial & Engineering Chemistry Research, 1988. **27**(11): p. 2161-2164.
153. Ma, S., M. Odgaard, and E. Skou, *Carbon dioxide permeability of proton exchange membranes for fuel cells.* Solid State Ionics, 2005. **176**(39–40): p. 2923-2927.
154. Ramani, V., H.R. Kunz, and J.M. Fenton, *Investigation of Nafion®/HPA composite membranes for high temperature/low relative humidity PEMFC operation.* Journal of Membrane Science, 2004. **232**(1–2): p. 31-44.
155. Antonucci, P.L., et al., *Investigation of a direct methanol fuel cell based on a composite Nafion®-silica electrolyte for high temperature operation.* Solid State Ionics, 1999. **125**(1–4): p. 431-437.
156. Jalani, N.H. and R. Datta, *The effect of equivalent weight, temperature, cationic forms, sorbates, and nanoinorganic additives on the sorption behavior of Nafion®.* Journal of Membrane Science, 2005. **264**(1–2): p. 167-175.
157. Hallinan, D.T., et al., *Non-Fickian Diffusion of Water in Nafion.* Macromolecules, 2010. **43**(10): p. 4667-4678.
158. Ma, S. and E. Skou, *CO2 permeability in Nafion® EW1100 at elevated temperature.* Solid State Ionics, 2007. **178**(7-10): p. 615-619.
159. Hensley, J.E. and J.D. Way, *The relationship between proton conductivity and water permeability in composite carboxylate/sulfonate perfluorinated ionomer membranes.* Journal of Power Sources, 2007. **172**(1): p. 57-66.

160. Liu, S., F. Wang, and T. Chen, *Synthesis of Poly(ether ether ketone)s with High Content of Sodium Sulfonate Groups as Gas Dehumidification Membrane Materials.* Macromolecular Rapid Communications, 2001. **22**(8): p. 579-582.
161. Jiang, R., H.R. Kunz, and J.M. Fenton, *Investigation of membrane property and fuel cell behavior with sulfonated poly(ether ether ketone) electrolyte: Temperature and relative humidity effects.* Journal of Power Sources, 2005. **150**(0): p. 120-128.
162. Xing, P., et al., *Synthesis and characterization of sulfonated poly(ether ether ketone) for proton exchange membranes.* Journal of Membrane Science, 2004. **229**(1-2): p. 95-106.
163. Wang, F., et al., *Synthesis of poly(ether ether ketone) with high content of sodium sulfonate groups and its membrane characteristics.* Polymer, 1999. **40**(3): p. 795-799.
164. Li, L., J. Zhang, and Y. Wang, *Sulfonated poly(ether ether ketone) membranes for direct methanol fuel cell.* Journal of Membrane Science, 2003. **226**(1–2): p. 159-167.
165. Manea, C. and M. Mulder, *Characterization of polymer blends of polyethersulfone/sulfonated polysulfone and polyethersulfone/sulfonated polyetheretherketone for direct methanol fuel cell applications.* Journal of Membrane Science, 2002. **206**(1–2): p. 443-453.
166. Gil, M., et al., *Direct synthesis of sulfonated aromatic poly(ether ether ketone) proton exchange membranes for fuel cell applications.* Journal of Membrane Science, 2004. **234**(1–2): p. 75-81.
167. Drioli, E., et al., *Sulfonated PEEK-WC membranes for possible fuel cell applications.* Journal of Membrane Science, 2004. **228**(2): p. 139-148.
168. Xing, P., et al., *Synthesis and characterization of sulfonated poly(ether ether ketone) for proton exchange membranes.* Journal of Membrane Science, 2004. **229**(1–2): p. 95-106.
169. Wilhelm, F.G., et al., *Cation permeable membranes from blends of sulfonated poly(ether ether ketone) and poly(ether sulfone).* Journal of Membrane Science, 2002. **199**(1-2): p. 167-176.
170. Arigonda, M., A.P. Deshpande, and S. Varughese, *Effect of PES on the morphology and properties of proton conducting blends with sulfonated poly(ether ether ketone).* Journal of Applied Polymer Science, 2013. **127**(6): p. 5100-5110.
171. Huang, R.Y.M., et al., *Pervaporation separation of water/isopropanol mixture using sulfonated poly(ether ether ketone) (SPEEK) membranes: transport mechanism and*

separation performance. Journal of Membrane Science, 2001. **192**(1–2): p. 115-127.

172. Zaidi, S.M.J., et al., *Proton conducting composite membranes from polyether ether ketone and heteropolyacids for fuel cell applications.* Journal of Membrane Science, 2000. **173**(1): p. 17-34.
173. Li, Y. and T.S. Chung, *Highly selective sulfonated polyethersulfone (SPES)-based membranes with transition metal counterions for hydrogen recovery and natural gas separation.* Journal of Membrane Science, 2008. **308**(1–2): p. 128-135.
174. Chen, W.-J. and C.R. Martin, *Gas-transport properties of sulfonated polystyrenes.* Journal of Membrane Science, 1994. **95**(1): p. 51-61.
175. Krause, B., et al., *Microcellular Foaming of Amorphous High-Tg Polymers Using Carbon Dioxide.* Macromolecules, 2001. **34**(4): p. 874-884.
176. Davis, E.M. and Y.A. Elabd, *Water Clustering in Glassy Polymers.* The Journal of Physical Chemistry B, 2013. **117**(36): p. 10629-10640.
177. Arce, A., et al., *Sorption and transport of water vapor in thin polymer films at 35 [degree]C.* Physical Chemistry Chemical Physics, 2004. **6**(1): p. 103-108.
178. Detallante, V., et al., *Kinetics of water vapor sorption in sulfonated polyimide membranes.* Desalination, 2002. **148**(1–3): p. 333-339.
179. Khan, A.L., X. Li, and I.F.J. Vankelecom, *Mixed-gas CO2/CH4 and CO2/N2 separation with sulfonated PEEK membranes.* Journal of Membrane Science, 2011. **372**(1–2): p. 87-96.
180. Wang, Z., T. Chen, and J. Xu, *Gas and Water Vapor Transport through a Series of Novel Poly(aryl ether sulfone) Membranes.* Macromolecules, 2001. **34**(26): p. 9015-9022.
181. Chen, G., et al., *Synthesis, properties, and gas permeation performance of cardo poly(arylene ether sulfone)s containing phthalimide side groups.* Journal of Applied Polymer Science, 2007. **106**(4): p. 2808-2816.
182. Piroux, F., et al., *Gas transport mechanism in sulfonated polyimides: Consequences on gas selectivity.* Journal of Membrane Science, 2002. **209**(1): p. 241-253.
183. Piroux, F., E. Espuche, and R. Mercier, *The effects of humidity on gas transport properties of sulfonated copolyimides.* Journal of Membrane Science, 2004. **232**(1-2): p. 115-122.
184. Tanaka, K., et al., *Gas permeation and separation properties of sulfonated polyimide membranes.* Polymer, 2006. **47**(12): p. 4370-4377.

185. Staudt-Bickel, C. and W. J. Koros, *Improvement of CO2/CH4 separation characteristics of polyimides by chemical crosslinking.* Journal of Membrane Science, 1999. **155**(1): p. 145-154.
186. Powell, C.E., et al., *Reversible diamine cross-linking of polyimide membranes.* Journal of Membrane Science, 2007. **291**(1–2): p. 199-209.
187. Tanaka, K., et al., *Effect of methyl substituents on permeability and permselectivity of gases in polyimides prepared from methyl-substituted phenylenediamines.* Journal of Polymer Science Part B: Polymer Physics, 1992. **30**(8): p. 907-914.
188. Chiou, J.S., J.W. Barlow, and D.R. Paul, *Plasticization of glassy polymers by CO2.* Journal of Applied Polymer Science, 1985. **30**(6): p. 2633-2642.
189. Agag, T., T. Koga, and T. Takeichi, *Studies on thermal and mechanical properties of polyimide–clay nanocomposites.* Polymer, 2001. **42**(8): p. 3399-3408.
190. Tyan, H.-L., Y.-C. Liu, and K.-H. Wei, *Thermally and Mechanically Enhanced Clay/Polyimide Nanocomposite via Reactive Organoclay.* Chemistry of Materials, 1999. **11**(7): p. 1942-1947.
191. Lin, W.-H. and T.-S. Chung, *Gas permeability, diffusivity, solubility, and aging characteristics of 6FDA - durene polyimide membranes.* Journal of Membrane Science, 2001. **186**(2): p. 183-193.
192. Seo, J., et al., *Water sorption and activation energy in polyimide thin films.* Journal of Polymer Science Part B: Polymer Physics, 2000. **38**(21): p. 2714-2720.
193. Watari, T., et al., *Water vapor sorption and diffusion properties of sulfonated polyimide membranes.* Journal of Membrane Science, 2003. **219**(1–2): p. 137-147.
194. Ansaloni, L., et al., *Effect of relative humidity and temperature on gas transport in Matrimid®: Experimental study and modeling.* Journal of Membrane Science, 2014. **471**(0): p. 392-401.
195. Okamoto, K.-I., et al., *The effect of morphology on sorption and transport of carbon dioxide in a polyimide from 3,3′,4,4′-biphenyltetracarboxylic dianhydride and 4,4′-oxydianiline.* Journal of Polymer Science Part B: Polymer Physics, 1989. **27**(6): p. 1221-1233.
196. Oberbroeckling, K.J., et al., *Density of Nafion Exchanged with Transition Metal Complexes and Tetramethyl Ammonium, Ferrous, and Hydrogen Ions: Commercial and Recast Films.* Analytical Chemistry, 2002. **74**(18): p. 4794-4799.
197. Fan, Y., et al., *Viscoelastic and gas transport properties of a series of multiblock copolymer ionomers.* Polymer, 2011. **52**(18): p. 3963-3969.

198. Wang, J., et al., *A facile surface modification of Nafion membrane by the formation of self-polymerized dopamine nano-layer to enhance the methanol barrier property.* Journal of Power Sources, 2009. **192**(2): p. 336-343.
199. Smith, Z.P., et al., *Influence of Diffusivity and Sorption on Helium and Hydrogen Separations in Hydrocarbon, Silicon, and Fluorocarbon-Based Polymers.* Macromolecules, 2014. **47**(9): p. 3170-3184.
200. Yeo, S.C. and A. Eisenberg, *Physical properties and supermolecular structure of perfluorinated ion-containing (nafion) polymers.* Journal of Applied Polymer Science, 1977. **21**(4): p. 875-898.
201. Kundu, S., et al., *Mechanical properties of Nafion(TM) electrolyte membranes under hydrated conditions.* Polymer, 2005. **46**(25): p. 11707-11715.
202. Kwon, O., S. Wu, and D.-M. Zhu, *Configuration Changes of Conducting Channel Network in Nafion Membranes due to Thermal Annealing.* The Journal of Physical Chemistry B, 2010. **114**(46): p. 14989-14994.
203. Park, J.-S., et al., *A study on fabrication of sulfonated poly(ether ether ketone)-based membrane-electrode assemblies for polymer electrolyte membrane fuel cells.* Journal of Power Sources, 2008. **178**(2): p. 642-650.
204. Wang, J., et al., *Enhancing proton conduction and methanol barrier performance of sulfonated poly(ether ether ketone) membrane by incorporated polymer carboxylic acid spheres.* Journal of Membrane Science, 2010. **364**(1-2): p. 253-262.
205. Huang, R.Y.M., et al., *Sulfonation of poly(ether ether ketone)(PEEK): Kinetic study and characterization.* Journal of Applied Polymer Science, 2001. **82**(11): p. 2651-2660.
206. Paturzo, L., et al., *High temperature proton exchange membrane fuel cell using a sulfonated membrane obtained via H2SO4 treatment of PEEK-WC.* Catalysis Today, 2005. **104**(2-4): p. 213-218.
207. Cheng, S.Z.D., M.Y. Cao, and B. Wunderlich, *Glass transition and melting behavior of poly(oxy-1,4-phenyleneoxy-1,4-phenylenecarbonyl-1,4-phenylene) (PEEK).* Macromolecules, 1986. **19**(7): p. 1868-1876.
208. Lin, W.-H., R.H. Vora, and T.-S. Chung, *Gas transport properties of 6FDA - durene/1,4-phenylenediamine (pPDA) copolyimides.* Journal of Polymer Science Part B: Polymer Physics, 2000. **38**(21): p. 2703-2713.
209. Gates, C.M. and J. Newman, *Equilibrium and diffusion of methanol and water in a nafion 117 membrane.* AIChE Journal, 2000. **46**(10): p. 2076-2085.

210. Liu, S.L., et al., *Effect of diamine composition on the gas transport properties in 6FDA - durene/3,3′-diaminodiphenyl sulfone copolyimides.* Journal of Membrane Science, 2002. **202**(1–2): p. 165-176.
211. ASTM, *Standard Test Methods for Density and Specific Gravity (Relative Density) of Plastics by Displacement*. 1993: ASTM International: West Conshohocken.
212. Hosseini, S.S., M.M. Teoh, and T.S. Chung, *Hydrogen separation and purification in membranes of miscible polymer blends with interpenetration networks.* Polymer, 2008. **49**(6): p. 1594-1603.
213. Zaidi, S.J., *Polymer sulfonation-A versatile route to prepare proton-conducting membrane material for advanced technologies.* Arabian Journal for Science and Engineering, 2003. **28**(2): p. 183-194.
214. Kusanagi, H. and S. Yukawa, *Fourier transform infra-red spectroscopic studies of water molecules sorbed in solid polymers.* Polymer, 1994. **35**(26): p. 5637-5640.
215. Duthie, X.J., *A study of polyimide gas separation membranes: Carbon Dioxide-induced plasticization and the influence of temperature*, in *Department of Chemical and Biomolecular Engineering* 2007, The University of Melbourne: Melbourne.
216. Hirschfelder, J.O., et al., *Molecular theory of gases and liquids*. 1954: Wiley.
217. Devanathan, R., A. Venkatnathan, and M. Dupuis, *Atomistic Simulation of Nafion Membrane: I. Effect of Hydration on Membrane Nanostructure.* The Journal of Physical Chemistry B, 2007. **111**(28): p. 8069-8079.
218. Devanathan, R., A. Venkatnathan, and M. Dupuis, *Atomistic Simulation of Nafion Membrane. 2. Dynamics of Water Molecules and Hydronium Ions.* The Journal of Physical Chemistry B, 2007. **111**(45): p. 13006-13013.
219. Venkatnathan, A., R. Devanathan, and M. Dupuis, *Atomistic Simulations of Hydrated Nafion and Temperature Effects on Hydronium Ion Mobility.* The Journal of Physical Chemistry B, 2007. **111**(25): p. 7234-7244.
220. Lee, J., et al., *Water vapor sorption and free volume in the aromatic polyamide layer of reverse osmosis membranes.* Journal of Membrane Science, 2013. **425–426**(0): p. 217-226.
221. Rivin, D., et al., *Solubility and transport behavior of water and alcohols in Nafion(TM).* Polymer, 2001. **42**(2): p. 623-635.
222. Kim, Y.S., et al., *State of Water in Disulfonated Poly(arylene ether sulfone) Copolymers and a Perfluorosulfonic Acid Copolymer (Nafion) and Its Effect on Physical and Electrochemical Properties.* Macromolecules, 2003. **36**(17): p. 6281-6285.

223. Mohamed, H.F.M., et al., *Free volume and permeabilities of O2 and H2 in Nafion membranes for polymer electrolyte fuel cells.* Polymer, 2008. **49**(13–14): p. 3091-3097.

224. Catalano, J., et al., *Gas and water vapor permeation in a short-side-chain PFSI membrane.* Desalination, 2009. **240**(1–3): p. 341-346.

225. Hande, V.R., et al., *Cross-linked sulfonated poly (ether ether ketone) (SPEEK)/reactive organoclay nanocomposite proton exchange membranes (PEM).* Journal of Membrane Science, 2011. **372**(1–2): p. 40-48.

226. Al Lafi, A.G. and J.N. Hay, *State of the water in crosslinked sulfonated poly(ether ether ketone).* Journal of Applied Polymer Science, 2013. **128**(5): p. 3000-3009.

227. Knauth, P., et al., *Thermogravimetric analysis of SPEEK membranes: Thermal stability, degree of sulfonation and cross-linking reaction.* Journal of Analytical and Applied Pyrolysis, 2011. **92**(2): p. 361-365.

228. Di Vona, M.L., et al., *Analysis of Temperature-Promoted and Solvent-Assisted Cross-Linking in Sulfonated Poly(ether ether ketone) (SPEEK) Proton-Conducting Membranes.* The Journal of Physical Chemistry B, 2009. **113**(21): p. 7505-7512.

229. Di Vona, M.L., et al., *High performance sulfonated aromatic ionomers by solvothermal macromolecular synthesis.* International Journal of Hydrogen Energy, 2012. **37**(10): p. 8672-8680.

230. Muthu Lakshmi, R.T.S., V. Choudhary, and I.K. Varma, *Sulphonated poly(ether ether ketone): Synthesis and characterisation.* Journal of Materials Science, 2005. **40**(3): p. 629-636.

231. Vico, S., B. Palys, and C. Buess-Herman, *Hydration of a Polysulfone Anion-Exchange Membrane Studied by Vibrational Spectroscopy.* Langmuir, 2003. **19**(8): p. 3282-3287.

232. Kittur, A.A., et al., *Pervaporation separation of water–isopropanol mixtures using ZSM-5 zeolite incorporated poly(vinyl alcohol) membranes.* Journal of Applied Polymer Science, 2003. **90**(9): p. 2441-2448.

233. Chang, M.-J., A.S. Myerson, and T.K. Kwei, *The effect of hydrogen bonding on vapor diffusion in water-soluble polymers.* Journal of Applied Polymer Science, 1997. **66**(2): p. 279-291.

234. Armstrong, A.A. and V. Stannett, *Temperature effects during the sorption and desorption of water vapor in high polymers. I. Fibers with particular reference to wool.* Die Makromolekulare Chemie, 1966. **90**(1): p. 145-160.

235. Chung, T.-S., W.F. Guo, and Y. Liu, *Enhanced Matrimid membranes for pervaporation by homogenous blends with polybenzimidazole (PBI).* Journal of Membrane Science, 2006. **271**(1–2): p. 221-231.
236. Zolandz, R., Fleming, G., *Membrane Handbook,*. 1992, New York City, USA: VNR.
237. Qader A, H.B., *Latrobe Valley Post-Combustion Carbon Capture (LVPCC): CO2CRC-IPRH Stream (Carbon Dioxide Capture Technologies for Brown Coal Power Generation)*. 2011, CO2CRC.
238. Merkel, T.C., et al., *Power plant post-combustion carbon dioxide capture: An opportunity for membranes.* Journal of Membrane Science, 2010. **359**(1–2): p. 126-139.

Appendix A: Experimental Methods

A.1. Pure Gas Permeability Calculation

Pure permeabilities for CO_2 and N_2 are measured on the CVVP apparatus discussed in section 3.3.1. The permeabilities are calculated according to Equation 3.2. A sample calculation for SPEEK IEC 1.6 meq/g at 30 °C is presented in Table A.1.

Table A.1: Sample calculation for N_2 and CO_2 permeability through SPEEK IEC 1.6 meq/g.

Gas	Blank	N_2	CO_2
Permeate Volume, Vp (cm^3)		1913.7	1913.7
Membrane Area, A (cm^2)		11.95	11.95
Membrane Thickness, l (cm)		0.003	0.003
Permeate Temperature, T (K)		303	303
Feed Pressure, pf (kPa)		492	503
Steady state permeate pressure gradient (torr/s)	4.786×10^{-7}	1.741×10^{-6}	2.821×10^{-5}
Adjusted steady state permeate pressure gradient (torr/s)		1.261×10^{-6}	2.773×10^{-5}
Permeability (Barrer)		0.019	0.412

A.2. High Temperature Mixed Gas Permeability Calculation

Mixed gas permeances for binary mixtures H_2O/CO_2 and H_2O/N_2 are measured on the high temperature mixed gas apparatus discussed in section 3.3.3. A sample calculation for Nafion 115 at 130 °C is presented in Table A.2.

Table A.2: Sample calculation for water, N_2 and CO_2 permeance through Nafion 115.

Gas	H_2O	N_2	CO_2
Permeate flowrate, Q_{per} (cm^3/min)	-	80	80
Membrane Area, A (cm^2)	15.91	15.91	15.91
Permeate Temperature, T (K)	403	403	403
Feed water partial pressure, p_f (hPa)	1000	-	-
Permeate water partial pressure, p_p (hPa)	509	-	-
Feed pressure (kPa)	-	1750	1750
Permeate pressure (kPa)	-	101.3	101.3
Permeate gas concentration, x_{gas}	-	0.008%	0.058%
Vapour activity, a	0.79	-	-
Permeance (GPU)	1803	0.78	1.04

A.3. Gravimetric Sorption Calculation

Water concentration sorbed in Nafion 115 was measured using the gravimetric sorption analyzer discussed in section 3.6.1 and calculated using equation 3.5. The sample calculation is presented in Table A.3.

Table A.3: Sample calculation for water concentration in Nafion 115 at 40 °C.

Component	H_2O
Vapour activity, a	0.20
Temperature, T (K)	313
Initial mass (mg)	21.9
Final mass (mg)	22.7
Density of polymer, ρ (g/cm³)	1.82
MW (g/mol)	18
Universal gas constant, R (J/mol.K)	8.314
STP	273K, 1 atm
Concentration, C (cm³ [STP]/cm³ polymer)	85.4

A.4. Theoretical T_g Calculation

The theoretical T_g was calculated from the water mass uptake in Nafion 115 at 40 °C and a vapour activity of 0.2 using the Fox Equation (Equation 2.4). A sample calculation is presented in Table A.4.

Table A.4: Sample calculation for theoretical T_g in Nafion 115 at 40 °C.

Component	H_2O
Vapour activity, a	0.20
Temperature, T (K)	313
Initial mass (mg)	22.3
Final mass (mg)	23.0
Density of polymer, ρ (g/cm³)	1.82
$T_{g,polymer}$ *(K)*	393
$T_{g,\ water}$ *(K)*	135
$T_{g,\ theoretical}$ *(K)*	51.2